Variabilité naturelle de la composition atmosphérique et influence anthropique en Patagonie. Contribution à l'étude des transports Equateur-Moyennes latitudes-Pôle

Isabel Moreno

THÈSE

En vue de l'obtention du

DOCTORAT DE L'UNIVERSITÉ DE GRENOBLE
(Arrêté ministériel du 7 août 2006)

Spécialité **Sciences de la Terre, de l'Univers et de l'Environnement**

Présentée et soutenue publiquement par

C. Isabel MORENO RIVADENEIRA

Le 19 janvier 2011

Variabilité naturelle de la composition atmosphérique et influence anthropique en Patagonie. Contribution à l'étude des transports Equateur-Moyennes latitudes-Pôle

---

Natural variability of the atmospheric composition and anthropogenic influence in Patagonia. Contribution to the understanding of transport pathways along the Equator-Mid latitudes-Pole transect

---

JURY

René Garreaud	Professeur, University of Chile, Santiago, Chili	Rapporteur
Karl Kreutz	Professeur, University of Maine, USA	Rapporteur
Luc Ortlieb	Directeur de Recherche IRD, IRD, LOCEAN	Examinateur
Catherine Chauvel	Directrice de Recherche CNRS, LGCA	Examinatrice
Anne Alexandre	Chargée de Recherche CNRS, CEREGE	Examinatrice
Jean-Robert Petit	Directeur de Recherche CNRS, LGGE	Directeur de thèse
Françoise Vimeux	Chargée de Recherche IRD, HSM-LSCE	Co-directrice de thèse
Martine de Angelis	Ingénieur de Recherche CNRS, LGGE	Co-encadrante

Thèse préparée au sein du **Laboratoire de Glaciologie et de Géophysique de l'Environnement (LGGE)** dans **l'École Doctorale Terre, Univers, Environnement** financée par le **Département de Soutien à la Formation (DSF) de l'Institut de Recherche pour le Développement (IRD)** dans le cadre du projet **ANR-SANVALLOR**

IRD
Institut de recherche pour le développement

LGGE
Laboratoire de Glaciologie et Géophysique de l'Environnement

Acknowledgments

This is the end
my only friend, the end
(The Doors, 1967)

...Although I learned that in science, there is no end. However, the completion of this project is a propitious opportunity to offer my gratitude to all of those who have supported me in any aspect during these last years.

First of all, I am very thankful to my advisors Françoise Vimeux and Martine de Angelis, whose encouragement, supervision and support facilitated the developing and understanding of this subject. I learned a lot from their different and complementary ways of tackling both difficult scientific and non-scientific problems. I feel that it was a privilege to work with you.

I sincerely thank Patrick Ginot for providing me the opportunity to join the SANVALLOR project, and also for his support and original as well as insightful discussions.

I also deeply appreciated the support and availability from Jean-Robert Petit from the beginning to the completion of this study.

Working with Julien, Nicolas, Olivier, Jean-Denis, Pamela, Gino, Mireille, Rémi, Fred, and all the other members of the SANVALLOR team was a very enriching experience and I wish that new projects as interesting as this one may emerge for them.

I also would like to thank all the scientists from the Centro de Estudios Científicos (CECs) in Valdivia for their warm welcoming and discussions. Paulina Lopez′s instantaneous and graceful help also contributed to this project.

Rene Garreaud, whose advice I truly appreciate, facilitated the short but insightful sojourn at the Geophysics Department (DGF) of the Universidad de Chile. I thank him, Mark, Patricio, Alejandra, Rodrigo, Laura, Martín, Angie and all the members of the DGF because in one way or another they contributed to answering my newbie questions about the vast domain of climatology.

I would also like to thank my colleagues at the Instituto de Hidráulica e Hidrología (IHH) in Bolivia, where I always had a door open and a desk at which to work comfortably.

Working at the LGGE was a fantastic experience and countless interactions made this period very rich in all aspects. It was a pleasure to share doctoral studies and life with wonderful people like Alvaro, Christine, Daph, Cécile, Josué, Ludo, JC, Julie, Julien, Bruno, Greg, Steph, Vincent F., Yves and all the others who are not listed here. Thank you all for the laughing and relief to go through the tortuous graduate student life.

Finally, I thank my lovely family for the support that underpins all the rest.

This project was financed by the Departament de Soutien et Formation (DSF) of the Insitut de Récherche pour le Développement (IRD) and the ANR project number ANR-06-BLAN-0245. The sojourn at the DGF was possible thanks to the funding provided by the ED TUE (Terre Univers et Environnement) graduate school.

Abstract

Although tropical and subtropical South America play an important role in atmospheric global and hemispheric chemistry due to the coexistence of big reservoirs with large-scale atmospheric patterns, exchanges between tropics and higher latitudes have remained poorly documented. During the last few decades, the study of past climate and atmospheric composition has benefited greatly by information provided by ice core analysis. In the Southern Hemisphere, a large amount of data is now available from polar ice cores and more recently from ice cores recovered in the Andes. Despite a few studies on climate reconstruction, there is a lack of information on past atmospheric composition in Southern mid-latitudes, in terms of both natural variability and anthropogenic impact.

This work is based on the analysis of a 122 m ice core extracted from a high altitude site in the Northern Patagonian Icefield (Monte San Valentin 46°35′S, 73°19′ W, summit at 4032 m.a.s.l., drilling plateau at 3723 m.a.s.l.). Besides high-resolution measurements of mineral and organic ions, a study of the precipitation events likely to influence the site was conducted in order to provide a basis for the interpretation of the ice archive.

The selected site registers precipitation events of marine and continental origin. We have demonstrated that marine primary and biogenic contributions are not synchronous and they are very likely underrepresented along the ice archive due to the effect of accumulation processes. Contrary to sea salt, a significant part of marine biogenic aerosol is associated with a complex and diluted continental fingerprint. The continental imprint was studied in terms of background trends and major events involving combustion processes, urban pollution, volcanic and soil emissions. This set of mixed sources is responsible for almost half of the total sulfate input. This important and ubiquitous sulfate concentration is related to that of nitrate and chloride and its understanding in terms of sources and transport needs further research. A comparison of our records with documented volcanic eruptions and Patagonian settlement periods allowed us to propose a few dating horizons, although an accurate dating of the entire core has not been possible so far. Background trends of continental species do not show any trend that can be clearly associated with an anthropogenic influence, except for ammonium, which increases likely in response to fertilizer consumption after ca. 1960.

Keywords : ice-core, chemistry, climate, Patagonia, southern hemisphere, atmosphere

Résumé

Au cours des dernieères décennies, l′étude des paléoenvironnements de l′Hemisphere Sud s′est développée avec les informations fournies par l′analyse des carottes de glace polaires et plus récemment à partir des carottes de glace prélevées dans les Andes. Bien que les zones tropicales et subtropicales de l′Amérique du Sud jouent un rôle majeur dans la chimie atmosphérique globale en raison de l′existence de réservoirs importants, les échanges entre l′équateur et les hautes latitudes sud restent encore peu documentés. Même si d′autres archives apportent des informations sur le climat passé, il existe peu de données de la composition atmosphérique des moyennes latitudes de l′Hémisphère Sud, aussi bien en termes de variabilité naturelle que d′impact anthropique.

Ce travail est basé sur l′analyse d'une carotte de glace de 122 m extraite d′un site d′altitude en Patagonie (Monte San Valentin 46°35′S, 73°19′ O, 3723 m). Outre l′établissement de profils à haute résolution des ions minéraux et organiques obtenus par chromatographie ionique, nous avons réalisé une étude des précipitations susceptibles d′influencer le site, fournissant ainsi une base pour l′interprétation de l′archive de glace.

Ce site se caractérise par l′enregistrement d′événements à caractère marin et continental. Nous avons démontré que, sur ce glacier, les contributions marines primaires et secondaires ne sont pas synchrones et qu′elles sont très probablement sousreprésentées dans le profil en raison de processus d'accumulation. Contrairement au sel de mer, une partie importante des aérosols biogéniques marins est associée à un apport influencé par des contributions continentales diluées. L′apport continental est complexe : il est composé d′événements ponctuels de combustion, de retombées volcaniques et d′émissions par les sols. Il correspond à presque la moitié de la quantité totale de sulfate déposé. Cette contribution importante et omniprésente de sulfate est associée au nitrate et au chlorure, mais mieux cerner son origine nécessiterait des recherches plus poussées. La comparaison de notre archive glaciochimique avec des éruptions volcaniques datées et le début de la colonisation en Patagonie nous a permis de proposer quelques repères pour la datation de la carotte, qui reste à ce jour encore incertaine. Enfin, aucune tendance anthropique claire n′a été décelée à partir de l′évolution du bruit de fond des espèces continentales, excepté l′ammonium, lui pouvant être mis en relation avec l′utilisation croissante d′engrais après les années 1960.

Contents

List of Figures

List of Tables

Introduction

Scientific motivation

For more than 20 years, ice core drillings have been recovered in the South American Central Andes glaciers at altitudes higher than 6000 m a.s.l. between 0°and 20°S, in order to reconstruct past tropical climate variability (see Thompson et al., 1995, 1998, 2000; Ramirez et al., 2003, for some examples). While Antarctic deep ice cores cover our climate history back to about 800,000 years albeit with a raw temporal resolution (EPICA, 2004), Andean ice cores allow to reconstruct past environmental changes only back to about 20,000 years, but with a higher temporal resolution varying from seasonal cycles over the last centuries to a few years over the last millennium (Vimeux et al., 2009).

The multi-proxy analytical approach previously used for polar studies, and mainly focused on water stable isotopes, ice chemical composition and insoluble particle content, has been applied to the tropical ice cores to obtain environmental and climatic parameters at high resolution. It was generally possible to establish seasonally resolved dating along the upper half part of the cores, i.e. at most over the last centuries (Simões et al., 2003; de Angelis et al., 2003). Post-depositional studies have also been conducted to better constrain the air-snow transfer-function for tropical glaciers, which is essential when reconstructing past mass balance and atmospheric composition (Ginot et al., 2001; Stichler et al., 2001). Thus, the climate variability at different timescales has been well documented at both low and high latitudes and using the same kind of archives (figure 1).

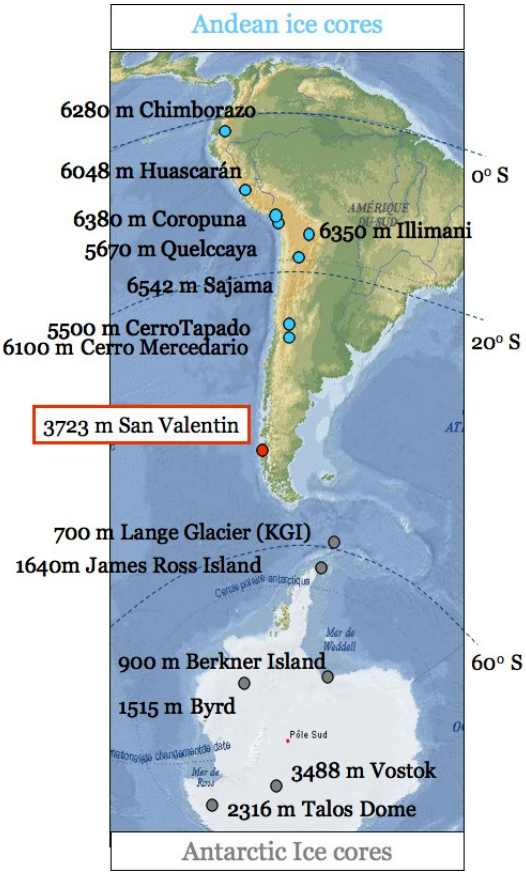

Figure 1: Drilling sites in South America (cyan circles) taken from (Vimeux et al., 2008, and references therein), some sites in Antarctica (grey dots) and the location of Monte San Valentin (this study).

However, a large gap exists along the Equator-Pole transect at mid southern latitudes, between 35°S and 60°S (Antarctic Peninsula). The documentation of past climate variability through continental archives in the Southern Hemisphere is very poor. Although marine sediment cores allow to reconstruct the past sea surface temperature history, only scarce data obtained at low temporal resolution are available at these latitudes. For instance, the influence of the recent global warming or El Niño-La Niña events on Patagonian glaciers is poorly documented.

Scientific questions remaining unanswered are numerous, among them: what was the past climate and environment variability of the Southern Hemisphere at mid-latitudes? What are the teleconnections linking Tropics and high latitudes? What are the key parameters of the climate

sensitivity at Southern mid latitudes? Can we detect an anthropogenic influence in this region and what can be its sources? What information is recorded in South American mid-latitude ice cores and what proxies are the most relevant for paleoenvironmental reconstructions?

The SANVALLOR project financed in 2007 by the Agence Nationale pour la Recherche (ANR) aimed at drilling deep ice cores in Patagonia to fill the abovementioned gap and to document the mid-latitude climatic and environmental history.

State of the art for Patagonian ice cores study before the SANVALLOR project

Many shallow ice cores have been drilled in Patagonia by different international groups during the past decades (Aristarain and Delmas, 1993; Matsuoka and Naruse, 1999; Shiraiwa et al., 2002, for the most recent examples). All these studies (mostly located in the Southern Patagonian Icefield) concerned glaciers at elevation lower than 2500 m a.s.l. where firn temperature close to 0°C does not allow a proper preservation of isotopic and chemical signals. Some soluble impurities are partly or totally (depending on the site) washed out making very questionable the interpretation of the glaciochemical profiles in term of past climate fluctuations. Moreover, all these sites have a very high annual accumulation rate (more than several meters per year), not suitable for paleoreconstructions. On the opposite, we found two glaciers at altitudes higher than 3500 m a.s.l., covered by several tens of meters of cold ice, and where the annual snow accumulation rate is moderate. They are presented in figure 2. The first site is the Monte San Valentin glacier (henceforward SV), the highest point of the Patagonian chain at ∼4000 m a.s.l., located on the Northern Patagonian Icefield (NPI). The second site is the San Lorenzo glacier at 3500 m a.s.l. Both sites appeared suitable for drilling operations (flat plateau-like surface and low ice flow) and appropriate to study the climate variability at various time scales (ENSO events as well as the glacial-interglacial transition) and to provide valuable information on the Equator-Pole connection. The drilling of two ice cores was mainly motivated by the very different

meteorological conditions expected to prevail at these two sites: the SV summit is located on the border of the humid area strongly influenced by the Pacific Ocean, while the San Lorenzo (∼100 km farther south-east) is located in the arid side of the Andes, likely under more continental and/or Atlantic influence. Moreover, concerning regional climate conditions, it was interesting to study two cores in order to investigate the very local variability when studying the imprint of specific short events at those latitudes (such as the Little Ice Age).

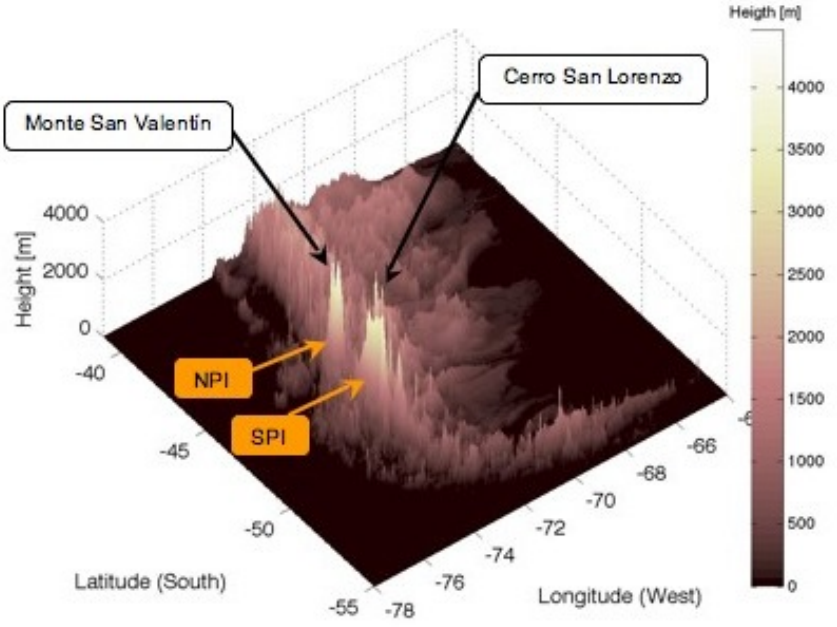

Figure 2: Topography of southern South America obtained from the GLOBE project (`http://www.ngdc.noaa.gov/mgg/topo/globe.html`), with a resolution of 1 degree and an error of ∼20 m. Note the abrupt topography of the Northern and Southern Patagonian Iciefields (NPI and SPI respectively). The location of the Monte San Valentin (4032 m a.s.l.) and Cerro San Lorenzo (3500 m a.s.l.) are indicated by black arrows.

Preliminary studies at Monte San Valentín

Site survey (march 2005)

Pre drilling site surveys of the Monte San Valentín and Cerro San Lorenzo were done in march 2005 by members of the Great Ice research unit of the IRD (Institut de Recherche pour le

Développement, France) and the CECS (Centro de Estudios Científicos, Valdivia, Chile). The San Lorenzo site survey demonstrated that the ice was too warm (∼0°C) to allow suitable paleoclimate reconstructions. It was then decided to explore the summit plateau of the SV (46°35′S, 73°19′W), located on the north eastern border of the NPI, in the upper accumulation area of Glacier San Rafael (Rivera et al., 2007).

The summit of Monte San Valentin has been assigned an altitude of 3910 m a.s.l. in the Chilean official maps (IGM, 1975), but a more precise altitude of 4032±1 m a.s.l. has been recently calculated using differential GPS (Wendt 2007, pers. comm.). It has an east-west extension of 1.5 km and spans an altitude range between 3700 m a.s.l and 3900 m a.s.l. It covers an area of about 2.1 km^2 and it is delimited by steep walls and icefalls as observed in the figure 3(a).

A 15.26 m long and 58 mm diameter shallow firn core (denoted SV2005 in the manuscript) was extracted on March 2005 on the summit plateau of SV site using the portable solar-powered electromechanical drilling system described by Ginot et al. (2002) (`http://www.canal.ird.fr/sommaires/missions_cp.htm`). The drilling site (46°35′19″S, 73°19′39″S, 3747 m a.s.l.) was chosen at the central section of the plateau, in the summit saddle area between the eastern and western peaks (red star in figure 3(a)).

Three radar profiles were obtained around the drilling site with a 9 MHz impulse radar system (Casassa et al., 1998) to show that the glacier thickness is 70 m close to the ice divide, increases to 100 m at the drilling site and reaches 170 m on the south-central portion of the summit plateau. Borehole temperature ranges from -11.9°C at 10 m to -11.6°C at 16 m depth, indicating that a well-preserved glaciochemical signal could be expected.

The 2005 firn core main results

The 15 m firn core extracted in 2005 was analysed in 2006 (Vimeux et al., 2008). The water stable isotopes content was analyzed at the LSCE (Laboratoire des Sciences du Climat et de l'Environnement, Saclay) in collaboration with the University of Copenhagen. Depth resolu-

(a) Picture of the Monte San Valentin taken from the east.

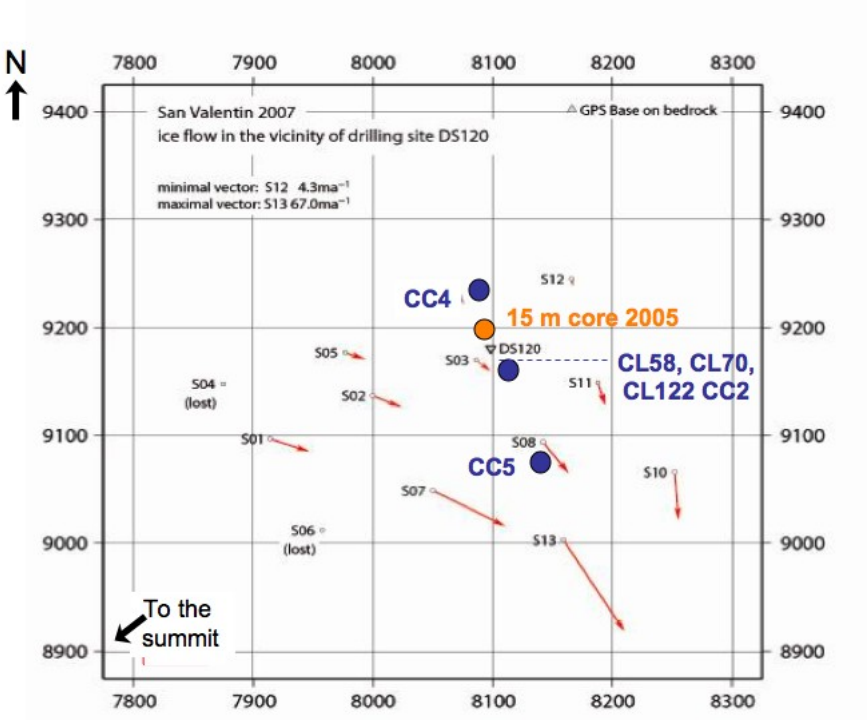

(b) View of the drilling site and stakes location in UTM coordinates.

Figure 3: (a) Picture of the highest peak, the summit plateau and the minor peak of the Monte San Valentin (46°35.323′ S, 73°19.671′ W). The picture was taken facing the west, thus the minor eastern peak the one closer to the airplane. Arrows show the flow direction of the glacier. The star corresponds to the drilling site (Vimeux et al., 2008). (b) Top view from the drilling site in UTM coordinates, including stake numbering (s01 to s12), the location of the shallow core retrieved in 2005 and some of the shallow and deep cores retrieved in 2007 (Ginot 2009, pers. comm.). Red arrows correspond to stake measurements of surface flow of the glacier during the drilling campaign (design is qualitative). Red arrows direction corresponds to the red arrow of the picture (a).

tion was approximately 10 cm for the two isotopes, deuterium and oxygen-18. Ionic species and radionuclides were analyzed at the LGGE (Laboratoire de Glaciologie et Géophysique de l′Environnement, Grenoble). The sampling resolution for ion analysis was approximately 5 cm. ^{7}Be (half time life: 54 days) was measured in the upper part of the core. The ^{210}Pb profile (half time life: 22.3 years) was established for the total length of the core. ^{137}Cs, ^{241}Am and ^{3}H (nuclear tests fallout of 1963-1965) were measured in the lower part of the core.

^{137}Cs, ^{241}Am and ^{3}H high activities observed at the bottom of the core combined with ^{210}Pb decay along the core showed that this 15 m-core covered roughly 40 years. This was in agreement with the assumption that chemical species like calcium present a seasonal cycle allowing annual layer counting. The mean snow accumulation rate was estimated around 0.36±0.03 m of snow per year.

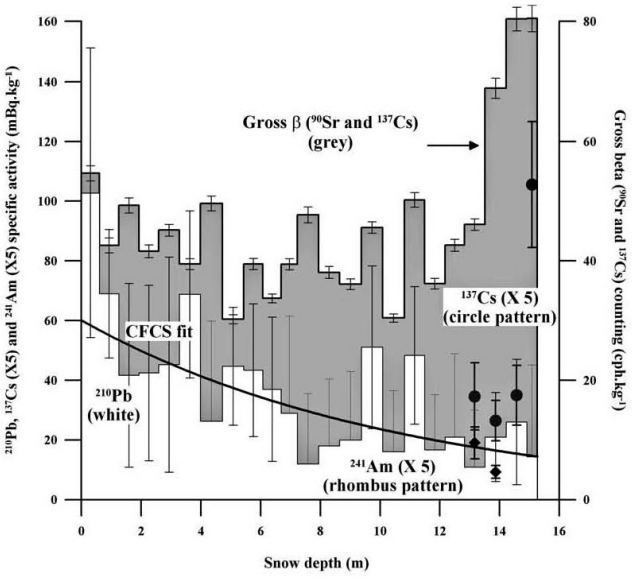

Figure 4: Radionuclide profiles (gamma emitters, ^{137}Cs, ^{210}Pb and ^{241}Am, as well as β emitters, ^{90}Sr plus ^{137}Cs) used for the San Valentin 2005 shallow firn core dating. The CFCS ^{210}Pb - derived model fit (bold line, n=23, r^2=0.5, p<0.05) is also presented. ^{210}Pb (white area), ^{137}Cs (gray circle) and ^{241}Am (black rhomb) are given in specific activities (mBq.kg^{-1}) while gross beta activities (grey area) are expressed in counts per hour per kilogram (cph.kg^{-1}). Error bars are expressed as 95% confidence level. ^{137}Cs and ^{241}Am scales are multiplied by 5 (Vimeux et al., 2008).

The comparison of isotopic and chemical profiles allowed Vimeux et al. (2008) to suggest that the SV area alternatively undergoes two kinds of influences, the relative importance of each one varying at interannual timescale: the site is influenced by air masses originating from the South Pacific and rapidly transported by western winds (high concentration of marine aerosol and deuterium excess, potential proxy of moisture source temperature, in figure 5), and a second very different mode, corresponding to air masses overflying the continent trough a N-NE circulation pattern containing the emissions of biomass, combustion events, , and erodible soils, is also observed. The later one may be mixed with aged marine air masses of polar origin (low concentration of marine aerosol, low level of deuterium excess in fig.5). Therefore, these results indicated that precipitation at that site was not controlled the whole-year long by westerlies and that meteorological patterns allowing aerosol and gas transport from eastern Patagonia and even Brazil regularly occur, which was an unexpected result.

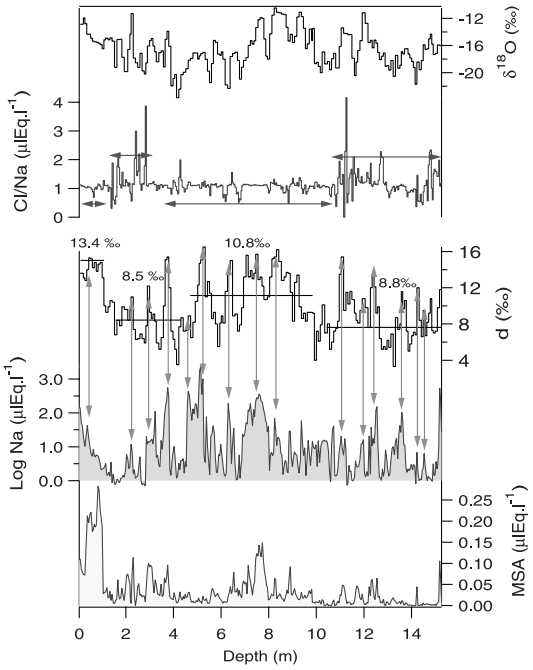

Figure 5: Selected chemical markers of marine inputs (μeq.L^{-1}), δ^{18}O and deuterium excess of the ice (%). Vertical arrows indicate similar occurrences in sodium concentration and deuterium excess (Vimeux et al., 2008).

The SANVALLOR project

Hypothesis underpinning a broader project

The preliminary studies conducted at the SV let to two main hypothesis:

- A deep ice core at this site could cover at least the last millennium given the low net accumulation observed.
- No years seem to be missing, and the register contains marine storms partly eroded by wind blowing and better conserved continental inputs.

These hypothesis set the basis for the franco-chilean SANVALLOR project, which aimed at retrieving and analyzing several cores at the SV summit plateau.

The San Valentin 2007 field campaign

After a failed drilling mission due to extreme weather conditions in 2006, a new attempt succeeded in April 2007. The expedition formed by members of the IRD, LGGE and CECS retrieved six new shallow cores (numbered CC1 to CC6), a 58-meter (CL58), a 70-meter (CL70) and a 122-meter deep core (CL122, reaching the bedrock) very close to the 2005 drilling site. Stake measurements of ice surface velocity were performed between the April 21^{th} and May $3rd$. The precise location where every core was recovered is reported in figure 3(b) along with surface velocity measurements. Red arrows show the surface flow direction deduced from stake measurements. The flow of the glacier would be deflected southward when passing through the depression between the main summit and the eastern peak, as suggested by arrows direction. CC2, CL58, CL70 andCL122 were recovered very close ($\sim$30 m) to the 2005 site. All 6 shallow and deep cores were recovered on a flat area along the glacier flow line, in the depression between the main summit (western peak) and the eastern peak (Ginot 2009, pers. comm.). New radar profiles were also obtained in order to complement those obtained in 2005 (Casassa 2009, pers. comm.).

We may expect some difficulties in core interpretation due to wind blowing and the lack of information on ice flowing. We must first underline that, although the northern part of the

drilling area is likely partly sheltered from wind erosion by a rock wall, a Venturi-effect may strongly influence the net snow accumulation rate of the site through wind erosion windward and wind blown snow redeposition downwind. Another characteristic of the SV site is that the stratigraphy of the CL122 core is characterized by layers oblique to the surface (with an angle that can reach approximately 30°). Below the close off level, visually found at 45 m, air bubbles were not spherical but prolated and slanted. Moreover, the ice was very fractured and broken from 73 to 105 m depth. Gas bubble form along with the presence of a continuous and more than 30 m thick layer of brittle ice at a depth where the hydrostatic pressure is too low to induce relaxation problems are very likely due to strong shearing processes within the glacier and led us to be aware of a possible discontinuity in ice archive occurring in the brittle zone. All this has important implications on dating hypotheses as the accumulation at this site is very likely influenced by the ice flow, which remains poorly characterized.

Objectives of this work

The SANVALLOR project involved an extensive set of analyses performed by five laboratories: Radiogenic isotopes (^{7}Be, ^{210}Pb, ^{137}Cs, ^{90}Sr and ^{241}Pu, ^{241}Am), major and minor ions, organic matter (levoglucosan, aldehydes) measurements and the study of ice crystallographic properties were done at the LGGE, water stable isotopes were measured by the LSCE and the LAMA (LAboratoire Mutualisé d′Analyse des isotopes stables de l′eau), pollen and inorganic trace elements were studied by the LMTG (Laboratoire des Mécanismes de Transfert en Géologie), microalgae identification was performed at the CECS and tritium measurements at the Physics Institute of the University of Bern. The sampling resolution and the depth covered by each dataset depended on the species under consideration and the time period expected to be covered. Only ionic species and water stable isotopes were measured continuously and at high resolution along the CL122 core. Radiogenic isotopes were analyzed along the CL70 core, algae and pollen along one of the shallow cores (CC2). Discontinuous samples for trace elements and specific samples for additional studies (electron microscopy, organic matter, crystallography) were taken along

CL122 when ice was available or along CL70.

Within this framework, the proposed for my doctoral research were:

1. To reconstruct the paleoenvironnmental conditions at southern mid-latitudes trough

   - The generation of a complete database of inorganic and organic ions from the SV ice.

   The interpretation of the data would be made by comparing the SV information with other available ice-core records.

2. To understand the transport processes responsible for the continental and the marine inputs, through

   - The identification of regional active sources likely to affect this site
   - The understanding of transport and deposit phenomena involved using a backtrajectories study related to precipitating conditions in this zone.

The analytical work and most of the interpretation was made in Grenoble, France. However, as established by the scholarship terms (DSF, Département de Soutien et Formation of the IRD), I spent six months in Bolivia mostly for interpreting data. As climatic studies appeared as key elements for a better understanding of our data (the second objective), I spent one month in fall 2009 at the Geophysics Department of the University of Chile (DGF), gathering useful meteorological data (precipitation and wind observations) and modeling outputs (e.g. precipitation predictions at SV site) as well as basic training on the use of the tools necessary for further work with meteorological and climatic datasets.

Presentation of the manuscript

In chapter 1 we present the complete analytical procedure used to obtain continuous high resolution profiles of major and minor ions, with a focus on carboxylate and contamination estimates. CL122 ionic profiles are reported and compared with data from the 2005 shallow core, and the

current dating hypothesis for both cores are presented. In chapter 2 we present a review of the climatology governing southern South America with a focus on Patagonia, and the main characteristics of precipitation events likely to influence the SV site. In chapter 3 we identify the marine primary and secondary contributions along the CL122 core. Corresponding inputs are discussed in regard of chapter 2. In chapter 4 we aim to disentangle the complex continental signature found in the core, starting from combustion markers. In the conclusion, we summarize our major results along with perspectives for future research on this interesting site.

Chapter 1

Analytical methods and complete chemical profile

1.1 Introduction

The comprehensive study of the 15-meter shallow core (SV2005) extracted in 2005 from the summit plateau of the Monte San Valentin (SV) (46°35.323′ S, 73°19.671′ W, 3723 m.a.s.l.) demonstrated the suitability of this site for high-resolution glaciochemical reconstructions (Vimeux et al., 2008). In this chapter we present a detailed description of the analytic methods used for the analysis of the CL122 core and average concentrations obtained (section 1.2). The CL122 record is then compared with SV2005 (section 1.3). This comparison raised unexpected questions on the dating proposed by Vimeux et al. (2008) and on the spatial and/or temporal variability of the accumulation. We discuss this issue in the last sections using additional information provided by field glaciological studies and the preliminary results of the analysis of the shallow cores CC4 and CC5.

1.2 Analytical methods

1.2.1 Ion chromatography (IC)

1.2.1.1 Sample preparation

To prevent gaseous contamination for organic species every core section was directly wrapped into aluminium foil in the field, and then stored into sealed polyethylene bags until the decontamination step. Samples for ion chromatography were prepared in the clean cold room facilities (-15°C) of the LGGE. 2 cm tick slices were cut along every core section with a bandsaw, and the outer part of each of them was mechanically removed by scraping with a plane. Decontaminated ice slices were then manually cut in samples of approximately 2 cm length and stored in frozen state in Coulter polycarbonate accuvettes closed with polyethylene caps. This procedure has been previously used for antarctic as well as alpine and tropical firn and ice samples. The sampling resolution slightly decreased when passing from firn to ice and is summarized in table 1.1. Analyses were performed by conductivity-suppressed ion chromatography using a Dionex ICS 3000 apparatus and a Dionex AS40 autosampler placed in the clean room facilities of the LGGE. Samples were melted inside the accuvettes, transferred into Dionex polycarbonate vials previously rinsed with ultrapure Millipore water (conductivity>18 mΩ, TOC<10 ng.g^{-1}) and analyzed less than 24 hours after melting.

My contribution to the analytical part of the SANVALLOR project was to provide continuous and high resolution profiles of ionic species including major and minor inorganic ions (sodium, Na^+; potassium K^+; ammonium, NH_4^+; calcium, Ca^{2+}; magnesium, Mg^{2+}; fluoride, F^-; bromide, Br^-; chloride, Cl^-; sulfate, SO_4^{2-}; nitrate, $NO_3^-$and nitrite, NO_2^-) as well as methanesulfonate, $MS^-$and mono and dicarboxylates (formate, acetate, lactate, pyruvate, propionate, oxalate, succinate and glutarate) of the 73 upper meters and the 14 bottom meters of CL122. Complementary analysis by Scanning Electron Microscopy (SEM) were performed on a few selected samples corresponding to specific events. According to the accumulation rates deduced from the study of the 2005 shallow core, the 73 upper meters of CL122 were expected

to cover a few centuries and the deepest ice, i.e. from 105 m to the bedrock (119 m), were likely representative of the Holocene natural background. The analyses I performed cover 75% of the whole core and account for 4692 samples (see table 1.1).

The brittle ice (73-105 m) was processed very recently. Each piece of broken ice was wrapped in aluminum foil to prevent contamination by gaseous diffusion, placed in a sealed polyethylene bag and transported frozen to the clean room for processing. Samples were directly rinsed under running ultrapure Millipore water (conductivity>18 mΩ, TOC<10 ng.g^{-1}), melted in capped polypropylene bottles and analysed within 3 hours after melting. My contribution to this part of the core study was to test and validate the decontamination process and the suitability of polyropylene for the study of organic traces. Moreover, I estimated the dilution of small volume samples by residual water droplets remaining on the ice surface after the rinsing step. Concentrations were corrected for this dilution effect, that accounted for $\approx$ 2%. No significant carboxylate increase was observed during 3 hours storage in polypropylene bottles. Part of the data concerning the brittle zone will be used in the following sections to help to a better interpretation of our results.

Table 1.1: Sampling details for the ion-chromatography analysis of the 122 m deep core (CL122)

Depth m (m weq)	**Tube number**	**Sample numbering**	**Total samples**	**Resolution cm**	**Comments**
0-45.05 (0-28.29)	1-61	1-2269	2261	2.01± 0.30	Firn
45.05-73.17 (28.29-51.99)	62-100	2270-3927	1622	1.70± 0.28	Ice
73.17-105.26 (51.99-79.89)	101-148	-	-	-	Only tubes 127,128 and 130 were analyzed in 2009 as part of this work
105.26-119.02 (79.89-87.88)	149-169	F0001-F0880	810	1.72± 0.27	Bottom ice to the bedrock

1.2.1.2 Analytical conditions

The Dionex ICS3000 equipment allows the simultaneous analysis of anions and cations by injecting an aliquot of the same sample into the injection loop of each chromatographic module. The remnant was left in the cuvette, refrozen and stored as a reserve for complementary analyses. Due to the large number of samples, the analyses were run 24 hours per day with stops only during weekends. As we intended to characterize the potential influence of continental biomass, specific care was taken for carboxylic acids measurements.

The operating conditions we used are presented in table 1.2.

Table 1.2: Operating conditions for the ion chromatograph Dionex ICS 3000 for the analyses of the deep core CL122

	Anions	**Cations**
Injection system	Autosampler	Autosampler
Separation column	AS11-HC 2mm	CS16 2mm
Guard column	AG11-HC 2mm	CG16 2mm
Suppressor	ASRS-300 2mm	CSRS-300 2mm
Injected volume μL	300	300
Eluent	KOH	MSA
Eluent flow rate mL.min^{-1}	0.38	0.50
Eluent concentration	Gradient from 3 to 30 mM	Isocratic, first 30 mM and later diminished to 24 mM
Regenerant	H_2O	H_2O
Temperature in °C	37 C	37
Run time in minutes	23	15, but increased to 23 to be synchronous with the cations run time

1.2.1.3 Control and validation of measurements

The main difficulty in obtaining reliable measurements was the evaluation of contamination due to sample storage in not 100% air-tight containers (accuvettes, autosampler vials) and to analytical issues (adsorption/desorption of different ions in the lines of the equipment, standard solution preparation).

Calibration The detector signal (conductivity in μS) is proportional to the concentration of the ion in the sample. To determine the relationship between conductivity and ion concentrations, we established daily calibration curves using mixed solutions of known concentrations, called *standard* solutions. The standard solutions were prepared in two steps: a first dilution was made from *concentrated* solutions (500-1000 mg.g^{-1}) to prepare *intermediate* solutions (0.4-20 mg.g^{-1}), and then a second dilution from the intermediate solutions was made to prepare the final standard solutions used for calibration (0.2-20 ng.g^{-1}for minor ions 1-100 ng.g^{-1}for major ions).

While intermediate solutions were renewed twice or three times per month for inorganic ions, they were weekly renewed for organic ions, the latter to prevent losses by bacterial contamination or gaseous exchanges. Standard solutions were prepared daily. The uncertainty related to the preparation of standard solutions is in average less than 1%. Uncertainty ranges corresponding to highest and lowest concentrations in standard solutions are [0.7-3.0%] for $F^-$and Br^-; [0.8-3.6%] for oxalate, succinate, pyruvate, lacate, propionate and glutarate; [0.4-1.8%] for acetate and formate; [0.4-0.6%] for $MS^-$and Mg^{2+}; [0.7-0.9%] for $K^+$and NH_4^+; and [0.3-0.4%] for Na^+, Cl^-, Ca^{2+}, $NO_3^-$and SO_4^{2-}. Intermediate solutions were monitored at the beginning and at the end of daily set of analysis to verify that no losses or exchanges took place during storage and also allowed testing the stability of column behavior.

Each calibration curve consisted of 6 points and was fitted by a linear function (for Na^+, F^-, Cl^-, Br^-, NO_2^-, NO_3^-, SO_4^{2-}, lactate, acetate, formate, oxalate) or quadratic (for other ions), passing or not through the origin. Some calibration curves showed a positive Y-intercept at the origin (F^-, NO_2^-, Ca^{2+}, acetate, formate, oxalate). The concentration to be added to the theoretical values of the standards to compensate this intercept was determined graphically and the calibration curve offset was then forced to zero (dashed line in figure 1.1). This initial offset value is generally very close to the value of the procedure blanks that are described in the next section and in table 1.3. It corresponds either to contamination related to standard preparation or to contamination produced inside the autosampler or the ICS3000. It was deduced from final concentrations only in this last case.

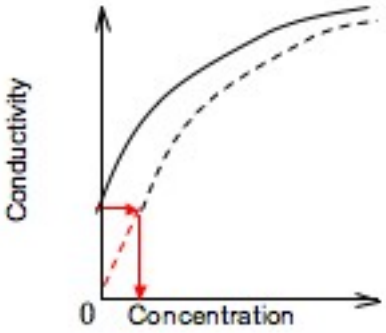

Figure 1.1: Schematic representation of a calibration curve with a Y-intercept (continuous black line). After adding a the graphically determined concentration, the offset is forced to be zero (dashed line). The graphically-determined concentrations were close to the procedure blank values obtained by injecting ultrapure Millipore water in the chromatograph (see table 1.3).

Procedure blanks Every day, various procedure blanks consisting in a few milliliters of ultrapure Millipore water were prepared and analysed in exactly the same way as the samples. This procedure accounts for the influence on measurements of water impurity content, and contamination occurring during sample transfer and analysis. Blank concentrations usually fit Y-intercept of calibration curves (fig. 1.1) and are presented in table 1.3.

A significant decrease of procedure blanks was observed for F^-, acetate, formate and $Ca^{2+}$when the injection was done manually (i.e., when samples were directly injected with a syringe into the injection port without using the autosampler) Acetate, oxalate and Ca^{2+}blank values tended to decrease gradually the longer the equipment was used mostly due to the progressive rinsing of autosampler loops and injection lines leading to significantly lower desorption from plastic tubings. For instance, Ca^{2+}contamination was higher for the first 10-12 samples analyzed after a weekend off and also in samples analysed just after more concentrated samples (Ca^{2+}>50 μeq.L^{-1}). The origin of the F^-blank is uncertain: it is probably due to an interference with an organic ion desorbed by PEEK (polyetherehetketone) Dionex connections. It remained constant during all our measurements.

Blanks of formate, acetate and $NO_2^-$are due to gaseous contamination. Once placed on the

Table 1.3: Y-intercept of the calibration curve and procedure blank values in ng.g^{-1}obtained before and after changing the anions column (at sample number 1937, 38.5 m of snow corresponding to 23.4 m w.e.). The rows marked with an A correspond to measurements obtained with the old separation column, N with the new separation column. m stands for the mean value, CI* for the confidence interval at 95%. Minimum and maximum values are also reported.

Species	Column	Y-intercept of the calibration curve				Procedure blanks					Source
						Using the autosampler				Manual injection	
		m	CI*	min	max	m	CI*	min	max	m	
F^-	A	0,07	0,03	0	0,40	0,18	0,02	0,00	0,87		Interference with PEEK of the sampling line (?)
	N	0,02	0,01	0	0,15	0,06	0,01	0,02	0,24	0,10	
Acetate	A	0,80	0,17	0,05	3,00	1,70	0,23	0,00	6,76		Gazeous contamination during sample preparation and during stagnation in the autosampler enclosure.
	N	0,19	0,07	0	1,50	0,73	0,15	0,14	3,54	0,31	
Lactate	A	0,69	0,10	0	1,10	1,00	0,17	0,00	1,93		
	N	0,08	0,03	0	0,40	0,19	0,02	0,02	0,52	0,22	
Formate	A	1,03	0,20	0	4,00	1,55	0,16	0,00	6,46		Idem as Acetate and Lactate and also desorption of formate increasing with the aging of the separation column.
	N	1,56	0,35	0	6,40	3,34	0,41	0,04	7,92	0,69	
NO_2-	A	0,21	0,10	0	1,50	0,78	0,11	0,11	2,06		Gazeous contamination during stagnation in the autosampler enclosure.
	N	0,28	0,11	0	1,70	0,56	0,08	0,02	1,82	0,00	
Ox^-	A	0,69	0,09	0	1,10	0,91	0,08	0,21	2,67		Desorption of oxalate increasing with the aging of the separation column.
	N	0,02	0,02	0	0,30	0,16	0,04	0,01	0,87	0,55	
Ca^{2+}		1,60	0,5	0,03	2,3	1,49	0,14	0,07	3,75		Adsorption of Ca^{2+} (and little Mg^{2+}) in the lines of the device.

autosampler rack, samples remained between a few minutes and more than 12 hours within the autosampler enclosure before the injection into the chromatograph lines. Contamination was higher for samples stored for longer time in the autosampler, very likely due to slow air penetration through the pre-pierced septa of the Dionex vials. A slight gaseous contamination may also occur when water microdroplets remain in vials once rinsed. Based on all these observations, blanks were minimized by improving the techniques of vial rinsing (in particular by avoiding inner wet residues), by renewing the vials and septa after every four to five uses and by analyzing the anions before the cations (so the septum will be pierced first for the gaseous contamination sensible samples). Contamination for formate and NO_2^-were significantly reduced, but it was not possible to avoid acetate increase during the batch duration (note the seesaw pattern in the first meters of the acetate profile in fig. 1.3). However, considering that values were close to the detection limit, acetate concentrations were not corrected for this progressive increase in the dataset produced as major peaks of theses species would be noticeable, if any.

By the end of our analytical work, an unidentified formate source induced a significant blank increase ($>$0.14 μeq.L^{-1}) and we decided to substract the blank value from the measured concentrations. Oxalate and lactate blank values increased with the aging of the separation column. We replaced this column once during the analyses (on 12/04/2008, at sample number 1937, 38.5 m = 23.4 m w.e.), which induced a significant decrease of blank values.. This is the reason why we present two values of procedure blanks and detection limits in tables 1.3 and 1.4.

In conclusion, to correct daily measurements of formate, acteate, oxalate and Ca^{2+}, we subtracted the corresponding values daily measured for procedure blanks from sample concentrations. The whole profile of oxalate was corrected for blank measurements made with the first separation column.

Instrument Detection Limit The instrument detection limit (DL) is the lowest concentration of a species that is just distinguishable from zero. DL was calculated with the equation:

$$DL = 3s * b \tag{1.1}$$

where b is the value of background noise and s is the standard deviation of a system blank. A system blank corresponds to the passage of the eluent alone, i.e., without injection of water or sample. Both b and s are calculated between the start and the end time where the peak of a given analyte must be located. These values are presented in table 1.4. The presence of spurious peaks in the anions′ baseline significantly increased the detection limit of pyruvate, succinate and glutarate, increasing corresponding uncertainties given the low concentrations of these ions. The baseline distortion problems were due to a suppressor defect identified only very recently by Dionex.

Missing data and unexplainable outliers were replaced by DL values, as they are indicators of the uncertainty of the measurements.

1.2.2 Microscopy

A few samples were investigated by optical and then by Scanning Electron Microscopy:

- Optical microscopy (OM) was used to make a preliminary identification of particles in filtered samples. This was done at the LGGE with an Olympus BH-2 microscope with a magnification of 100.
- Conventional SEM was used for the qualitative chemical and morphological characterization of insoluble particles. This was done with a microscope Jeol JSM-6400 at the Consortium des Moyens Technologiques Communs (CMTC -INPG) (Grenoble).

1.2.2.1 Sample preparation

Two kinds of samples were selected: samples corresponding to particular events and samples containing one or few visible particles. The particular events selected here were a biomass burning like event, a very important arrival of marine primary aerosols, an event presumed to be volcanic, and an arrival of soil dust (i.e. a Ca^{2+}concentrated sample). We also prepared one sample corresponding to clean air conditions (natural background sample equivalent to low concentrations of all ions). These samples were filtered with or without preliminary dilution (as

Table 1.4: Detection limit in μS, ng.g^{-1} and μeq.L^{-1}for all the species detected by conductivity-suppressed ion chromatography. Values corresponds to old and new separation columns (anions) and conductivity suppressors (cations). Mean, standard deviation (italics) and maximum concentrations along the entire CL122 core are also presented in μeq.L^{-1}. DL influenced by procedure blanks is marked with an asterisk (Ca^{2+}, oxalate by progressive adsorption in the apparatus sampling lines, succinate by spurious peaks

	Detection limit						**Mean**	**Standard deviation**	**Maximum**
	Old separation column			**New separation column**					
	µS	**ng.g^{-1}**	**µeq.L^{-1}**	**µS**	**ng.g^{-1}**	**µeq.L^{-1}**	**µeq.L^{-1}**	**µeq.L^{-1}**	**µeq.L^{-1}**
F^-	0,0018	0,02	0,001	0,0020	0,02	0,001	0,006	*(0,024)*	1,264
Cl^-	0,0014	0,26	0,007	0,0056	0,12	0,003	1,511	*(4,273)*	111,6
Br^-	0,0037	0,10	0,001	0,0030	0,16	0,002	0,006	*(0,008)*	0,215
MS^-	0,0039	0,25	0,003	0,0020	0,14	0,002	0,021	*(0,029)*	0,715
NO_2^-	0,0019	0,04	0,001	0,0039	0,11	0,002	0,018	*(0,017)*	0,229
NO_3^-	0,0090	0,30	0,005	0,0029	0,12	0,002	0,307	*(0,344)*	7,798
SO_4^{2-}	0,0141	0,51	0,011	0,0046	0,20	0,004	0,782	*(1,007)*	18,92
Formate (C1)	0,0015	0,21	0,005	0,0023	0,07	0,001	0,196	*(0,130)*	3,358
Acetate (C2)	0,0019	0,09	0,001	0,0019	0,12	0,002	0,047	*(0,096)*	6,819
Lactate (C3)	0,0008	0,06	0,001	0,0017	0,08	0,001	0,005	*(0,038)*	1,928
Propionate (C3)	0,0076	0,07	0,001	0,0018	0,15	0,002	0,006	*(0,010)*	0,246
Pyruvate (C3)	0,0039	0,43	0,005	0,0014	0,19	0,002	0,001	*(0,006)*	0,225
Oxalate (C2)	0,0359	1,21*	0,027	0,0056	0,2	0,005	0,020	*(0,156)*	6,821
Succinate (C4)	0,0070	0,87*	0,015	0,0022	0,5	0,008	0,007	*(0,018)*	0,535
Glutarate (C5)	0,0033	0,23	0,004	0,0042	0,52	0,008	0,002	*(0,006)*	0,160
	Old conductivity supressor			**New conductivity supressor**					
Na^+	0,0005	0,01	0,000	0,0003	0,01	0,000	1,350	*(4,062)*	105,00
NH_4^+	0,0003	0,01	0,000	0,0003	0,01	0,001	0,153	*(0,377)*	11,64
K^+	0,0005	0,05	0,001	0,0003	0,03	0,001	0,061	*(0,180)*	6,178
Mg^{2+}	0,0004	0,04	0,003	0,0003	0,01	0,001	0,311	*(0,774)*	21,29
Ca^{2+}	0,0003	0,03	0,001	0,0015	0,13*	0,006	0,553	*(2,949)*	179,2

seen in table 1.5). Two filters were prepared for each level of interest: one for both OM and SEM and the other as a reserve for further analysis like Transmission Electron Microscopy (TEM) or black carbon.

Samples for microscopy were pipetted from accuvettes containing IC residual melted ice and vacuum filtered in a Millipore stainless steel hub through polycarbonate membranes (13 mm diameter, 0.4 μm pore diameter). Filters for SEM analysis were fixed on aluminium holders using double-sided adhesive tape. For filters dedicated to TEM studies, only a small piece of adhesive was put between the holder and the filter edge. Sample holders were stored in accuvettes previously rinsed three times with ultrapure water.

Only two samples containing visible particles were found among the ca 4600 analyzed. This is not surprising since SV is dominated by oceanic winds and soil dust transport is favored neither by atmospheric circulation nor by site altitude. We allowed larger particles to sediment for 24 hours and then proceeded as explained above for the supernatant. We prepared a third filter with the largest particles (5 μm pore diameter) that was stored on a covered filter holder. Table 1.5 presents the characteristics of samples prepared for SEM studies, which were conditioned by carbon metallization directly at the CMTC-INPG by the technician in charge of the equipment.

Table 1.5: Sampling for microscopy analyses for the 122 m deep core (CL122)

	nssCa^{2+} peak	**Background**		**Volcanic event**	**Marine event**	**Forest fire**		**Particle tube 87**	**Particle tube 97**	**Blank**
Depth (bottom) m	20.44	17.15	17.17	16.52	18.36	22.17	22.19	∼63.7	70.39	-
Depth (bottom) m w.e.	10.92	8.95	8.96	8.59	9.66	11.95	11.96	43.86	49.56	
Sample number	1030	860	861	827	923	1116	1117	P−87	3767	-
Dilution	1:2	1:2	1:2	1:2	1:2	1:1	1:2	1:4	1:4	-
Filtered volume mL	2	4	3.2	4	2	2	3	4	2	4

1.2.2.2 Microscopy procedure blanks

Blanks were prepared with ultrapure Millipore water following the same procedure as for samples. The contamination procedure is characterized by the presence of carbon rich fibers, very likely

threads from garment and fine plastic debris from the accuvettes making a few tens of microns and easy to identify. Less than 7% of all the analysed samples showed fiber-type contamination. A few very fine stainless steel fragments coming from the filtering device were also observed but they did not interfere with our measurements, as they were easily recognizable through their density and composition.

1.3 Complete ionic profiles

The complete set of concentration profiles for the entire CL122 core is presented in figure 1.2 for inorganic: Na^+,Cl^-, F^-, Br^-, MS^-, NH_4^+, Mg^{2+}, Ca^{2+}, $NO_3^-$and $SO_4^{2-}$and in figure 1.3 for organic ions: formate, acetate, lactate, propionate, pyruvate, glutarate, oxalate et succinate. Concentrations of all ions are expressed in μeq.$L^{-1}$and depth in m. Organic profiles are less accurate due to low level concentrations close to the DL of most of the species. Here we will briefly describe these profiles because they will be discussed in detail in following chapters.

No regular cycles can be observed for any ions (MS^-cycle-like record may be due to diffusion of this species in the ice). A zone located between 35 and 45 m shows very low concentrations of for all ions except for $Ca^{2+}$and MS^-. A change in concentration variability and magnitude is observed in the bottom part of the core, starting at ∼100 m, for most of the species.

The only region where discontinuities can be possible is the brittle zone (located below 73 m) and profiles seem continuous until 80 m, where an increase in the frequency of peaks of Na^+, K^+, Mg^{2+}, $Ca^{2+}$and NH_4^+points to a changing of the register. From 80 to 100 m, we observe a variability increase for the mentioned ions and the highest concentrations of formate and oxalate at 85 m.

Bottom ice ionic profiles show marked transitions that coincide with $\delta^{18}O$ profiles at 112.5 m, where variability of most species diminishes; at 116.7 m where Ca^{2+}, NH_4^+, K^+, Mg^{2+}, oxalate and $\delta^{18}O$ recover some variability; and at 118.0 m where a steep increase of the concentrations of $\delta^{18}O$ and most of the species (Ca^{2+}, Mg^{2+}, K^+, oxalate, NH_4^+, SO_4^{2-}, F^-) is observed. Ion concentrations increase in the bottom ice is probably due to bedrock dissolving. The only species

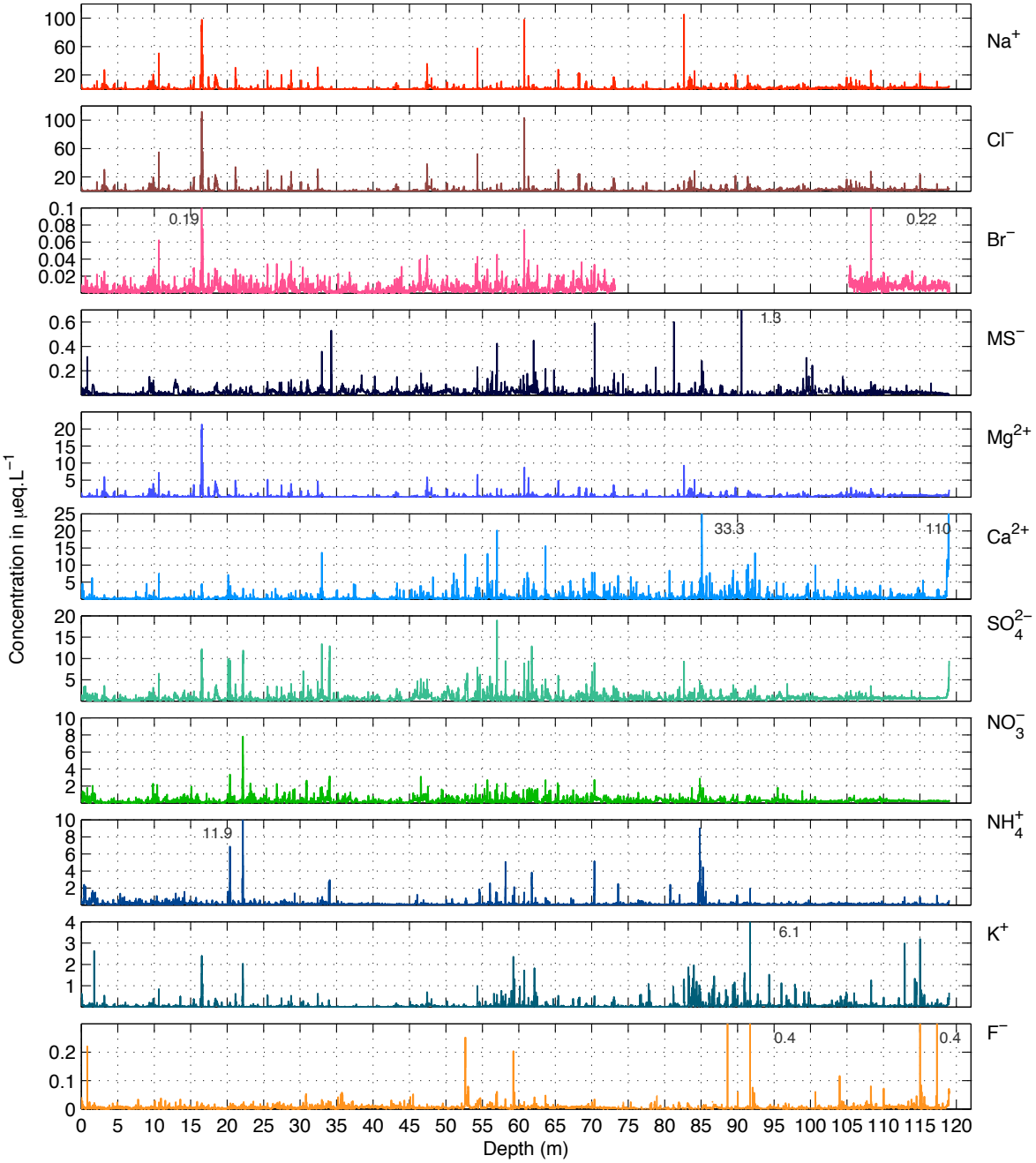

Figure 1.2: Complete profiles of inorganic ions along the CL122 core. Depth is given in m, concentrations in μeq.L^{-1}. The bedrock level corresponds to 119 m. $Br^-$was not measured in the brittle zone.

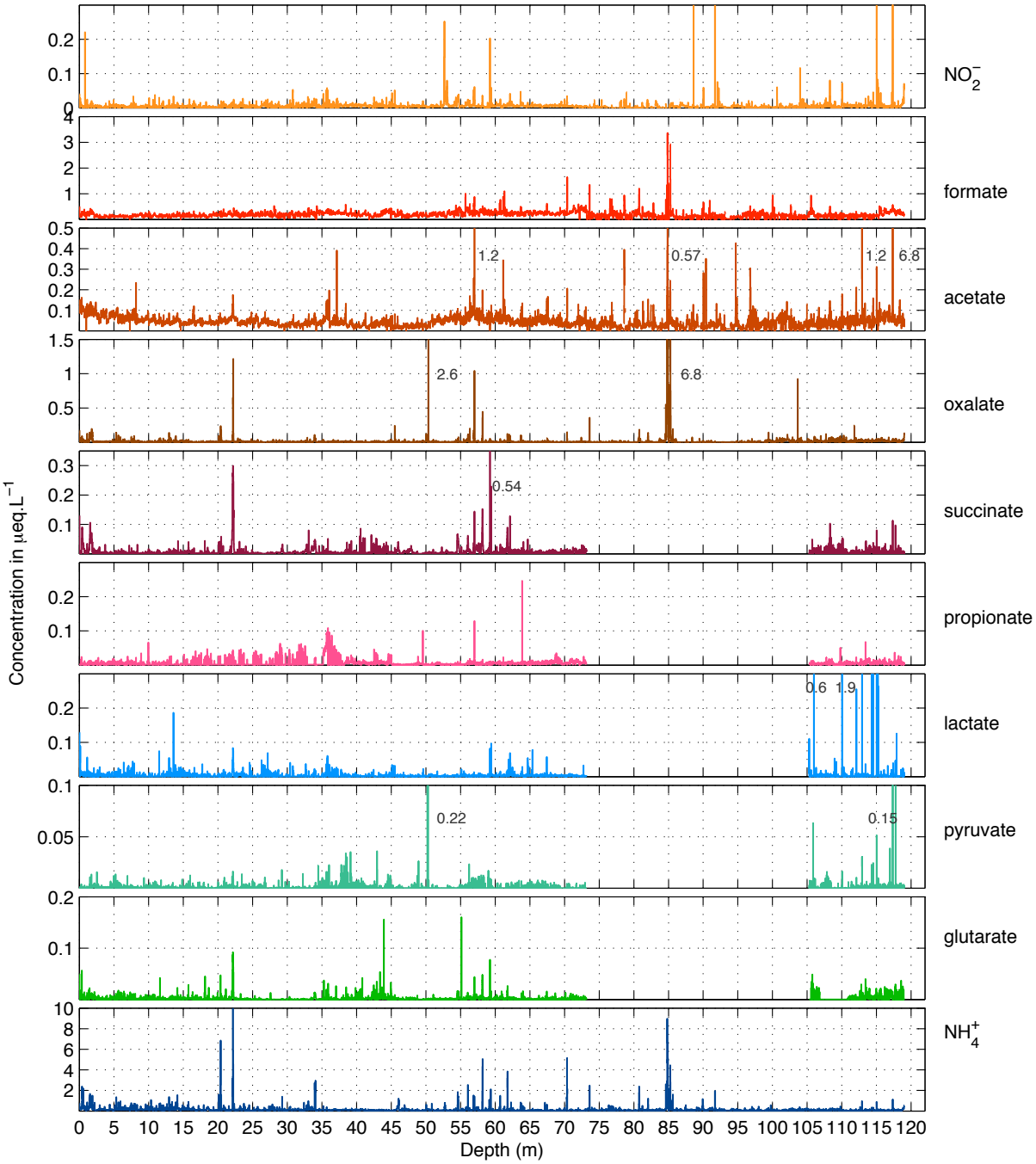

Figure 1.3: Complete profiles of NO_2^- and organic ions along the CL122 core. NH_4^+ profile is included here to provide a reference of the ions presented in figure 1.2. Depth is given in m, concentrations in μeq.L^{-1}. The bedrock level corresponds to 119 m. The baseline drifting due to column aging was only corrected for oxalate.

showing a decrease tendency for bottom ice are $MS^-$and $\delta^{18}O$.

In conclusion the ionic profile of CL122 seems continuous except for the brittle zone. Other indicators of a discontinuity below 80 m are the loss of isotopic variability (F. Vimeux, pers. comm. 2008) and recent SEM profiles of the 85 m oxalate event (M. de Angelis, pers. comm 2011). Thus, old ice would be probably conserved below 80 m and this is sustained by the $\delta^{18}O$ content of air bubbles from bottom ice, which indicates that ice near the bedrock would not be more than 4000 years old (A. Landais, pers. comm. 2008)

1.3.1 Comparison between the chemical profiles of 2005 (SV2005) and 2007 (CL122)

In figure 1.4, we present the complete MS^-profile and the most outstanding features of the Na^+, $NO_3^-$and $nssCa^{2+}$depth profiles for the 15.3 m SV2005 shallow core and the first 30 m of the CL122 deep-core, the latter being recovered at a site located ∼30 m away from the 2005 drilling site. . The chemical register obtained in SV2005 is easily recognized between 12.6 and 25.6 m (6.4-14.2 m w.e.) of the deep-core CL122 (as it was the case for the isotopic profiles, Herreros, 2010). The main features identified are:

(1) The 70 cm wide MS^-peak located between 0.3 and 1.0 m along SV2005 is found between 12.7 and 13.3 in CL122. The maximum concentration for this event is 0.28 μeq.$L^{-1}$for SV2005 and 0.13 μeq.$L^{-1}$for CL122. Such a difference could tentatively be explained by a loss of 53% of MS^-in 2 years. MS^-post depositional losses have been previously observed at sites of very low accumulation rates (see for instance Weller et al., 2004). Our finding here suggests that MS^-loss due to ventilation of the snowpack may be also a significant post depositional process even at sites with high accumulation values (note that the peak itself spans almost 1 m of snow).

(2) The layer containing a very concentrated Na^+layer (∼100μeq.L^{-1}, blue profile) found at 5.0-5.3 m in SV2005 and attributed to halite from the 1991 Cerro Hudson eruption is located between 16.3 and 16.7 m in CL122.

(3) The large marine event ($Na^+ \sim 20 \mu eq.L^{-1}$, $MS^- \sim 0.11 \mu eq.L^{-1}$) identified between 7.4 and 8.0 m in SV2005 is observed between 18.4 and 18.9 m in CL122.

(4) The largest $nssCa^{2+}$peak observed in SV2005 between 9.2 and 10.0 m is observed with a higher resolution between 20.0 and 20.8 m in CL122 (black profile in fig.1.4). This event overlaps with a prominent peak of NO_3^-(magenta profile) in both cases.

(5) The huge NO_3^-peak of $\sim 6 \mu eq.L^{-1}$(associated with SO_4^{2-}, $NH_4^+$and Cl^-, not shown) between 10.9 and 11.3 m along SV2005 and attributed to biomass burning is found between 22.0 and 22.5 m in CL122.

(6) The 1965 horizon found at 12.1-14.2m along SV2005 is found at 25.0-25.4 m in CL70 according to β decay and radionuclides counting (Magand 2008, pers. comm.) and at 25.02-25.39 according to ^3H decay (Schotterer 2009, pers. comm.). As CL70 was recovered in the same drilling tent as CL122, we assume that the same events should be found at very similar depths in both cores.

In SV2005, the first 2.59 m contained ^7Be, a marker of snow younger than 18 months, but this ^7Be rich zone was not detected in CL122 (although it coincides with the 70 cm wide MS^-peak) probably because radiogenic samples were too diluted.

Other common facies not detailed here may also be inferred from fig.1.4. Average concentrations for all ions and the isotope cycles are similar in both SV2005 and CL122 cores. Only a few thin sections found along SV2005 are missing in CL122. We present an example of this for succinate profiles in figure 1.5. The respective locations of 1965 and 2005 horizons on CL122, C70 and SV2005 cores lead to propose a slightly lower mean accumulation rate for CL122 ($\sim$13%) than for the shallow core on the common section.

No obvious differences exist between the glaciochemical profiles below and above 12.6 m: the snow presents the same mean composition, similar amplitude of isotopic cycles, and similar characteristics of ionic peaks. When extrapolating the methodology used for dating the SV2005 to the CL122 core, for the 2005-2007 period, more than two years can be counted: 17 isotopic

cycles (Herreros, 2010) and 6 nssCa^{2+}peaks (covering more than 2 samples that alternate with Na^{+}peaks).

Finding the same chemical (this study) and isotopic (Herreros, 2010) profiles along CL122 and SV2005 but with a 12.6 m gap was unexpected and raised several questions about accumulation processes at this site and this discussion will be resumed in next section.

1.4 Dating hypothesis and spatial variability of the register at SV site

1.4.1 Dating hypothesis

The net accumulation measured between 2005-2007 is 10 times higher than the net accumulation between 1965-2005. This raised a relevant question: How does the net snow accumulation rate vary at SV? And consequently, if high net accumulation values are usual here, is there any discontinuity between the 2005 (surface layer of SV2005) and deeper (older) ice? So far, three hypothesis may proposed to tentatively explained the observed discrepancy (the first two were proposed by Herreros (2010), and the third one is proposed here as more data was obtained in this regard):

1. A recent local change in precipitation rates and/or important snow redeposit driven by wind blowing between 2005 and 2007, which according to Herreros (2010) would explain the abrupt change of net accumulation values for this period (12.6 meters of snow in 2 years = 3.24 m w.e. per year).

2. The top 2.59 m of the SV2005 core contained ^{7}Be, setting an absolute dating horizon for this layer (maximum snow age: november 2003). The transition towards ^{7}Be below the detection level is abrupt. In consequence, Herreros (2010) proposed that these 2.59 m corresponds to fresh snow deposited at the surface of eroded ice that would have suffered permanent ablation (for several years) due to wind scouring. Assuming that isotopic vari-

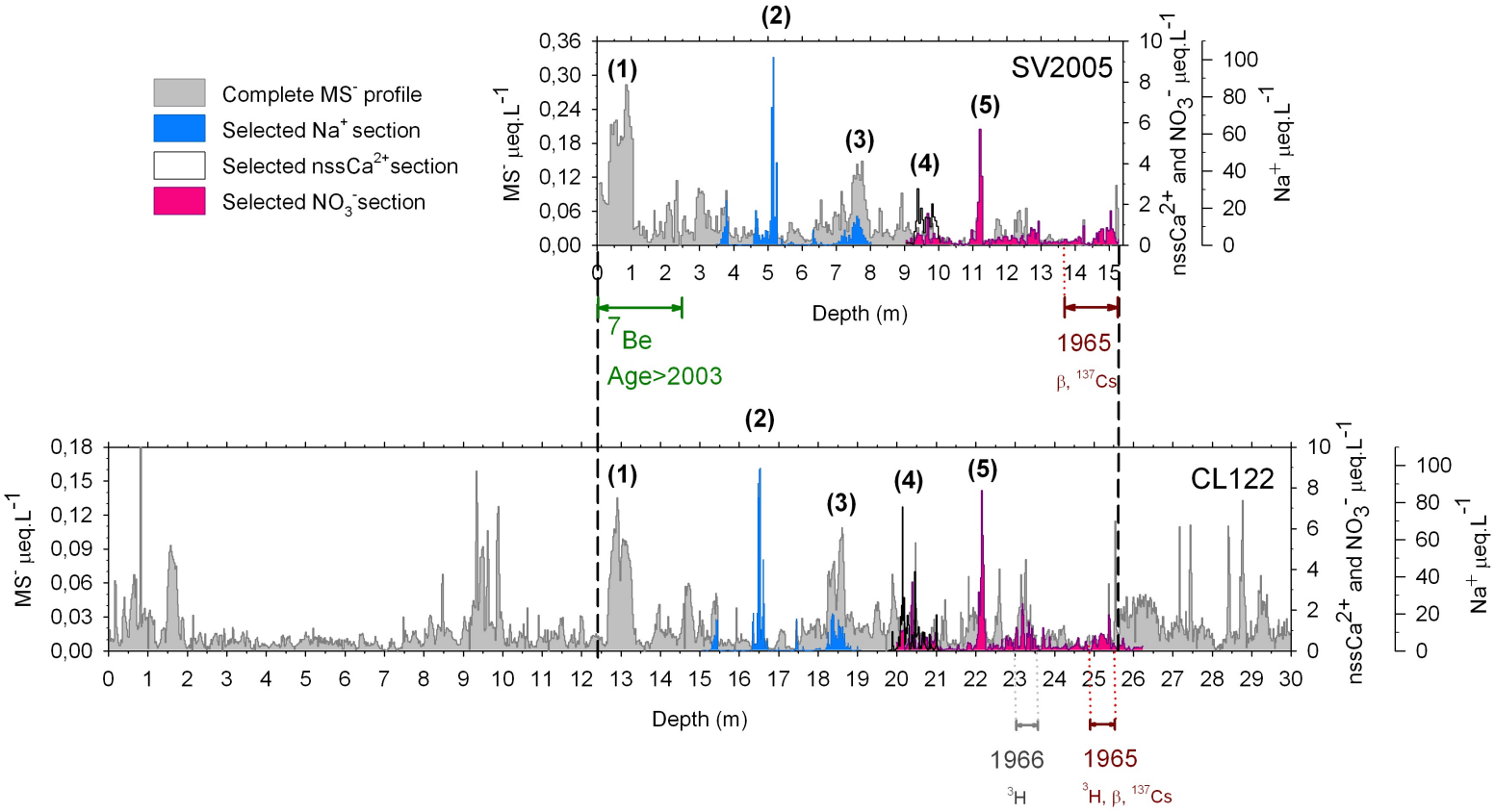

Figure 1.4: Comparison between the 15.26 m firn core retrieved in 2005 (resolution 4-5 cm, top) and the first 30 m of the CL122 deep core retrieved in 2007 (resolution ∼2 cm, bottom). The complete MS^-profile and selected continuous sections of NO_3^-, $Na^+$and $nssCa^{2+}$profiles are presented. ^7Be, a proxy used for dating show layers younger than 18 months was only measured in the SV2005 core. The 1965 horizons at CL122 are reported from the measurements made in the neighboring CL70. No more than 20 cm of depth shift between CL70 and CL122 is expected (P. Ginot, M. de Angelis, pers.comm.). The most relevant features common to both profiles are: (1) The widest and largest MS^-peak (2) A very concentrated Na^+layer (3) A large marine event (4) The largest $nssCa^{2+}$peak of SV2005 associated with NO_3^-(5) A huge NO_3^-peak likely due to biomass burning.

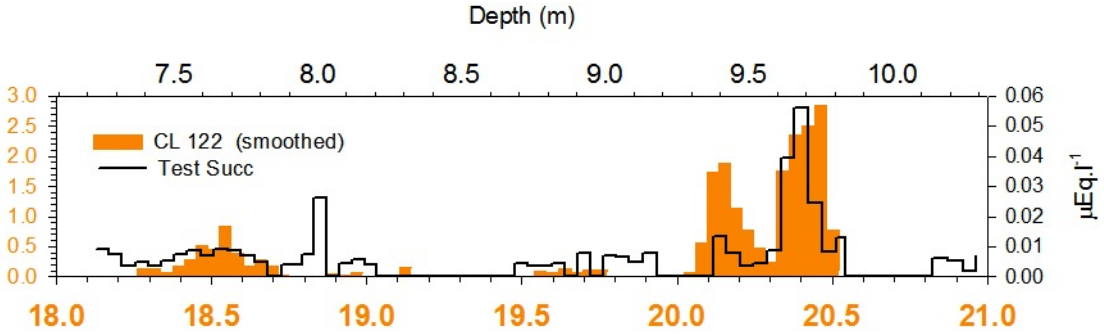

Figure 1.5: Comparison of the succinate profiles obtained for the SV2005 shallow core (black, top depth scale) and the CL122 deep core (filled orange, bottom depth scale). An example of a missing part of the record is the black peak of succinate found between 7.9 and 8.1 m in SV2005 that is absent in CL122, where it should have been located between 18.7 and 19.0 m.

ations correspond to seasonal cycles, Herreros (2010) proposed that the surface over which the 2005 snow was deposited corresponded to 1987 and in consequence a big hiatus of 18 years would exist in our register. The reason why the net accumulation rate was positive in 2005 remained unclear.

3. The SV cores do not contain any major hiatus and the changes in net snow accumulation rates observed along the cores are not abrupt but progressive and somehow governed by net accumulation occurring along the glacier flow line.

All these hypotheses are represented in figure 1.6 and will be discussed in the next section.

In this work we will prefer the third hypothesis, and our choice is based on the evidence presented in the next section.

1.4.2 Spatial variability of the register at the SV site

The 12.6 m difference between the 2005 and 2007 surfaces, together with the slanted stratigraphic profiles, the high surface velocity and the increasing distance between the radar isochrones for southward locations (fig. 1.6(b)) point to an important spatial variability on the accumulation at SV site.

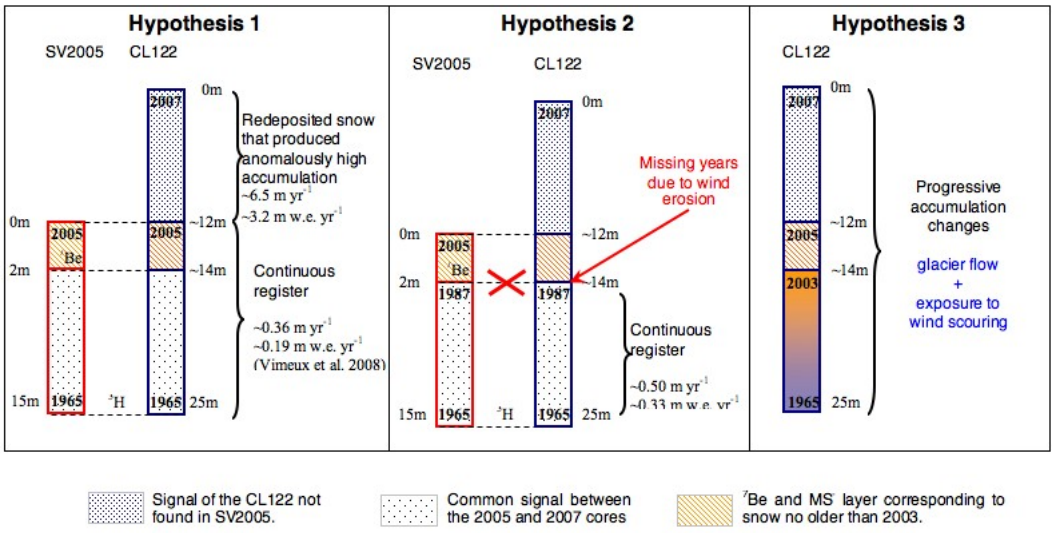

Figure 1.6: Dating hypothesis proposed to explain the 12.6 m lag between SV2005 and CL122, adapted from Herreros (2010).

In order to characterize the geographical variability of the snow accumulation and to obtain more information to choose one of the aforementioned hypotheses, complementary ionic and isotopic analyses were conducted on the shallow cores CC4 and CC5 recovered along the NNW-SSE flow line (see figures 3(b) on page 6 and 1.8(a) on page 35). CC4 is located in a zone where the surface velocity is close to zero, whereas the surface velocity corresponding to CC5 can be higher than 10 m per year. CC4, CC5, SV2005 and CL122 were compared with a multiproxy approach that included MS^-, NO_3^-, $NH_4^+$and $Na^+$for the identification of common layers (de Angelis 2010, pers. comm.). Different depth shifts among the cores were identified by this method and results are in good agreement with the reflective layers considered as isochrones on the radar profile, as observed in figure 1.7. The identification of common events (from 25 facies identified) in the four cores allowed to conclude that:

1. All the cores conserve a common and coherent signal with small (few centimeters) hiatuses among them.

2. For all the cores, the firn covering the last 2-3 years corresponds to net accumulation rates

significantly higher than older ice, but no signs of anomalous wind erosion were observed in any of these cores, not even in CC4, the core recovered at the site the most exposed to wind scouring.

3. For core sections corresponding to the 2005 to 2007 period, the net accumulation rate was 3 times higher at the site with highest surface velocity (CC5) compared to the site with near zero surface velocity (CC4). Higher surface velocity values are certainly related to higher snow accumulation rates.

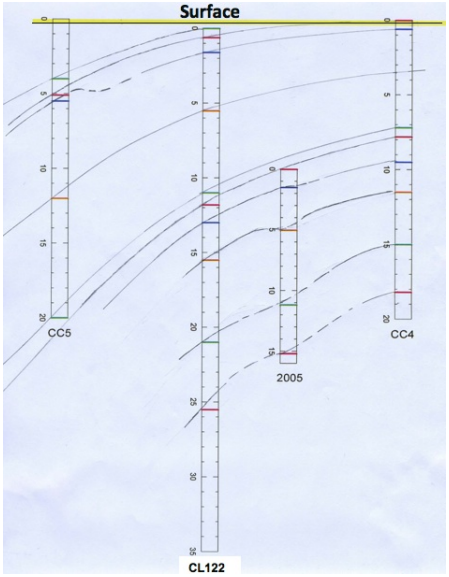

(a) Common facies for CC4, CC5, CL122 and SV2005 (de Angelis 2010, pers. comm.).

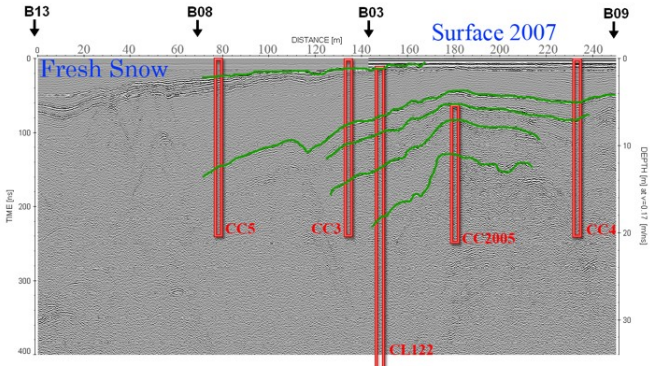

(b) Radar profile of the site (Ginot et al., 2009).

Figure 1.7: (a)Multi core study of the site along the transect marked by blue dots on fig.3(b) (page 6) and red stars in figure 1.8. Common facies for all the cores show that CC4 is located in a zone where accumulation is stronger than CC4. (b)Radar profile showing the SV cores and their possible common horizons according to the isochrones of the radar sounding.

Net accumulation rates at sites with rather low surface velocity (CC4, SV2005 and CL122) are consistent among the cores. Mean net accumulation values calculated using facies common to the three cores and covering roughly the 1965-2005 time period show a marked decrease from the most upwind site (CC4, 9 m) to downwind sites like the CL122 (13 m) and SV2005 (15 m).

An abrupt accumulation change seems unlikely as the chemical and isotopic profiles show very similar trends below and above the 2005 level.

An broader inspection of the SV site allows a better understanding of the spatial variability of the net accumulation. As illustrated in figure 1.8(a) (and also in fig. 3(a) on page 6), the accumulation zone of the summit plateau is located upstream of the glacier flow line. Most of the plateau seems to be exposed to wind blowing, while the drilling site would be somehow sheltered by a rockwall (located northward). It can be then argued that the glacier is constituted by an accumulation zone (the upper part of the summit), a zone more influenced by wind scouring, located in the depression between the western (highest) and the eastern peaks of the glacier, and a more sheltered zone located before the change of flow direction. The rock wall would protect a part of the flat area where the ice-cores were extracted, but would not prevent over accumulation of snow further downwind. This is sustained by the net accumulation measured with stakes and the intercomparison of the shallow ice-cores. Thus, under or over accumulation processes may be responsible of the changes in accumulation rates observed in our records.

It is difficult to precisely assess the accumulation changes at the surface at this flowing glacier given the lack of data for modeling. However, given the described characteristics of this site, it can be hypothesized that the surface of the flowing ice would be successively exposed to strong and weak wind blowing. The bidimensional flow model described by Vincent et al. (1997) was applied to this glacier to obtain the net accumulation along the flow line based on surface velocity measurements and the available dating constrains (presented in section 4.4.5), assuming that the glacier thickness is constant over time (given the surface and bedrock heights, cf. fig. 1.8(b)). The net effect of ice movement would be a change in accumulation rates estimated from a few tens of cm per year to several meters for the CL122 core as seen in the orange line in figure 1.8(b) (Ginot 2009, pers. comm.).

For all the exposed above, we think that progressive changes in the net accumulation, which led to high accumulation values in the last few years, are the result of the ice flow towards a zone less affected by wind scouring, and this favors the third dating hypothesis.

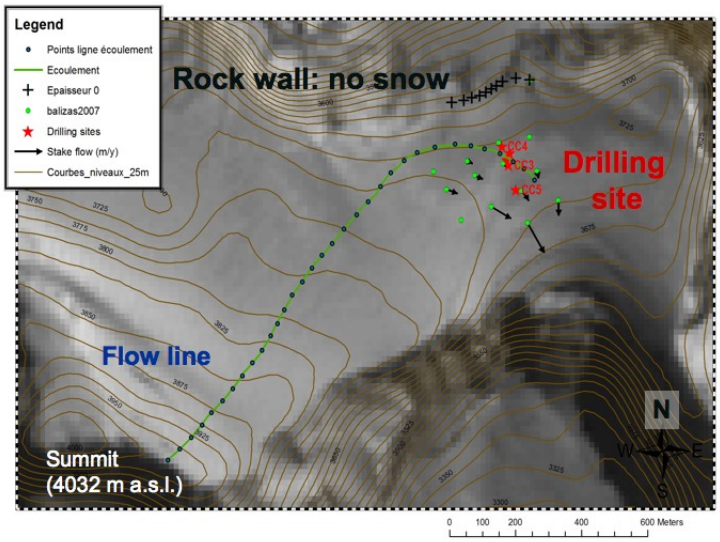

(a) Topography of the summit plateau of the Mount San Valentin.

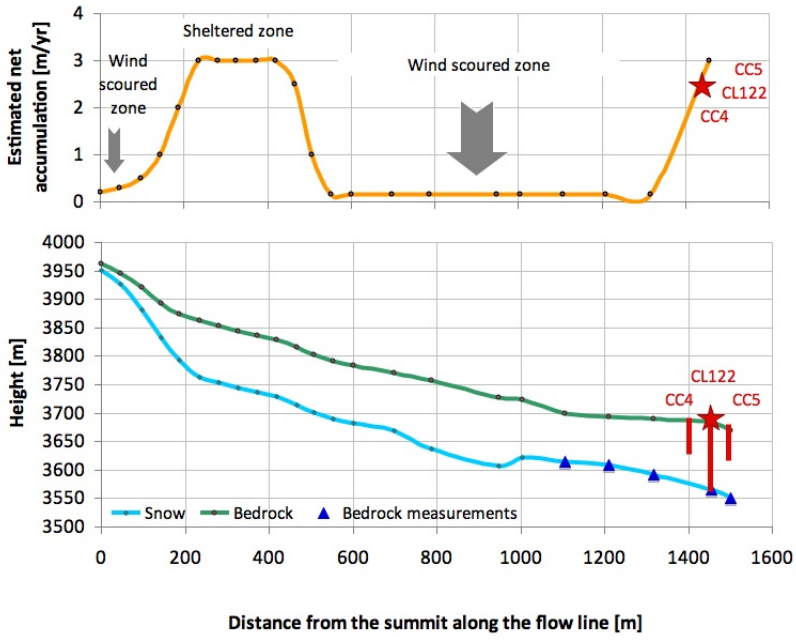

(b) Estimated net accumulation

Figure 1.8: (a) Topography of the summit plateau of the Monte San Valentin obtained from an ASTER image (Ginot 2009, pers. comm.). The green dotted line corresponds to the estimated flow line. Green circles correspond to stakes′ location during the drilling campaign and the red stars correspond to CC4, CL122 and CC5 cores. (b) Estimated net accumulation (orange line, atop), surface height (green line) and bedrock height (blue line) along the flow line depicted in (a). Dots correspond to the points where accumulation was calculated with by the flow model described by Vincent et al. (1997) and adapted to the SV to fit the observed changes (Ginot 2009, pers. comm.). Snow can be subjected to important wind scouring near the summit and in most of the summit plateau, thus expected net accumulation is very low (grey arrows). The drilling site corresponds to a zone where net accumulation increases progressively probably due to a sheltering effect of the rock wall located northward. Triangles on the bedrock profile correspond to radar sounding measurements (Casassa 2009, pers.comm.) and dots to estimations. The location of the CL122 core is denoted by a red star. Approximate CC4 and CC5 locations are also shown.

Finally, an additional proxy that sustains the fact that accumulation is rather irregular at this site is the algal biovolume (see figure 3.5 on page 109). Algal blooms (high observed biovolumes) have been used as tracers of summer on temperate glaciers (Kohshima et al., 2007; Santibañez et al., 2008; Uetake et al., 2006). Preliminary algal profiles for the first 6 m of CC2 (nez 2008, pers. comm.) show 2 important peaks (thus summer-like conditions) at 0.8 m and 1.4 m, and no other important peaks below. This could imply that for the first 6 m of the core, we account for more than 4 m of snow accumulated in only one year. Whether the first two major peaks correspond to one or two years is still under debate, but in any case, they point to irregular accumulation processes at this site.

1.5 Conclusions

Small-scale spatial variability in ice core chemical records is a known issue, especially in wind scoured sites with low accumulation rates. Conversely, even if the different zones of SV summit are affected in different ways by snow blowing and redeposition (e.g. the accumulation estimated for CC5 is 3-times higher than for CC4), all the cores conserve a consistent archive of events influencing the site, as shown by the comparison of the chemical and isotopic profiles of CC4, SV2005 and CL122 (de Angelis 2010; Patris 2009, pers. comm.). Nevertheless, it has to be kept in mind that small hiatuses (from a few cm to ca.20 cm) identified by missing events may be observed from one record to the other (for an example see figure 1.5).

The high net accumulation rate evidenced for the recent years by the 12.6 m lag between SV2005 and CL122 homologous records lead us to ask the pertinent question of how much precipitation can we expect at this site. Part of records are certainly missing due to wind blowing. However, we argue that individual events (or part of events) may have been blown away but not entire seasons and in consequence, temporal trends, if any, will remain visible.

The lack of a robust and accurate dating for the CL122 core makes difficult the interpretation of our record. For this reason, my work was firstly oriented towards the comprehension of the climatology governing SV site and to provide a link between active sources, transport and events

observed in the record. Then, the characterization of those events will provide an estimate of the representativeness of this site in terms of environmental archive. Lastly, in order to contribute to the dating of the ice core, I also tried to unveil an anthropogenic impact (settlers arrival to Patagonia, industrialization of the region) as well as absolute time makers such as volcanic eruptions.

Chapter 2

Climatology on the Northern Patagonian Icefield

2.1 Motivations

The Monte San Valentin is located approximately 30 km inland of the fjords and western protrusions of the Andes cordillera. Even if it is very close to and under the influence of the Pacific Ocean, it conserves a record of continental proxies, as it was observed by the alternation of marine and continental arrivals in the 15 m firn core drilled in 2005 (Vimeux et al., 2008). Marine arrivals are dominated by marine salts (e.g. sodium chloride) and originate from the nearby Pacific Ocean, located west of the Northern Patagonian Icefield (NPI). Continental arrivals contain other specific chemical markers, such as calcium (indicating soil erosion) or ammonia (emitted by forest fires or by soil biological activity, Andreae et al., 1988; Schlesinger, 1996), but their precise sources were not identified.

In this chapter we intend to construct a conceptual framework for the interpretation of the ice-core chemical (and isotopic) signals based on our understanding of transport of air masses advected to SV and, consequently, retrace their possible origin. We will emphasize the origin of air masses other than the strong westerlies to determine the location of continental sources

influencing this site. We will relate each type of trajectory to precipitating and non-precipitating events on a daily and a seasonal time scale (the interannual-scale is not explored here).

To achieve this, we will explore daily data of forecasted precipitation, reanalysis data and wind-based backtrajectories mainly from 2005 to 2007.We choose this short period due to the data availability for forecasted precipitation at SV site and for wind measurements at the nearby stations (San Pedro and Cabo Raper), the latter allowing models validation. Additionally, this period overlaps to a study of the cloudiness over the SV region based on MODIS satellite images made for the 2000 to 2008 period (Vimeux et al., 2011)).

Alongside this main objective, we also intend to estimate the total annual precipitation at SV drilling site. This is because depending on the choice of the dating hypotheses (which differ by more than 10 times), SV average net accumulation can have three different values given in millimeters of water equivalent (in this chapter we use the notation in mm to be consistent with precipitation data): 1) 190 mm.yr^{-1}, between 1965 and 2005 according to the shallow core radiogenic and nssCa^{2+}profiles interpretation (Vimeux et al., 2008), 2) 330 mm.yr^{-1}between 1965 and 1987 according to isotopic cycles counting (Herreros, 2010) or 3) 3240 mm.yr^{-1}between 2005 and 2007 according to the comparison between the 2005 and 2007 chemical and isotopic records. Actually, net accumulation arises from the combination of total accumulation (precipitation and blown snow redeposit) minus ablation (wind erosion, sublimation or melting plus evaporation). By exploring the upper limit of total accumulation, given by precipitation, we will evaluate whether an accumulation of 3240 mm.yr^{-1}is realistic and/or estimate the magnitude of the ablation leading to small net accumulation values.

A review of mid-latitudes and Patagonian climate studies is presented on section 2.2. The methodology and the data used are presented in section 2.3. The results and implications for the chemical signal are presented in section 2.4.

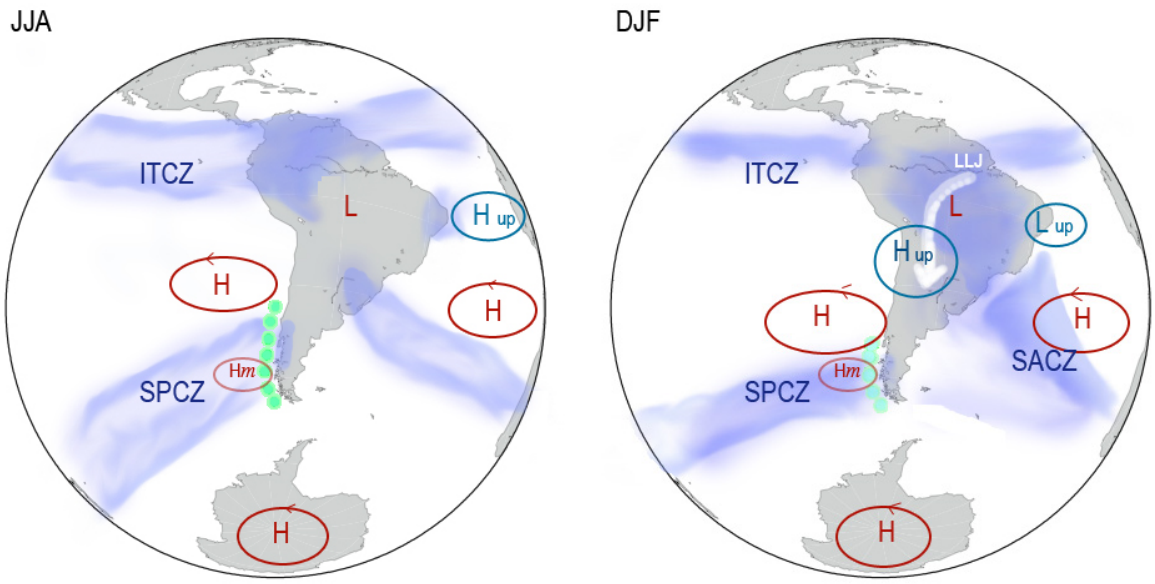

(a) Winter season: June July August

(b) Summer season: December January February

Figure 2.1: South America climate components for (a) winter (JJA) and (b) summer (DJF) (Adapted from Garreaud and Aceituno, 2007; Sinclair, 1996) H= low-level anticyclones (only those lasting more than 2 days in average) Hm= low-level migratory anticyclones region (synoptic feature) L= low pressure center. Green dots: Westerlies band (persistent cyclonic band). It is worth noting that migratory cyclones also pass through the southern tip of South America. In red, low level features, in cyan, upper level (200hPa) features. LLJ = low level jet. ITCZ, SACZ, SPCZ = precipitation zones: Intertropical Convergence Zone, South Atlantic Convergence Zone, South Pacific Convergence zones.

2.2 Introduction

2.2.1 Wind and synoptic features at mid-latitudes

Mid-latitudes (40-50°S) mid-tropospheric flow at a synoptic scale (2-10 days) follows a geostrophic behavior, i.e., roughly, wind direction depends only on the Earth rotation because the pressure gradient force is in balance with the Coriolis effect. Westerly wind flow, a highly zonal flow, is a consequence of this geostrophic behavior (Holton, 2004, sections 2.3, 2.4). The Patagonian Icefields are located in the belt of the *Westerlies* (40-55°S, green dots in fig. 2.1), which tends to coincide with the storm track where mid-latitude waves move (including cyclonic and anticyclonic disturbances).

North of the Westerlies belt and over the Antarctic plateau there are zones of persistent high-pressure centers or anticyclones. The more persistent anticyclones (lasting more than 2 days and denoted by H in fig. 2.1) are found astride South America at around 35°S, from the eastern Pacific (90°W) to the western Atlantic (0°) (Sinclair, 1996).

In winter (JJA), the mid-latitude thermal gradient is weaker, leading to a diminution of the pressure gradient over Patagonia and in consequence a weakening of low-level Westerlies, particularly near 50°S (Garreaud et al., 2007), approximately from 14.3 $m.s^{-1}$in summer to 10.9 $m.s^{-1}$in winter. At this season, consequently to the weakening of the pressure gradient, the Pacific anticyclone moves approximately 4°northward from its summer/fall position (Sinclair, 1996), so it is centered at ∼30°S, schematically depicted in figures 2.1(a) and (b). Winter is more propitious for calm wind situations, as detected by Paruelo et al. (1998) in 25% of the observations from meteorological stations at Eastern Patagonia. However, note that calm wind situations are not necessarily synonymous of stagnant atmospheric conditions at the synoptic scale (blocking), as over the southeast Pacific, spring and summer (SONDJ) are the most propitious seasons for blocking (which is more frequent September and October) (Renwick, 1998; Renwick and Revell, 1999).

In summer (DJF), the equator to pole temperature gradient is stronger. The Pacific anticyclone is more intense (Sinclair, 1996), and an enhanced pressure gradient induces stronger Westerlies, which peak between 45°S and 55°S (Garreaud et al., 2007). Maximum low-level westerly speed was observed in SONDJ in the Argentinean Patagonia (Paruelo et al., 1998). At the upper-level (600hPa, this work, not shown), no important seasonal wind speed differences were detected using ERA40 reanalysis data (from the European Centre for Medium-range Weather Forecast, available at ∼125 km and available over the 1957-2002 period, Uppala et al., 2005).

2.2.2 Precipitation at mid-latitudes and in Patagonia

Precipitation at mid-latitudes is driven by the mean westerly flow (Garreaud, 2007; Garreaud and Aceituno, 2007): note that in fig. 2.1 the South Pacific Convergence Zone coincides with

the mean flow. Precipitation is produced mostly by stratiform clouds formed along extratropical (warm/cold) *frontal* systems and at mountainous regions it is *orographically* enhanced (Garreaud and Aceituno, 2007).

Nonlinear interactions, lateral shear in the jetsteam and the release of latent heat in precipitating systems produce exceptions to the geostrophic flow aforementioned. In consequence, low-pressure centers (cyclones) are asymmetrical, elongated, with the strongest winds and largest temperature gradients concentrated along narrow bands. These narrow bands are called *fronts* (Holton, 2004, sections 3.4 and 6.1). Precipitation at mid-latitudes is primarily produced by deep stratiform clouds and embedded convective cells that develop along these fronts that can be either cold or warm (Garreaud, 2007).

The orographic effect is due to condensation promoted by an adiabatic uplift of atmospheric water vapor (Garreaud, 2007), which produces a leeward moisture depletion of air masses, called *Foehn effect* or *rain shadow*. This is noticeable at the Patagonian Icefields (Fujiyoshi et al., 1987; Paruelo et al., 1998), where precipitation can reach values higher than 2000 mm.yr^{-1}at the NPI zone (Matsuoka and Naruse, 1999; Paruelo et al., 1998; Yamada, 1987) and higher than 6500 mm.yr^{-1}at the SPI zone (Schneider et al., 2003). On the piedmont areas of the eastern side of the NPI, the annual amount of precipitation is reduced dramatically to approximately 1500 mm (Enomoto and Nakajima, 1985) and further east can be lower than 200 mm (Paruelo et al., 1998).

The zonal wind strength is a precipitation proxy at mid-latitudes, especially in mountain regions under windward oceanic influence (Garreaud, 2007; Moy et al., 2007). For the southern hemisphere, Moy et al. (2007) found a strong correlation of precipitation ($r>0.6$) with zonal wind at 700 hPa, whereas Garreaud (2007) observed that the orographic effect is more patent when using wind at 850 hPa than at 300 hPa near the mountain ranges.

2.2.3 Climatic and glaciological studies at the NPI region

Various glaciological and climatic studies are available for the Patagonian Andes (Rivera et al., 2007; Rignot et al., 2003; Schneider et al., 2003; Schneider and Gies, 2004; Rasmussen et al., 2007; Lopez et al., 2008; Smith and Evans, 2007) and we report various net accumulation values for the Patagonian icefields in table 2.1 (in correspondence with figure 2.2(a)). However, for the interpretation of the San Valentin ice core, we need very accurate and fine-scale studies. The only available glaciological study relating climatic controls at both sides of the cordillera and accumulation at the NPI (71 km from West to East, 125 km from North to South) with a very fine geographical resolution is the one of Lopez et al. (2008), who observed that snow cover fluctuations at NPI behave differently depending on whether they are located east or west of the internal mountain divide showed in figure 2.2(b). The western board is controlled by a maritime temperate climate and oceanic fronts, with neither intraseasonal nor inter-annual variability of precipitation, whereas the eastern side of the NPI is governed by a colder continental climate, having a precipitation maximum in JJA. This east-west divide can also be deduced by observing the vegetation cover of the region (Paruelo et al., 2001; Smith and Evans, 2007) but the precise divide location can only be identified by a glaciological study such as the one performed by Lopez et al. (2008). The precise accumulation processes at the SV site are difficult to assess, but it can be hypothesized to have a mixed behavior, recording west and east climate fluctuations.

Table 2.1: Summary of net accumulation measurements in Patagonian glaciers presented in fig. 2.2(a). Net accumulation of this table corresponds to the X-axis of fig. 2.14

Glacier	**Altitude m a.s.l.**	**Net accumulation m.yr^{-1}**	**Longitude W**	**Latitude S**	**Reference**
Glacier Nef	1500	2.2	73.3	46.93	Matsuoka and Naruse 1999
San Rafael	1296	3.5	73.5	46.73	Yamada 1987
Ice divide Moreno	2680	1.2	73.25	50.63	Aristarain and Delmas 1993
Gorra Blanca	2300	1	73.15	49.15	Schwikowski et al. 2006
Pio XI	2600	∼6	73.35	49.27	nez 2008, pers. comm.
Tyndall	1756	14	73.52	50.98	Shiraiwa et al. 2002
San Valentin	3723	0,19	73,32	46,58	Vimeux et al. 2008
		0,33			Herreros 2010
		3,25			Herreros 2010

An ongoing study of MODIS daily images from 2000 to 2008 at the SV site (Vimeux et al.,

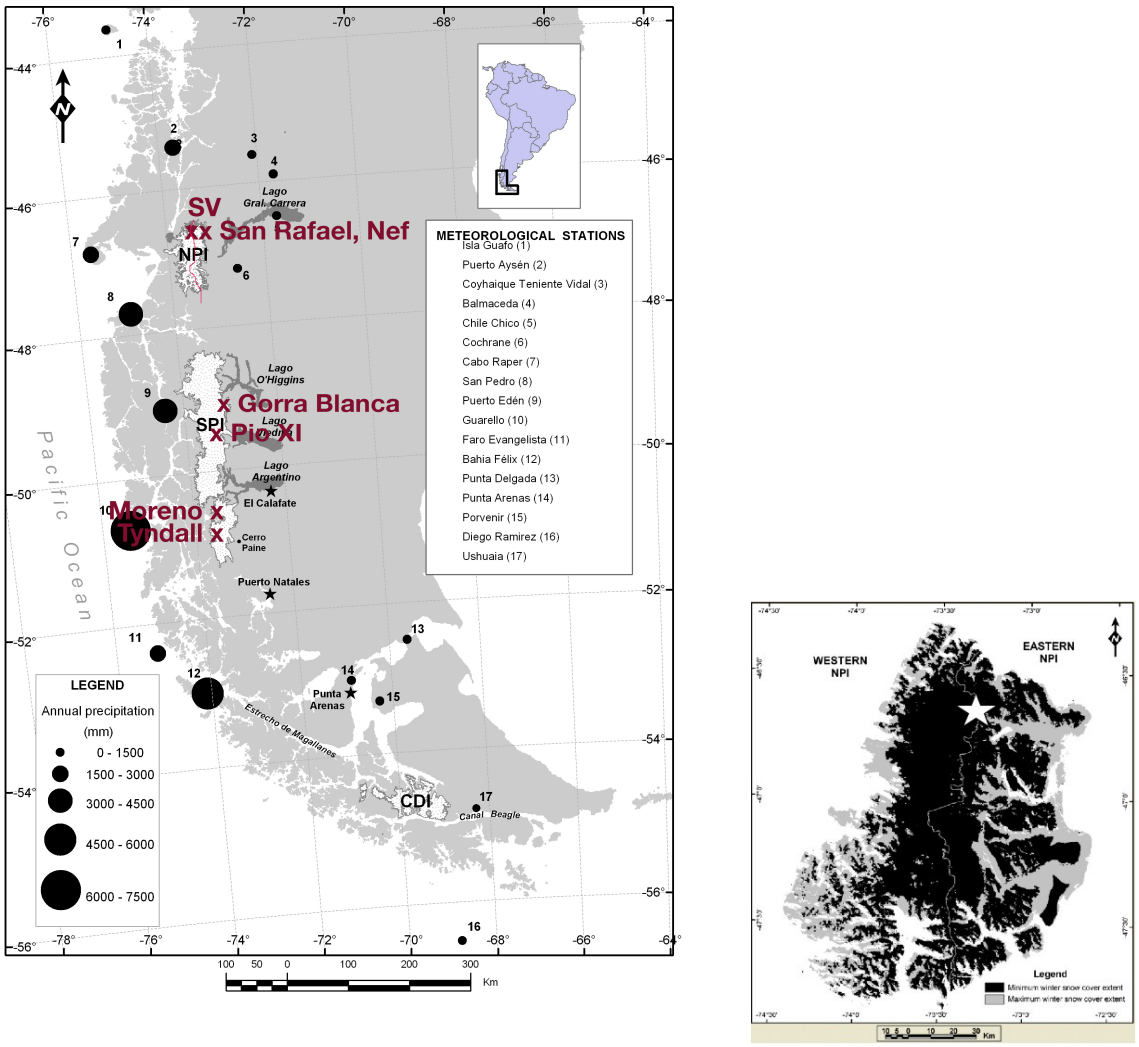

(a) Stations locations, other ice-coring studies

(b) Precipitation divide in the Northern Patagonian Icefield

Figure 2.2: (a) Locations of ground stations where data is available, adapted from Lopez et al. (2010). Black circles: Precipitation stations and mean yearly value. Red marks: Glaciological measurements as reported in table 2.1. The pink line shows the division between eastern and western sides of the Northern Patagonian Icefield, according to the teledectection study of Lopez et al. (2008). (b) Precipitation divide of the Northern Patagonian Icefield with the location of the SV (white star). Adapted from Lopez et al. (2008).

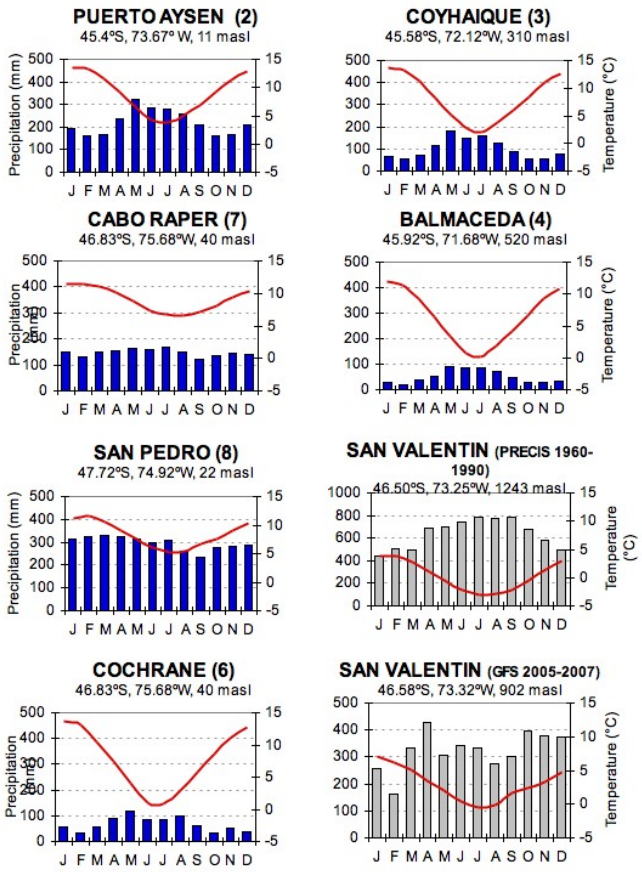

Figure 2.3: Blue bars: monthly mean precipitation (mm), red line: monthly mean temperature (°C) based on data from the Dirección Meteorológica Chilena, averaged for 1961-1990, graciously provided by Lopez (2007). The numbering corresponds to figure 2.2(a) For the SV location, data was generated with PRECIS and GFS models (this study)

2011) shows that its cloud cover is similar to the regional cloudiness in 54.4% of the cases. In 1.9% of the cases, the SV summit emerges over a partially or totally cloud covered region suggesting that the low net accumulation at that site does not have to be attributed to a lower cloud cover over the summit area relative to the surroundings, as it was firstly proposed by airplane pilots. In 7.5 % of the cases, SV summit is clear while the southwest of the region is partially covered, while the rest of the cases correspond to different combinations between cloudiness over SV and over the SW and NE regions of the NPI.

Between 40 and 48 °S, soundings at Puerto Montt (41°43′S, 73°10′ W) and Comodoro Rivadavia (45°78′S, 67°50′ W) show that the freezing level varies from 880 to 780 hPa and in 3 of the 4 studied cases a moist top/inversion level appears, located at 750 hPa (Smith and Evans, 2007). This implies that the SV (approximately at 600 hPa) is undoubtedly influenced by icy-cloud precipitation, and in most cases it would seem that the stratified flow produced by the inversion cap would transport air masses to the SV from sources not located at the near low level.

Concerning the daily behavior of precipitation and wind, meteorological observations from Schneider et al. (2003) at 53°S showed that the strongest episodes of precipitation at the western side of the Andes were associated with strong Westerlies. When the pressure gradient diminishes (mostly in winter), Westerlies weaken allowing wind incursions from other directions (North, South, East, North East and South East) but no detailed information is available to relate these wind directions to the occurrence of precipitation over the NPI region.

Interannual variation of monthly precipitation around the NPI ranges from ∼14 to ∼30% according to the registers of the nearby stations (Herreros, 2010). In a study covering a broader area, Aravena and Luckman (2008) performed a Principal Component Analysis of homogenized Patagonian precipitation registers of 38 stations spanning at least 20 years with less than 30% of missing data. They found that the precipitation recorded at NPI neighboring stations Puerto Aysén, Coyhaique, Balmaceda, Chile Chico and Cochrane share a common pattern characterized by precipitation maxima in JJA, a decrease of precipitation since 1960 and a 12-year cycle that is negatively correlated with the Antarctic Oscillation Index, which is unique and different from

the rest of Patagonia (see fig. 2.4). Note, however, that the authors did not use any western, i.e., windward, stations such as Guarello, Cabo Raper, San Pedro or Puerto Edén. As orographic rain is important in this region, this study depicts only the behavior of leeward stations in the region neighboring the NPI, or the eastern half of the NPI.

In the rainfall series of Puerto Aysén, Coyhaique, Balmaceda, Chile Chico and Cochrane, that cover the 1950-2001 period, the highest precipitation rates were observed in the mid 1960′s (2000-2500 mm.yr^{-1}), followed by a decreasing trend (1500-2000 mm.yr^{-1}, fig. 2.4(b)). The 1976 shift of the Pacific Decadal Oscillation (PDO) is also observed, although no correlation between the PDO and the principal component of the precipitation pattern was observed over 1950-2000. However, Aravena and Luckman (2008) noticed a highly significant anticorrelation with the Antarctic Oscillation Index which depicts latitudinal pressure gradient fluctuations in the Southern Hemisphere. Thus, the precipitation at SV (if conserved) could keep a history of the pressure gradient fluctuations of the region.

Concerning temperature, as shown by meteorological stations around NPI (Puerto Chacabuco, Puerto Aysen, Bahia Murta, Coyhaique, Chile Chico, Puerto Ibáñez, Cabo Raper, Caleta Tortel presented in figures 2.2 and 2.3), the monthly mean minimum temperature is 2.8°C higher on the western stations than on the stations located eastward the cordillera. Moreover, monthly mean maximum temperature is 3.5°C lower on the western side than in the eastern side of the Andes (Lopez et al., 2008). This indicates that eastern stations present a higher seasonal difference ($T_{jan} - T_{july}$ ∼11°C), which is characteristic of continental locations. Temperature variations are buffered by the influence of the ocean in coastal stations ($T_{jan} - T_{july}$ ∼5°C).

At SV site, temperature obtained from reanalysis data ERA-40 (Uppala et al., 2005) and NCEP-NCAR (Kalnay et al., 1996, from National Centers for Environmental Prediction-National Center for Atmospherics Research Analysis, available since 1948) is governed by seasonal changes having the highest (lowest) values in summer (winter) -10.4±0.1°C (-17.1±0.1°C) (Vimeux et al., 2008). This seasonal amplitude of about 7°is also in agreement with measurements at Gran Campo (Schneider et al., 2003, at 53°S), where summer values are lowered by the influence of

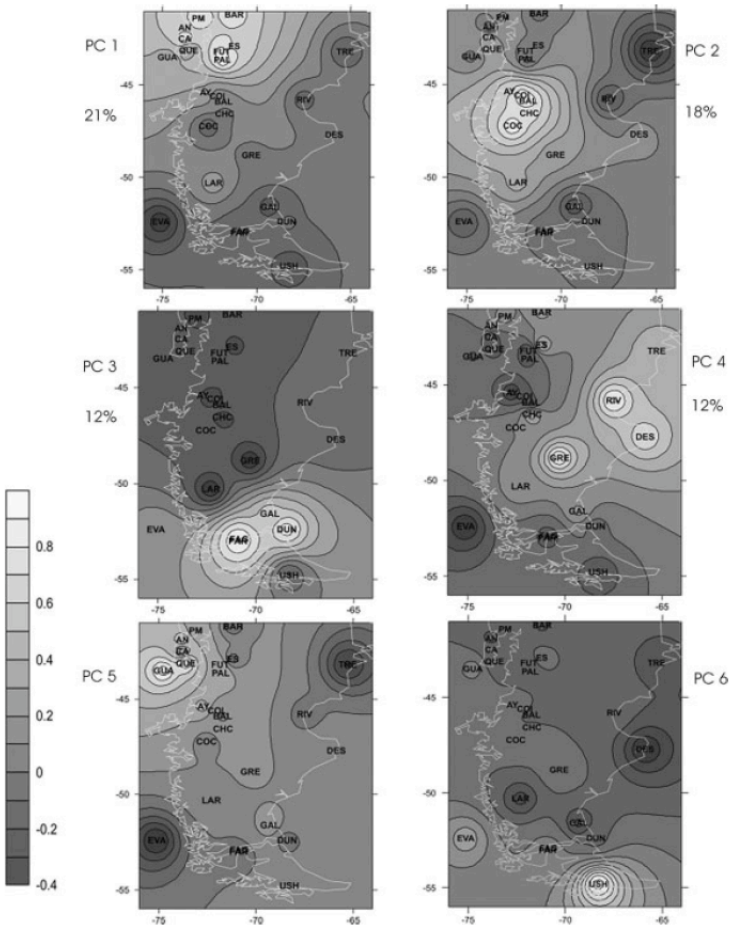

(a) Spatial patterns derived from a PCA of the annual rainfall records in Southern South America for the period 1961-2000. Bar scale to the left indicates the loading value ranges. The San Valentin is located in the region identified by the PC2.

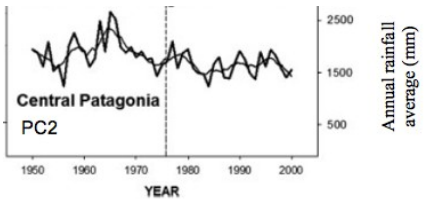

(b) Regional annual rainfall averages (bold lines) and 10-year low pass Gaussian filter (thin line) to show the low-frequency variations of the regional precipitation series. The vertical dashed line indicates the year 1976.

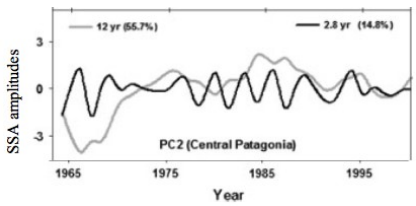

(c) Singular Spectrum Analysis (SSA) of PC2. The percentages of variance contributed by each wavelength are: 55.7% for the 12 yr, grey line and 14.8% for the 2.8 yr, black line.

Figure 2.4: Figures extracted from the work of Aravena and Luckman (2008). (a) Loadings of the Principal Component Analysis on rainfall series of southern South America. The region identified as PC2, comprises the Northern Patagonian Icefield (and the SV). Stations concerned for the SV case are: AY Puerto Aysén, COY Coyhaique, BAL Balmaceda, CHC Chile Chico, COC Cochrane. San Pedro y Cabo Raper were not taken into account as the series considered were incomplete (no more data after the 80′s). (b) A decrease of precipitation from 1960 for the NPI region. (c) The 12 year cycle identified by the SSA decomposition of the principal component PC2 seems in agreement with the Antarctic Oscillation Index (and also the Antarctic Pacific Oscillation Index) which accounts for the meridional changes of the pressure gradient over time.

the ice fields presence.

In a study performed with NCEP-NCAR reanalysis data, an increase of 0.5°C in the low level (850 hPa) air temperature around the Patagonian icefields since 1955 is observed (Rasmussen et al., 2007). This is in agreement with a steady increase of ∼1.5°C in ground level measurements of minimum temperature between 46-53°S, from Aysén to Punta Arenas, since 1933 (Rosenblüth et al., 1997). On the contrary, further north, at around 41°S, a cooling trend of the atmosphere was observed between 1933 and 1992 of ∼2.3 °C, i.e. 0.2°C/decade (Rosenblüth et al., 1997).

2.3 Methodology

2.3.1 Datasets

We have used reanalysis data and observations, when available, of wind direction, temperature, specific/relative humidity and precipitation covering the 2005-2007 time period to estimate precipitation occurrences and air mass trajectories in the SV zone., as well as the long term mean values of precipitation and temperature. We have chosen two continental stations, Coyhaique and Balmaceda (leeward the Andes), and two coastal stations, Cabo Raper and San Pedro (westward the Andes), that are representative of NPI climate, as observed by Aravena and Luckman (2008) and Lopez et al. (2010). We have chosen to use complete registers from 2005 to 2007, in order to:

1. Cover the period of the puzzling dating hypothesis (very high accumulation over those 2 years), and

2. Span the same period with all datasets, including the few observations made during the drilling campaign.

The different datasets used are presented in figure 2.5.

Daily pluviometer measurements from 2005 to 2007 at Coyhaique and Balmaceda were provided by the Dirección Meteorológica Chilena (DMC). Daily wind magnitude and direction, as

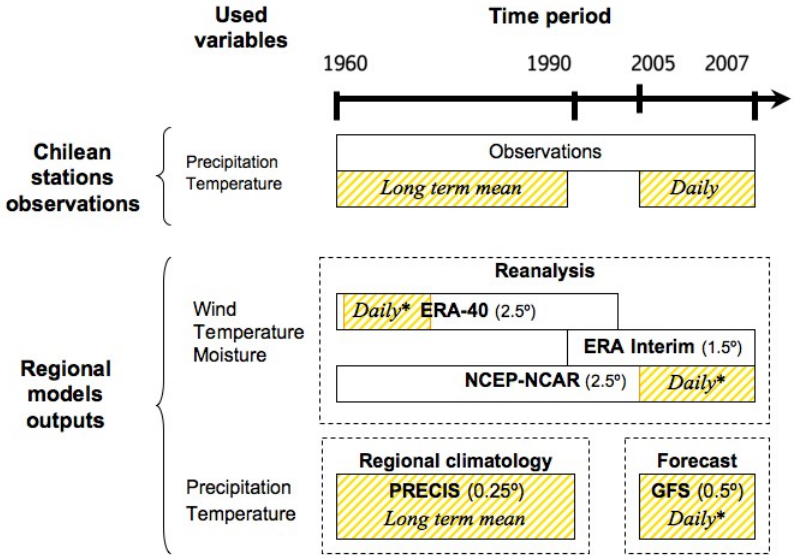

Figure 2.5: Available datasets and variables used in this study (cf. Table 2.3). The dashed portion of the bars correspond to the time period employed. Daily datasets marked with an * correspond to sub-daily datasets, i.e., data generated every 6h in the case of the reanalysis and 3h in the case of the forecast model.

well as pluviometer measurements at Cabo Raper and San Pedro were provided by the meteorological service of the Chilean Army (obtained by my own manual transcription of the written registers of precipitation, which also explains the short period 2005-2007 spanned). For both cases, access to data was granted via a scientific agreement between these institutions and the Geophysics Department (DGF) of the University of Chile. Note that pluviometer measurements are reported at different hours of the day: 0 UTC for the DMC, 4 UTC for the Chilean Army.

Long-term means of measured precipitation for the 1961-1990 period were provided by the Geophysics Department of the Universidad de Chile (DGF) through their website for interactive meteorology `http://www.atmosfera.cl/`.

During the 2007 drilling campaign (from April 22^{nd} to May 3^{rd}) a Gemini TGIS-1580 data-logger placed outside of one of the camping tents recorded relative humidity and temperature every 5 minutes (Ginot 2009, pers. comm.). Temperature measurements seem reliable as they show daily cycles and they are in good agreement with NCEP-NCAR reanalysis data; however, since this data-logger is designed to work indoors and the plastic cap is black, an artifact due to

radiative heating may affect the maximum values. Relative humidity data seem untrustworthy because values are close to saturation (100%) most of the time in spite of daily variability of temperature and wind direction. This can be related to a known hysteresis effect on those data-loggers after a long saturated period and that cannot be disregarded.

Besides the data-logger data, we also have qualitative observations of weather conditions: no snow, snow, and heavy snowing conditions, made during the drilling campaign (see table 2.2).

Table 2.2: Qualitative observations of snowing conditions in SV summit during the drilling campaign (Ginot 2009, pers. comm.). The value assigned is given in mm and it is only for drawing purposes, it does not represent the intensity of the precipitation. Missing observations are left in blank.

Date	**Observation**	**Value assigned [mm]**
21/04	clear sky	0
22/04	snow+wind	30
23/04	-	
24/04	covered/into the cloud/hoar formation/ snow	30
25/04	clear sky	0
26/04	clear sky	0
27/04	clear sky	0
28/04	-	
29/04	covered/into the cloud/hoar formation/snow only part of the day	30
30/04	-	
01/05	heavy snow	60
02/05	heavy snow (1 m accumulation in 2 days)	60
03/05	clear sky	0

Meteorological information is sparse in Patagonia and only a few stations have complete records. So, besides precipitation and wind measurements, we also used reconstructed data (so called *reanalysis* data) from global circulation models forced with meteorological, probe and satellite observations to complete the expanse of the datasets. The main limitation of reanalysis data is the lack of real observations to force the model, especially in the Southern Hemisphere. Nevertheless, reliability of these data has been tested by some authors. Monthly scale comparisons between NCEP-NCAR data and observations show a good agreement with observations after 1967 (when satellite data became available) for sea-level-pressure at the Southern Pacific (Marshall and Harangozo, 2000), for temperature around the NPI (Lopez, 2007; Lopez et al.,

2008) and for zonal wind at surface level even if zonal wind has a large uncertainty (50%) for NCEP-NCAR data (Schneider and Gies, 2004). Concerning precipitation, Schneider and Gies (2004) found that NCEP-NCAR data do not represent the daily variability of precipitation and underestimate the real values. This is due to a poor representation of the Andes cordillera at 53°S because the mountain range is too narrow to be well represented in the model grid: it is smoothed to less than 1000 m a.s.l., thus orographic precipitation is not correctly predicted. We have used the ERA-40 dataset for the 1963-1974 period for a preliminary inspection of the general climatic conditions, except for rain products that have high incertitudes as very few satellite observations were available at that time. This inspection was first made with the intention of characterizing the time period dated by radionuclides measurements, but as better datasets are available, we decided not to report the ERA-40 results here. The ERA-Interim dataset (available only from 1989 onwards, Berrisford et al., 2009) has not yet been validated for this region, however we use the precipitation included in this dataset to 1) test if precipitation is correctly depicted and 2) asses the percentage of convective and stratiform clouds in this region.

Being aware of the important caveats mentioned above, we use daily averages of sub-daily (every 6h) values of NCEP-NCAR wind and geopotential height 1) to calculate air-mass trajectories and 2) to obtain synoptic charts for an area covering 110-40°W and 20-70°S with a resolution of 2.5x2.5°(the only available data covering the entire study area). We present the results of the backtrajectories calculation in section 2.4.3. We used synoptic charts to complete the information on unusual backtrajectories.

Since no measurements of precipitation were available for the NPI, we have reconstructed it by means of the Global Forecast System (GFS) model (Kanamitsu, 1989; Kalnay et al., 1990). This is a global atmospheric weather prediction model based on the same algorithm of the NCEP-NCAR reanalysis, with the advantage of having a better horizontal resolution, i.e., topography (0.5x0.5°), which improves predictions (for an example, see Favier et al., 2009). Forecast data for Chile is only available from September 2005 and is archived at the Geophysics Department of the University de Chile (DGF). For this study we used data spanning from September 2005

to December 2007, which account for 724 days due to some missing registers.

Finally, we also use modeled climatic data produced by the regional model Providing REgional Climates for Impact Studies (PRECIS) (Jones et al., 2004) on a high-resolution grid (0.25x0.25°) where SV height is ∼1200 m a.s.l. This is an atmospheric model only, so sea surface temperature (SST) is prescribed. The atmospheric initial state is forced by the HadCM3 global circulation model (Gordon et al., 2000). Even if SST is prescribed, since HadCM3 is a coupled atmosphere-ocean model, changes in the SST affecting the atmosphere will also influence PRECIS. PRECIS was designed to run under different climate change scenarios, so we use only the baseline run output of this model, i.e., the long-term mean of precipitation for the 1960-1990 time period obtained from the average of daily outputs.

The characteristics and some application examples of these models are presented in table 2.3 and the reader is referred to the references therein for a more detailed explanation of each model. The datasets grids and series availability are resumed in table 2.4. Reanalysis grids are too coarse to fairly represent the NPI complex topography: the drilling plateau makes only 2.1 km^2, out of the 4197 km^2 of the NPI (Lopez, 2007) and the model′s grid covers an area of approximately 10^4 km^2. We are aware of these limitations, but reanalysis data and forecast data are the only available information that we can use to depict general transport patterns and climate conditions at this site.

2.3.2 Comparison and validation of used datasets

2.3.2.1 Precipitation

We compared the observed daily precipitation at ground stations with precipitation predicted by NCEP-NCAR, ERA-Interim and GFS models for the 2005 to 2007 period. The results are shown in figure 2.6. Note that all stations are located in different grid boxes (cf. table 2.4). As Schneider and Gies (2004), we observe a very poor prediction of daily precipitation variability with NCEP-NCAR data (the correlation coefficients range from 0.19 to 0.37) and a tendency to underestimate precipitation. ERA-Interim predictions slightly improve (the correlation coefficients range from

Table 2.3: Reanalysis and model characteristics

Model	Grid size	Description	Boundary conditions	Application in this study	Examples of application
NCEP-NCAR (Kalnay et al., 1996)	2.5x2.5 °(T62-gaussian for precipitation)	Historical data assimilation using state-of-the-art models in order to reconstruct environmental variables	General Circulation Model	Synoptic conditions study, climatology	Upper air conditions at the Patagonian Icefields (Rasmussen et al., 2007), Precipitation vs. circulation at mid-latitudes (Garreaud, 2007)
ERA 40 (Uppala et al., 2005)	2.5x2.5°	"	"	Climatology for the 1963-1974 period	
ERA Interim (Simmons et al., 2006; Berrisford et al., 2009)	1.5x1.5°	"	"	% of stratiform precipitation calculation. Comparison with NCEP-NCAR data	
PRECIS (Jones et al., 2004; DGF, 2007)	0.25x0.25°	A regional climate modelling system developed at the Hadley Centre to help generate high-resolution climate change information. The DGF runs a version with high-resolution topography of Chile	HadCM3 global model and prescribed SST	Climatology, site description	Precipitation along Chile (Falvey, 2009b), Andes influence upon low and high-level wind flow (Garreaud, 2009), 20th century climatic variability in Chile (DGF, 2007)
GFS (Kalnay et al., 1990; Kanamitsu, 1989)	0.5x0.5°	A NCEP weather prediction model that is run four times per day (00, 06, 12, 18 UTC), first, with resolution of 55-km out to 3.5 days, then 80-km from 3.5 to 7.5 days, and then 110-km resolution up to 16 days	Global horizontal domain	Only 55-km resolution runs were used to study precipitation variability at SV	Precipitation at high-altitude in a central Chilean valley (Favier et al., 2009).

Table 2.4: Period covered by the data used in this study, studied locations coordinates and corresponding grids of each model. For NCEP data, surface height here is the value of the geopotential height at the surface. ERA-Interim surface height is approximated by dividing the mean annual geopotential at the surface by g=9.81 $m.s^{-2}$. PRECIS surface height is the real topography of the model. GFS surface height is obtained by interpolating linearly the topography height for the neighboring nodules (Falvey 2009a, pers. comm.). The asterisk * stands for long-term mean values for the stated period and n.u. for ″not used in this study″.

	Rain stations and drilling site	**NCEP-NCAR**	**NCEP Precipitation**	**ERA-40**	**ERA-Interim**	**PRECIS (Chile)**	**GFS (Chile)**
Data availability	Variable daily	1948-present sub-daily	1948-present sub-daily	1957-2002 sub-daily	1989-present sub-daily	1961-1990 2010-2100 daily	2005-present sub-daily
Used data	2005-2007 1960-1990*	2005-2007	1968-1996* 2005-2007	1963-1974	2007	01/12/1960- 30/11/1990	5/09/2005- 31/12/2007
Coyhaique	45.58°S 72.12°W 310 masl	45 72.5 669	44.7611 71.25 819	n.u.	45 72 831	45.5 72 850	45.63 72.12 819
Balmaceda	45.92°S 71.68°W 520 masl	45 72.5 669	46.6558 71.25 366	n.u.	46.5 72 873	46 71.75 1040	45.92 71.68 749
Cabo Raper	46.83°S 75.68°W 40 masl	47.5 75 408	46.6558 75 280	n.u	46.5 75 97	46.75 75.75 0.31	46.83 75.68 4
San Pedro	47.72°S 74.92°W 22 masl	47,5 75 408	48,5705 75 439	n.u	48 75. 136	47,75 75 76	47.72 74.92 104
San Valentin	46.58°S 73.32°W 4032 masl	47.5 72.5 817	46.6558 73.125 698	47.5 72.5 3480=600hPa 2670=700hPa et al. (2004)	46.5 73.5 719 Kaallberg	46.5 73.25 1243	46.58 73.32 902

0.20 to 0.56) but with an overestimation of a factor 2-3. The only station that compares well with ERA-Interim is San Pedro (r=0.56). In contrast, GFS predicted precipitation is much more reliable, as shown in figure 2.6 (c), where we observe a significant improvement of the correlations: r=0.45 for Balmaceda, r=0.62 for Coyhaique, r=0.54 for Cabo Raper and r=0.71 for San Pedro.

A closer look at daily variability is shown in figure 2.7 for the period covering the 2007 drilling campaign (13 days). We observe that GFS (red line) may overestimate the precipitation for some events in the stations although occurrences are fairly depicted. The total annual amount of precipitation is overestimated by 20-25% (as also observed in figure 2.8 for yearly values). As the GFS model is reliable to capture the occurrence of our qualitative observations at SV (blue dots), we use it in the following to predict precipitation at SV summit and obtain monthly means, assess the seasonal behavior of precipitation and its relationship with air-masses origin.

In consequence, we need to correct the overestimation of the number of days without precipitation. For this, we use the *false alarm* method i.e., we calculate the average precipitation for days when the model incorrectly predicted precipitation occurrence and we consider that significant precipitation only took place above this average value (Favier 2010, pers. comm.; Favier et al. 2009). This method does not remove high overestimation values, but at least provides an idea of uncertainty of predictions below a certain threshold. In table 2.5 we present the number of rainy days at ground stations (Balmaceda, Coyhaique, San Pedro and Cabo Raper), which represent the reality, compared to the number of rainy days obtained with the GFS model before and after correction. We have no observations to correct the predictions at the SV site, but since it seems to have a mixed behavior between coastal and continental stations (as shown in figure 2.10 and discussed in section 2.4.1), we take a value close to the average of all stations: 2 mm per event, for minimal precipitation at the SV site. In conclusion, for further calculations, precipitation below 2 mm will be neglected at SV.

By applying this correction to the SV predictions, we removed 162 small events, which represent 23% of the occurrences. Their contribution to the total amount of precipitation is negligible (2%), thus figure 2.8 is drawn without correction.

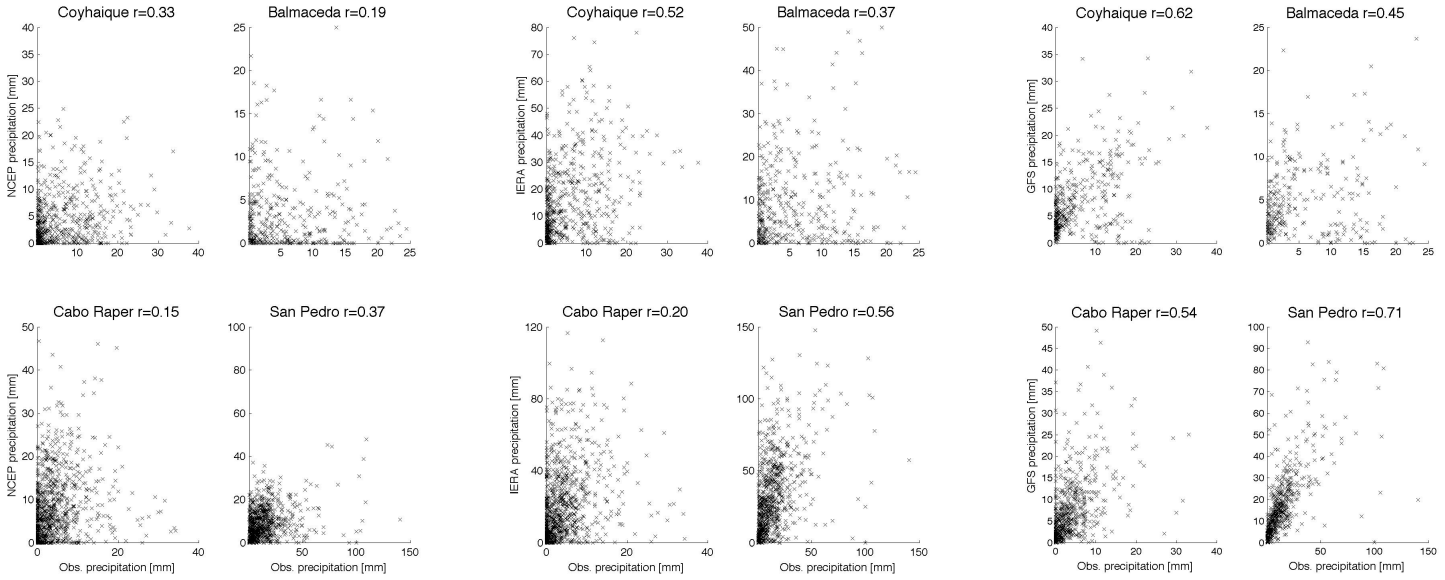

(a) NCEP precipitation vs. observations

(b) ERA-Interim precipitation vs. observations

(c) GFS precipitation vs. observations

Figure 2.6: Gauged rain measurements over 2005-2007 compared to reanalysis and forecast data. The grids corresponding to each station can be found on table 2.4. According their location relative to the Andes cordillera, the leeward stations are Coyhaique and Balmaceda and the windward stations are the stations Cabo Raper and San Pedro.

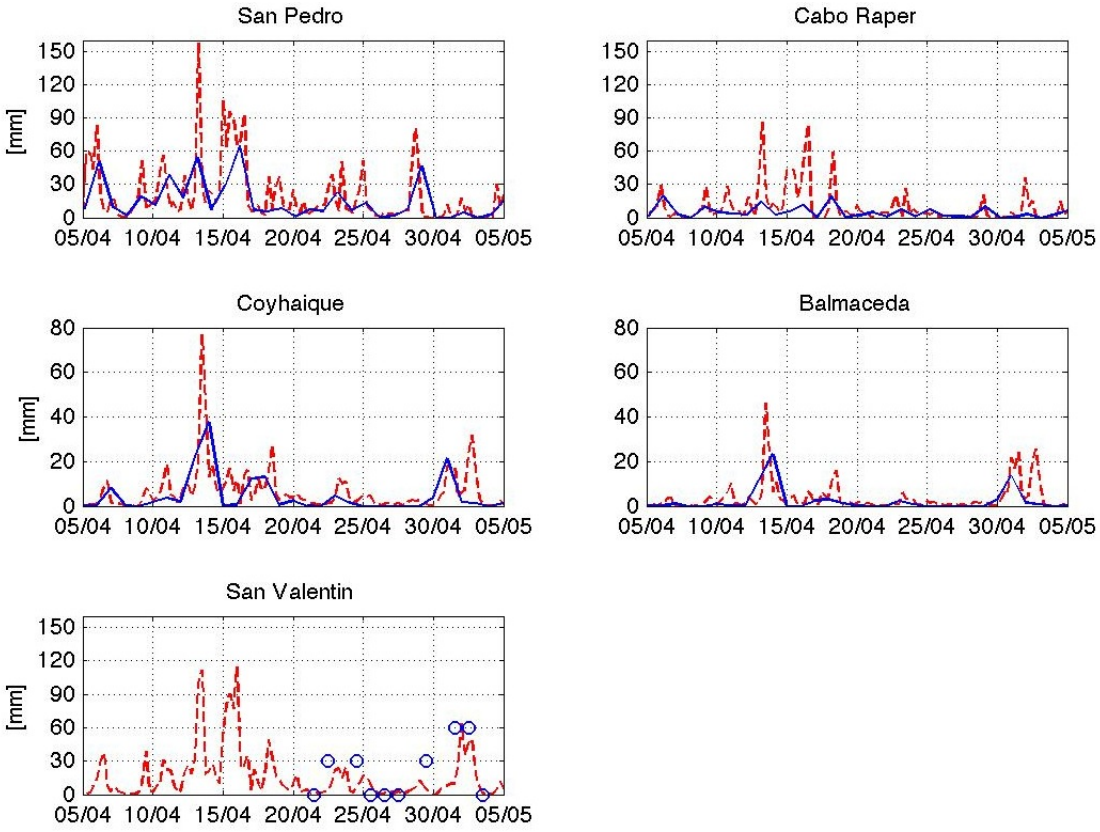

Figure 2.7: Comparison between observed precipitation (blue line) at meteorological stations and GFS predictions (red line). For the SV case, the blue dots represent qualitative observations reported during the drilling campaign (21/04/07 to 03/05/07, table 2.2): No snow=0, Snow=30, Heavy snow=60. The grids corresponding to each station can be found in table 2.4

In conclusion, we use the GFS model to produce a prediction of daily occurrence of precipitation at the SV drilling site. We apply the *false alarm* correction for calculations of section 2.4.3 (precipitation events according to wind direction) but not for other cases.

2.3.2.2 Wind

To validate the GFS wind data at the surface, we compare wind measurements at coastal stations, the Cabo Raper and San Pedro pharos, for the period 2005-2007 (we do not have data for continental stations nor for the SV site). This is shown in figure 2.9(a), where zonal and meridional observed wind components are compared with forecasted values. The resemblance

Table 2.5: Number of days with precipitation events for the period when GFS data is available (04/09/2005 to 31/12/2007) and without missing data at stations. Total days = 724. N_{real} stands for the number of days with precipitation measured at ground stations (reference of real precipitation events). N_{GFS}, for the number of days when precipitation is predicted with the GFS model. N_{false} is the number of days when precipitation was erroneously predicted, i.e., when a false alarm of precipitation was set. pp_{min} is the average precipitation for the cases when a false alarm was given (N_{false}). We estimate a value for the SV site based on the ground stations values. Finally, N_{corr} is the number of days taken from N_{GFS} with precipitation higher than the pp_{min} values. We use the latter as a prediction for SV precipitation

Location	$\mathbf{N}_{real}$	$\mathbf{N}_{GFS}$	$\mathbf{N}_{false}$	$\mathbf{pp}_{min}$ **[mm]**	$\mathbf{N}_{corr}$
Coyhaique	422	679	257	2.0	451
Balmaceda	305	674	369	1.3	369
Cabo Raper	526	680	154	2.7	429
San Pedro	563	700	137	2.6	560
San Valentin		702		*2.0*	540

is striking for San Pedro (r=0.59 and r=0.46 for zonal and meridional winds respectively) and puzzling for Cabo Raper, where only meridional wind (r=0.69) is relatively well depicted while zonal wind is overestimated (r=0.15).

This last issue could arise from a misrepresentation of topographical effects by the model and also from the manual register of observations, i.e., instantaneous wind would be registered instead of a time-averaged value. In that case it would seem that the GFS model does not depict Cabo Raper instantaneous zonal shear. It is also worth noting that for Cabo Raper some periods show a good correlation with the model and others do not. That may be due to a misrepresentation of different weather regimes and/or transition between them at this location, pointing again to a local topographical effect since predictions at San Pedro comply with the observations (e.g. note that the April 25^{th} to 27^{th} time period was under an easterly regime due to a strong blocking conditions according to the synoptic charts obtained with NCEP-NCAR data).

In section 2.4.3, we classify wind directions at the SV site and then we obtain the corresponding daily backtrajectories. Ideally, for the calculation of backtrajectories, we would have used the same GFS dataset that we have used to predict precipitation. However, this is not possible because GFS covers a region-limited domain. Thus, we use the NCEP-NCAR dataset

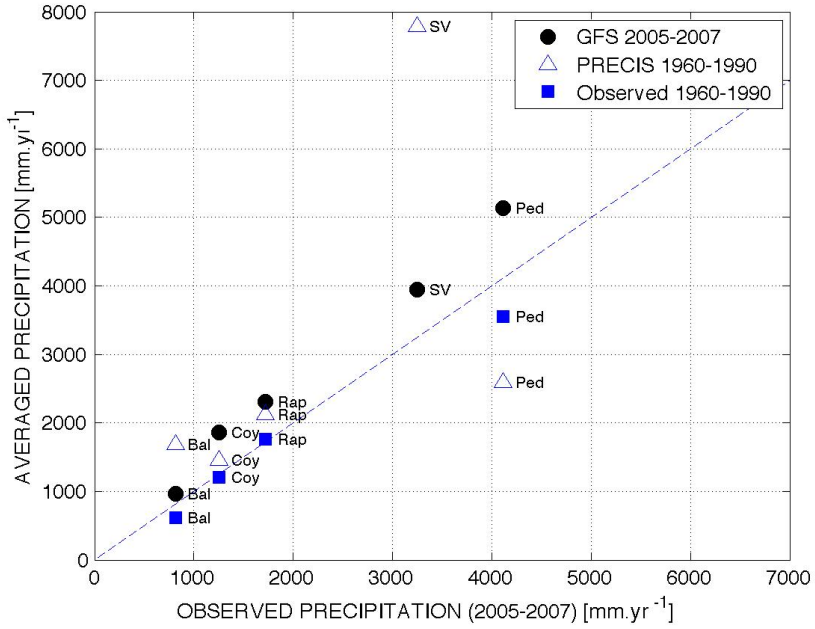

Figure 2.8: Predicted precipitation (dots for GFS, triangles for PRECIS) and long term mean precipitation (squares, from `http://www.atmosfera.cl/`) versus the mean precipitation observed between 2005-2007 in the San Pedro (P), Cabo Raper (R), Coyhaique (C) and Balmaceda (B) stations. For the San Valentin (SV) case we use the net accumulation value of 3240 $mm.yr^{-1}$for the x-axis and the GFS and PRECIS precipitation predictions for the y-axis. See table 2.4 and section 2.3.1 for more details.

to calculate backtrajectories . To assess the discrepancies between NCEP-NCAR data and GFS data we plot total wind speed for both datasets for the grids of Coyhaique, San Pedro and SV at 700 hPa (approximatively the SV altitude) in fig. 2.9(b). We observe consistency between the two models, r>0.9 (which is not surprising as both use the same algorithm to generate data). Given the consistent vertical structure of the atmosphere we argue that the validation performed at low level coastal stations would also validate the use of the NCEP-NCAR dataset at higher levels (i.e., for SV altitude).

As mentioned, GFS and NCEP-NCAR datasets are produced with the same algorithm, thus we favor the use of the NCEP-NCAR dataset for calculations, as it was the dataset available at the DGF (which was not the case of the ERA-Interim dataset). Nevertheless, we performed a fast crosschecking between NCEP-NCAR and ERA-Interim wind data by means of backtrajectory

calculations (using the same algorithm for both, for 2007, thus testing the zonal, meridional and vertical wind components at once) and we observe that both datasets are in agreement for 85% of the cases and only 10% show significant disagreement (especially for blocking events). We are not able to decide which dataset is more accurate, but given the high consistency between them we are confident of the use of NCEP-NCAR reanalysis.

2.3.3 Methodology used for trajectory calculations and their relationship with precipitation events at SV

Our methodology aims at exploring a possible link between wind direction at the SV site, the origin of airmasses arriving there and whether they are precipitating or not. For this, we first classify daily wind direction at SV (NCEP-NCAR grid) in eight classes: North (337.5-22.5°), North East (22.5-67.5°), East (67.5-112.5°), South East (112.5-57.5°), South (157.5-202.5°), South West (202.5 247.5°), West (247.5-292.5°) and North West (292.5-337.5°) for the 2005-2007 period (1095 days). Then, for each day we obtain the predicted precipitation at the SV site (GFS) corrected with the false alarm method. This allows us to deduce the corresponding number of precipitating events and the amount of precipitation expected for every wind direction, based on daily observations.

As we use subdaily NCEP-NCAR data (data available every 6h), the classification in wind classes is based on daily averages of wind direction. Total wind is obtained from zonal and meridional wind components at the SV site, which is assumed to be at the 700 hPa level (2670 m a.s.l.) instead of 600 hPa (3840 m a.s.l.), the latter being too high for the topography included in the NCEP-NCAR dataset.

Also, in order to relate potential sources with air masses arrivals, we calculate 7-day backtrajectories starting every day at SV grid (47.5°S, 72.5°W, 700 hPa, see table 2.4) for each of the aforementioned classes. Then, we average all calculated backtrajectories to obtain a mean path for each wind direction.

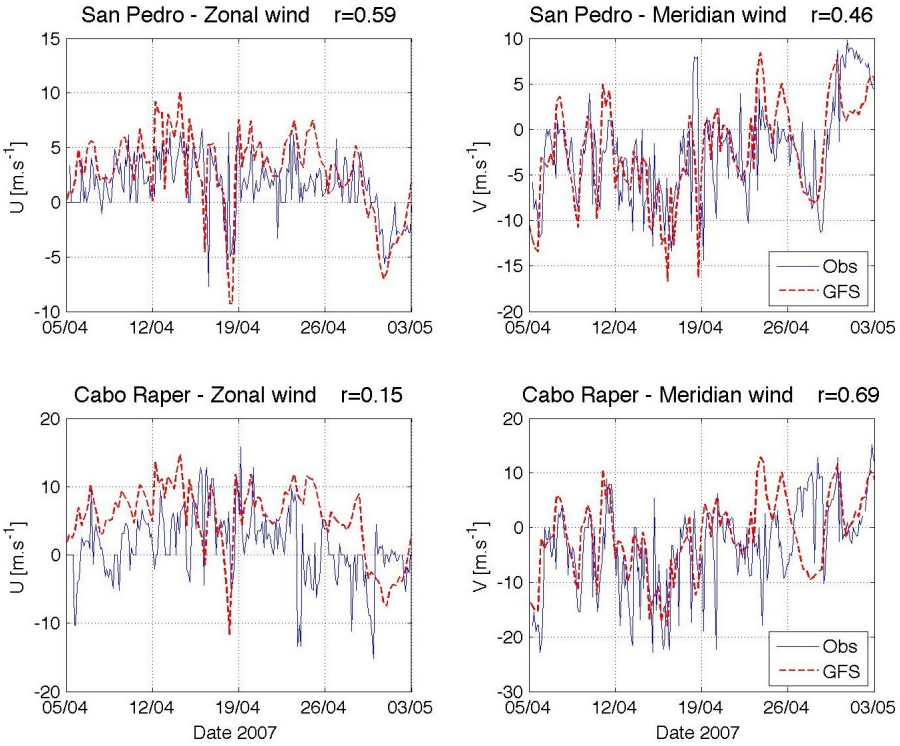

(a) GFS wind compared to observations

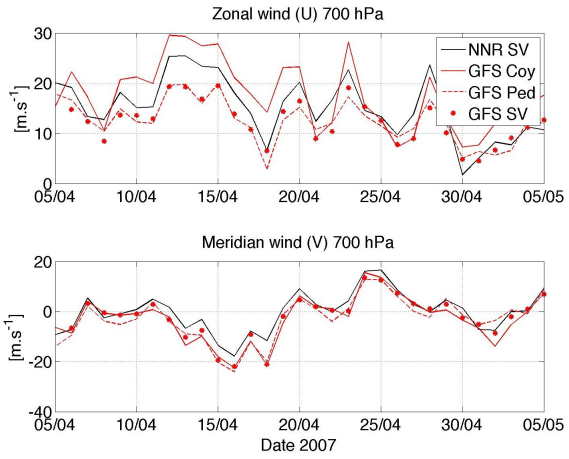

(b) NCEP-NCAR and GFS wind

Figure 2.9: (a) Comparison between measured wind and forecast zonal and meridional wind components at coastal stations (San Pedro and Raper). Focus on April 2007. Red line = GFS data at 1000 hPa. Blue line = transcription of handwritten observations at the stations.) (b) Comparison between GFS and NCEP-NCAR reanalysis data for zonal and meridional wind components at 700 hPa (the SV level) for San Pedro, Cabo Raper and Coyhaique. Focus on April 2007. Red line = GFS data. Black line = NCEP-NCAR observations.

Backtrajectories were calculated at the DGF (Molina 2009, pers. comm.) with a backward step linear interpolation every 6h from U and V wind components, and corrected for topographical effects (air parcels are forced to go upslope when they enter the topography domain, otherwise, the interpolation would be done for unrealistic wind values that fill the topography domain in). We compared some selected trajectories of 2007 with the HYSPLIT model (Draxler and Rolph, 2003) and our calculations are in good agreement with HYSPLIT calculations.

Note however the broad character of the trajectories, given the grid resolution (2.5x2.5°). Thus, they are not intended to resolve fine scale transport the results, but are useful to depict general transport patterns and provide a rough idea of the source regions affecting this site.

2.4 Results

2.4.1 SV precipitation compared to continental and coastal stations

In this section we compare SV precipitation as predicted by GFS with the nearby stations in order to better understand if the SV site follows either a maritime or a continental behavior (Aravena and Luckman, 2008; Lopez et al., 2008, did not explore the mountain divide).

In figure 2.10, we draw a scatter plot of GFS precipitation magnitude as a function of zonal wind (U) and meridional wind (V) for coastal stations (San Pedro, Cabo Raper), and continental stationss (Coyhaique, Balmaceda), as well as for the SV site.

For most of the cases, the highest precipitation values are associated with high zonal wind ($\sim$10 m.s^{-1}), but not necessarily with the highest zonal wind gusts ($\sim$20 m.s^{-1}). For continental stations, the few highest precipitation events take place under westerly flow, when air masses traversing the cordillera have enough moisture to produce rain at those sites, after having suffered an orographic moisture depletion. Balmaceda, the station located most inland, shows that important precipitation events can take place under easterly flow (U<0) conditions. In this case, the moisture would originate in the Atlantic Ocean (Garreaud and Aceituno, 2007).

In figure 2.10 we oberve that at Cabo Raper an easterly component of the zonal flow (U<0)

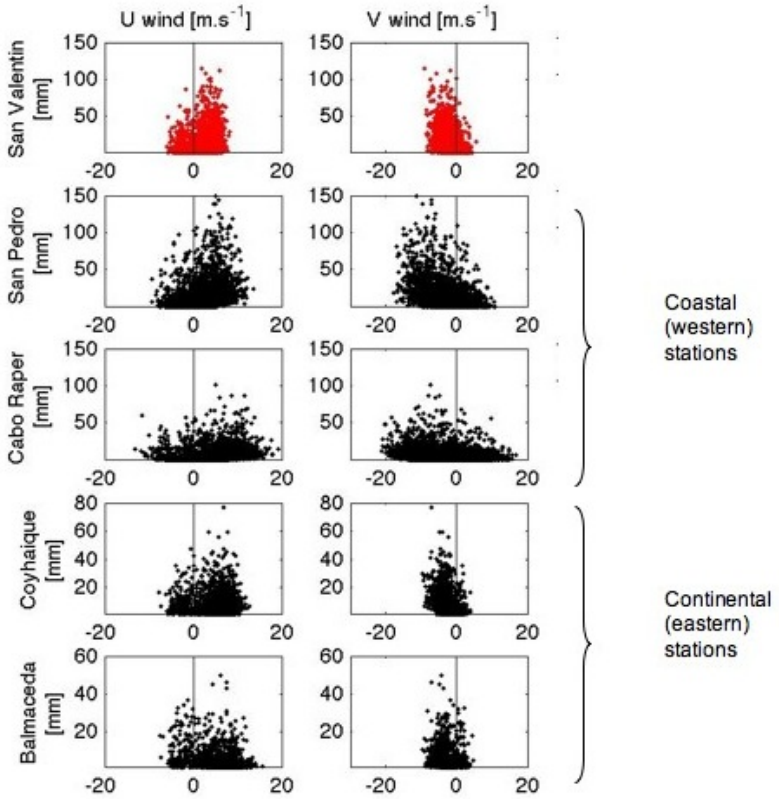

Figure 2.10: Precipitation [mm] vs. zonal (U) and meridional (V) wind speeds [m.s^{-1}], air temperature and relative humidity around the Northern Patagonian Icefield and San Valentin grid. All data were obtained with the GFS model at surface level and were validated by observations at the stations. U>0 for Westerly wind and V>0 for Southerly wind. Wind components at 10m instead of surface wind show a narrower distribution but the same behavior. Using 2 m temperature instead of surface level values yields the same result. Surface and 2 m relative humidity at the Cabo Raper and SV sites seem to be biased toward values <90%. Data spans from 04/09/2005 to 31/12/2007 (724 days, cf. table 2.5) when GFS data are available.

is predicted by GFS (and this is supported by observations). However, for this station, located on the coast, the easterly wind component would rather reflect turbulence of the fronts while encountering the continental relief rather than a real easterly regional wind flow. In contrast, San Pedro, also a coastal station, shows a clear dependency of strong precipitation on Westerlies, yet important precipitation events at San Pedro also take place under easterly conditions (figure 2.10). San Pedro is located in a fjord between the Northern and Southern Patagonian Icefields,

where wind can be tunneled (see 2.2 (a)). Indeed the only free low level path for easterly flow is between the NPI and the SPI. This may explain the high precipitation rate at San Pedro (∼3000 mm.yr^{-1}) which receives precipitation under both easterly and westerly conditions whereas Cabo Raper (∼1700 mm.yr^{-1}) does not.

Precipitation events at the coastal stations can be related to cyclonic systems that traverse this region bringing frontal precipitation associated with high turbulence (frontal eddies of cyclonic systems). The maritime behavior of San Pedro and Capo Raper is also denoted by a more frequent precipitation than at continental stations, as observed in table 2.5, which is also the case at SV.

Concerning meridional wind (V), coastal stations are under the influence of both southerly (V>0) and northerly (V<0) arrivals, with a more important contribution of northern transport to precipitation (see fig. 2.10). In contrast, continental stations narrow distribution of meridional wind evidences their almost entire dependency on zonal wind strength (U), since meridional wind (V) is virtually centered at zero, albeit with a small northerly component. This confirms that, on a regional scale, northwesterly transport bring most of the precipitation to all these sites.

SV site shows a narrow zonal wind (U) distribution, similar to San Pedro, but a meridional wind (V) distribution similar to Coyhaique (cf. figure 2.10). This implies that SV is affected by a more complex circulation than low-level stations: mixing between marine stratified air masses and continental transport, would be more frequent at this altitude than at low levels. Moreover, at the SV site, both westerly and easterly zonal transport can bring precipitation (which is not the case of Balmaceda, for instance, a station mostly influenced by easterly zonal wind bringing precipitation). Finally, at the SV site, few precipitation events associated with southerly flow (V>0 and pp>2mm) are likely to take place. On the contrary, most of the precipitation would be associated with northerly flow (V<0 and pp>2mm). This is in agreement with the NCEP-NCAR reanalysis data table 2.6, in which the moistest air masses are clearly coming from the northwest. Furthermore, according to GFS outputs, westerly storms arrive with the warmest air masses (∼281K).

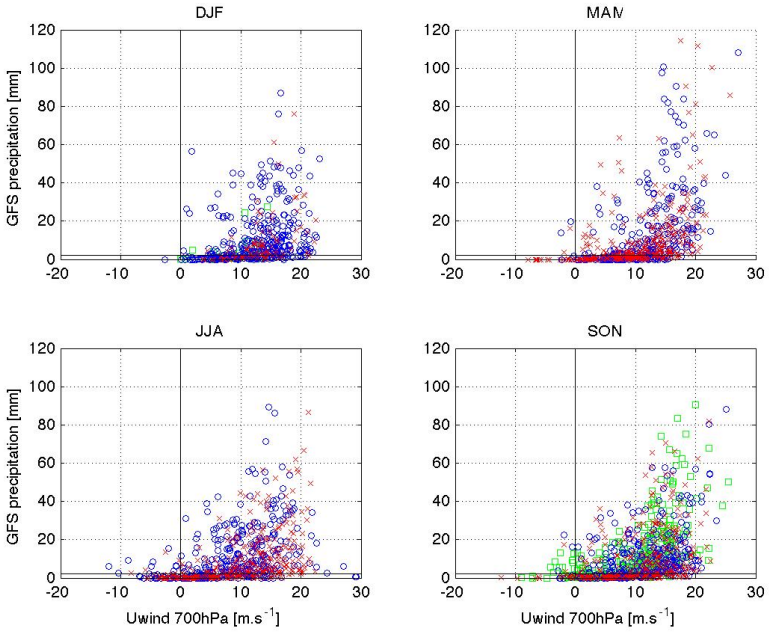

(a) Zonal wind (W - E)

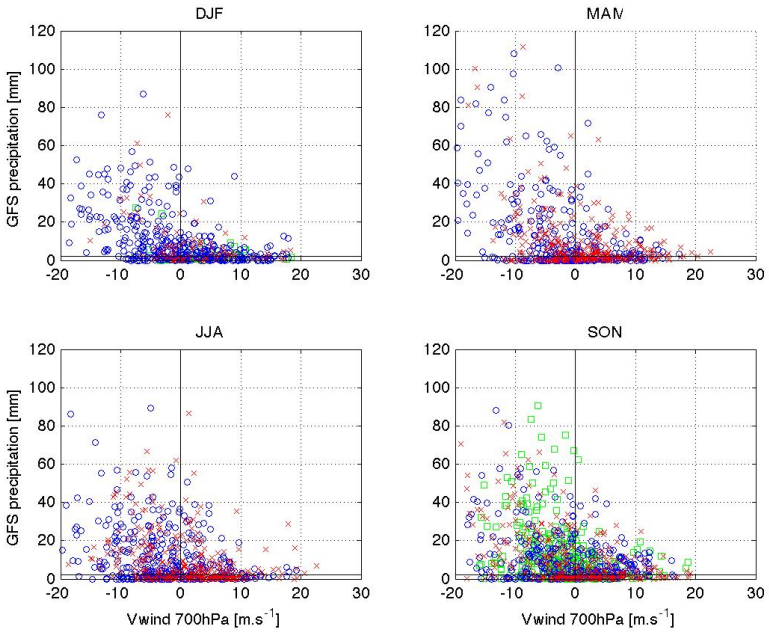

(b) Meridional wind (N - S)

Figure 2.11: Precipitation vs. (a) zonal and (b) meridional wind obtained with the GFS model, for each season and for the SV grid (cf. table 2.4). Wind was obtained for the 700 hPa level to account for San Valentin location, above the inversion cap. GFS precipitation is considered to take place only if values exceed 2 mm (cf. table 2.5), thus values located below the line in the bottom of each graph are neglected. Each year is represented by a different color: 2005 green, 2006 blue, 2007 red.

In the next section we explore in more detail the relationship between precipitation and wind direction, and we complete this climatological study.

2.4.2 Seasonality of predicted precipitation and temperature by PRECIS and GFS models (2005-2007).

The dependency of precipitation in U and V regardless the season has been presented in figure 2.10. In figure 2.11, we explore the precipitation occurrence and strength according to zonal (a) and meridional (b) wind components for each season with GFS data. We observe that the high values of monthly precipitation are determined by the occurrence of single important precipitation events (>60 mm.day^{-1}) that would take place under a strong zonal wind (i.e., under westerly conditions), and this is especially true for MAM and SON. Westerlies are stronger in summer (DJF) but it is tricky to relate high precipitating events with this season since less cloudiness is observed. In contrast, according to fig. 2.11, the most important precipitating arrivals would take place in SON or MAM.

In winter (JJA), an easterly component appears in the zonal wind (negative values in fig. 2.11(a)) and this is consistent with the decrease of the latitudinal pressure gradient during this season, which greatly favors . Easterly flow is associated with low precipitation values (<30 mm.day^{-1}). Note that transition seasons also show a few easterly zonal wind arrivals associated with precipitation. Finally, another important feature of figure 2.11 is that we observe important precipitation events (>60 mm per event) associated with northerly meridional wind (fig.2.11(a)) in MAM, more than for the other reasons.

In order to assess monthly variability on precipitation at the SV site we use reconstructed variability of precipitation and temperature obtained with both PRECIS (for long-term means) and GFS (for the 2005-2007 period) models and this is seen in figure 2.12. Total predicted precipitation at the SV site is 8000mm.yr^{-1}according to PRECIS (climatological surrogate between 1960-1990, average for those 30 years) and 4000 mm.yr^{-1}according to forecast data of GFS (average for 2005-2007). In section 2.4.4 we will discuss the implication of these values for

the dating of the ice-core.

As we observe in fig. 2.12, PRECIS predictions show a smooth transition between two regimes: maximum precipitation would take place in JJAS, with monthly precipitation values of ∼800 mm, and lower precipitation in DJFM ∼500 mm. The transition month towards upper values would be April. According to PRECIS results, precipitation seasonality in the SV is similar to leeward stations, notably, more precipitation in winter than in summer. This would be in agreement with the findings of Schneider et al. (2003), who observed that precipitation maxima takes place before the highest point of the mountain range. Analogously, the SV has in average a similar behavior to the drier side of the mountain range (leeward stations). This behavior has an implication on the interpretation of our ice register: continental precipitation could be higher than previously expected.

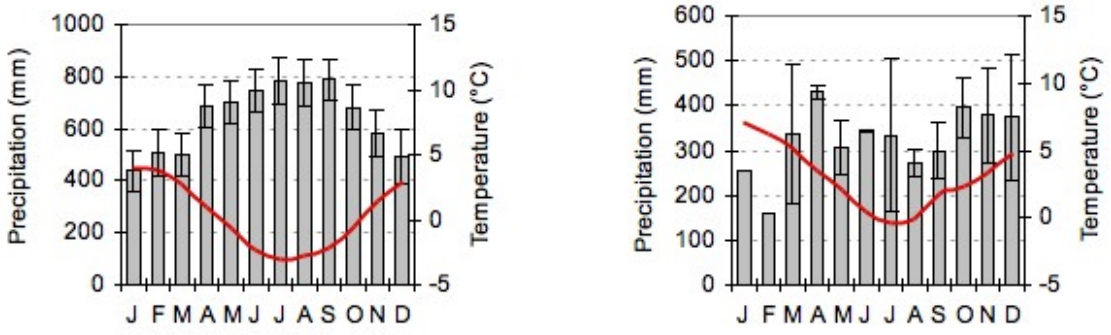

(a) PRECIS (1960-1990)

(b) GFS (2005-2007)

Figure 2.12: Predicted monthly precipitation at the Monte San Valentin. (a) PRECIS predictions are based in 10300 days (1960-1990), at the following coordinates: 46.50°S, 73.25°W, 1243 m a.s.l.) (b) GFS predictions are based in 724 days (2005-2007), at the following coordinates: 46.58°S, 73.32°W, 902 m a.s.l. January and February correspond only to the year 2007 (no data available for 2005, 2006)

Precipitation at the SV site according to table 2.5 is as frequent as San Pedro station (560 occurrences for San Pedro, 540 for SV). However, it would be granted only if air masses have not been readily depleted before by orographic precipitation, which seems to be the case for most of the year: according to GFS, precipitation at SV, 4000 mm, is twice precipitation at Cohyaique,

implying that there is still enough precipitating water in this level of the atmosphere likely to produce precipitation events.

Concerning GFS predictions, figure 2.12(b), precipitation for the SV site shows a highly variable distribution over the year. A only notable feature is the low precipitation in January and February (256 and 160 mm.yr^{-1}respectively) when compared with rest of the year (>300 mm.yr^{-1}). Interestingly, this prediction is in good agreement with cloudiness observations over the SV site from 2000 to 2008: cloudiness exhibits a minimum in february (Vimeux et al., 2011). Moreover, january and february low precipitation values would also correspond to a more frequent jutting out of the SV summit from the cloud cover during these months.

Precipitation maxima, according to GFS data, would take place in April and in OND (∼400 mm.month^{-1}). This seems in agreement with the observed cloudiness over the NPI, but, as pointed out by Vimeux et al. it is not possible to quantitatively deduce precipitation based only in the cloud cover density. For example, the persistent cloudiness observed over the whole NPI region in july (Vimeux et al., 2011), does not imply that july is the rainiest month (∼350 mm.month^{-1}). As GFS predictions span a shorter period than PRECIS predictions, we are certainly not fully sampling of the variability of the system, although the cloudiness study goes in favor of GFS predictions. The discrepancies in the seasonality predicted by PRECIS (1960-1990) and GFS (2005-2007) may be due to discordances between both models or a change in seasonality in the recent years.

In conclusion, with respect to precipitation, we argue that GFS predictions correctly reflect the daily and monthly variability in the studied zone. Complementary to this, PRECIS outputs would represent the average behavior of the SV site. Seasonal maxima is difficult to establish, however, the months with minimum precipitation are January and February (the months with persistent westerly transport and practically deprived of easterly transport). The seasons undergoing high precipitation events (>60 mm per event) are spring (SOND) and fall (MAM), which are associated with strong northwesterly winds, while winter (DJF) precipitation would be moderate and also include easterly transport producing less than 10 mm per event. The most

important northern meridional winds would take place in fall. Summer precipitation events would rarely exceed 60 mm per event, even if this season corresponds to the highest moisture content of the atmosphere and the strongest westerly winds (peaking between 45 and 55°S). This may probably due to a weaker influence of frontal precipitation during summer (and not a more important orographic depletion). Finally, summer is a good candidate for the most wind blowing season, given a combination of higher wind speed (which is the case) and less precipitation at SV site. Thus, wind could blow most of the unconsolidated snow.

Although stratiform precipitation dominates mid-latitude precipitation, convective precipitation near the NPI site would range between 20 and 40%, according to ERA-Interim data, with no clear seasonal behavior. In contrast, the Atmopsheric General Circulation Model ECHAM4 (Hoffmann et al., 1998) simulates between 0 to 10% convective precipitation in JJA and approximately 40% (the maximum) in January (Hoffmann 2009, pers. comm.). Thus, convective precipitation cannot be neglected at this site and may be responsible for the uplift of low-level air masses than can precipitate at the SV site. As summer precipitation has mostly a westerly origin (i.e., Pacific Ocean), according to the ECHAM4 model, marine airmasses entrainment into the atmosphere would be more important in summer. On the contrary, continental air masses uplift by convection seems to be less important in JJA.

Finally, concerning temperature, according to both GFS and PRECIS models 2.3, the January (T $_{jan}$) to July (T $_{july}$) difference at SV would be of 6.5°C , which is in agreement with the estimate of Vimeux et al. (2008) based on reanalysis data, that is of 7°C. Coastal stations show also a moderate seasonal difference: $T_{jan} - T_{july}$ ∼5°C, since ocean proximity buffers temperature (Lopez et al., 2008). In contrast, continental stations show larger seasonal variations: $T_{jan} - T_{july}$ ∼11°C. According to this, temperature behavior at the SV site is closer to coastal stations (i.e., moderate seasonal differences) and this can be explained by the constant influence of marine air masses at this site.

2.4.3 Backtrajectories and precipitation dependency on wind direction

A backtrajectory is the backward calculation of the trajectory followed by an air parcel during a given number of days to a given location. In this section we present the results of backtrajectories starting at the 2.5x2.5°grid containing the Monte San Valentin in the NCEP-NCAR model (47.5°S 72.5°W) for the 2005-2007 period. The objective of this calculation is to relate each transport direction to a source region and precipitating conditions. Nevertheless, it has to be kept in mind the broad character of these trajectories, which do not account for mixing of air parcels.

Results are presented in tables 2.6 and 2.7 and figure 2.13. In table 2.6 we present the distribution of days according to eight wind classes (N, NE, E, SE, S, SE, W, NW) at the SV site and the corresponding days with precipitation at ground stations. We also present averaged conditions at the SV grid point for total wind speed, specific and relative humidity (from NCEP-NCAR) and precipitation amount per event. Days with precipitation are based on observations at ground stations. Averaged precipitations per event are calculated with GFS forecast data and corrected with the false alarm method (sec. 2.3.2.1). Table 2.7 presents a seasonal distribution of precipitation events at the SV site as forecasted by the GFS model for the 2005-2007 period. A summary of both tables is presented in table 2.8. In figure 2.13, we plot the averaged backtrajectories (from table 2.6) for each wind class in a latitude-longitude equidistant projection and the average vertical profile of bactktrajectories in an altitude-longitude graph. For clarity, the colors corresponding to the various trajectories are also shown in tables 2.6 to 2.8.

We observe that all air masses have an oceanic origin between 40 and 70°S. The changing in circulation patterns have an influence on trajectories only 2 days before the arrival or air masses to the SV site, and this is specially true for the air masses that flow over the continent.

Westerly (NW, SW and W) transport is the most frequent (92.1%, tab. 2.6). Backtrajectories are associated with high values of total wind, indicating a fast transport of moist air masses to SV (wind speed of $\sim$15m.s^{-1}, SH$\sim$0.0020 kg.kg^{-1}, RH$\sim$65%). Most of the time, NW and W

Table 2.6: Daily distribution according to wind direction at the San Valentin NCEP-NCAR grid (47.5°S, 72.5°W, 700 hPa). Wind direction as stated in section 2.3.3. The table contains the number of days of the 2005-2007 period for the specified wind direction, the number of precipitation events registered at ground stations and average conditions for the SV grid. Wind speed, specific humidity, relative humidity and temperature are calculated from NCEP-NCAR data (that are in agreement with the GFS model) and precipitation average is predicted with GFS and corrected with the false alarm method (*=observations, **= GFS, no marker=NCEP-NCAR data).

	N	NE	E	SE	S	SW	W	NW	Total
Days for each class	**30**	**7**	**5**	**6**	**39**	**253**	**555**	**200**	1095
	2,7%	0,6%	0,5%	0,5%	3,6%	23,1%	50,7%	18,3%	
Days with pp at Coyhaique *	18	6	3	5	24	116	326	118	616
Days with pp at Balmaceda *	20	6	2	6	23	62	225	97	441
Days with pp at Cabo Raper *	14			4	16	164	433	148	779
Days with pp at San Pedro *	15			3	7	186	472	147	830
Total wind at SV (m/s)	8,7	7,3	5,5	7,9	9,0	15,4	17,0	14,4	15,5
Specific humidity at SV (kg/kg)	0,0023	0,0015	0,0007	0,0007	0,0008	0,0018	0,0023	0,0025	0,0021
Precip. per event at SV (mm) **	13,5	4,9		4,8	10,9	8,1	15,7	18,3	14,3
Temperature (ºC)	-6,3	-9,7	-9,7	-11,5	-10,4	-7,5	-6,8	-5,4	-8

Table 2.7: Seasonal precipitation events distribution according to wind direction for the SV site in the GFS grid (46.58°S, 73.32°W, 902 masl). Wind direction is as stated in section 2.3.3. To avoid oversampling for SON 2005, we removed those months from the analysis. Total days = 639. The table contains the number of days with precipitation, the sum of all precipitation events (mm) and the average temperature (°C) for the specified wind directions, per season.

		N	NE	E	SE	S	SW	W	NW	Total
DJF	**Days with precipitation**	**1**					**22**	**63**	**16**	**102**
	Total pp [mm/season]	*29*					*114*	*802*	*263*	*1207*
	Temperature (ºC)	-0,5					-7,0	-5,4	-4,1	-5,4
MAM	**Days with precipitation**	**3**					**33**	**68**	**17**	**121**
	Total pp [mm/season]	*37*					*298*	*1171*	*457*	*1962*
	Temperature (ºC)	-1,3					-8,0	-6,1	-4,5	-6,3
JJA	**Days with precipitation**	**4**	**2**			**4**	**23**	**71**	**25**	**129**
	Total pp [mm/season]	*33*	*10*			*52*	*212*	*1073*	*416*	*1796*
	Temperature (ºC)	-7,4	-12,35			-13,87	-12,6	-10,2	-7,7	-10,2
SON	**Days with precipitation**	**4**				**2**	**28**	**67**	**25**	**126**
	Total pp [mm/season]	*69*				*21*	*198*	*1069*	*423*	*1780*
	Temperature (ºC)	-7,4				-11,62	-10,1	-8,8	-7,7	-8,9
Total	**Days with precipitation**	**12**	**2**			**6**	**106**	**269**	**83**	**478**
	Total pp [mm/year]	*168*	*10*			*73*	*822*	*4115*	*1559*	*6746*

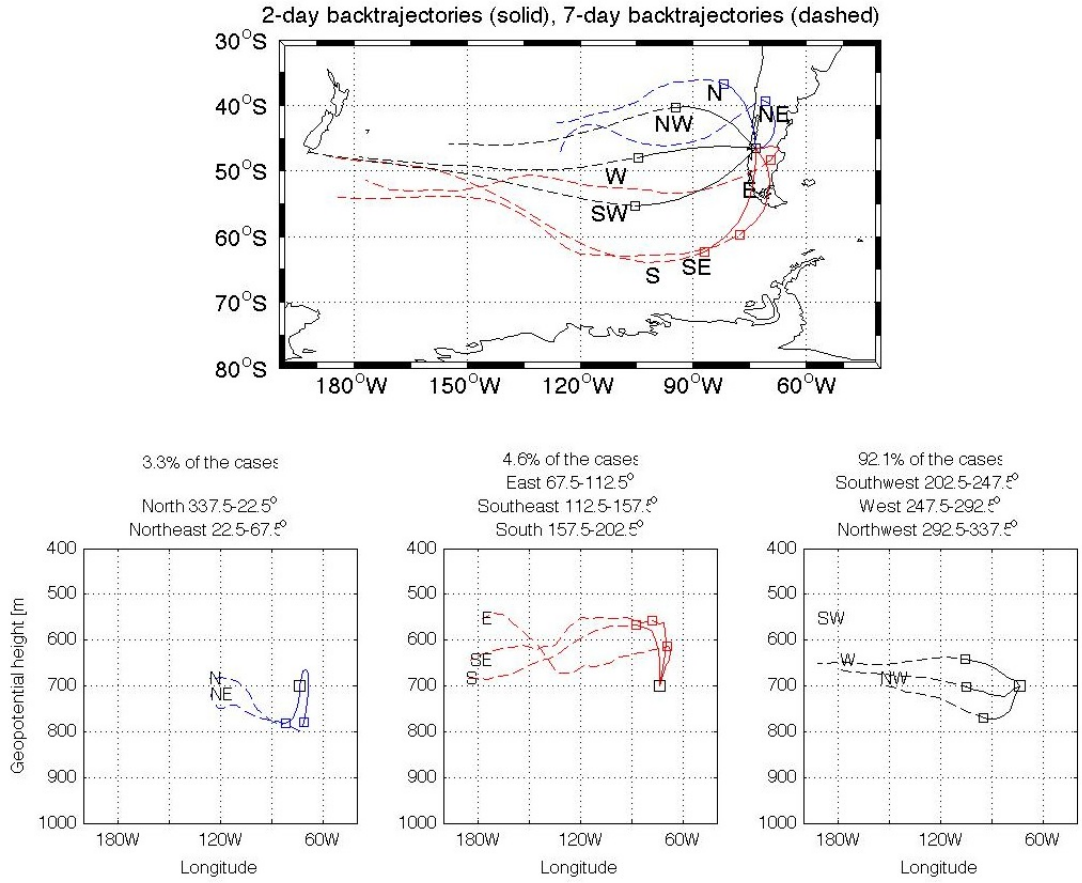

Figure 2.13: Averaged backtrajectories for 2005-2007, classified by wind direction starting at the San Valentin grid. Blue lines correspond to N, NE directions; black to NW, W and SW; and red to S, SE and E. Calculations were obtained with NCEP-NCAR data. 7-day backtrajectories (dashed lines) and 2-day backtrajectories (solid lines) are shown. The squares at the trajectories show the end point of 2-day backtrajectories. For clarity, confidence intervals were not drawn, but it should be kept in mind that S/SE trajectories may originate as far as the Antarctic plateau. The three lower panes depict the same groups of trajectories as a function of geopotential height (hPa) for the same longitudes as depicted in the map. Total days = 1095.

Table 2.8: Percentage of days and contribution to annual precipitation at SV site according to wind directions. Data obtained for the 2005-2007 time period, based on GFS and NCEP-NCAR data validated by observations at ground stations (see tables 2.6 and 2.7 for more details). This summary constitutes the basis for the interpretation of the ice archive of CL122.

	N	NE	E	SE	S	SW	W	NW
% days	2,7%	0,6%	0,5%	0,5%	3,6%	23,1%	50,7%	18,3%
% precipitation	2,5%	0,1%	0,0%	0,0%	1,1%	12,2%	61,0%	23,1%

conditions produce precipitation (>75%), mainly at coastal stations, but also at leeward stations (>50%). When SW transport takes place, precipitation is frequent on the coast (>65% of the cases) but rare at the continental stations (>25%). At the SV site, both NW and W transport (73.8%) bring moisture from atmospheric low-levels above the open ocean (height expressed as geopotential range from 600-900 hPa, fig.2.13). They account for 84% of the precipitation at SV.

NW and W transport can bring moisture for a wide latitudinal range of open ocean (20-70°S) over short periods, such as 3 days (not shown in fig.2.13, whereas SW transport do not come further ∼30°S (they would be blocked by the subtropical Pacific anticyclone), and thus do not substantially contribute to SV precipitation.

At the SV site, transport from the SW produce 2-times less precipitation than NW transport for a similar frequency of occurrence (see totals in table 2.7) as they come, in average, from the free troposphere, which is drier than lower-levels (RH∼57% vs. 70%). SW trajectories (not shown) coming from low-levels (∼800 hPa) are likely to bring precipitation while those coming from higher levels (∼600 hPa) are not as likely. SW precipitation account for 12% of precipitation at SV.

SW, N and NW transport take place all year round (table 2.7), but they bring less precipitation during DJF due to less cloudiness .

In contrast, transport with and easterly zonal component (E, NE, SE) at SV are very scarce (1.6% of the days, table 2.8) and they are associated with calmer weather conditions at the SV site: dry air and lower wind speed than westerly wind (6 to 9 $m.s^{-1}$). E, NE and SE transport

produces precipitation in most of the cases (>65%) at continental stations (∼5 mm per event) and in very few cases (<15% of the cases) at the coast. Occasionally (<0.5% of the cases), SE transport produces important precipitation events (∼12 mm) at coastal stations mostly due to the invoked wind tunneling effect between the Patagonian Icefields (notorious in the figures 2.2(a) and 2) that allows transport of moisture from the Argentinean Patagonia to the Pacific board. However, at the SV site, E/SE transport is associated with dry conditions (SH is around 0.0007 kg.kg^{-1}, RH∼30%) and do not produce precipitation (empty cases in table 2.7, 0% in table 2.8), likely because they come from the mid-level atmosphere (500-700 hPa).

Usually, NE, E and SE transport is the consequence of blocking events (stagnant synoptic conditions), with the blocking pattern located mostly westward the Andes. For instance, the blocking event lasting from 25/07/2006 to 28/07/2006 produced successively NE and SE transport at SV. It brought precipitation at Coyhaique and Balmaceda (20 mm in 4 days) and exceptionally to the SV site (10 mm in 4 days according to GFS, note however the low precipitation value) but not to coastal stations. This type of synoptic situation lasts a few days and it is associated with higher air temperatures than the seasonal average.

NE transport (SH=0.0015 kg.kg^{-1}, 58% RH), that take place seldom (0.6% of the days) and likely to occur in JJA, can bring precipitation at the SV site but accounting for less tan 1% of total yearly precipitation. Backtrajectories for these cases show that airmasses may come from lower-levels (900-700 hPa) and go upslope the Northern Patagonian Icefield.

Northerly transport (2.7% of the days) bring wetter airmasses than from the NE (SH∼0.0023 kg.kg^{-1}, RH∼70%, wind speed of ∼9 m.s^{-1}) and also transports marine moisture upslope the NPI from low levels (900-700 hPa). Precipitation associated with N transport accounts for 3% of total precipitation. Northerly transport produce more precipitation at continental stations than in coastal stations (65% vs. 50% of the cases) probably because the low level flux (850 hPa) remains blocked by the mountain massif. At the SV site, N transport would take place year round but precipitation events are more intense in SON (30 vs. ∼15mm.yr^{-1}). It is worth keeping in mind that the model output discussed here is for a coarse topography and real climatic

conditions may be different because wind flow may be deflected by the NPI foothills (which are not accounted for in the models) and thus and may not result in precipitation at the plateau of the SV.

Finally, Southerly transport (SH∼0.0008 kg.kg^{-1}, RH∼35%, wind speed of ∼9 m.s^{-1}) accounts for 3.5% of the arrivals. They bring moisture mostly from the mid troposphere (700-500 hPa) and produce precipitation in 60% of the cases in the continental stations and less frequently in the coastal stations: to Cabo Raper in 40% of the cases and to San Pedro in less than 20% of the cases. At the SV site, S transport is rather rare and occur during JJASON. They would be responsible only of 1% of total precipitation expected to fall in one year. Southerly/South Westerly transport can bring air masses from as far as the Amundsen Sea, near the Antarctic coast and can arrive with polar fronts sweeping the Patagonian plateau (Paruelo et al., 1998; Schneider et al., 2003).

In conclusion, low-level (600-900 hPa) westerly arrivals are the most common at the SV site because NW/W transport account for 84% of the precipitation. Conversely, easterly (E, SE, NE) arrivals are infrequent (1.6 %) and mostly dry. Southerly arrivals (SW, S) are drier, colder and they bring upper-level (400-700 hPa) polar air to the SV site, where they account for 12% of total precipitation. Northerly arrivals (N, 2.7%+ NE, 0.6%) would bring moisture and low-level tracers as they may go upslope the Northern Patagonian Icefield. Nevertheless, a caveat must be kept in mind: the SV site is located in the free troposphere and the backtrajectories do not account for mixing of air masses in the atmosphere, thus only a general path can be retraced and no precise start points of the retrotrajectories can be defined.

2.4.4 Long-term mean precipitation compared to 2005-2007 period and implications on accumulation hypotheses

This section aims to explore the feasibility of a very high net accumulation rate, as the mean net accumulation that was measured for the 2005-2007 period (3250 mm w.e.). For that period we use GFS predictions, and for the 1960-1990 period we use PRECIS data. We also compare

with the long-term annual mean precipitation (1960-1990, used as a reference for the regional climatology).

PRECIS predicts a long-term-mean precipitation at SV of 8000 mm.yr^{-1}and GFS predicts 4000 mm.yr^{-1}. Escobar et al. (1992) estimated 6700 mm.yr^{-1}for the NPI. The correct value of precipitation is difficult to assess since PRECIS has a better topography grid (0.25 km and SV height is ∼1200 m a.s.l. vs. 0.5 km and ∼900 m a.s.l. for GFS) whereas the GFS model depicts better precipitation variability (see sections 2.3.2 and 2.4.2). In any case, the 3250 mm.yr^{-1}net accumulation appears to be realistic if most of the precipitation has been conserved.

In figure 2.8 we present comparisons between the observed values of precipitation in 2005-2007 at the aforementioned stations and long term means obtained by averaging observations (squares marked as climatology), GFS outputs, and PRECIS long-term mean. The mean precipitation for the 2005-2007 period is in good agreement with the long-term mean of measured data, and thus in average, precipitiation conditions over 2005-2007 are not exceptional. In fig. 2.8, we observe that the GFS model is positively biased and overestimates precipitation, whereas PRECIS modeled climatology shows a larger incertitude, overestimating precipitation for Balmaceda and Cabo Raper and underestimating it at Coyhaique and San Pedro. Nonetheless, no aberrant values show up when comparing modeled data with observations showing the robustness of both models.

Thus based on both GFS and PRECIS models we can conclude that the SV site lies in a very rainy (snowy) environment, and high accumulation values should not be surprising if all precipitation has been conserved. As a first approximation, this may be the case for the first meters of the deep ice-core (CL122), i.e., after 2003-2005. The increase of the net accumulation observed for the recent years should be driven by ice flow combined with wind blowing and site topography (see more details in section 1.4.2 and figure 1.8).

We can indirectly explore whether these accumulation values are likely to be conserved by comparing the net accumulation outputs of PRECIS with other sites where glaciological measurements are available at the Patagonian Icefields (GFS data on net accumulation were not available). This is shown in figure 2.14 where reported glaciological measurements from table 2.1

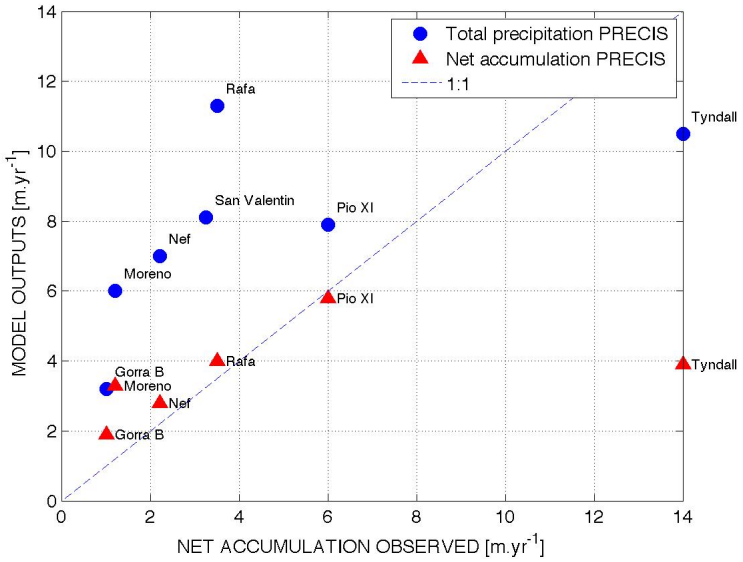

Figure 2.14: Comparison between precipitation and net accumulation obtained by PRECIS and glaciological measurements of net accumulation in the Patagonian Ice Fields. Blue dots represent total precipitation (solid+liquid) and red triangles, modeled net accumulation both obtained with PRECIS model (1960-1990 average). As the ablation is calculated by melting and no wind blowing effect is considered, the net accumulation for the SV is not reported here. Dashed line and x-axis correspond to net accumulation measurements of locations presented in fig.2.2(a) at the glaciers San Rafael (Yamada, 1987), Nef (Matsuoka and Naruse, 1999), Tyndall (Shiraiwa et al., 2002), Gorra Blanca (Schwikowski et al., 2006), Moreno ice divide (Aristarain and Delmas, 1993), Pio XI (nez 2008, pers. comm.) and San Valentin (3250 m.yr^{-1} for 2005-2007) . See table 2.1 for more details.

are compared with PRECIS predictions. Indeed, the PRECIS model is able to calculate ablation which accounts for melting and sublimation but not for wind blowing, which is not realistic for the SV case (whose topography is underestimated by ∼2000 m).

In fig. 2.14 we observe that the net accumulation for lower altitude sites is well represented by PRECIS.The eastern flank of the NPI is mountainous and produces precipitation depletion (Lopez et al., 2008) for glaciers located eastward the massif. The glaciers Nef 1500 m a.s.l., Gorra Blanca 2300 m a.s.l. and Moreno 2700 m a.s.l. are located leeward the massif, and they show smaller net accumulation values compared to westward located glaciers (San Rafael 1300 m a.s.l., Pio XI 2600 m a.s.l., Tyndall 1750 m a.s.l.). Thus, the PRECIS model captures fairly

well the behavior of Patagonian temperate glaciers: precipitation (Falvey, 2009b) and ablation (by melting and sublimation) are correctly estimated. The only exception is the Tyndall glacier, for which the net accumulation of 14 m.yr^{-1} (water equivalent) is underestimated by the model. This could be due to accumulation of redeposition of snow given the high wind speed measured at this site (15m.s^{-1} Shiraiwa et al., 2002).

For the SV site, melting is not likely to occur given the low borehole temperature measurements (annual mean temperature is approximately -10 °C) and sublimation should be negligible given the hindering of solar radiation due to its continuous cloud coverage, high moisture and air temperature. Other process, such as wind blowing, influence the net accumulation value at this site. Besides, it is worth noting that when ice particles are suspended by wind, their sublimation is enhanced (Pomeroy et al., 1997) and the PRECIS model does not account for this mechanism. For that reason we have not reported the net predicted accumulation by PRECIS in fig. 2.14

Wind blowing at SV is possible given the high permeability of the snow pack: no wet metamorphism nor important wind-packed snow layers protect the snow pack from blowing. At this site, precipitation and snow metamorphism take place under dry conditions (signs of wet metamorphism are only found at 2 and 14 m depth) and the wind-packed snow layers are thin (1-2 mm) and discontinuous. Similar conditions are found in an open prairie (Li and Pomeroy, 1997, Canada) where the measured minimum wind speed required to remobilize snow is 7.7m.s^{-1}. For SV, GFS data at 700hPa show that wind is above this value 76% of the time. Thus it is very likely that snow deposition associated with westerly stormy arrivals is remobilized and lost, and even snow previously deposited can be blown (eroded).

Therefore, ablation is certainly driven mostly by wind blowing. Wind blowing losses can take place all year round under a westerly wind flow. No snow blowing is expected under calm conditions, which take place seldom and mostly when the zonal wind is easterly, thus leading a conservation of these precipitation events in our glaciological register.

In conclusion, even if high accumulation rates are possible at SV (4000-8000 mm.yr^{-1}), for the 2005-2007 period (characterized by normal precipitation values at ground stations), a net

accumulation value of 3250 mm.yr^{-1}would only be explained by little wind blowing or by snow redeposit. The 2005-2007 period was not less windy than the 1990-1960 average (NCEP-NCAR data). A changing in the precipitation regime at this site could partially explain this, however, it is unlikely that precipitation changes from a factor 10 in few years. Thus, we argue that the SV drilling site was either sheltered by topographical effect that prevented wind losses or accumulated redeposited snow over this period.

Other net accumulation values (190, 330 mm.yr^{-1}) can be only explained by high rates of wind erosion. This lead us to confirm that there are local processes (likely the glacier flow) that govern these changes in the net accumulation observed along CL122.

Nevertheless, for a complete glaciological interpretation, it is important to keep in mind that geophysical mechanisms related to glacier flow can generate hiatuses on the register, and that may lead to the miscalculation of net accumulation rate (cf. section 1.4.2 of the previous chapter)

2.5 Conclusions

At the SV site, precipitation can range from 4000 to 8000 mm.yr^{-1}according to GFS and PRECIS predictions, respectively. To explain the change of measured values of net accumulation at this site: 190 mm.yr^{-1}for 1965-2005 (SV2005 core Vimeux et al., 2008), 330mm.yr^{-1}1965-1987 (Herreros, 2010), 3250 mm.yr^{-1}for 2005-2007 (CL122, this study), we can conclude that ablation is certainly not driven by melting nor sublimation, but driven mostly by wind blowing, probably in a combination with ice flow and site topography.

Periods with important precipitation at SV turn out to be the intermediary seasons: spring (SOND ∼1900 mm) and fall (MAM, 1900 mm), with precipitation events associated mostly with northwesterly flow. In contrast, summer (DJF) is the less rainy season (1200 mm), partly related to a lower cloudiness in january and february than in the rest of the year (Vimeux et al., 2011). Wintertime (JJA) precipitation (1800 mm) takes place under a wider range of wind directions than in the other seasons, including more frequent S/SW transport.

It seems that summer precipitation (DJF) is not the most conserved, firstly due to the

occurrence of modest precipitation events (<20 mm) and also due to a strong wind blowing that may erode the deposited snow. Summertime snow blowing can also erode older snow, namely part of springtime contributions. Conversely, wintertime events (JJA) are likely to be better conserved since they are associated with weaker winds are more frequent at this season.

JJA calm conditions are associated with SE, E and NE flow, which usually does not bring precipitation, thus favoring dry deposition of continental markers. As marine contributions seem to be underrepresented, we conclude that although rare, continental chemical markers associated with eastward transport are likely to be well conserved in the SV ice archive. We are aware though that the backtrajectories calculations are less accurate under blocking conditions (this is confirmed by the divergence of 10% of the cases when comparing ERA-Interim and NCEP-NCAR datasets).

Winter (JJA) and spring (SON) are characterized with more frequent Southerly and Northerly transport and produce respectively 1.1% and 2.5% of the total precipitation at the SV site. Northerly transport brings moisture from low levels (900-700 hPa) probably incorporating dust or other emissions from the arid regions close the NPI or even further subtropical locations (40°S). Southerly transport brings airmasses from higher levels (500 hPa) and that can come from remote locations such as the circumantarctic region.

Westerly zonal flow (NW, W, SW) brings 92% of precipitation at the SV site, entraining Pacific Ocean moisture from low levels (600-900 hPa). Since NW, W, SW contributions take place year round, we should expect an important contribution of marine sources to the ice core record. But this is not the case, as we will see in chapter 3, which leads us to an oversampling of continental events (cf. chapter 4) as suggested by weaker zonal wind during Northerly and Southerly transport (and thus a better conservation of snow layer as mentioned above).

Cyclonic circulation is very effective to suspend Patagonian dust (Iriondo, 2000), and other continental tracers to the troposphere, thus creating a reservoir of a wide variety of species of continental origin (anthropogenic pollution, dust and forests emissions, biomass burning). The location of the SV in the free troposphere favors the mixing of stratified westerly flow (containing

marine aerosol) with this continental reservoir.

All that provided reliable arguments to sustain the hypothesis of Vimeux et al. (2008) that the SV core contains an important register of continental contributions.

To resume, we propose the following for the interpretation of our ice-core:

- The ocean is the main source of moisture, thus an important marine signature is expected.
- The circulation changes affects air masses only 2 days prior to their arrival to the SV site. These 2 days would be the period when a strong continental effect changes the chemical and isotopic composition of the initially marine air masses.
- This site lies in a very rainy environment, thus high accumulation rates are possible even without accounting for snowdrift.
- A continental wet contribution is expected for N, NW, S flow mostly in spring and autumn
- Continental dry deposit can take place under NE, E, SE flow, although seldom and according to our calculations, only in JJA.
- The glaciochemical record of the SV should be interpreted in terms of event types, associated with wind direction arrivals.
- Chemical/isotopic signals must be interpreted carefully since wind losses and ventilation effects can be important at this site.

Chapter 3

Marine contributions to San Valentin ice

3.1 Motivations

As discussed in chapter 2, air masses arriving to the San Valentin site from the SW-NW range would be associated with the most important precipitation events, especially in spring and fall. Thus, the Pacific Ocean is obviously the main source affecting this altitude site, and its influence is examined in the following sections in terms of primary and secondary marine aerosol contributions. In theory, precipitation associated with these transport directions should account for ∼96% of the ice archive. Our objective is to quantify the different marine contributions to test the representativeness of this site in terms of a marine archive.

Along the shallow core (SV2005), it was observed that marine primary aerosol arrivals, traced by Na^+, alternate with continental arrivals, traced by $nssCa^{2+}$. Here we identify different kinds of sea salt arrivals and we determine their characteristics. Then, we also characterize secondary marine aerosol arrivals, traced by methanesulfonate (MS^-) (Legrand and de Angelis, 1995). We discuss primary and secondary marine aerosol arrivals in relation with other chemical species (Na^+, Cl^-, Br^-, SO_4^{2-}, K^+, Ca^{2+}, carboxylic acids) and the isotopic composition of ice (oxygen-

18 and deuterium and for selected samples we also include microalgal biovolumes and SEM data.

Raw concentrations inμeq.L^{-1}have been presented in chapter 1. Depth was expressed in m (real depth). In the following, and to counterbalance the influence of snow densification depths, depth will be expressed in meters of water equivalent (m w.e.). We discuss here only ionic profiles along the first 52 m w.e. (73 m of CL122, i.e. the part of the core located above the brittle zone). We include the high-resolution isotope dataset obtained at the LAMA (δD , δ^{18}O and deuterium excess from Herreros, 2010) for the first 33 m w.e. (50 m) of CL122, and microalgal biovolumes obtained at the CECS over the upper 2.8 m w.e. (6m) of a neighboring shallow core (CC2).

In section 3.2 we present a review of the proxies used, in section 3.3 the methodology to identify and to statistically characterize marine contributions along the CL122 core. In section 3.4 we present the results of this characterization and a comparison with data from other sites, water stable isotopes and we discuss them in terms of atmospheric circulation / seasonality to finally conclude in section 3.5.

3.2 Introduction

3.2.1 The oceanic contribution in terms of chemical tracers

Whereas marine primary aerosol (dominated by Na^+, Cl^-, SO_4^{2-}, K^+, $Mg^{2+}$and Ca^{2+}) is produced by bubble bursting processes occurring at the surface of the ocean, secondary biogenic aerosol is produced by the oxydation of gaseous species emitted by the phytoplankton.

Marine primary aerosol contains large amounts of chloride compounds. However its initial composition may be altered by chemical reactions occuring during transport and leading to chloride losses. Indeed, marine primary aerosol can act as a support for heterogeneous reactions involving acidic gases. It has extensively been observed that chloride in marine primary aerosol can be removed by strong acidic compounds (see for instance Legrand and Delmas, 1988; Ker-

minen et al., 1998; Song and Carmichael, 1999). Chloride is emitted as HCl, Cl_2, HOCl and $ClNO_2$. The three latter are rapidly converted to HCl following photolysis and H-abstractions with hydrocarbons (Graedel and Keene, 1995). Thus, the mechanism leading to chloride losses from marine primary aerosol can be summarized as follows:

$$HA + NaCl \rightarrow NaA + HCl \tag{3.1}$$

Where HA stands for H_2SO_4 (Legrand and Delmas, 1988; Kerminen et al., 1998), HNO_3 (Pakkanen et al., 1996; Kerminen et al., 1998) or methanesulfonic acid (MSA) (Kerminen et al., 2000).

Part of phytoplankton emissions is transformed into dimethylsulfide (DMS) in the atmosphere, which is in turn oxidized into MSA and SO_2 following different reaction pathways. The latter is then transformed in sulfuric acid (found as SO_4^{2-}in the aqueous phase). MSA formation takes place preferentially at lower temperatures than SO_2 and at different altitudes (see Finlayson-Pitts and Pitts, 2000, for a review of reaction mechanisms). DMS is almost exclusively produced by marine biota (96% of the global DMS burden, as calculated by (Gondwe et al., 2003). Note that whereas MSA is only produced by DMS oxidation, SO_4^{2-}can have other anthropogenic or natural sources including combustion and volcanism. In remote marine atmosphere, methanesulfonate (MS^-) and the part of sulfate not associated to marine primary aerosol (called non-sea-salt sulfate, $nssSO_4^{2-}$) can be used as tracers of phytoplankton blooms, that in turn depend on the location of nutrients and the seasons (see fig.3.1 for an example). The MS^-:$nssSO_4^{2-}$ratio increases towards higher latitudes in summer because colder temperatures favor MS^-production by OH, and it has typically a summer maximum and a winter minimum at high southern latitudes (Bates et al., 1992; Leck and Persson, 1996; Legrand and de Angelis, 1995).

Phytoplankton emits other volatile organic species, such as unsaturated fatty acids that are transformed to dicarboxyilic acids (Kawamura et al., 1996) from which succinate (C4) and oxalate (C2) dominate over azelaic (C9), adipic (C6) and malonic (C3) acids, and to monocarboxylic

acids such as formate (C1), acetate (C2) and propionate (C3) (Arlander et al., 1990). As a general rule, monocarboxyilic acids are found preferentially in the gas phase while dicarboxylic acids in the aqueous and aerosol phases (Chebbi and Carlier, 1996).

Oceanic emissions also include ammonium NH_4^+(15% of the global NH_4^+burden according to Bouwman et al., 1997), as evidenced by aerosol and ice-core measurements in coastal Antarctic sites not influenced by penguin excreta emissions (Neumayer, Berkner Island, D10, South Pole, according to Legrand et al., 1998). While individual species (NH_4^+, MS^-, $nssSO_4^{2-}$) peak in summer, the season where phytoplankton blooms occur, the ratio $NH_4^+/(MS^-+nssSO_4^{2-})$ has a winter maxima. The authors explained this feature by 1) uncertainties of winter MS^-+ $nssSO_4^{2-}$calculations 2) a winter $nssSO_4^{2-}$contribution from marine biogenic sources located farther north 50 °S. This ratio is approximately 2.5 % weight (13 % molar) for central Antarctic locations and 7-8% weight in Neumayer, where NH_4^+a continental influence may be present.

In figure 3.1 we present the seasonal variations of DMS, $MS^-$and total sulfate fluxes, obtained with the climatic-chemical coupled model MOCAGE (Peuch, 1999) for the Southern hemisphere (south of 20°S) and averaged over the 2000 to 2005 period (simulation number 11, Ménégoz 2010, pers. comm.). This model uses the AEROCOM inventory Dentener et al. (2006) for emissions. It has been demonstrated that the year-to-year variability of the atmospheric content of MSA and marine biogenic SO_4^{2-}(and expectably other species) depends mostly on climatic variability (Ménégoz, 2009). For this reason, figure 3.1 does not have to be considered as an absolute reference of the total column content of these species but only as a geographical reference of major MSA and SO_4^{2-}production zones in the Southern Hemisphere.

Figure 3.1 shows that DMS maximum production takes place in summer around Antarctica with noticeable regional maxima in Amundsen, Bellingshausen and Weddell seas. Fall (MAM) sources of DMS are located in the South Indian and South Pacific Oceans, with a regional maximum near the Chilean coast along 30-50°S. Significant winter production is limited to the Chilean coast, with a maximum shifted equatorward compared to fall production. Finally, springtime sources are sparse and emit 4-5 times less DMS than summertime sources. They are

located between 30-50°S with regional maxima located in the Tasman Sea, South Eastern and Western Atlantic Ocean. Note that the Pacific Ocean shows no important phytoplankton blooms in this season other than the already identified band along the Chilean coast.

MSA production takes place in the atmosphere and follows phytoplankton blooms traced by DMS, although more widely distributed. In summer, MSA maximum concentrations are found in the circumpolar belt (50-70 °S) and in the subtropical Eastern South Pacific. In fall, maximum MSA concentrations are located over the subtropical Eastern South Pacific and in a circumpolar band (30-50 °S) showing concentrations 2-times lower than summertime maximum. A weak winter MSA production is observed only close to the tropics. springtime production is rather homogeneously distributed in the Southern Hemisphere with values 3 to 4 times lower than in summertime. A regional maximum is observed along the northern Chilean coast.

Although the AEROCOM inventory remains lacunary for South American countries (as all current inventories, Lamarque et al., 2010), sulfate emissions are dominated by anthropogenic sources and pollution transports follow the general eastward circulation pattern. Nevertheless, sulfate concentrations over most of the Pacific Ocean are unsignificant in winter and spring, likely due to very efficient wet deposition processes leeward of the sources. Maximum biogenic sulfate production seems to follow DMS production in summer and to a lesser extent in fall.

3.2.2 Water stable isotopes

Water stable isotopes (oxygen-18 and deuterium) are widely used to study atmopsheric water cycle and to accurately reconstruct past temperature variations in high latitude environments (Jouzel et al., 2007).

The enrichment or depletion in heavy water molecules relatively to the international standard V-SMOW (Vienna Standard Mean Ocean Water) is expressed as:

$$\delta = (R_{sample}/R_{standard} - 1) \times 1000 \tag{3.2}$$

where R = (X*/X) where * stands for heavy molecules

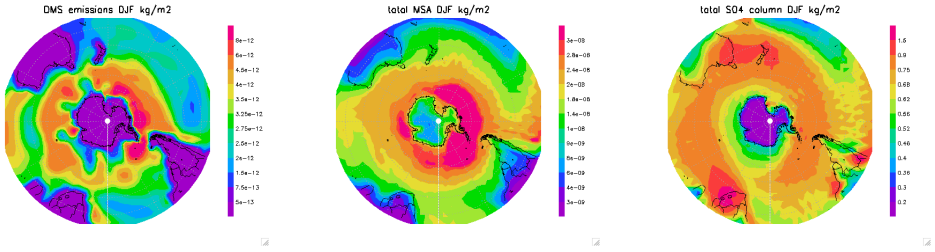

(a) DMS - MSA - SO_4^{2-}distributions in summer (DJF)

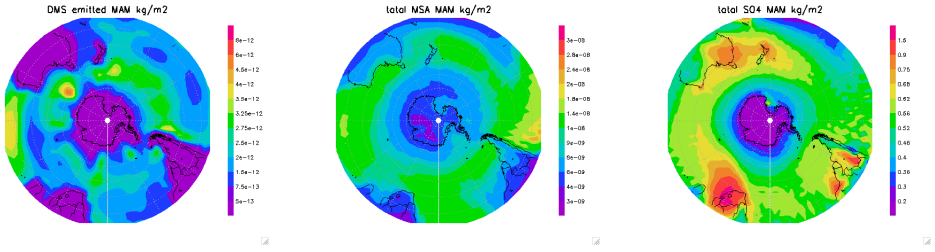

(b) DMS - MSA - SO_4^{2-}distributions in fall (MAM)

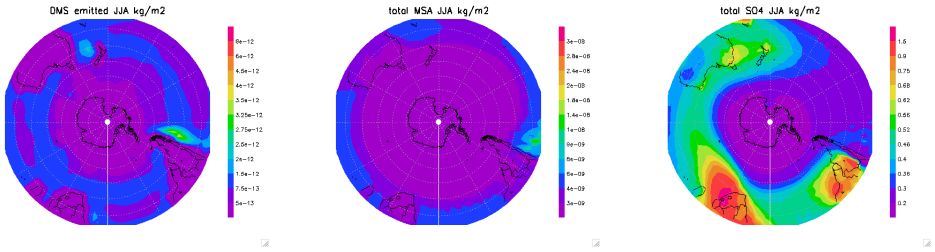

(c) DMS - MSA - SO_4^{2-}distributions in winter (JJA)

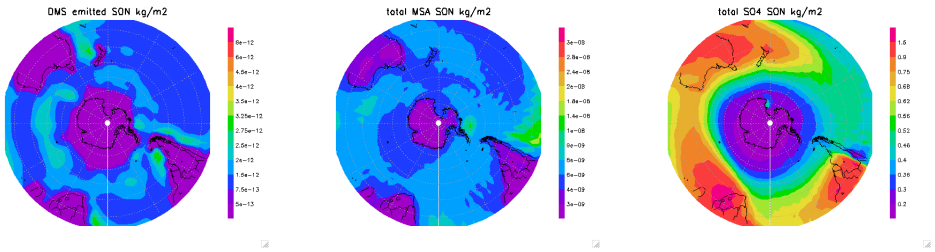

(d) DMS - MSA - SO_4^{2-}distributions in spring (SON)

Figure 3.1: DMS, MSA, sulfate mass concentrations integrated over the atmospheric column. Seasonal variations were obtained from the outputs of the MOCAGE climatic-chemical model, averaged for the 2000 to 2005 period (Ménégoz 2010, pers. comm.). The graphics here are intended to be a reference of DMS sources location and MSA and SO_4^{2-}total columns and should not be taken as absolute reference, since year to year variability in the oxidation of DMS into MSA and $SO_4^{2-}$is governed by climatic variability (Ménégoz, 2009). Left: DMS emitted ($kg.m^2$). Center: Total MSA column ($kg.m^2$) Right: Total SO_4^{2-}column ($kg.m^2$).

We will use δD measurements at SV ice to retrace the regional temperature. We will also use the second order parameter, deuterium excess (Dansgaard, 1964), defined as:

$$d = \delta D - 8 \times \delta^{18}O \tag{3.3}$$

This parameter depends on kinetic fractionation occurring during airmasses history, mainly the evaporation from oceanic surface and snow formation (Merlivat and Jouzel, 1979; Jouzel and Merlivat, 1984). Multiple processes can influence d. However, here, we will assume that a positive linear relationship exists between d and the mean oceanic source temperature, mimicking the interpretation of d in polar ice cores (Vimeux et al., 1999) as the water atmospheric cycle is not so different from an isotopic fractionation point of view between mid-latitudes and the poles. We are aware that in this regard we formulate an important hypothesis that will need to be addressed in future work. Therefore, in SV ice, high d values have been related to transport of marine air masses from Pacific with a moisture source at mid-latitudes whereas lower d values have been related to airmasses originating southward, in polar regions (Vimeux et al., 2008). Post-depositional effects affecting deuterium excess have been neglected: actually, no melting in surface is pointed out by water isotopes (Herreros, 2010) and we are not able to relate the few ice layers found in the CL122 core with specific deuterium excess values.

3.3 Methodology

The methodology described here was used for all chemical species considered as potential source markers.

3.3.1 Data distribution and peak definition

First we have removed the few unexplainable outliers found in chemical depth profiles (extremely high values in one single sample not explained by contamination or correlation with other species) and drawn the frequency distribution for all chemical species (cf. chapter 1). Concentration

distributions follow a Weibull distribution (cf. appendix 188), however, we use statistics corresponding to normal (Gaussian) distributions for simplicity and because corresponding tools are commonly available. Ionic profiles show peaks of variable amplitude that have been classified in major and minor peaks according to the following definitions:

- For a given ion X, we define a major peak as a contiguous group of samples flanked by relative minima and that contains at least one sample with concentration given by equation 3.4

$$C \geq m + s \tag{3.4}$$

  where:

  C = concentration of the ion X in the sample

  m = mean concentration of X calculated over the first 52 m w.e. of the profile

  s = standard deviation of X calculated over the first 52 m w.e. of the profile

- We define a minor peak as a contiguous group of samples flanked by relative minima that contains at least one sample with concentration given by equation 3.5 and that does not contain any samples comprised in a major peak

$$m + s > C \geq min \tag{3.5}$$

  where:

  min = mean of the minimum values of 10-sample bins in the data (the average of minimum values extracted every 10 contiguous samples along the profile)

- Consequently, the remaining samples, considered as covering background emission for X, are defined by eq. 3.6

$$Background < min \tag{3.6}$$

Samples remaining after having removed significant marine signals constitute the register of continental contributions that will be addressed in the following chapter. Note that only major MS^-contributions are observed along the SV core so that the definition of MS^-minor peak is irrelevant.

Mean values used in this chapter for the identification of $Na^+$and MS^-peaks are presented in table 3.1.

Table 3.1: $Na^+$and MS^-mean concentration, standard deviation and the averaged minimum values along the first 52 m w.e. of the deep core.

	m	**s**	**min**
	μeq.L^{-1}	μeq.L^{-1}	μeq.L^{-1}
Na^+	1.350	4.280	0.314
MS^-	0.022	0.032	0.009

3.3.2 Correlation matrices and species ratios

The three groups of samples corresponding to major peaks, minor peaks and background values of X, respectively, are characterized statistically through correlation matrices and concentration ratios of ions of interest. Correlation matrices and ions$'$ ratios are calculated sample by sample, but we are aware that statistical calculations can be biased by deposition artefacts and/or post depositional effects (e.g. ions diffusion) in the ice.

3.3.3 Non-sea-salt contributions

As cyclonic circulation favors Pacific Ocean contributions to the SV site (and given that halite sources from arid zones of South America lie more than 1600 km farther north), the marine primary aerosol contribution can be traced by Na^+concentrations (Keene et al., 1986).We calculate

the non-sea-salt (nss) contribution of ions other than sodium according to:

$$nssX = [X] - (X/Na)_{bsw} \times [Na^+] \tag{3.7}$$

where: nssX= non sea salt fraction of ion X

[X]= concentration of X in snow

$(X/Na)_{bsw}$ = X to Na^+ratio in bulk sea water (reference values from Keene et al., 1986)

$[Na^+]$ = sodium concentration in snow (or ice)

Negative values of nssX imply either that part of X is lost when marine aerosol is formed (e.g. Wagenbach et al. (1998) observed this for sulfate in winter Antarctic aerosol, when mirabilite losses occur at temperature lower than -8°C), or the existence of another sporadic source of sodium leading to overestimate the marine component of X. Negative values are not included in correlations or ratios calculations.

HCl arrivals or chloride depleted marine primary aerosol reaching the SV site may respectively increase or decrease snow concentrations of Cl^-compared to the contribution expected from the marine primary emission alone. The corresponding amount, called excess chloride and denoted $Cl^-_{exc}$is calculated in the same way as other non sea salt components but may be effectively positive or negative (the latter retracing chloride depletion).

3.3.4 Ionic balance

The snow acidity given inμeq.L^{-1}can be calculated from the ionic balance and it is defined as:

$$H^+ = \Sigma anions - \Sigma cations \tag{3.8}$$

It has been demonstrated (Delmas et al., 1992; Legrand and de Angelis, 1995) that in slightly acidic snow (H^+>0), the snow acidity may be valuably estimated by H^+. This will be the case for the SV ice core, where pH was not measured.

3.4 Results

3.4.1 Primary aerosol

Data concerning Na^+major and minor peaks are summarized in table **??**. Na^+major contributions (32 peaks) represent 6.4 m w.e. corresponding to 12.2% of the studied core section whereas minor contributions account for 8.9 m w.e., i.e., 17.1% of the core section.

Table 3.2: Number of samples, N (out of 3882) and their total contribution to the first 52 m w.e. of the deep core in meters of water equivalent and in percentage, for Na^+major and minor peaks and MS^-narrow and wide peaks.

	N	**Sum (m w.e.)**	**%**
Na^+major peaks	505	6.364	12.2
Na^+minor peaks	680	8.891	17.1
Na^+(total)	1185	15.455	29.3
MS^-associated with $Na^+$and Ca^{2+}	282	3.788	7.3
MS^-wide	301	4.033	7.7
MS^-(total)	583	7.812	15.0

In the previous chapter we have estimated that ∼96% of precipitation at SV site is expected to have an oceanic origin (61% due to westerly transport + 23% NW + 12% SW). In contrast, precipitation containing an important marine salt contribution, as recorded in the ice-core by adding all the layers containing Na^+major and minor contributions, corresponds only to 29% of the ice thickness. This confirms that wind erosion strongly influences the net snow accumulation rate and that our register does not represent the real precipitation distribution in terms of moisture origin: influences other than westerlies are very likely over-represented in the ice core.

3.4.1.1 Na^+major arrivals (major peaks)

In ice-cores studies, concentration peaks are generally associated to seasonal maxima (Legrand and Mayewski, 1997). At the SV site wind blowing certainly induces changes in net snow accumulation rates between upwind and downwind zones of the summit area. Thus, the net accumulation variability (observed in the CC4, CC5, CL122, SV2005 cores), depends on the area

where the snow was initially deposited. Net accumulation values significantly higher than 1 m w.e. may be observed (for instance the 2005-2007 time period along CL122) while the mean value calculated along the 2005 shallow core (1965-2005) is only 0.19 m w.e. Moreover, in CL122 we observe that some major Na^+peaks span ∼0.50 m w.e. depth (see for instance peak number 27 in 3.2), which is larger than the mean net accumulation measured along the shallow 2005 core. Finally, mid-latitudes weather is mostly governed by synoptic conditions at a timescale of few days, and storms take place under strong zonal wind (westerly) conditions. All these considerations led us to interpret Na^+peaks as punctual events rather than seasonal markers and to suggest that they are tracers of the occurrence of heavy storms, i.e., moist conditions in this site.

The occurrence of marine storms can be related to specific seasons (september to may), thus the record of marine storms might indirectly retrace seasonality at SV site. In figure **??** we present Na^+, NH_4^+, Cl_{exc}^-, nss$SO_4^{2-}$and MS^-concentrations corresponding to Na^+major and minor peaks. Major Na^+peaks are depicted in black, whereas minor Na^+peaks are depicted in orange. Heavy precipitation events produced by strong marine storms, can be conserved as Na^+single peaks spanning 0.15 to 0.50 m w.e. (i.e., a precipitation event of 150-500 mm). These values exceed the maximum precipitation rate per event predicted by the GFS model for the SV site (65 mm in MAM).

Major peaks are unevenly distributed along the first 52 m w.e. of the ice-core. They are more frequent, taller and wider along the first 10 m w.e., between 26 and 35 m w.e. and between 47 to 52 m w.e.; they are scarcer, shorter and generally narrower between 10 and 20 m w.e. and between 35 and 42 m w.e.; finally no significant peaks are observed between 20-26 and 42-47 m w.e.. This heterogeneous distribution along CL122 does not reflect the expected imprint of climatic conditions at this site: westerly storms are frequent at this latitude (cf. chapter 2) and the fact that we find large zones deprived of Na^+peaks reflects accumulation processes leading to a loss of large part of marine events. On the opposite, layers containing frequent and wide peaks may originate from over-accumulating zones (the first 10 m w.e. and between 26 and 35

m w.e.).

Cyclonic systems at open ocean can produce fast uplift of air masses, transporting coarse mode marine aerosol from the marine boundary layer (Covert et al., 1996, 900 hPa over the South Pacific) up to the free troposphere. At Torres del Paine National Park (51°S south of SV location) (Galloway et al., 1996), it has been observed that Na^+concentrations in precipitation are higher in spring in relation with increased wind speed. The strongest precipitation events predicted at SV would take place during the transition seasons (MAM, SON cf. fig. 2.11 on page 67). Thus major wet deposition of primary marine aerosol would take place preferentially in fall (MAM) or spring(SON). Assuming that the observations of Galloway et al. (1996) are valuable at the SV latitude, maximum Na^+concentrations could be spring markers. Peak maxima concentrations at SV are generally close to 20 and 30μeq.$L^{-1}$for $Na^+$and Cl^-, respectively, which is in the same range as data from a lower altitude site, Pio XI glacier (2900 m a.s.l., maximum $Cl^- = 20\mu$eq.L^{-1}, (Schläppi et al., 2009) suggesting that both sites intercept the same marine environment.

However, a few Na^+peaks (located at 9.7, 41.3 and 60.3 m w.e.) contain very high concentrations of $Na^+(Cl^-)$, close to 100 (112)μeq.L^{-1}. These extreme values are close to maximum values measured in firn cores retrieved in Antarctic Peninsula (Simões et al., 2004, 120μeq.$L^{-1}$for Cl^-at Lange Glacier, 690 m a.s.l., less than 10 km from open ocean,) and in the Southern Patagonian Icefield where Na^+can be higher than 130μeq.$L^{-1}$and Cl^-higher than 300μeq.L^{-1}(Shiraiwa et al., 2002, Tyndall glacier 1756 m a.s.l., 150 km from open ocean,). See figure 2.2 (45) for the location of the above mentioned glaciers. Such high concentrations at SV are puzzling. A tentative explanation may involve strong storms combined with long living clouds precipitating only at high altitudes. As observed at higher latitudes, mixed phase clouds are frequent in spring and fall and their life time is longer than for single phase clouds (Prenni et al., 2009). SV is located above the freezing level, 750 hPa (Smith and Evans, 2007), and is certainly influenced by mixed phase clouds where washout remained moderate allowing precipitation to entrap large amounts of marine primary aerosol.

Cl^-_{exc}/Cl^-(eq.eq $^{-1}$) ratios corresponding to highest Na^+concentrations in Na^+major peaks

(i.e., values of $Na^+ > 1\mu eq.L^{-1}$) ranges from -0.30 to 0.45 and the median value is -0.05 (i.e., 5%). As chloride replacement is produced by heterogeneous reactions taking place at the aerosol surface, its relative importance is expected to increase with aerosol aging and to be also dependent on the surface to volume ratio of aerosol: the smaller the particle the higher the loss of chloride. For instance, Antarctic aerosol measurements (Aboa, western Queen Maud Land, 500 m a.s.l., 150 from open ocean) show chloride replacement rates ranging from -0.67 to -1.0 for particles of 4.5-8.6μm and from -0.15 to -1.0 for particles of 0.8-1.1μm (Kerminen et al., 2000). The low values observed at SV point then to the fast transport of relatively large marine aerosols to this high altitude site.

In figure 3.2(b) we present an example of the composition of Na^+major peak, where we can observe the relationship between $Na^+$and Cl^-_{exc}in more detail (red arrows): Na^+maxima correspond to slightly Cl^-depleted values and are surrounded by $Cl^-_{exc} > 0$ in the peak′s tail (i.e., when $Na^+ < 1\mu eq.L^{-1}$). This phenomenon may suggest that air masses arriving under calmer conditions at the beginning or at the end of stormy events contain marine aerosol along with HCl provided by a tropospheric reservoir of continental (as discussed in the following chapter) or marine origin leading to positive Cl^-_{exc}values. On the opposite, stronger winds occurring during the most intense phase of the storm provide the site with marine air masses containing freshly produced primary aerosol slightly chloride depleted ($Cl^-_{exc} < 0$). Note that this behavior is not found in Na^+minor peaks (fig. 3.2(c)) and would be only associated with strong marine storms.

The detailed study of inter ion relationships in samples corresponding to Na^+major peaks allows to better investigate the composition of marine primary aerosol at SV. Correlation matrix is presented in table 3.3, and ratios between significantly correlated elements (r>0.6) are shown in table 3.4.

Cl^-, Br^-,$K^+$and Mg^{2+}show a strong correlation (r>0.85) not only with Na^+but also among each other and their respective ratios to $Na^+$are in good agreement with reference values for marine primary aerosol (table 3.4)

$SO_4^{2-}$is quite well correlated with Na^+, Cl^-, Br^-, K^+, $Mg^{2+}$and Ca^{2+}(r>0.75). This high

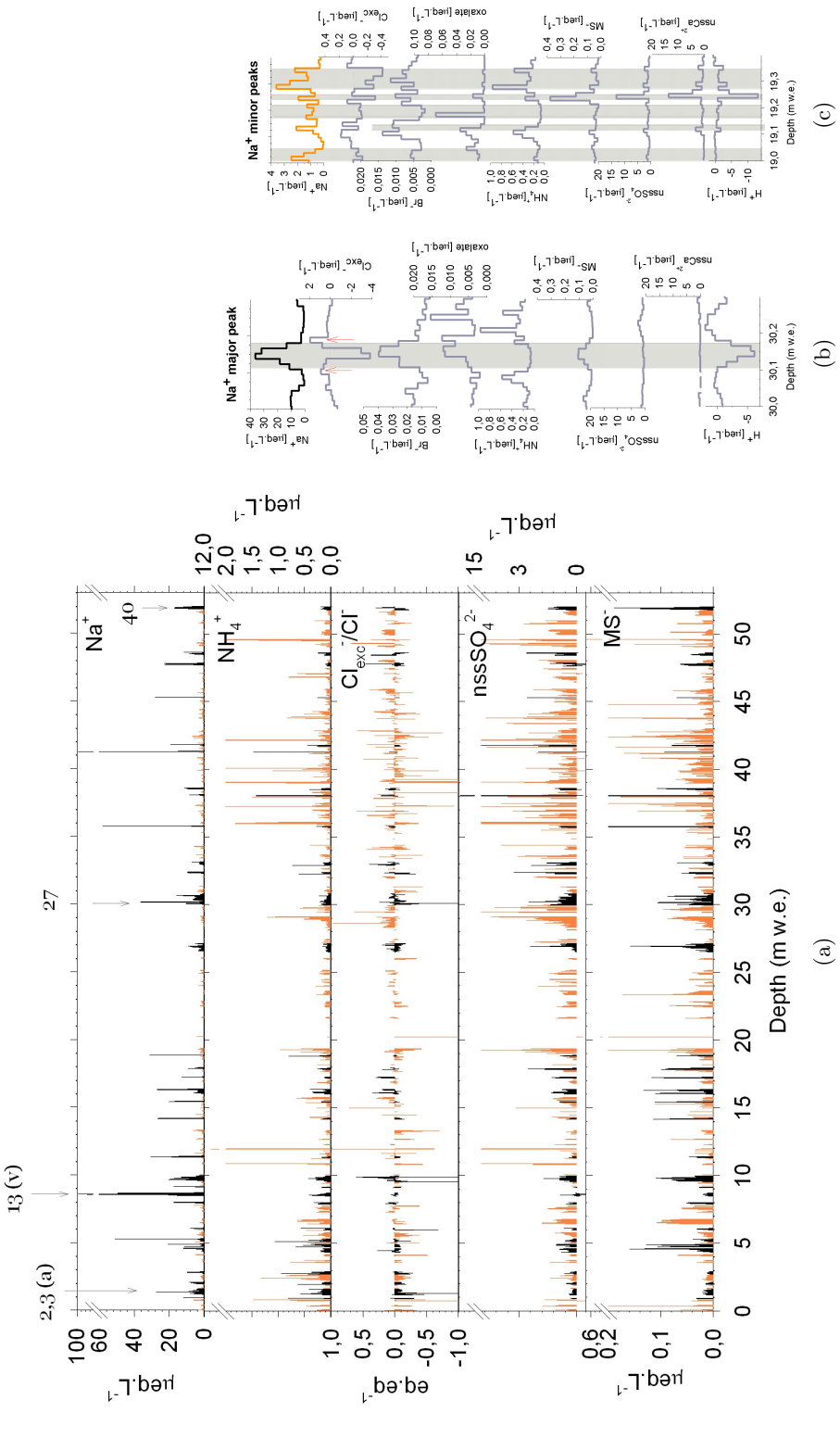

Figure 3.2: (a) Na^+, NH_4^+, Cl^-_{exc}, $nssSO_4^{2-}$ and MS^- distributions for the first 52 m w.e. of the CL122 ice-core. Values associated with Na^+>m+s are depicted in black (40 peaks), whereas values associated with sodium concentrations in the range m+s>Na^+>0.31μeq.L^{-1} are depicted in orange. Major Na^+peaks number 2 and 3 are associated with algal inputs (cf. section 3.4.1.3), peak number 13 corresponds likely to a mixed marine and volcanic input (cf. section 3.4.1.2) and peak number 27 is associated with a NH_4^+major peak (cf. section 4.4.2.2). (b) An example of a major Na^+peak (shaded zone) . (c) An example of a minor Na^+peaks (shaded zones).

Table 3.3: Correlation matrices for the first 52 m w.e. of CL122 for **(a)** Na^+major peaks and **(b)** Na^+minor peaks. See section 3.3 for details on the definition of Na^+peaks.

(a)	Na^+	Cl^-	Br^-	K^+	Mg^{2+}	Ca^{2+}	MSA	SO_4^{2-}	NH_4^+	NO_3^-	Oxalate	Succinate	Cl_{exc}^-	$nssSO_4^{2-}$
Cl^-	**1,00**													
Br^-	**0,88**	**0,90**											Color code	
K^+	**0,96**	**0,97**	**0,88**										**r□|0,60|**	
Mg^{2+}	**0,92**	**0,95**	**0,91**	**0,93**									|0,60|□r>|0,40|	
Ca^{2+}	0,39	0,38	0,39	0,45	0,35								|0,40|□r>|0,30|	
MSA	0,27	0,25	0,19	0,32	0,24	0,58								
SO_4^{2-}	**0,77**	**0,77**	**0,76**	**0,80**	**0,76**	**0,73**	0,55							
NH_4^+	0,09	0,09	0,16	0,15	0,10	0,36	0,22	0,36						
NO_3^-	-0,06	-0,07	0,05	-0,03	-0,08	0,29	0,11	0,25	0,32					
Oxalate	0,02	0,02	0,10	0,12	0,03	**0,73**	0,52	0,53	0,49	0,31				
Succinate	0,07	0,07	0,11	0,18	0,06	**0,60**	0,49	0,46	0,33	0,22	**0,75**			
Cl_{exc}^-	-0,59	-0,53	-0,33	-0,49	-0,30	-0,30	-0,36	-0,45	-0,08	-0,01	-0,03	-0,08		
$nssSO_4^{2-}$	-0,08	-0,08	0,05	0,02	0,00	**0,65**	0,52	0,57	0,44	0,48	**0,80**	**0,63**	0,07	
H^+	-0,34	-0,31	-0,20	-0,33	-0,26	-0,52	-0,32	-0,21	-0,10	0,33	-0,12	-0,12	0,51	0,10

(b)	Na^+	Cl^-	Br^-	K^+	Mg^{2+}	Ca^{2+}	MSA	SO_4^{2-}	NH_4^+	NO_3^-	Oxalate	Succinate	Cl_{exc}^-	$nssSO_4^{2-}$
Cl^-	**0,95**													
Br^-	0,30	0,34											Color code	
K^+	0,20	0,10	0,18										**r□|0,60|**	
Mg^{2+}	**0,82**	**0,84**	0,39	0,10									|0,60|□r>|0,40|	
Ca^{2+}	0,15	0,16	0,26	0,14	0,28								|0,40|□r>|0,30|	
MSA	0,15	0,08	0,09	0,06	0,13	0,46								
SO_4^{2-}	0,14	0,16	0,40	0,38	0,33	0,56	0,27							
NH_4^+	-0,02	-0,02	0,25	0,58	0,08	0,16	0,06	**0,69**						
NO_3^-	-0,01	0,05	0,45	0,52	0,12	0,37	0,15	**0,69**	**0,76**					
Oxalate	0,01	-0,01	0,18	0,56	0,11	0,19	0,08	**0,61**	**0,75**	**0,63**				
Succinate	0,02	0,00	0,18	**0,64**	0,07	0,08	0,04	0,55	**0,74**	**0,62**	**0,77**			
Cl_{exc}^-	-0,35	-0,03	0,06	-0,35	-0,10	-0,02	-0,23	0,02	0,00	0,15	-0,08	-0,06		
$nssSO_4^{2-}$	0,05	0,07	0,37	0,37	0,25	**0,55**	0,26	**1,00**	**0,70**	**0,69**	**0,61**	0,56	0,06	
H^+	-0,14	0,01	0,24	0,00	-0,01	-0,34	-0,17	**0,45**	0,35	**0,44**	0,30	0,35	0,45	0,46

Table 3.4: Median, mean and standard deviation of the concentrations of selected species and species ratios sorted out by event type. Mean concentrations of Na^+, Ca^{2+}, $H^+$are given in μeq.L^{-1}. $Cl^-_{exc}/Cl^-$and other concentration ratios are given in eq.eq $^{-1}$except for the MS^-:nssSO_4^{2-}ratio, which is given in molar units (the latter to facilitate comparisons with aerosol measurements that are usually given in molar ratio).

	Na^+	Ca^{2+}	H^+	Cl_{exc}^-/Cl^-	$Cl_{exc}^-/Cl^-<0$	$Cl_{exc}^-/Cl^->0$	Cl^-/Na^+	Br^-/Na^+	K^+/Na^+	Mg^{2+}/Na^+	Ca^{2+}/Na^+	SO_4^{2-}/Na^+	MSA:nssSO_4^{2-} (molar)
Major Na Peaks													
Median	3,171	0,290	0,095	-0,05	-0,07	0,07	1,114	0,002	0,021	0,225	0,077	0,250	0,032
Mean	6,418	0,673	0,036	-0,02	-0,09	0,14	1,201	0,005	0,030	0,323	0,497	0,625	0,569
Std. Dev.	*11,277*	*1,410*	*1,127*	*0,16*	*0,08*	*0,17*	*0,490*	*0,012*	*0,034*	*0,449*	*2,610*	*1,412*	*2,707*
Minor Na Peaks													
Median	1,052	0,182	0,427	-0,03	-0,06	0,05	1,132	0,004	0,025	0,231	0,163	0,663	0,080
Mean	1,331	0,571	0,570	-0,72	-1,18	0,09	1,148	0,006	0,061	0,269	0,560	1,167	0,127
Std. Dev.	*1,064*	*1,247*	*1,215*	*7,68*	*0,04*	*0,11*	*0,230*	*0,006*	*0,181*	*0,139*	*1,105*	*1,782*	*0,186*
Background													
Median	0,078	0,114	0,300	0,21	-0,11	0,29	1,468	0,040	0,101	0,548	1,525	4,406	0,094
Mean	0,145	0,268	0,514	0,16	-0,47	0,33	1,938	0,094	0,186	0,939	3,918	9,240	0,233
Std. Dev.	*0,178*	*0,671*	*1,083*	*1,16*	2,35	0,23	*1,812*	*0,252*	*0,375*	*1,155*	*8,134*	*16,444*	*2,853*
Reference values													
Keene et al. 1986							1,166		0,022	0,231	0,044	0,121	

correlation implies that a significant SO_4^{2-}fraction is associated with the sea-salt contributions. Nevertheless, SO_4^{2-}/Na^+(0.250eq.eq $^{-1}$) and Ca^{2+}/Na^+(0.077eq.eq $^{-1}$) ratios twice as high as sea water references (0.121 and 0.044 eq.eq $^{-1}$, respectively, as shown in table 3.4) are likely due to the influence of important sources of both non-sea-salt $SO_4^{2-}$and Ca^{2+}.

The Ca^{2+}variability is only moderately associated with marine primary aerosol (r$\sim$0.40 with all aforementioned ions). Combined with high and scattered Ca/Na^+ratios, this points to the quasi permanent influence of a regional scale semi-arid continental reservoir. This hypothesis is in agreement with SEM studies that show microparticles of aluminosilicates in a sample corresponding to the Na^+major peak centered at 9.64 m w.e. (see figure 3.3).

$MS^-$is also weakly correlated (r<0.40) to marine primary aerosol, and is better correlated with Ca^{2+}(r$\sim$0.6). This association will be discussed in section 3.4.2.1.

In samples corresponding to Na^+major peaks, succinate and oxalate are not correlated with marine primary aerosol, but they are strongly correlated (r>0.75) with $Ca^{2+}$and to a lesser extent with marine secondary aerosol (MS^-, SO_4^{2-}) and nitrogen containing compounds(NH_4^+, NO_3^-) (0.6>r>0.3). This suggests either two different sources for these species (marine biogenic origin and continental) or the ubiquitous presence of this species in the regional atmosphere.

Acetate and formate not shown in table 3.3(a), are well correlated in sodium major peaks (r=0.62) . They are partly associated with continental markers and anticorrelated with oxalate and succinate, suggesting that a marine source of dicarboxylic acids is significant at SV site, although difficult to estimate given the low concentrations of oxalate and succinate often close to the detection limit (0.005μeq.$L^{-1}$for oxalate and 0.008μeq.$L^{-1}$for succinate).

Finally, SEM investigations of the sample at 9.64 m w.e. show a large contribution of organic insoluble material mainly composed of carbon and oxygen. Some examples are presented in figure 3.3. These organic objects contain various amounts of Cl, K, Ca, S sometimes P, and also fine metallic inclusions (Ti, Fe, Cr, Cu). They may correspond to bacterial exopolymers and biofilms that are known to be abundant in hostile marine environments, in particular the nutriment poor Southern Ocean and to be able to accumulate trace metals (Hardy, 1982; Nichols et al., 2005).

The main information provided by this study is that the most important contribution of insoluble organic matter at high altitude sites of southern mid-latitudes originates from the ocean and not from the continent.

3.4.1.2 The 8.4-8.6 m w.e. Na^+major peak

The huge Na^+peak at 8.5-8.6 m w.e. presents a specific signal. It is the only peak containing several samples with Na^+concentrations close to 100μeq.L^{-1}, i.e. the highest values of the whole profile. Part of these very high Na^+concentrations are associated with significant amounts of Cl^-_{exc}reaching severalμeq.$L^{-1}$and leading to an acidic signal, which is not the case for other major marine peaks. Based on the hypothesis that the alternation of $Na^+$and nssCa^{2+}peaks corresponds to successive years, this event, located between 2.2 and 2.6 m.w.e. in the 2005 shallow core, was attributed by Vimeux et al. (2008) to halite rich deposits from the 1991 Cerro Hudson eruption mixed with marine primary aerosol.

We have completed the analysis of this event by SEM studies, which allow to obtain information about the sample′s surface topography and composition. Some examples of our findings are presented in figure3.4. Note that SEM analyses do not allow inner structure identification of the sample (as is the case of transmission electron microscopy, TEM) thus it was not possible to determine if amorphous volcanic glass shards were present in the sample. A few examples of particles investigated are presented in figure 3.4. Particles are mainly minerals (often aluminosilicates), some of them showing metallic inclusions or coating. Their sizes range from 1 to 50 μm. Only one large organic particle (300 μm) was found. The presence of mineral particles containing Ni, Cr, Fe is surprising as these metals are the main constituents of stainless steel. If such particles were formed in smelter exhaust, they should be found in other core sections. Moreover, the only important smelter of the region is located far north in Neuquén, Argentina, (Sierca, 38°S 68°W); a neighboring smaller smelter located in Sierra Grande (Hipasam, 41°S, 65°W) was not operating between 1990 and 2006 (Patagonia-Argentina, 2010; Infobae, 2006). Thus, the smelter hypothesis does not seem valid.

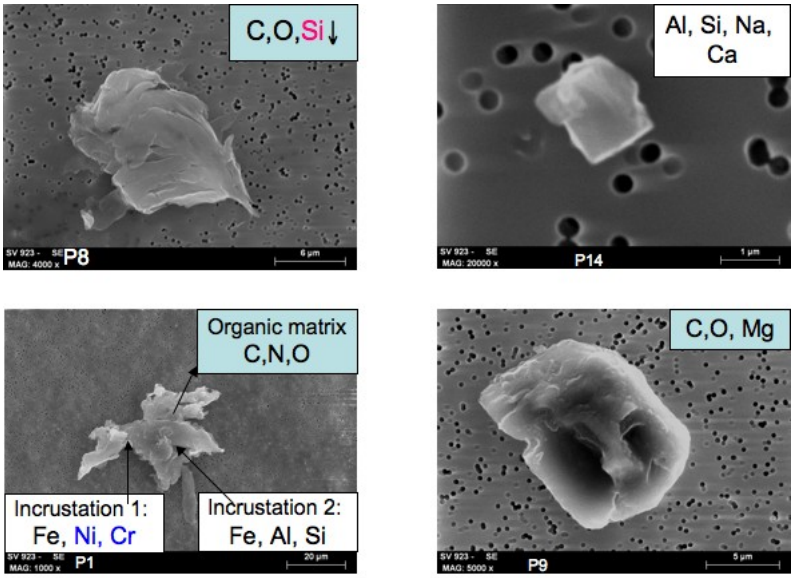

(a) Mixed organic and metallic matter, dust.

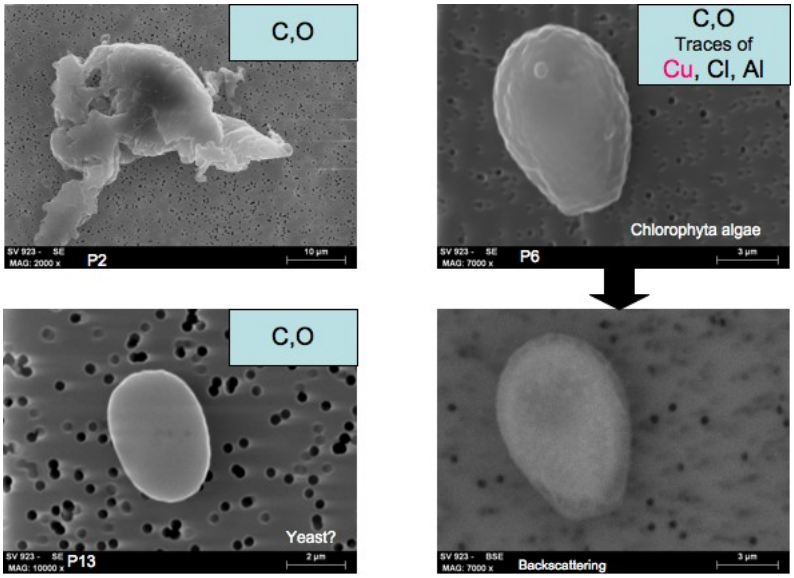

(b) Organic matter

Figure 3.3: Selected images obtained by SEM of insoluble particles found in the marine peak spanning 9.5-10.0 m w.e. (sample number 923, 18.2 m). (a) Organic particles with metallic inclusions (probably bacterial exopolymers) and dust microparticles ($<5\mu$m). (b) Organic matter chunk, yeast and microalgae (showing both SEM and backscattering images). The microalgae is similar to the morphotype chlorophyta found on the CC2 core analyzed at the CECS (nez 2008, pers. comm.)

Interestingly, similar observations (SEM studies) were made on ice cores recovered from the Lange Glacier (Dalia Pereira et al., 2004, in King George Island) and at South Pole Station (Parungo et al., 1979). Mineral particles containing Ni, Cr, Fe (and Ti) were found at both sites. They were considered of unclear continental (Dalia Pereira et al., 2004) and possibly extra-terrestrial origin (Parungo et al., 1979). Taking into account the fingerprint of particles long-range transported from lower latitude (deprived of SiO_2 or tephra) to the Lange Glacier, Dalia Pereira et al. (2004) suggested that the Lange Glacier was under the volcanic influence of the nearby Deception Island from where metal rich particles may originate. Similarly, we can invoke the short-range transport of volcanic particles to SV.

Lastly, very high concentrations of Zirconium (160.8 $ng.g^{-1}$) and Yttrium (10.3 $ng.g^{-1}$) considered as potential volcanic markers were found by ICPMS (Fredier 2009, pers. comm.) in a contiguous sample. All that supports the hypothesis of a volcanic contribution to this event and we can invoke a short-range transport of volcanic particles. The large organic debris may be of marine origin due to the mixing of marine air masses with a local volcanic plume, or come from continental biomass (burned plants for instance).

3.4.1.3 Algae arrivals with Na^+major peaks

A complementary proxy for glacier characterization is the algae population. Major algal peaks (algal blooms) have been used as summer markers of warmer conditions in temperate glaciers, whereas minor algal peaks represent dormant algae (Kohshima et al., 2007; Santibañez et al., 2008; Uetake et al., 2006). However, the origin of algae in glaciers is still on debate. In this section we only discuss the association between Na^+peaks and small algal peaks. This is interesting, as the presence of freshwater algae associated with marine peaks is unexpected and it has not been observed at such a fine scale. This could provide information, if not on the precise origin, at least on the transport pathways of algae observed in Patagonian glaciers.

In figure 3.5 we present the profiles of the total biovolume of algae and some selected ions of biogenic origin besides Na^+. Algae were analysed at the CECs in a firn core (CC2) extracted very

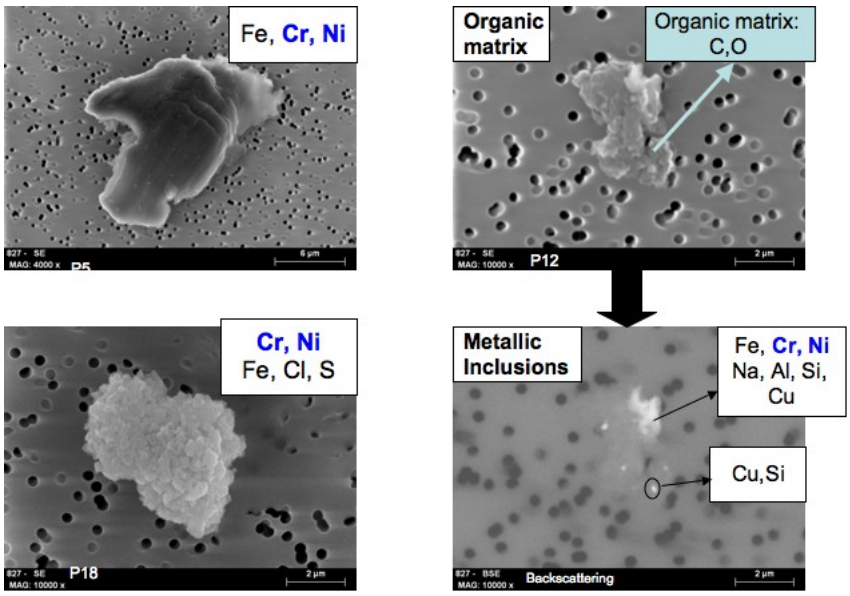

Figure 3.4: Selected images obtained by SEM of insoluble particles found in the marine peak located between 8.4-8.6 m w.e. likely mixed with a volcanic contribution (sample number 827, 16.5 m). The marine influence on this peak can be retraced by the organic matter present in the sample (bacterial exopolymers found in the ocean). The volcano-like influence is retraced by the presence of heavy metals: Ni, Cr, Fe, Cu.

close to the deep CL122 core (2 m apart). We focus here on the dormant algae peaks between 2.8 and 3.9 m and between 4.2 and 4.8 m closely related to Na^+peaks (major algal peaks were discussed in the section 1.4.2).

Algae remain dormant either when the glacier surface temperature is not high enough to produce a liquid water layer where they can reproduce or when they are buried by a thick layer of freshly fallen snow (stormy arrivals) that diminishes the sunlight income. Algae identified at SV are of the genus chlorophyta (nez 2008, pers. comm.) which are frequently observed in glaciers overall in the world and even in remote locations such as Antarctica (Guiry and Guiry, 2010).

The repetitiveness of the four algal and Na^+peaks indicates that deposition conditions were similar for the four events. The absence of continental markers (NH_4^+, nss$Ca^{2+}$and others not shown in the figure) suggests that marine arrivals alternate with pristine precipitation. The association with high δD values (-100$^o/_{oo}$) would indicate that those events take place in warmer months (or under warm conditions).

Provided that there is no depth shift between the two cores, we observe that Na^+peaks alternate with small algal peaks, i.e., with algal growth (fig. 3.5(a)). This could suggest that algae were transported in clean air masses and deposited under calm conditions, after a stormy event, over a warming snow surface. Clean snow layer may correspond to moisture precipitation from aloft or to air masses previously submitted to rain/snow out.

Another explanation is possible if we shift CC2 10 cm with respect to the deep-core (which is possible, but was not investigated): algae peaks would overlap Na^+peaks. (fig. 3.5(b)). This may be supported by SEM observations : a freshwater alga identical to the morphotype identified in the major algae peaks was found in the Na^+major peak at 9.64 m w.e (figure 3.3).

If this last hypothesis holds, we could explain the presence of freshwater algae in marine air masses by the presence of long range transported algae in the air aloft (chloronomas and chlorophyta genus are known to be resistant and quasi ubiquitous), or even invoke the presence of dormant freshwater algae in the ocean. Algae small peaks would not be indicators of algal

growth but only reflect a higher number of algae present in the ice as a consequence of heavy precipitation that would produce a sort of algal rain-out.

Given the absence of precise depth fitting between both cores, we cannot clearly conclude on the origin and deposition way of glacier living algae at SV. More precise studies are needed with a focus on the algae biovolume and its relationship with marine storm occurrences (as well as on synoptic conditions associated to these precipitation events.

3.4.1.4 Na^+minor peaks

The average Na^+concentration in minor peaks is $0.85\mu eq.L^{-1}$. The minor peaks distribution is depicted in orange in figure 3.2. Peaks are rather regularly distributed along the profile, although more densely between 35 and 40 m w.e. They are narrower than major peaks, spanning less than 0.1 m w.e. except between 5 and 10 m w.e. and 28 and 32 m w.e where they can be larger than 0.2 m w.e. and associated with MS^-. Below 35 m w.e., minor peaks are associated with MS^-, $NH_4^+$and $nssSO_4^{2-}$.

Chloride replacement rates range between -0.40 and 0.25 (with a median value of -0.07), which is similar to what was observed in Na^+major peaks. This slight chloride depletion indicates restricted aging processes i.e., direct transport from the Pacific Ocean. Na^+maximum concentrations are 10 to 100 times smaller than in major peaks, possibly due to weaker uplift of marine air masses or to the dilution of highly concentrated marine air-masses with continental air (or Na^+depleted) during transport.

The correlation matrix corresponding to Na^+minor peaks is shown in table 3.3(b) As for Na^+major peaks, Cl^-, Na^+, Mg^{2+}contributions are highly correlated ($r>0.8$), but the correlation coefficient of other species with Na^+diminishes to less than 0.3 ($r=0.15$ for Ca^{2+}, $r=0.14$ for SO_4^{2-}) and moreover, their ratios to Na^+increase. This implies that other sources gain relevance as marine influence decreases. As in major peaks, MS^-, is moderately correlated to Ca^{2+}arrivals ($r\sim0.42$).

The correlation of $Br^-$with marine primary aerosol is weaker in Na^+minor peaks ($r\sim0.35$),

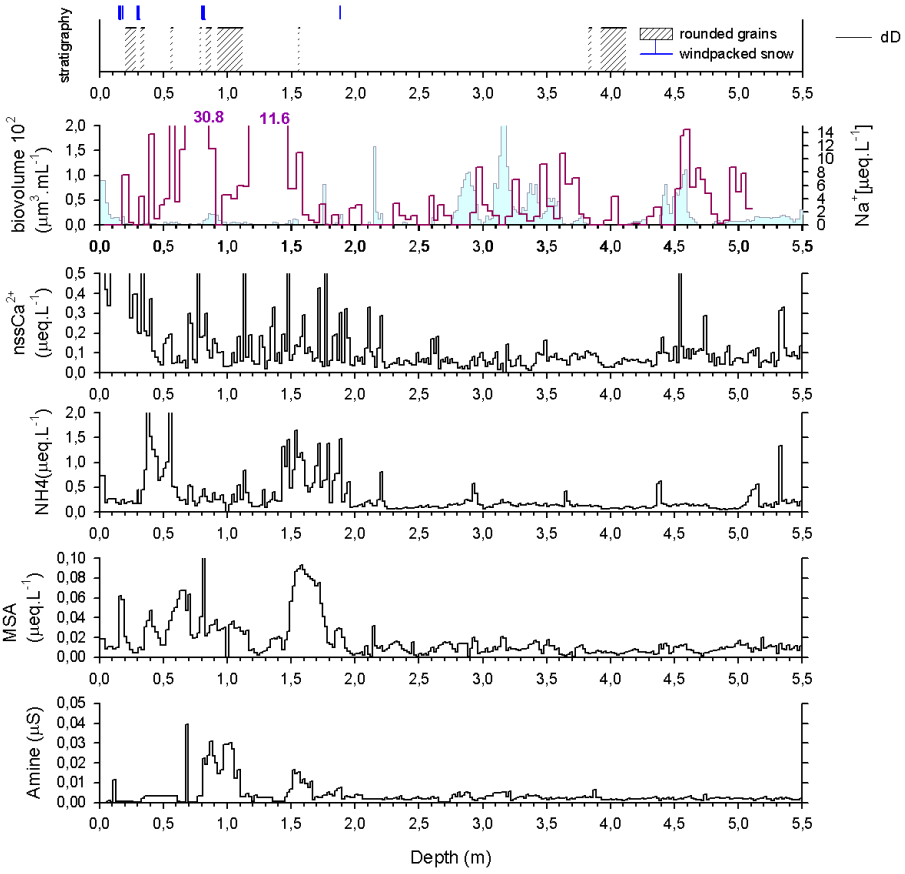

(a) Surface is the same for both cores

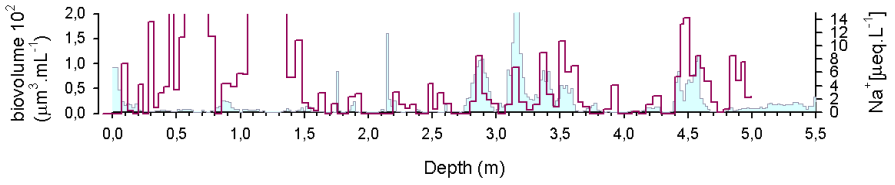

(b) Surface with a 10 cm lag (CC2 shifted upwards)

Figure 3.5: From top to bottom, stratigraphy, total biovolume algal (red line, obtained at the CECs), Na^+(light blue shaded profile) and some selected ions likely of biogenic origin (unidentified aminoacid, succinate, NO_3^-, NH_4^+). The first two big peaks of algal biovolume would be related to summer maxima (dating horizons, according to nez 2008, pers. comm.) but will not be discussed here. Focus is on dormant algae between 2.8 and 2.8 and 4.5 and 5 m. Algae identification was made in the shallow core CC2 retrieved next to the CL122 in the same drilling tent. Note that the depth is given in meters (not m w.e.)

than in major peaks (r∼0.88), that can be explained by the presence of another source of this ion. Bromine is released from sea salt aerosol, emitted by volcanic eruptions and produced by the photolytic decomposition of bromocarbons (either anthropogenic or biogenic) or their oxidation by OH (Salawitch and Ross, 2006). Higher $Br^-$to Na^+ratios are observed in Na^+minor peaks (0.004 eq.eq $^{-1}$) than in major peaks (0.002 eq.eq $^{-1}$), which again points to the influence of sources other than marine under less stormy conditions.

A strong relationship between SO_4^{2-}, K^+, dicarboxylic acids (oxalate, succinate) and nitrogen containing compounds (NH_4^+, NO_3^-) is observed (0.75>r>0.55) in table 3.3(b) Ionic balance H^+shows a moderate correlation (r∼0.4) with those species, pointing to the presence of acidic gases partly neutralized in the atmosphere. The association of marine primary aerosol with NH_4^+, $NO_3^-$and nssSO_4^{2-}has been previously observed in other marine sites influenced by the anthropogenic activity (Yeatman et al., 2001). Thus, several continental sources may be proposed for these species (among them biomass burning, soil or anthropogenic emissions).

3.4.1.5 Na^+background concentrations: the non-marine component

Na^+background concentrations are lower than 0.31μeq.$L^{-1}$and correspond to a non-marine component that may have a local continental origin (NW transport for instance) resulting from the mixing of marine moisture with air masses long range transported in the free troposphere (high level SW transport, for instance), or even partly account for stratospheric contributions. Note that the primary source of moisture at this site is the ocean, even for the samples that do not contain important contributions of primary marine aerosol. So, pristine samples that have very low concentrations of all ions, would have initially a marine origin. Thus, by studying Na^+background concentrations we are focusing on the non-marine (i.e. continental) contribution to the soluble fraction of the precipitation at this site and not the moisture origin. Continental contributions to SV snow, as defined here, will be addressed in the following chapter.

3.4.1.6 Marine primary arrivals and water stable isotopes

Major Na^+peaks are characterized by very high values and a ratio between maximal and minimal concentrations of approximately 10^5. For that reason, a logarithmic representation of $Na^+$is useful for some comparisons, particularly with water stable isotopes.

Figure 3.6 depicts δD , d, $MS^-$and the logarithm of Na^+concentrations for the first 33 m w.e. of ice-core, where the high resolution dataset of water stable isotopes is available. As a general rule, logNa^+trends follows both δD (r=0.28) and d (r=0.31) trends.

In figure 3.7 we present separately the δD distribution for each type of marine arrivals (major, minor and background sodium concentrations). We clearly observe a trimodal distribution for major Na^+arrivals (>m+s). They are associated with δD values centered 1) at -120$^o/_{oo}$ 2) at -100$^o/_{oo}$ and 3) between -80 to -60$^o/_{oo}$. Considering a gradient of about 5$^o/_{oo}$ per °C (according to LMDZ-iso isotopical modeling, Vimeux 2010, pers. comm.), all this represents a difference of temperature between 1) and 2); and 2) and 3) of 4°C that is equivalent to an interseasonal difference; and between 1) and 3) of 8-12°C that is equivalent to the difference between January and July temperatures. The interseasonal difference of temperatures of 4°C is also predicted by reanalysis data at this site. However, the summer to winter difference of 8-12°C is higher than the reanalysis predictions for SV (7°C according to NCEP-NCAR data). In contrast, 8-12°C is in the range of continental stations. The fact that SV ice archives this temperature difference remains to be explained.

When counting the number of peaks corresponding to each δD value, we confirm that 31% of major Na^+arrivals are associated with cold conditions (case 1), 56% with temperate conditions (case 2) and 12% with the warmest conditions (case 3) (4 peaks from which 2 are related to wide MS^-peaks). If δD reflects regional temperature (Vimeux 2009, pers. comm.), the fact that 56% of the major Na^+peaks are associated with δD values of -100$^o/_{oo}$ (temperate conditions) would indicate that marine storms take place preferentially under temperate conditions, from October to May but not in summer (DJF). Summer precipitation would be restrained to a few cases that are sometimes associated with MSA transport.

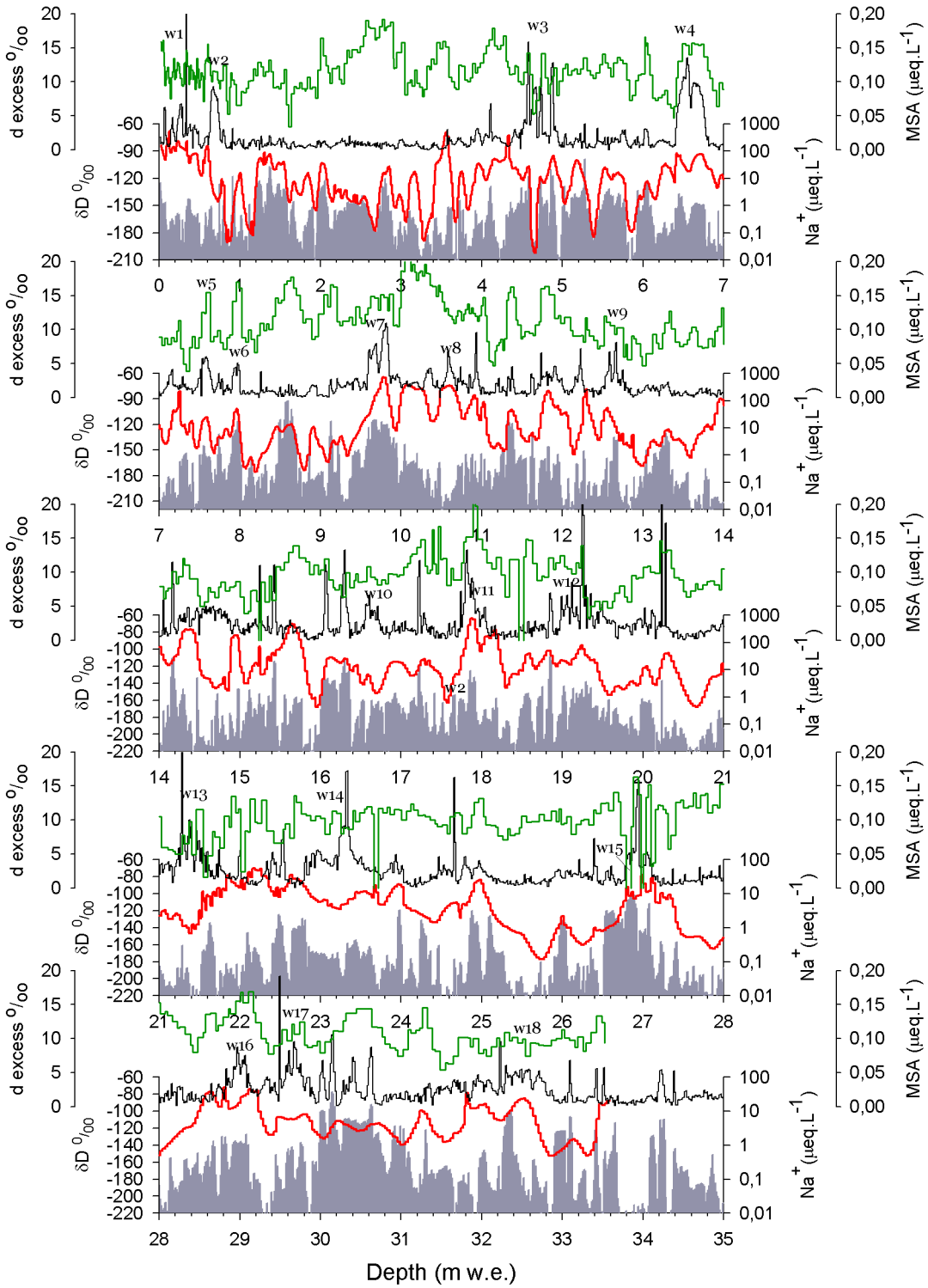

Figure 3.6: Deuterium excess (green, left-hand scale), δD (red, left-hand scale), log Na^+(shaded gray, right scale) and MS^-(black, right scale) profiles for the first 33 m w.e. of the CL 122 core where fine resolution measurements of stable water isotopes are available. Isotopes measurements were made at the LAMA (Herreros, 2010). Wide peaks of $MS^-$are numbered from w1 to w18 in this section of the core.

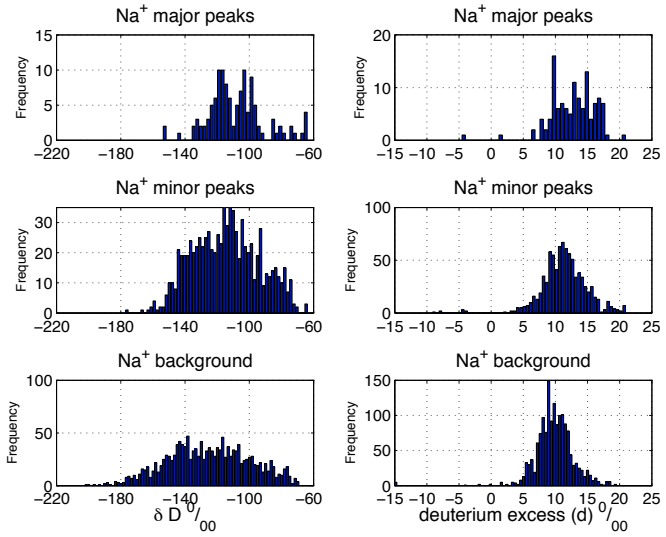

Figure 3.7: Frequency distribution of samples corresponding to major, minor and background Na^+contribution according to their δD (left-hand) and deuterium excess (right) content. All the samples contained in a peak are taken into account.

Minor Na^+arrivals (m+s>Na^+>0.31) include a wider range of isotope values (-160 to -60$^o/_{oo}$) with a maximum centered between -118 to -110$^o/_{oo}$. This indicates that although minor oceanic contributions arrive to the SV site during warm and cold seasons, their transport takes place preferentially during colder months.

Finally, Na^+background values show the broadest range of all contributions (-200 to -60$^o/_{oo}$) and, interestingly, the lowest isotope values. This would indicate that winter season precipitation would favor the transport of continental (non marine) markers.

Deuterium excess values associated with major Na^+peaks (r=0.31) can be classified in two groups: those having d<12$^o/_{oo}$ (40% of the peaks) and those having d>12$^o/_{oo}$ (60% of the cases, which can be subdivided in: 42% having d centered at 14$^o/_{oo}$ and the remaining 18% having d centered at 18$^o/_{oo}$).

Values significantly lower than the mean deuterium excess value calculated along the ice core (10.7$^o/_{oo}$) would retrace the Southern Ocean source and this is not the case in CL122 as very few samples associated to Na^+peaks have d<5$^o/_{oo}$. Thus, Na^+major peaks retrace the mid-

latitudes oceanic contribution rather than the Southern Ocean source. The different modes of the frequency distribution of the Na^+major peaks (d centered at 10, 14 and $18^o/_{oo}$, fig. 3.7) would then retrace seasonal conditions influencing the Pacific Ocean. It is worth noting that the source characterized by d values between 15 and $20^o/_{oo}$ (18%) is usually associated to high δD values (summertime temperature conditions). Thus, Na^+major peaks having a high δD (>-$100^o/_{oo}$) and a high d ($18^o/_{oo}$) would retrace summer precipitation originated in the Pacific Ocean.

Minor Na^+peaks and background level are associated with a broader range of values of d (from 5 to $20^o/_{oo}$) and this indicates that many sources/transport conditions influence the minor Na^+peaks occurrences (which include continental inputs).

3.4.2 Marine biogenic contribution

As explained in the introduction of this chapter, the molar $MS^-$to nssSO_4^{2-}ratio is often used to estimate the contribution of marine biogenic sources to total sulphate (see Bates et al., 1992; Legrand et al., 1992, for some references).

Nevertheless and as shown in 3.4.1, apart from the sea salt contribution, the nssSO_4^{2-}contribution at SV site is not only composed by biogenic SO_4^{2-}but probably also influenced by continental sources including volcanic degassing, the transport of pollutants from subtropical megacities and emissions due to local human activities.

In this section we intend to better understand MS^-sources and deposition processes and to provide an estimate of the marine biogenic fraction of nssSO_4^{2-}.

3.4.2.1 MSA major contributions

In figure 3.8(a) we present high resolution depth profiles of MS^-, nssSO_4^{2-}concentrations and of the molar MS^-: nssSO_4^{2-}ratio. We will first discuss the MS^-profile.

MS^-major contributions are defined by equation 3.4. They can be classified in narrow peaks spanning approximately 0.02 to 0.08 m w.e. (18 peaks) and wide peaks spanning 0.08 to 0.80 m w.e. (33 peaks). MS^-peaks, whatever their type (wide or narrow), are more frequent in the

deepest 35 to 52 m w.e. of the core.

Table 3.5: Correlation matrix for the first 52 m w.e. of CL122 for MS^-major contributions including both wide and narrow peaks.

(a)	Na+	Cl-	Br-	K+	Mg2+	MSA	nssSO4	NH4+	NO3-	Clexc	Oxalate	Succinate	nssK	nssMg	nssCa
Cl-	**0,99**														
Br-	**0,74**	**0,76**													
K+	0,57	0,56	0,50												
Mg2+	**0,85**	**0,88**	**0,75**	0,51											
MSA	0,21	0,19	0,22	0,14	0,19										
nssSO4	-0,08	-0,07	0,27	0,26	0,02	0,28									
NH4+	-0,02	-0,02	0,17	0,49	0,00	0,04	**0,59**								
NO3-	-0,07	-0,07	0,22	0,36	-0,08	0,09	**0,66**	**0,73**							
'Clexc'	**-0,73**	**-0,65**	-0,43	-0,47	-0,37	-0,25	0,09	0,01	0,07						
Ox	0,00	-0,01	0,19	0,42	0,02	0,19	**0,69**	**0,67**	0,57	-0,02					
Succ	-0,04	-0,05	0,09	0,42	-0,06	0,01	0,46	**0,69**	0,58	0,02	0,64				
'nssK'	-0,15	-0,16	-0,02	**0,73**	-0,09	0,00	0,37	**0,60**	0,50	0,04	0,51	0,55			
'nssMg'	**-0,65**	**-0,60**	-0,31	-0,34	-0,15	-0,11	0,17	0,03	0,03	**0,83**	0,03	0,00	0,14		
'nssCa'	0,02	0,02	0,20	0,10	0,04	0,42	**0,59**	0,12	0,34	-0,03	0,36	0,07	0,11	0,02	
'H+maj'	-0,27	-0,24	-0,09	-0,14	-0,23	-0,27	0,25	0,24	0,33	0,37	0,15	0,28	0,05	0,17	-0,52

Color code
r>|0,6|
|0,6|>r>|0,4|
|0,4|>r>|0,3|

In figure 3.9 we present detailed sections of MS^-, $Na^+$and $nssCa^{2+}$profiles chosen in the firn part and in deeper ice of CL122. We observe that MS^-narrow peaks are often associated with Na^+peaks and/or $nssCa^{2+}$peaks ($> 2\mu eq.L^{-1}$), compared to only 20% of the wide peaks. This is likely due to MSA uptake by alkaline aerosol. Indeed, it has been observed that MS^-(and other secondary aerosol) can condensate on the coarse mode of marine primary aerosol or continental particles (Kerminen et al., 2000; Yeatman et al., 2001). When MS^-arrivals are not concomitant with high Na^+or $nssCa^{2+}$concentrations, peaks tend to spread out possibly by diffusion, as observed in Antarctic cores (Pasteur and Mulvaney, 2000). This phenomenon is more visible in the deeper ice than in firn, suggesting that MS^-migration would require several years to fully take place. Thus, we may assume that part of MSA arriving at SV is transported by air masses containing sea salt (marine origin) or soil dust (continental origin) particles, heterogeneous reactions at the surface of these particles preventing MSA diffusion and leading to the conservation of narrow peaks spanning a few samples. The other part is transported by air masses that do not contain any important continental or marine fraction, and in that case, wide MS^-peaks are observed.

The sum of MS^-major contributions represents 15% of the first 52 m w.e. of the ice core (cf. table 3.2), peaks associated with Ca^{2+}or Na^+(mostly narrow) accounting for 7.3% and wide

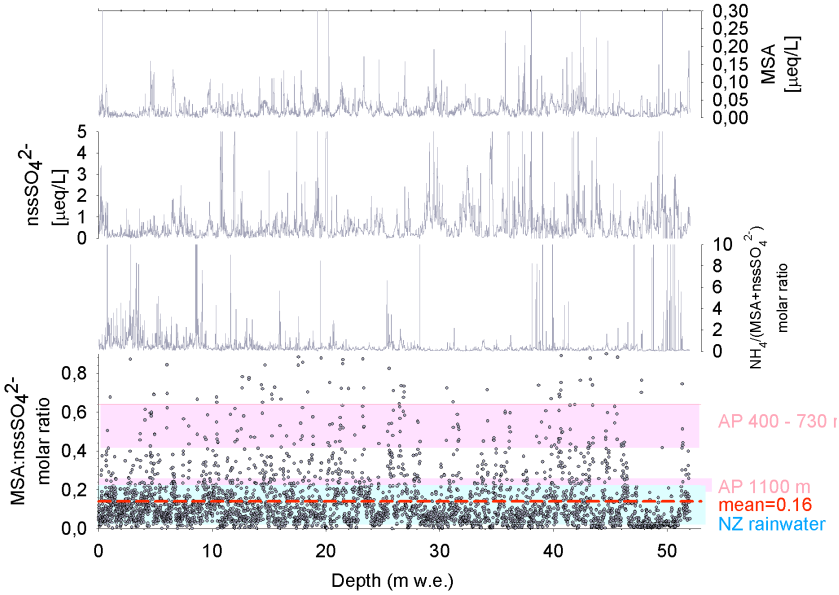

(a) Complete profile, all samples included. (R_T).

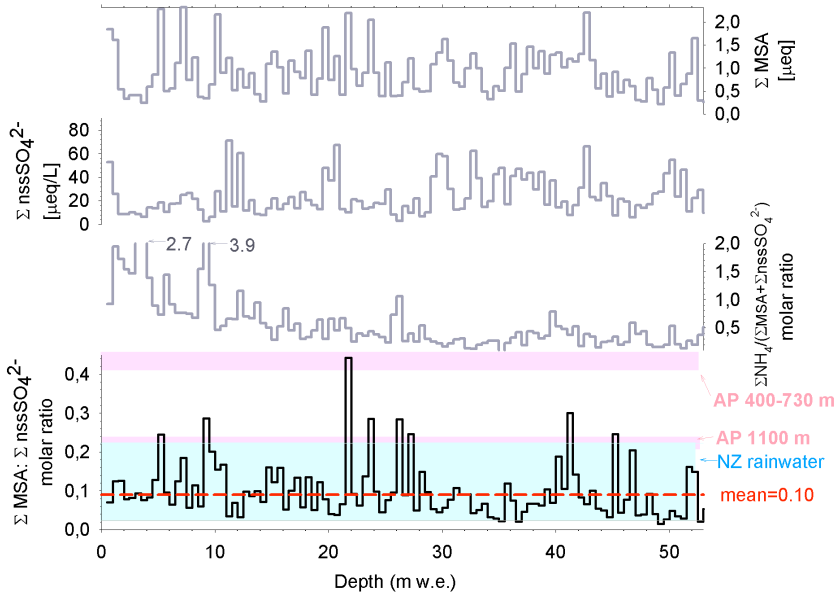

(b) Integrated values over 0.5 m w.e. depth bins. (R_S).

Figure 3.8: MS^-, $nssSO_4^{2-}$, the molar NH_4^+:(MS^-+$nssSO_4^{2-}$)and the molar MS^-:$nssSO_4^{2-}$ratios along the first 52 m w.e. of CL122. $MS^-$and $nssSO_4^{2-}$are given inμeq.L^{-1}, the ratios are molar. In (a) we observe sample by sample measurements and the MS^-:$nssSO_4^{2-}$ratio calculated with equation 3.11. In (b) we observe the same variables for 0.5 m w.e. bins, calculated with equation 3.12. In red, the mean value of the MS^-:$nssSO_4^{2-}$ratio. In light blue, the range of MS^-:$nssSO_4^{2-}$measurements of rainwater in coastal Eastern New Zealand (300 m a.s.l.) (Wylie and Mora, 1996). In pink, the range of MS^-:$nssSO_4^{2-}$measurements of various firn samples in the Antarctic peninsula, for sites ranging from 400 to 730 m a.s.l. and higher than 1100 m a.s.l. (Pasteur and Mulvaney, 2000) (cf. table 3.6).

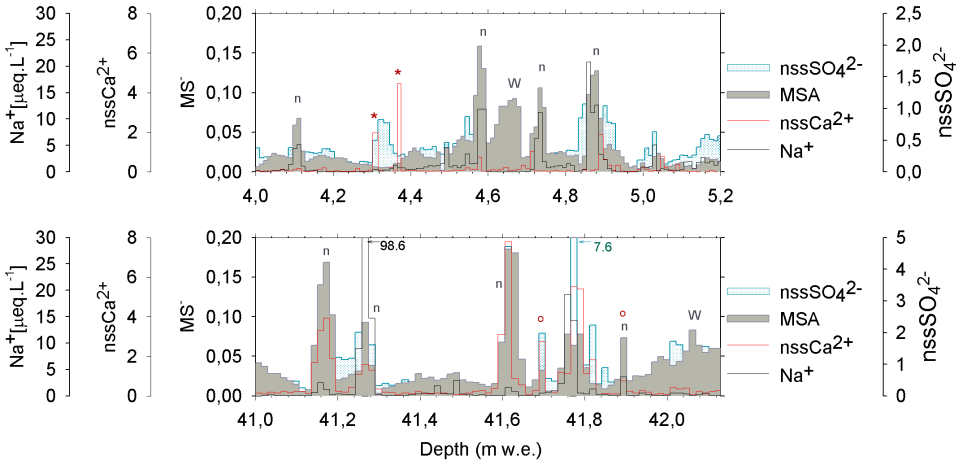

Figure 3.9: Example of the association of MS^-(gray) with Na^+(black) and $nssCa^{2+}$(red) spikes in the firn (top) and in the ice (bottom) of the San Valentin deep core. The $nssSO_4^{2-}$profile is also presented (green). Note that migration of MS^-on one-sample $nssCa^{2+}$spikes is more obvious in ice (bottom panel) than in firn (top panel). *n* denotes narrow peaks and *w* denotes wide peaks.

peaks only for 7.7%. As stated in section 3.4.1.1, most of the MS^-arrivals are not associated with Na^+major peaks. Thus, adding both primary and secondary marine contributions, it appears that only ∼40% of the SV snow has a strong marine imprint, which is, again, lower than the value of 96% predicted for oceanic precipitation (cf. chapter 2)

In table 3.5 we present the correlation matrix determined for major MS^-arrivals (including narrow and wide peaks). $MS^-$is not correlated to Na^+($r<0.27$), and shows, instead, a better correlation with $nssCa^{2+}$($r>0.45$) because MS^-narrow peaks associated with $nssCa^{2+}$tend to be slightly wider and more frequent than the ones associated with Na^+. Three different fingerprints appear: a marine primary aerosol component, a continental mixed source including $nssSO_4^{2-}$, NH_4^+, NO_3^-, and a marine biogenic source traced by MS^-alone.

The cluster corresponding to marine primary aerosol is clearly recognizable by the strong relationship linking Na^+, Cl^-, Br^-, K^+, and Mg^{2+}($1>r>0.5$). Note, that mean Na^+concentrations in MS^-peaks are lower ($0.44\mu eq.L^{-1}$for wide peaks and $4.44\mu eq.L^{-1}$for narrow peaks) than in Na^+peaks ($0.86\mu eq.L^{-1}$for minor peaks and $6.41\mu eq.L^{-1}$for major peaks). This supports the previous observation that most of MS^-deposit takes place under different synoptic conditions

than Na^+major arrivals. However, a few cases of overlapping between $Na^+$and MS^-major peaks may be observed. This could correspond to the arrival of marine storms taking place in summer and fall (the seasons of important production of MSA).

The presence of a cluster of $nssSO_4^{2-}$, NH_4^+, NO_3^-, oxalate and succinate in the correlation matrix suggests that marine biogenic species are brought to SV by mixed air-masses influenced by both a weak primary marine and a significant continental source.

Concerning MS^-, it is moderately correlated with $nssCa^{2+}$(r=0.42) and very poorly correlated with $nssSO_4^{2-}$(r=0.28). This points again on the possible existence of another sulfate source. MS^-maximum concentrations generally range between 0.12 and 0.25μeq.L^{-1}, with few samples values higher than 0.30 and sometimes reaching 0.63μeq.L^{-1}. This compares rather well with glaciochemical data from South Pole Station, 0.20-0.30μeq.L^{-1}(Meyerson et al., 2002) and Pio XI glacier, 0.25μeq.L^{-1}(Schläppi et al., 2009).

Table 3.6: Reference values for MS^-:$nssSO_4^{2-}$molar ratio and used in figure 3.8 for Eastern New Zealand (300masl) (Wylie and Mora, 1996) and Antarctic Peninsula (Pasteur and Mulvaney, 2000).

Site	**Elevation m a.s.l.**	**Sample type**	MS^-:$nssSO_4^{2-}$molar ratio
Antarctic Peninsula	>1100	Firn	20-24%
Antarctic Peninsula	400-730	Firn	42-64%
Eastern New Zealand	300	Rainwater	2.4-22.3%

3.4.2.2 The $MS^-$to $nssSO_4^{2-}$ratio

As shown in figure 3.8(a). the depth profile of the $MS^-$to $nssSO_4^{2-}$molar ratio is highly scattered (s>700%) and becomes even more scattered below 12 m w.e. Beside very high and meaningless values corresponding to very low $MS^-$and $nssSO_4^{2-}$concentrations, such an high scattering is certainly partly due to the fact that not all $nssSO_4^{2-}$has a marine biogenic origin, MSA diffusion (Pasteur and Mulvaney, 2000) and/or MSA association to coarse alkaline particles (Kerminen et al., 2000; Yeatman et al., 2001). The mean value of the $MS^-$to $nssSO_4^{2-}$ratio calculated taking into account every sample is 0.161$\pm$0.008.

To counterbalance the bias related to MS^-possible tightening /relocation, we calculate $MS^-$to $nssSO_4^{2-}$ratios, for 0.5 m w.e. section-integrated values of $MS^-$and $nssSO_4^{2-}$(i.e., deposition fluxes calculated for contiguous ice sections 0.5 m w.e. thick). This depth interval may allow to cover a full event, even wide. However part of the information concerning the short timescale variability will be lost. Corresponding MS^-, $nssSO_4^{2-}$and MS^-:$nssSO_4^{2-}$molar ratio depth profiles are shown in figure 3.8(b). The mean value of the MS^-:$nssSO_4^{2-}$ratio calculated using section-integrated concentrations is 0.100±0.014 (see section 3.4.2.4 for mathematical details) which is lower than the mean ratio calculated using all individual values.

Data from other sites are reported in table 3.6 and in figure 3.8 (the shaded zones). The average MS^-:$nssSO_4^{2-}$molar ratio at SV ($\sim$ 10% or $\sim$16% depending on the method employed) is close to data obtained near the sea surface in mid-latitudes marine atmosphere (2.4 to 22%, Eastern New Zealand rainwater sampled at 300 m a.s.l. (Wylie and Mora, 1996)). They are slightly lower than data from Antarctic Peninsula (20-24%, firn sampled at 1100 m a.s.l. Pasteur and Mulvaney, 2000) which may be partly due to the existence of a $nssSO_4^{2-}$source other than marine biogenic in southern mid-latitudes (biomass combustion, volcanic background, anthropogenic activity). Despite these slight differences, the good agreement between SV data and data from lower altitude or higher latitude remote sites confirms that significant amounts of MS^-, although mainly produced within the boundary layer in the mid-latitudes, reach the upper troposphere and high altitude sites.

3.4.2.3 MS^-sources traced by water stable isotopes

In this section we compare MS^-wide and narrow peaks, an also the remaining background signal with deuterium (δD) and deuterium excess (d).

In figure 3.6 we present the complete MS^-, Na^+, δD and d profiles. We observe that in general, wide MS^-peaks are associated with high δD (r=0.28) values and this is logic as MSA production takes place in warmer seasons rather than during the cold months. This association is clearer for well-defined wide MS^-peaks than for peaks subjected to diffusion (notoriously below

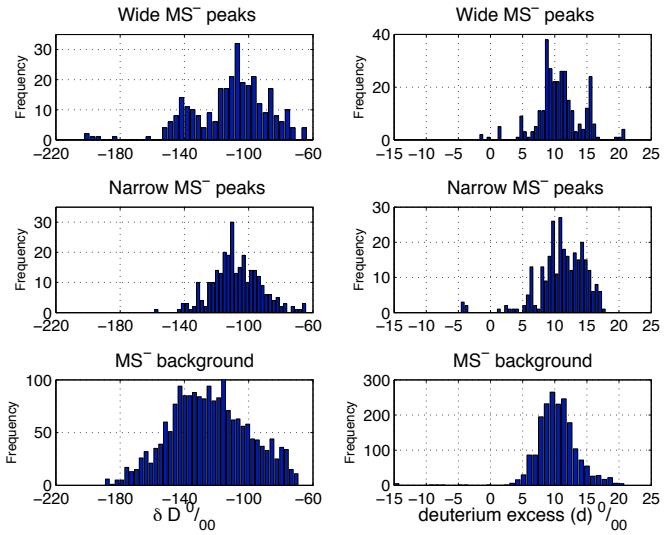

Figure 3.10: Frequency distribution of samples corresponding to wide, narrow and background MS^-peaks for δD (left-hand) and deuterium excess (right). All the samples contained in a peak are taken into account.

20 m w.e.).

There is no evident correlation between $MS^-$and d (r=0.08), except for some well-defined wide peaks (located at 6.4-6.8, 9.8-10 and 17.7 -18.1 m w.e.) where high d values ($> 15^o/_{oo}$) are associated with high concentrations of $Na^+$and $MS^-$and δD values of approximately -90$^o/_{oo}$. Note that $MS^-$and Na^+concentrations are variable (not necessarily correlated), but the similar values of d for all these contributions indicate a common source. Vimeux et al. (2008) proposed a fast transport from a warm source of this type of association, probably the Pacific Ocean (mid-latitudes).

Taking into account all MS^-peaks (wide and narrow), we obltain the frequency distribution of isotopic values (δD and d) for corresponding samples. This is presented in figure 3.10.

Wide MS^-peaks present a bimodal distribution of δD , centered at -140 and -110 $^o/_{oo}$ and this could be related to two different seasons when MSA contributions take place. The temperature difference between january and july at SV is of approximately 7°C, (NCEP-NCAR data at 700hPa). This would be in agreement with the intermodal δD difference (a 30$^o/_{oo}$ difference

represents 6°C).

According to seasonal variations of DMS production 3.1, no production of MSA takes place in JJA (winter) at high latitudes and the only noticeable source of MSA is the tropical Pacific. The highest MSA production takes place around Antarctica, particularly over the Ross Sea in summer (DJF). In fall (MAM) the tropical source gains relevance. In consequence, the δD mode centered at -140$^o/_{oo}$, could reflect fall arrivals (as in winter there is no MSA production) and the -110$^o/_{oo}$ mode can reflect summer or spring arrivals. Deuterium excess provides some additional information: there are also two possible sources of moisture: one traced by 15$^o/_{oo}$ values and another by 10$^o/_{oo}$ values of d.

When combining both δD and d, it would seem that wide MS^-peaks retrace:

- summer phytoplankton activity when δD is higher than -100$^o/_{oo}$. It would originate and be transported from the Southern Ocean if d is less than 10$^o/_{oo}$ and from mid-latitudes for d higher than 10$^o/_{oo}$.

- MAM or SON production when δD is in between -100 and -150$^o/_{oo}$ for d between 10 and 5$^o/_{oo}$. However, the precise source location is difficult to identify.

- Winter production when δD is lower than -150 $^o/_{oo}$ and the only possible source is the subtropics as the phytoplankton or the circumantarctic circle is not active due to the presence of the ice-shelf and the low temperature. We do not observe any of these peaks in our record, except one peak of MS^-located at 4.6 m w.e., number *w3* in fig. 3.6, that seems to contradict this: it has low δD (-200$^o/_{oo}$) and low d (8$^o/_{oo}$).

  The puzzling case of peak *w3* may be tentatively attributed to the combination of narrow and wide (diffusing) MS^-peaks related to a single event (traced by successive deposits of $Na^+$and Ca^{2+}) rather to several events, which is possible given the very high accumulation rate for this section of the core. This would lead to unrealistic d values in terms of source when sampling the entire event, but may retrace precipitating processes. However, as *w3* is the only case out of 18 presenting this unrealistic isotopic signature, we are confident for

the rest of the MS^-wide peaks.

Backtrajectory studies showed that NW/W air masses can bring MSA from the tropics and subtropics in 3-4 days. SW air masses bringing MSA can come from a wide variety of environments as the Ross Sea or near Antarctica (55-70°S) for 2-3 days backtrajectories, or from the subtropics (30-40°S) for 3-6 days backtrajectories.

Concerning narrow MS^-arrivals, we observe that they are also centered at δD = -110 $^o/_{oo}$ but the distribution is narrower than for wide MS^-peaks. However, due to diffusion of $MS^-$and relocation over $Na^+$and Ca^{2+}layers, this distribution can be biased and reflect the precipitation conditions of air masses rich in $Na^+$and $Ca^{2+}$and not necessarily MS^-production.

Background MS^-contributions encompass a wide range of deuterium (-150 to -100$^o/_{oo}$, equivalent to 10°C), as Na^+background contribution. As for Na^+, the lowest δD values, reflecting a cold season, are found in this distribution. As $MS^-$and Na^+background represent continental contributions, we can expect polar incursions to arrive with continental (or at least non marine) markers.

3.4.2.4 Biogenic and residual SO_4^{2-}obtained from MS^-contributions

The MS^-:nssSO_4^{2-}ratio is often used to calculate the contribution of marine biogenic sources to the SO_4^{2-}budget (Bates et al., 1992), and, as a consequence the non marine SO_4^{2-}component. Here we only discuss the marine biogenic contribution, denoted biogSO_4^{2-}. The residual component of SO_4^{2-}denoted ResSO_4^{2-}will be discussed in the next chapter.

Marine biogenic and residual sulfate are given by:

$$biogSO_4^{2-} = \frac{MS^-}{R_{MS^-:nssSO_4^{2-}}} \tag{3.9}$$

$$ResSO_4^{2-} = nssSO_4^{2-} - biogSO_4^{2-} \tag{3.10}$$

We used three different ways of estimating MS^-:nssSO_4^{2-}molar ratios :

1. The average ratio including every sample i calculated along the complete profile, denoted R_T:

$$R_T = \frac{\sum_{i=1}^{N} (MS^- : nssSO_4^{2-})_i}{N} \tag{3.11}$$

Where

N = number of samples along the profile

This calculation yields R_T=0.161±0.008 (molar)

2. The average of ratios calculated for j contiguous 0.5 m w.e. ice sections (as depicted in figure 3.8(b)), denoted R_S. We choose 0.5 m w.e. intervals because lower values may split strong marine arrivals (that can span 0.5 m w.e.).

$$R_S = \frac{\sum_{j=1}^{S} (\sum_{i=1}^{Ns} MS^- : \sum_{i=1}^{Ns} nssSO_4^{2-})_j}{S} \tag{3.12}$$

Where

S= Number of 0.5 m w.e. sections (bins)

Ns= Number of samples per 0.5 m w.e. section

This calculation yields R_S=0.100±0.014 (molar)

3. The running ratio of 0.5 m w.e. integrated sections, successively centered at every individual sample depth, R_g. When approaching the first and last samples of a given 0.25 m w.e. interval, neighboring lags were progressively reduced. The running ratio calculated for the sample i is given by

$$R_g(d_i) = \sum_{i=1}^{Ng} MS^- : \sum_{i=1}^{Ng} nssSO_4^{2-} \tag{3.13}$$

where

di= depth of the sample i

Ng= Number of samples per moving 0.5 m w.e. section (from d_i-0.25 m w.e. to d_i+0.25 m w.e.)

Calculation made using equation 3.11 makes no sense for very low MS^- or $nssSO_4^{2-}$ concentrations and also includes possibly biased values, like high MS^- concentrations corresponding to tightening on continental or sea salt particles. Also included are high SO_4^{2-} concentrations due to events other than marine, such as biomass burning or volcanic eruptions, which lead to anomalously low ratios. In contrast, the averaged calculation performed with equation 3.12 will smooth these punctual influences, but has the disadvantage to be based on an arbitrary depth dicretization (event cutting, loss of high resolution information). When using 3) the influence of the discretization will diminish although remaining arbitrary with a persistent risk of information loss. In table 3.7, we present the relative contributions of $biogSO_4^{2-}$ to total SO_4^{2-} along the first 52 m w.e. of the ice core and calculated using successively the three above mentioned ratios. The marine $biogSO_4^{2-}$ contribution to total sulfate is 31%, 40% and 50%, when using R_T, R_S and R_g, respectively. Conversely and taking into account the sea salt contribution, this means that the non marine sulfate component represents between 20 and 50% of the total SO_4^{2-} input at this site expected to be mostly influenced by marine air-masses.

In figure 3.11 we present a comparison of the different estimates of marine biogenic (bottom) and residual (top) $nssSO_4^{2-}$ along with MS^- profiles.

Table 3.7: Sulfate budget (in %) for the first 52 m w.e. of the CL122 core, calculated using different MS^- to $nssSO_4^{2-}$ ratios (R) to determine the biogenic fraction. See details in section 3.4.2.4.

Source	$\mathbf{R}_T$	$\mathbf{R}_S$	$\mathbf{R}_g$
Sea salt	21	21	21
Biota emissions	31	40	50
Residual	49	39	29

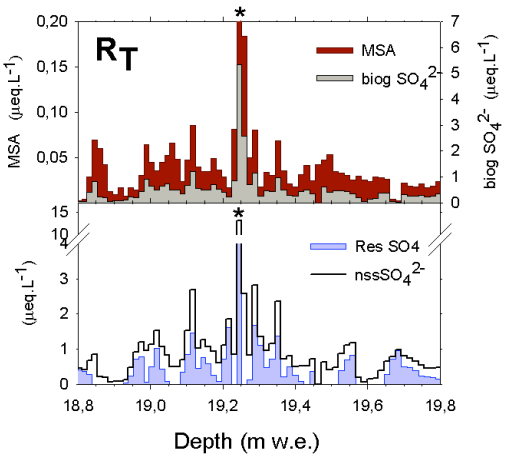

(a) $ResSO_4^{2-}$ calculated with the mean value of individual samples

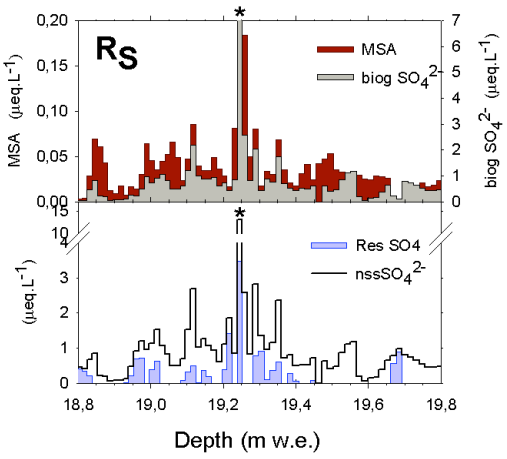

(b) $ResSO_4^{2-}$ calculated with the mean value of 0.5 m w.e. depth bins

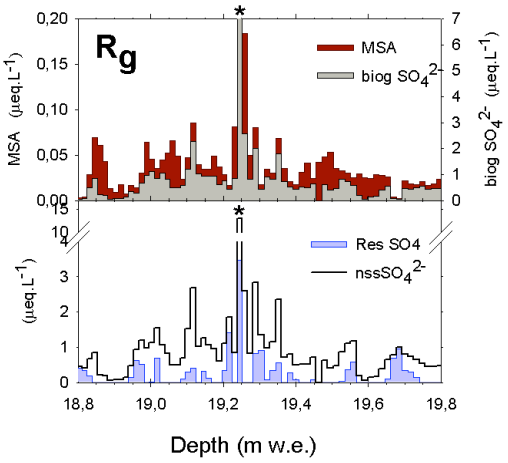

(c) $ResSO_4^{2-}$ calculated with the mean value of moving 0.5 m w.e. depth bins

Figure 3.11: An example of the calculation of $ResSO_4^{2-}$. $nssSO_4^{2-}$, $ResSO_4^{2-}$, $biogSO_4^{2-}$ and MS^- profiles are presented. $ResSO_4^{2-}$ was obtained using MS^- as reference species with different MS^-:$nssSO_4^{2-}$ ratios, according to (a) equation 3.11, (b) equation 3.12, (c) equation 3.13

3.4.2.5 The ammonium to $MS^-$and $nssSO_4^{2-}$ratio

While NH_4^+contributions can be important at sites under marine influence with $NH_4^+$to Na^+concentration ratios in snow ranging between 0.1 and 0.01 (Legrand et al., 1998). NH_4^+concentrations in samples corresponding to Na^+major peaks at SV are close to $0.15\mu eq.L^{-1}$which corresponds to significantly lower values of the ratio. On the other hand many NH_4^+peaks as high as several $\mu eq.L^{-1}$are observed along the core. This allows to conclude that the relative contribution of marine primary aerosol to NH_4^+at SV is very small, which is supported by the lack of any significant correlation between $Na^+$and NH_4^+(r$\sim$0.03). A poor correlation with $MS^-$is also observed (r$\sim$0.03)

Nevertheless, we present the depth profiles of the NH_4^+:(MS^-+ $nssSO_4^{2-}$) molar ratio calculated using the concentrations of all individual samples or deposition fluxes corresponding to 0.5 m w.e. integrated sections: from 52 m w.e. to 22 m w.e. the ratio corresponding to integrated sections varies between a few % and $\sim$50% . Upper, it progressively increases up to approximately 150% with a very high peak of 300% around 10 m w.e. that is related to combustion and will be discussed in the following chapter. All these values are significantly higher than what is observed at coastal Antarctic stations under pure marine conditions and even higher than under more continental influence when a maximum of $\sim$50% is found. We can conclude that the marine biogenic component of NH_4^+at SV is also small. Despite a very large scattering, the same observation may be made using ratios calculated with individual concentrations.

All that demonstrates that most of NH_4^+at SV is of continental (natural and/or anthropogenic) origin.

3.5 Conclusions

The presence in the SV ice core of layers with Na^+concentrations of the same magnitude of those found at lower sites (Pio XI, Tyndall, King George Island) along with chloride concentrations corresponding to quite moderate chloride losses from marine primary aerosol (5 to 7%) is an

evidence of fast transport of marine air at this altitude site, which would be more frequent in spring (SON) or fall (MAM), according to predicted precipitation (cf. chapter 2). The high δD values associated to Na^+peaks go in favor of a warm season for these contributions.

For more diluted marine air masses (Na^+minor peaks), we observe that even if the major moisture source is the ocean, the regional/local atmosphere is permanently influenced by a continental source identifiable by nitrogen containing compounds and non marine biogenic SO_4^{2-}. A free-tropospheric reservoir of aerosols and gases of continental origin can also be responsible of this mixing. Strong marine storms associated to eddy activity in the windward flanks of the cordillera as they go upslope (Garreaud, 2007), would favor mixing between oceanic (below) and continental (aloft) air masses.

Layers concentrated in Na^+, combined with the δD and deuterium excess of the snow, retrace the occurrences of marine storms from the Pacific Ocean, confirming that they take place all year round, with a lower frequency in DJF (18%). Layers concentrated in MS^-, alongside with δD and d, indicate that both the Pacific and Southern oceans have an imprint on the precipitation at this site all year round except in winter. Both primary and secondary marine sources represent 45% of the ice archive, a low value for a precipitation expected to be 96% marine, indicating that the marine influence at this site is not fully conserved. This is certainly due to wind scouring and also accumulation processes.

Wide MS^-peaks recorded along the ice core seem roughly related to nssSO_4^{2-}arrivals. Narrow MS^-peaks are mostly associated with alkaline particles (marine aerosol and eventually continental nssCa^{2+}) either by condensation on these particles during precipitation or possibly if MS^-diffusion occurs in the ice, MS^-tending to be fixed on Na^+or nssCa^{2+}rich layers

The MS^-:nssSO_4^{2-}ratio is in the range of what is observed in the same latitude band at low altitude, which demonstrates that significant amounts of MSA are transported aloft. The marine biogenic contribution to this site ranges from 30 to 50% to the total SO_4^{2-}budget, depending on the way it is calculated. This is rather low given the climatic conditions that produce an important oceanic contribution to the SV site.

Chapter 4

Continental contributions to San Valentin ice

4.1 Motivations

The marine contribution along the CL122 core has been discussed in the preceding chapter. Important sea salt arrivals (Na^+peaks) account for ∼29% of the snow of the upper part of the CL122 core, above the brittle zone (i.e. 52 m w.e.). In terms of ice archive, they represent its principal constituent. The second constituent, methanesulfonate (MS^-), tracking the marine biogenic input, covers ∼15% of the core. Two main conclusions were inferred from this observation concerning the ice record: part of the precipitation of marine origin is missing (likely due to wind scouring) as the total marine inputs should account for ∼96% according to the study conducted in chapter 2, and another non marine reservoir accounts for more than 50% of the imprint in CL122 ice. Note however that by non marine reservoir we mean the soluble contribution of continental sources to the precipitation at SV, whose primary origin is, in any case, oceanic moisture.

In section 4.2, we will describe continental sources likely to influence the San Valentin area. For every source, we will summarize what was inferred from previous ice core studies and what

could be expected from the SV core. In section 4.3 we present the methodology used. Then, in section 4.4 we will investigate the non marine fingerprint characterized by a complex cluster of carboxylic acids, NO_3^-, NH_4^+, $SO_4^{2-}$and Cl_{exc}^-. The discussion will be focused on ions origin and depth trends, and will also include a tentative dating of the core. In section 4.4.6 we will briefly present some other proxies not fully studied here but worth to mention.

4.2 Introduction

As a general rule, the main continental sources, natural or anthropogenic, to be taken into account are:

- Biomass burning (natural or intentional)
- Direct gaseous emissions from the continental biomass: natural soil emissions and emissions related to manure and chemical fertilization, vegetation emissions and litter decomposition.
- Urban centers and industrial activities (including fossil fuel consumption)
- Volcanoes
- Erodible soils

The more relevant reservoirs for this study are reported in figure 4.1.

4.2.1 Biomass combustion

Most of intentional or natural burning occurs in the tropics and the subtropics, and over the last 150 years, burning has become more influenced by human practices than natural factors (Denman et al., 2007). Present global fire activity (1982 to 1999) has been characterized with satellite observations, providing information of the seasonality of their occurrences (Carmona-Moreno et al., 2005).

- June to August are the months of maximum fire activity in the South American tropics 0-20°S and African Tropics 0-30°S.

- September to November, in subtropical regions of South America (central 20-40°S and eastern 0-30°S), Africa (0-30°S) and Australia (10-35°S).

- December to February, in South American subtropics and mid-latitudes (30-50°S) and Australia (30-40°S), February corresponding to the most intense fire activity in the Pampa and Northern Patagonia.

Emissions from biomass burning include reactive and non-reactive species such as NO_x, sulfur species (mainly SO_2), non methane hydrocarbons, VOCs, carboxylic acids, nssK^+, Cl^-, $NH_4^+$and a wide variety of organic and elemental matter. Different amounts of soil dust may also be remobilized as a result of enhanced convective activity over fires. The intensity of fire events, the composition of fire plumes and the altitude that they reach depend not only on the type of the burned vegetation but also on the meteorological conditions prevailing when fires occur. The chemical composition of biomass burning plumes has been characterized mostly in tropical areas and northern hemisphere higher latitudes (Talbot et al., 1988; Andreae et al., 1988; Sillanpä et al., 2005, see for instance).

Flaming fires may emit more NO_x than smoldering fires (Lebel et al., 1990) as they are more oxidizing. Smoldering of biomass can last for days or weeks after flaming has ceased (Reid et al., 2004).

Atmospheric compounds emitted during fire events can be transported to remote locations. For instance, it has been demonstrated that plumes of Amazon fires taking place from July to October can be transported southwards by the low level jet flowing eastward the Andes cordillera and reach Antarctic Peninsula owing to the subsidence produced by cyclones passing trough the Drake passage (Prospero et al., 2002).

Although little data on biomass burning chemical composition is available for southern mid-latitudes and even less for Patagonia, some information may be found in technical reports (In-

ternational Forest Fires News, for the last decades) and dendrochronologic records (for the last centuries). Seasonal intentional biomass burning is not a common practice in Patagonia, as it is the case in the Amazon basin. Patagonia was affected by an intense period of land clearing between ca.1890 and ca.1950 due to colonization. The intensive use of fire for land clearing in Eastern Patagonia (Argentina) took place mostly between 1850 and 1910 (del Valle et al., 1998; IFFN, 2000; Kitzberger and Veblen, 1999; Kitzberger et al., 1997) firstly due to indigenous newly acquired practices and then to sheep farming by settlers, whereas in Western Patagonia (Chile) an intense period of fire land clearing aiming to cattle grazing took place later, around 1890, peaking after 1937 as consequence of Chilean colonization policies (Gonzales and Veblen, 2007; Rodrigo S. and Orrego S., 2007). According to Chilean historical archives (museum of the city of Coyhaique), in the surroundings of the NPI, land clearing with fire produced long lasting uncontrolled subsurface (smoldering) fires that spread out to higher elevations (not aimed for grazing) due to strong winds. These fires lasted several months sometime between 1930 and 1950. On the Argentinean side, after 1910, intentional fire cessation and fire exclusion limited the burning of remaining vegetation until 1970, when an internal migratory wave populated the region. Since then, biomass burning has monotonically increased, 93% of the fires being produced by humans (IFFN, 2000). On the Chilean side, protection policies and also settlers retreat reduced human influence on fires since ca. 1960 (Gonzales and Veblen, 2007).

Ice core studies: Andean glaciochemical signature in terms of biomass burning contributions has been hitherto poorly studied. Conversely, boreal biomass burning has been extensively studied on Greenland deep ice cores (Alexander et al., 2004; Legrand and de Angelis, 1996; Savarino and Legrand, 1998; Whitlow et al., 1994). Boreal biomass burning contributes between 20 and 30% to the formate, oxalate, glycolate and ammonium deposited on central Greenland. The glaciochemical imprint of most boreal fires recorded in Greenland ice is characterized by a molar ratio NH_4^+/formate close to 1 related to smoldering events. However, a few cases having an imprint of flaming fires were observed, with NH_4^+/(formate+NO_3^-) ratios close to 1 (Legrand and de Angelis, 1996). Furthermore, a decrease of background levels of formate is noticeable

when background levels of acidity increase in the snow (Legrand and de Angelis, 1996).

Burning events along the CL122 core will be identified mainly based on NH_4^+ peaks. Then we aim to investigate the biomass burning fingerprint in relation with the different types of vegetation likely to be burned. We also will try to locate time markers in relation with documented human influences: besides a better understanding of the chemical composition of the local atmosphere, this could help to provide a tentative core dating.

4.2.2 Urban centers, industrial emissions

Industrial and urban emissions include a wide variety of compounds: carboxylic acids, nitrogen oxides, ozone, sulfur species, heavy metals, etc. (Seinfeld and Pandis, 1998). Usually, these emissions contribute only locally to the composition of the atmosphere as they do not penetrate the free troposphere (Chebbi and Carlier, 1996). South American industry and urban areas have experienced a fast growth since the mid of the 20th century. Subtropical and tropical biggest megacities viz. Buenos Aires, Rio de Janeiro, Santiago and Sao Paulo gather more than 12, 11, 6, 18 million inhabitants, respectively (Molina and Molina, 2004), and indubitably influence the atmospheric composition at a regional scale. However this influence is not yet fully studied. For instance, a study of the dispersion of SO_x emissions by copper smelters and urban areas around Santiago showed that around 40% of the emitted sulfur (i.e. 436 Gg S.yr^{-1} between 1997 and 1999) are transported southward 34°S (Olivares et al., 2002) but transport to Patagonia (the land located south of 37°S, as historically defined) is uncertain as it was not documented.

In Patagonia, cities do not exceed the million inhabitants. The principal urban centers are Neuquén, San Carlos de Bariloche, Coyhaique, Río Gallegos, Comodoro Rivadavia, Punta Arenas and Ushuaia (figure 4.1). Oil extraction began in December 1907 (1908 henceforward) and it is the principal industrial activity in Eastern Patagonia (Argentina). As far as we know, Siderca is the only smelter located in this region (38°S, Neuquén), and Sierra Grande a small iron and steel processor (41°S, 65°W). Patagonia is mostly dedicated to cattle, sheep breeding and salmon farming.

Ice core studies: No long-term high resolution registers of anthropogenic pollution are available for the last centuries for Patagonia. Further south, Antarctic glaciochemical records seem unresponsive to the increase of $SO_4^{2-}$and NO_3^-precursors due to urban growth and industrialization of the southern hemisphere during the last century (Legrand, 1997). On the contrary, nitrate and sulfate records on ice-cores retrieved in the northern hemisphere at high (Greenland) or mid latitudes (French Alps) sites are strongly influenced by atmospheric anthropogenic pollution (Fischer et al., 1998a,b; Goto-Azuma and Koerner, 2001; Preunkert et al., 2001, 2003; Yalcin and Wake, 2001; Hong et al., 1996): SO_4^{2-}shows a notorious concentration increase following industrial revolution (ca. 1890) whereas NO_3^-increase began in 1940/1950. Preunkert et al. (2001) demonstrated that high elevation alpine sites were influenced in winter by the long range transport through the free troposphere of combustion products from eastern Europe. For the case of tropical Andean glaciers, the few investigations available show a marked increase of trace metal concentrations starting at the onset of mining industry and markedly enhanced since the beginning of the last century (Hong et al., 2003; Ferrari et al., 2001; Correia et al., 2003).

Along the SV core, we will investigate the possible anthropogenic impact of lower latitude megacities and more restricted mid-latitudes activity (sporadic occurrence of pollution plumes, background trends and/or change in the composition of combustion events).

4.2.3 Natural and agricultural soils and manure emissions

Microorganisms (fungi and bacteria) are responsible of the two main biogeochemical transformations taking place in soils, namely nitrification (oxidation of ammonia into NO_2^- and NO_3^-) and ammonification (transformation of N into NH_4^+). Gaseous products and by products of these transformations are: NH_3, NO, N_2O and N_2. The three latter enter the subsequent steps in the nitrogen cycle to be finally transformed to aqueous atmospheric HNO_3^-(Seinfeld and Pandis, 1998). In soils, ammonium may be converted to ammonia that is released to the atmosphere. The reaction $NH_4OH \rightleftharpoons NH_3 + H_2O$ is favored in dry soils and deserts where accumulation of $CaCO_3$ maintains alkaline pH. Low cation exchange capacity and low rates of nitrification

maximize the production and loss of NH_3 (Schlesinger, 1996). In semi-arid environments, the respective importance of nitrification and ammonification seems to depend on the number and duration of precipitation events (Yahdjian and Sala, 2008).

The decomposition of urea, dung and dead organisms is responsible of the emission of significant amounts of NH_3. Emissions from cleared, cultivated and fertilized soils are greater than from forests. Part of NH_3 can be oxidized to NO_x (then NO_3^-) in the atmosphere and some redeposited as aqueous or inorganic NH_4^+. Gaseous NH_3 increases the alkalinity of the atmosphere immediately downwind the source. Consumption of nitrogenous fertilizers followed by redistribution alters the nitrogen cycle through enhanced ammonia and nitrous oxide emission (Schlesinger, 1996). Consumption of nitrogenous, phosphate and potash fertilizers in South America shows a marked increase in the early 1960′s according to estimates based on population growth (Zhang and Zhang, 2007). Nitrogenous fertilizers used in Chile and Argentina are mainly ammonium sulfate and urea, with significant amounts of sodium nitrate only in Chile (Matthews, 1994, inventory for 1984)

Human settlements in semi-arid or arids lands and, in particular, burning practices change the vegetation and soil properties leading to progressive desertification (Villagra et al., 2009). On the Chilean side of the Andes, after the incursion of settlers only 56% of the original forests persist in the Valdivian ecoregion (Lara et al., 1999) but not all burned land has now an agricultural use: only 0.03% of the region has really been transformed into agricultural fields, the remaining part became unproductive land prone to erosion (Eyzaguirre, 2010; Rodrigo S. and Orrego S., 2007).

4.2.4 Vegetation emissions

Biomass emission depends on the vegetation cover. In particular, forest emissions depend on the tree species composing the forest. Besides NH_3 production from senescent leaves, isoprenes are the most important emitted species. The Valdivian forest (conifers) that surrounds the NPI emits mostly monoterpenes (Centritto et al., 2008) while Amazonian forests emit mostly isoterpenes

(Schlesinger, 1996). The end products of these emissions are dicarboxylic acids.

Ice core studies: Very few information concerning vegetation and soil emissions has been inferred from ice core studies. Changes in carboxylate concentrations in Greenland deep ice cores have been related to the rebuilding of the boreal vegetal cover following the Laurentide retreat at the end of the last glacial period (Legrand and de Angelis, 1996). Seasonal variation of nitrogen species related to summer soil emissions have been observed in ice cores from the Mont Blanc, French Alps (Preunkert et al., 2001, 2003). Lastly, Kellerhals et al. (2010) propose to relate the long term ammonium variations observed along a tropical ice core to the temperature, through soil and vegetation emissions (although vegetation itself does not emit NH_4^+).

The question that arises is whether change in soil emissions after forest clearing is visible in our ice core, or in the evolution of the fires composition. A possible link between the background trend of nitrogen species and climate markers may also be investigated.

4.2.5 Volcanoes

Volcanic eruptions are responsible of the emission of volatile gases (mainly S_2, SO_2, H_2S, HCl and HBr) and solid matter (ash and minerals remobilized from the substratum). Interaction between volcanic gases and other atmospheric compounds like ammonia and soil dust particles may significantly modify atmospheric properties at a regional or even global scale.

Although more than one hundred active volcanoes have been inventoried along the Andes (Simkin and Siebert, 2002), the emission of only a few of them have undergone detailed studies until now, namely Láscar (23°S, Amigo, 2004; Tassi et al., 2009) and Cerro Hudson (46°S, Haberle and Lumley, 1998; Gutierrez et al., 2005). As a general rule the volcanic contribution to the $SO_4^{2-}$and halogene atmospheric content remains poorly documented in South America.

The most active volcanoes of extratropical South America are located between 33°S and 46°S, from which the most prominent examples are: Tinguiririca, Quizapu, Villarica, Mocho-Chosuenco, Chaitén and Cerro Hudson. Between 47°S and 55°S, volcanism is much less active

(given the slower subduction rate of the Antarctic plate in this region). The location of the most active volcanoes in the last decades in this region (Simkin and Siebert, 2002) is denoted by triangles in figure 4.1. A more detailed list of active volcanoes located near the SV is presented in the appendix (pag. 188).

Ice core studies: Non-sea-salt sulfate peaks have been used to locate the stratospheric deposits of major eruptions in polar ice cores and, thus, to provide dating tools (Cole-Dai et al., 2000, see for instance). Under favorable transport conditions even tropospheric large plumes may be observed in remote locations: once removed the non biogenic component, Antarctic ice-cores keep a record of the 1991 Cerro Hudson eruption (Legrand and Wagenbach, 1999; Baroni, 2006; Cole-Dai et al., 2000).

The influence of tropical Andean volcanism superimposed to major events of global importance has been reconstructed by de Angelis et al. (2003) for the last century. This study was based on sulfate and halogen measurements. These authors have also shown that atmospheric acidity was notably enhanced by volcanic emission in the tropical belt, leading to the ubiquitous presence of water soluble gypsum aerosols formed trough the interaction between volcanic SO_2 and carbonate particles.

At mid-latitudes, the ash plume of the 1991 eruption of the Cerro Hudson was mostly directed to the southeast and there is no evidence of its influence in the NPI even if the event lasted several days, except for the mixed marine and possibly volcanic peak (centered at 8.5 m w.e.) discussed in section 3.4.1.2 of the previous chapter. We must also keep in mind that due to wind scouring affecting this site, we can miss individual events. However, we may expect to conserve the imprint of sustained periods of volcanic activity, if any.

4.2.6 Dust particles from erodible soils

The major dust sources of South America are located on the Bolivian Altiplano (15-26 °S, 76-66°W), in Western Argentina (27-34°S, 67-70°W) and in Argentinean Patagonia (38-48°S

Neuquén, Río Negro and Santa Cruz provinces) (Prospero et al., 2002). The Patagonian Andes, lying athwart the Westerlies, foster an important climate divide that results on a very moist side westwards and a semi-arid side eastwards (Paruelo et al., 1998; Warren and Sugden, 1993). Cyclones passing through Eastern Patagonia are very effective for pumping dust into the troposphere (Iriondo, 2000) allowing their subsequent long-range transport. It is now well established that Patagonian dust plumes reached central sites of the East Antarctic Plateau during glacial periods, at a time of increased aridity and enhanced atmospheric circulation. For present time and based on aerosol (Dalia Pereira et al., 2004) and ^{222}Rn sampling performed at Punta Arenas, and on firn core studies at King George Island and Lange Glacier, it has been demonstrated that 95% of the bulk mode of dust particles found in the Antarctic Peninsula have a Patagonian origin (Dalia Pereira et al., 2004).

Semi-arid soils of the Argentinean Patagonia have suffered severe degradation during the last century, in relation with human activity. As ∼67% of them are now in a moderate to very severe state of erosion (del Valle et al., 1998) we could expect to observe a corresponding increase of nssCa^{2+}along the SV core.

Ice core studies: In the tropical belt, Correia et al. (2003) observed increased crustal input at high altitude during dry season. Concerning Patagonian sources, one of the very interesting finding of these last decades is that Patagonia was the most important supplier for dust to central East Antarctica during Quaternary glaciations (for a review, see Delmonte et al., 2010). This supports the effective injection of Patagonian plumes into the free troposphere.

4.3 Methodology

Major, minor and background contributions of NH_4^+were identified using the same methodology as for Na^+described in section 3.3 of the previous chapter, but with a variant: major contributions are those having a maximum value ≥m+2s and minor contributions are those above the standard deviation value (not the minimum *min* value of equation 3.6). This choice is justified

by the background NH_4^+variability, which is higher compared to Na^+steady background levels. NH_4^+average value and standard deviation used here are reported in table 4.1.

Table 4.1: NH_4^+mean concentration and standard deviation values along the first 52 m w.e. of CL122.

	m	**s**
	μeq.L^{-1}	μeq.L^{-1}
NH_4^+	0.1643	0.3734

Two additional smoothing techniques have been applied to the complete profile: singular spectrum analysis (Vautard and Ghil, 1989, SSA) and running averages (for 31 points, covering roughly 0.3 m w.e.). Principal Component Analysis (PCA) was used in a few cases as a deconvolution tool for intricate contributions. For SSA and PCA analysis, we used the software Analyseries and data series were resampled at a regular step (Paillard et al., 1996).

4.4 Results

As evidenced in sections 3.4.1.5 and 3.4.2.4 of the previous chapter, when the Na^+contribution weakens, a mixed chemical signal composed mostly by NO_3^-, NH_4^+, nssSO_4^{2-}, nssCa^{2+}(that corresponds in fact to total Ca^{2+}) is observed. In this section, we investigate this signal and its possible sources.

In order to locate any possible anthropogenic or climatic trend likely to help to core dating, data from the whole core (i.e. not only the part we analyzed) are used in part of the following sections.

4.4.1 Non marine sulfate

As shown in section 3.4.2.4, where calculation ways are reported in detail, the contributions of continental sources to total sulfate along the SV core may be approximated by the residual fraction of SO_4^{2-}. The residual SO_4^{2-}(ResSO_4^{2-}) relative contribution accounts from ∼30% to∼50%

of total SO_4^{2-}depending on the calculation approach (see table 3.7 from previous chapter). Nevertheless, given the uncertainties encountered in estimating residual SO_4^{2-}, we finally decided to use total nssSO_4^{2-}in the following sections (although both nss$SO_4^{2-}$and Res$SO_4^{2-}$are depicted in some of the figures, to allow a rough comparison). Moreover, most of residual SO_4^{2-}peaks tightly fit nssSO_4^{2-}peaks, which confirms that nss$SO_4^{2-}$is a good estimate of non marine sulfate out of significant marine influence (whereas biogenic SO_4^{2-}corresponds to the low frequency variability of SO_4^{2-}).

We first calculate the correlation matrix for the first 52 m w.e., once the samples corresponding to major Na^+peaks are removed (i.e., the remaining signal corresponds to Na^+background and Na^+minor peaks). This takes into account sections containing a significant continental contribution along with weak marine inputs. Results are reported in table 4.2. The most important features of this table are that nss$SO_4^{2-}$is well correlated with NO_3^-(r=0.63) and NH_4^+(r=0.60), moderately with succinate (r=0.42) and nssCa^{2+}(r=0.48) and residually with nssK^+(r=0.32), oxalate (r=0.32) and F^-(r=0.23). ResSO_4^{2-}follows rather closely nssSO_4^{2-}correlations with the aforementioned species, which retrace different origins: nssK^+can be used as tracer of biomass burning emissions of different types of vegetation (Gao et al., 2003), $F^-$is a proxy of volcanic activity (de Angelis and Legrand, 1994) and dicarboxylic acids can have both continental and marine origins (Chebbi and Carlier, 1996). This convoluted signature will be explored in more detail in the following sections.

In table 4.2 we also present the marine biogenic SO_4^{2-}(obtained using MS^-as the reference species). Interestingly, succinate is slightly correlated with both residual (r=0.42) and marine biogenic sulfate (r=0.22). This could be explained by the ubiquitous presence of succinate of both marine and continental origins in the atmosphere. Part of the succinate of continental origin may be related to pyroconvective activity produced by fires (as we will see later). As previously suggested for MS^-, the correlation of succinate with biogenic SO_4^{2-}could also be due to succinate tightening on eolian dust particles (Sillanpä et al., 2005) identified by nssCa^{2+}present in mixed air masses containing biogenic marine aerosol and continent derived species.

PCA of the triplet NH_4^+, NO_3^-, residual SO_4^{2-}shows that even if most of the variability is explained by the common variation of these three compounds (PC1=43% when using $ResSO_4^{2-}$, PC1=41% when using $nssSO_4^{2-}$), the residual variability of the signal (the remaining PCs) depends on the association of varying relative contributions of NH_4^+, NO_3^-, and $nssSO_4^{2-}$which will be discussed in detail in section 4.4.4.

4.4.2 NH_4^+major contributions

As demonstrated in the previous chapter, $NH_4^+$is mostly of continental origin in the SV core. The existence in South America of several large reservoirs for this ion (e.g. soils, biomass likely to burn) led us to consider NH_4^+peaks as valuable markers of continental events.

As shown in table 4.3, NH_4^+major contributions represent only 3.2% of the first 52 m w.e. of CL122 and minor contributions 9.9%. Excepting a few cases (cf. section 4.4.2.2), NH_4^+peaks alternate with major Na^+peaks, indicating that NH_4^+deposit does not take place with marine storms driven by a strong zonal flow.

Major NH_4^+peaks are either quite narrow (0.02 - 0.06 m w.e.) or broad (0.10 and 0.21 m w.e.). Major peaks constituted by only one single sample (events located at 5.32 and 29.25 m w.e.) will not be taken into account in further analyses (except when calculating correlation matrix). Minor contributions are mostly Dirac′s delta shaped peaks constituted by one single sample (∼0.01 m w.e.).

4.4.2.1 Location on the profile, general characteristics

In figure 4.2 we present major (black) and minor (orange) NH_4^+contributions along the 52 m w.e. of the core together with NO_3^-, Cl_{exc}^-/Cl^-, $nssSO_4^{2-}$, formate, succinate and oxalate corresponding concentrations. NH_4^+peaks are heterogeneously distributed along the profile, which may be split in four zones:

I. The first 21 m w.e., where minor $NH_4^+$and NO_3^-arrivals are more frequent than in the remaining part of the profile. In this zone, $Cl_{exc}^-/Cl^-$is mostly negative and acidity shows

Table 4.2: Correlation matrix obtained by removing only Na^+major peaks from the profile along the first 52 m w.e. of CL122. Residual sulfate ($ResSO_4^{2-}$) and biogenic sulfate ($biogSO_4^{2-}$) obtained with a moving MS^-:$nssSO_4^{2-}$ratio (equation 3.13) are included. Numbers in italics indicate a dependency of both variables due to calculations, thus correlation is biased for this cases.

	F^-	Cl^-	Br^-	Cl_{exc}^-	NO_3^-	NH_4^+	Succinate	Oxalate	Ace+Glyc	Formate	MS^-	$nssK^+$	$nssMg^{2+}$	$nssCa^{2+}$	$nssSO_4^{2-}$	$biogSO_4^{2-}$
Cl^-	0,04															
Br^-	0,12	0,39													Color code	
Cl_{exc}^-	-0,06	-0,15	0,05												**r≥|0,60|**	
NO_3^-	0,17	0,21	0,48	0,17											|0,60|≥r>|0,40|	
NH_4^+	0,16	0,11	0,21	-0,03	**0,61**										|0,40|≥r>|0,20|	
Succinate	0,18	0,08	0,14	-0,06	0,42	**0,63**										
Oxalate	0,07	0,05	0,08	-0,05	0,30	0,41	0,37									
Ace+glyc	0,24	0,04	0,06	-0,09	0,15	0,27	0,29	0,15								
Formate	0,13	-0,17	-0,04	-0,08	-0,16	0,03	0,11	0,01	0,26							
MS^-	0,23	0,20	0,10	-0,22	0,16	0,10	0,11	0,08	0,16	0,23						
$nssK^+$	0,15	0,07	0,14	-0,30	0,42	0,56	0,53	0,31	0,21	0,03	0,07					
$nssMg^{2+}$	0,03	-0,22	0,05	0,02	0,16	0,14	0,04	0,08	0,08	0,14	-0,05	-0,11				
$nssCa^{2+}$	0,20	0,21	0,23	-0,02	0,33	0,17	0,09	0,11	0,15	0,24	0,41	0,13	0,18			
$nssSO_4^{2-}$	0,23	0,23	0,40	0,05	**0,63**	**0,60**	0,42	0,32	0,11	-0,06	0,27	0,32	0,24	0,48		
$biogSO_4^{2-}$	0,20	0,25	0,29	0,02	0,41	0,24	0,22	0,16	0,06	0,03	*0,54*	0,13	0,18	*0,60*	*0,72*	
$ResSO_4^{2-}$	0,17	0,14	0,35	0,04	0,57	**0,66**	0,42	0,32	0,11	-0,11	-0,03	0,35	0,20	0,21	*0,85*	0,26

Table 4.3: Number of samples (N, out of 3882) corresponding to NH_4^+major and minor peaks and their total contribution to the first 52 m w.e. of the deep core given as the sum of all samples and in percentage (of the depth in m w.e.).

	N	Sum(m w.e.)	%
NH_4^+major peaks	138	1.672	3.2
NH_4^+minor peaks	407	5.122	9.9
NH_4^+(total)	545	6.794	13.1

a decrease tendency from $\sim 0.5 \mu eq.L^{-1}$to values close to $0.0 \mu eq.L^{-1}$. Major peaks average composition is: NH_4^+=1.17±0.28 $\mu eq.L^{-1}$, NO_3^-=1.10±0.22 $\mu eq.L^{-1}$, nssSO_4^{2-}=2.50±0.60 $\mu eq.L^{-1}$.

II. From 21 to 28 m w.e., a zone deprived of any NH_4^+contributions. This zone coincides with a zone where Na^+major peaks are also absent (cf. figure 3.2) and may be considered as representative of present time background levels of all species, i.e., NH_4^+=0.13±0.02 $\mu eq.L^{-1}$, NO_3^-=0.26±0.01 $\mu eq.L^{-1}$, nssSO_4^{2-}=0.60±0.11 $\mu eq.L^{-1}$.

III. From 28 to 50 m w.e. a densely populated zone with minor and major NH_4^+peaks (NH_4^+=1.04±0.25 $\mu eq.L^{-1}$, NO_3^-=0.73±0.12$\mu eq.L^{-1}$, nssSO_4^{2-}=3.11±0.58 $\mu eq.L^{-1}$)

IV. Not shown in figure 4.2 but shown in figure 4.6. There is a group of peaks from 61.9 to 62.6 m w.e. characterized by their high content of oxalate (2-7$\mu eq.L^{-1}$), acetate ($0.6 \mu eq.L^{-1}$) and formate (1-3.6$\mu eq.L^{-1}$) .

In table 4.4**(a)** we present the correlation matrix for major NH_4^+arrivals (calculated including all peaks) where, besides marine contribution, we observe that:

- nssSO_4^{2-}, NO_3^-, NH_4^+, $H^+$are strongly correlated r$\sim$0.6 and to a less extent with dicarboxylic acids r<0.55
- Formate losses due to strong acidity are evidenced by the anticorrelation existing between formate and H^+r=-0.37

Table 4.4: Correlation matrices for the first 52 m w.e. of CL122 for **(a)** NH_4^+ major peaks **(b)** NH_4^+ minor peaks and **(c)** background levels of NH_4^+. See section 4.3 for NH_4^+ peaks definitions.

(a)	Na	MS^-	F^-	Br^-	Formate	Succ.	Oxalate	NO_3^-	NH_4^+	Cl_{exc}^-	$nssSO_4^{2-}$	$nssK^+$	$nssMg^{2+}$	$nssCa^{2+}$
MS^-	0,08													
F^-	0,17	-0,02												
Br^-	0,62	0,25	0,02											
Formate	0,06	0,33	0,00	-0,08										
Succinate	0,00	0,04	0,07	0,26	-0,18									
Oxalate	-0,02	0,10	-0,05	-0,16	0,59	-0,08								
NO_3^-	-0,06	0,09	-0,07	0,23	0,07	0,56	0,30							
NH_4^+	-0,05	0,02	-0,01	0,09	0,34	0,35	0,63	**0,79**						
Cl_{exc}^-	0,04	-0,03	0,03	0,25	-0,02	0,27	-0,01	0,31	0,25					
$nssSO_4^{2-}$	-0,06	0,26	-0,07	0,40	-0,04	0,38	0,09	0,67	0,50	0,14				
$nssK^+$	0,15	-0,05	0,49	0,05	0,04	0,17	0,14	0,21	0,29	0,17	0,03			
$nssMg^{2+}$	0,04	0,21	-0,04	0,21	0,21	-0,06	0,27	0,06	0,21	0,02	0,14	0,01		
$nssCa^{2+}$	0,08	0,60	0,05	0,24	0,36	-0,04	0,35	0,17	0,19	-0,05	0,43	0,06	0,28	
H^+	-0,08	-0,15	-0,06	0,23	**-0,26**	0,41	-0,11	0,62	0,33	0,18	0,73	0,00	-0,10	**-0,21**

Color code

r>=|0,60|

|0,60|>r>=|0,40|

|0,40|>r>=|0,20|

(b)	Na^+	MS^-	F^-	Br^-	Ace+ G	Forma	Succin	Oxalat	NO_3^-	NH_4^+	Cl_{exc}^-	$nssSO_4$	$nssK^+$	$nssMg$	$nssCa^2$
MS^-	0,15														
F^-	-0,03	0,21													
Br^-	0,83	0,12	-0,01												
Ace+ Gly	0,05	0,25	0,05	0,08											
Formate	-0,07	0,26	0,08	-0,02	0,47										
Succinate	-0,01	0,04	0,44	-0,03	0,01	0,13									
Oxalate	-0,04	0,20	0,14	-0,10	0,23	0,24	0,23								
NO_3^-	-0,08	0,18	0,16	0,23	0,08	0,01	-0,01	0,09							
NH_4^+	-0,10	-0,04	0,07	-0,07	0,01	-0,07	-0,03	0,35	0,17						
Cl_{exc}^-	-0,64	-0,20	0,00	-0,42	-0,10	0,06	-0,02	-0,06	0,21	0,04					
$nssSO_4^{2-}$	0,02	0,25	0,29	0,16	0,17	0,20	0,00	0,24	0,44	0,15	0,07				
$nssK^+$	-0,23	-0,01	0,44	-0,20	-0,01	0,13	0,21	0,20	0,07	0,07	0,13	0,03			
$nssMg^{2+}$	-0,32	-0,04	0,10	-0,18	0,18	0,31	0,08	0,17	0,17	0,15	0,46	0,32	0,18		
$nssCa^{2+}$	-0,02	0,34	0,40	0,06	0,28	0,53	0,03	0,31	0,39	0,06	0,05	0,48	0,08	0,24	
H^+	-0,13	-0,19	-0,24	0,01	-0,21	-0,45	-0,10	-0,22	0,19	-0,04	0,28	0,23	-0,10	-0,03	-0,66

Color code

r>=|0,60|

|0,60|>r>=|0,40|

|0,40|>r>=|0,20|

(c)	Na^+	MS^-	F^-	Br^-	Ace+ Gly	Formate	Succinate	Oxalate	NO_3^-	NH_4^+	Cl_{exc}^-	$nssSO_4^{2-}$	$nssK^+$	$nssMg^{2+}$	$nssCa^{2+}$
MS^-	0,22														
F^-	0,11	0,13													
Br^-	0,78	0,10	0,10												
Ace+ Gly	0,06	0,02	0,22	0,03											
Formate	-0,09	0,07	0,16	-0,07	0,15										
Succinate	0,01	0,11	0,23	0,01	0,09	0,17									
Oxalate	0,00	0,05	0,03	0,00	0,03	-0,02	0,03								
NO_3^-	-0,03	0,01	0,06	0,22	-0,05	-0,26	0,00	0,04							
NH_4^+	0,20	0,08	0,04	0,22	0,20	-0,33	-0,01	0,05	0,23						
Cl_{exc}^-	0,18	0,06	0,03	0,27	-0,01	-0,06	0,00	0,01	0,21	0,03					
$nssSO_4^{2-}$	0,01	0,17	0,05	0,21	-0,13	-0,18	0,03	0,08	0,53	0,23	0,17				
$nssK^+$	0,05	0,08	0,22	0,06	0,11	0,03	0,37	0,04	0,09	0,12	0,11	0,04			
$nssMg^{2+}$	0,11	0,09	0,02	0,13	0,00	0,01	0,02	0,00	0,01	0,00	0,76	0,07	0,07		
$nssCa^{2+}$	0,07	0,24	0,15	0,11	0,03	0,09	0,05	0,03	0,24	0,09	0,07	0,35	0,10	0,07	
H^+	-0,04	0,00	-0,01	0,22	-0,13	-0,28	0,00	0,13	0,71	0,16	0,25	0,78	-0,02	-0,02	-0,05

Color code

r>=|0,60|

|0,60|>r>=|0,40|

|0,40|>r>=|0,20|

- nss$Ca^{2+}$is moderately correlated with MS^-, acetate, formate and oxalate r>0.30, likely due to condensation/deposition of acidic gas/secondary aerosol on dust particles. nss$Ca^{2+}$is also well correlated with nssSO_4^{2-}, and in a few cases in stoichiometric equilibrium, which suggests the presence of gypsum . The anticorrelation observed between nss$Ca^{2+}$and H^+indicates that calcium rich minerals take a prominent part in the neutralization of atmospheric acidity in the SV latitude range.

As stated in chapter 3, NH_4^+:(MS^-+nssSO_4^{2-}) molar ratios strongly suggest that the marine biogenic component of ammonium is very low. This is supported by the absence of any strong MS^-- nssSO_4^{2-}-NH_4^+correlation in NH_4^+peaks when high NO_3^-concentrations are observed. Thus, we can definitely discard marine biomass as a source of NH_4^+significant arrivals. Four hypotheses may be then proposed to explain the presence of NH_4^+peaks:

1. Biomass burning, as the species associated to major NH_4^+peaks (viz. nssK, NO_3^-, nssSO_4^{2-}, nssCa and dicarboxylic acids) have also been found in aerosol measurements in biomass burning plumes (Andreae et al., 1988; Gao et al., 2003; Talbot et al., 1988, for some exemples).

2. Soil emissions and litter decomposition although the absence of strong continental convection in the SV area does not favor the transport of local emissions toward higher altitudes.

3. As suggested by the association of $NO_3^-$and nss$SO_4^{2-}$with NH_4^+, the long-range transport of combustion plumes containing fossil fuel emissions

4. The neutralization of volcanic SO_4^{2-}plumes by atmospheric $NH_4^+$and carbonate rich particles, especially in the samples where F^-(a proxy of volcanism (Mather et al., 2004b)) is present.

In a ternary plot (figure 4.3) we compare the respective contributions of SO_4^{2-}, $NO_3^-$and $NH_4^+$of individual major NH_4^+events as well as the mean value corresponding to NH_4^+background conditions with selected data available for precipitation:

i) Rainwater data for a site strongly impacted by coal combustion (Flues et al., 2002, Figueiras, Brasil) and a remote site (Galloway et al., 1996, Torres del Paine National Park). Note that the marine contribution to total sulphate has not been removed from this last set of data, leading certainly to overestimate the sulphur contribution.

ii) Data corresponding to boreal forest fire events and background conditions recorded in a Central Greenland deep ice core for the preindustrial Holocene time period (de Angelis 2010, pers. comm.), denoted by filled cyan circles. Concentrations in fire events once removed background mean values contain the highest relative abundance of ammonium of the whole graph due to most exclusively smoldering conditions.

iii) Data for winter and summer snows from the summit area of the French Alps covering the onset of anthropogenic activity ca. 1925 (Preunkert et al., 2001, 2003), also denoted by filled cyan circles. Summer data correspond to local emission influenced by soil emission, while winter data correspond to the free troposphere influenced by the long range transport of pollution from Eastern Europe.

iv) We have also reported reference values for biofuel combustions (Tissari et al., 2008) showing large variations of sulfur content (emission by oat and rape seed burning contain a rather high amount of sulfur while wood and other types of tropical and subtropical vegetation combustion are sulfur depleted). Note that experiments performed in burners are NH_4^+depleted due to complete combustion conditions (N is emitted as NO_x). Field fires involving similar vegetation would led to varying relative contributions of nitrate and ammonium, but the relative abundance of sulphate in emission will remain unchanged. Along with this dataset, we present some reference values for biomass burning average composition of biofuels; savanna, tropical and extratropical fires, agricultural waste and charcoal burning (Andreae and Merlet, 2001).

Our data show relative low ammonium proportions, varying between a few and ∼20%, in NH_4^+events and a background mean value close to ∼5%. Peak events may be classified in three

main groups on this ternary plot (figure 4.3):

1. Only three events fit rather well the composition of biofuel combustion (events 2, 4 and 33)

2. Roughly half of the events gather around Figueira and Torres del Paine data, showing strong sulphate enrichment (1, 2, 3, 5, 8, 11, 12, 13, 14, 15, 16, 17, 21, 22, 23 i.e.).

3. The remaining points are located in between these two groups (6, 18, 20, 24, 25, 27, 28, 30, 31, 32). Almost of all our samples (except two events showing rather low concentrations and located in the very upper part of the core), have nssSO_4^{2-}content always higher than average SO_4^{2-}values published for biomass combustion. Thus, given such high SO_4^{2-}contents and even if most events have a combustion-like composition in terms of species identified, emission from fossil fuel combustion (instead of biomass) as well a mixed signature with other sulphur rich atmospheric contributions cannot be discarded. This preliminary study will be compared with a detailed examination of the individual composition of some NH_4^+events.

4.4.2.2 Mixed $NH_4^+$and Na^+major contributions

In most of the record, an alternation between major peaks of NH_4^+(expected to have a continental origin) and Na^+(expected to have a marine origin) is observed, three NH_4^+major events show an overlapping between both $NH_4^+$and Na^+major peaks (events 4, 17, 21, depicted in blue in the ternary plot (cf. figure 4.3 and figure 4.4(a) for detailed compositions)

Note that the composition of event 4 is close to the composition of extratropical forest fires (ternary plot). The high $SO_4^{2-}$and F^-concentrations observed in event 17 may possibly be due to volcanic activity. If true, Na^+could come from volcanic ash solubilization by acidic gases. The composition of event 21 is relatively similar to rainwater in Torres del Paine National Park (Galloway et al., 1996), but also to rainwater sampled downwind a coal burner in Brazil (Flues et al., 2002). Taking into account our preceding remark on the influence of marine sulphate on

the precipitation composition at Torres del Paine, we think that the comparison with Figueiras data is more relevant. This could imply the existence of pollutant emissions from a reservoir influencing the whole Patagonian region, possibly mixed with marine air masses.

Aerosol measurement in an oceanic environment (Yeatman et al., 2001, Mace Head) under the influence of urban polluted areas showed evidence of the shift of NH_4HSO_4 and NH_4NO_3 from the fine mode of aerosols to the coarse mode when polluted air masses were mixed with marine air masses. Mechanisms invoked by the authors are chemical replacement, condensation and coagulation. This would imply that the presence of NH_4^+, SO_4^{2-}, NO_3^-in SV can be due to the long range transport of urban pollutants in the fine aerosol mode to this region. Their deposit on the snowpack would be only granted if coarse mode marine alkaline aerosols were available for gathering gaseous species or secondary aerosol.

This mixing of marine $Na^+$and NH_4^+peaks highlights the complex interactions between continental and marine emissions short and long-range transported at SV.

4.4.2.3 Can we identify biomass-burning events?

San Valentin NH_4^+major peaks contain mostly NO_3^-, nss$SO_4^{2-}$and dicarboxylic acids, species that have been measured in forest or more open canopy fire emissions (Andreae et al., 1988; Gao et al., 2003) and in sites under urban influence (Pio et al., 2008; Sillanpä et al., 2005). However, important differences arise: acetate and formate are absent in most imprints, which is not usually the case for combustion events, and very high nssSO_4^{2-}concentrations are always observed, which is puzzling.

The absence of formate in most of the SV events can be explained by snow acidity. This phenomenon has been observed in Greenland ice containing high amounts of sulphuric acid of volcanic origin, or in firn layers submitted to the growing impact of fossil fuel combustion on nitrate and sulphate budgets (Savarino and Legrand, 1998; Legrand and de Angelis, 1996). Formate losses were observed in samples with acidity higher than the typical Holocene background (i.e. H^+>1.5 to 2 μeq.L^{-1}) likely due to equilibrium shift that favours the presence of monocar-

boxyilic acids in vapor phase. Acetate and formate are kept by alkaline snow ($H^+ < 0 \mu eq.L^{-1}$), very likely entrapped on soil dust, ash or salts, as observed in several events below 19 m w.e. (events marked with circles in the ternary plot). The absence of acetate/formate due to higher acidity frequently observed in more recent events may track change in combustion type and/or atmospheric acidity with time. Nevertheless, the acidity in the upper 22 m w.e. of the ice core shows instead a decrease tendency (from $\sim 0.5 \mu eq.L^{-1}$to $\sim 0.0 \mu eq.L^{-1}$), and this would favor the hypothesis of a changing of combustion type (which includes vegetation changes induced by human practices).

The total contribution of $nssSO_4^{2-}$to the total soluble species budget (i.e., the sum of all ion concentrations, in this case, expressed in moles to facilitate the comparison with bibliographic values) ranges from 18 to 40%, which is 2 to 4 times higher than in boreal Holocene fires recorded in Central Greenland (10% according to de Angelis 2010, pers. comm.) and 2 to 6 times higher than in semi-arid and Amazonian fires (Talbot et al., 1988). Only events 2, 19, 20, 27, 28, 30 present a $nssSO_4^{2-}$molar fraction in the same range as semiarid or boreal fires. This could indicate that two kinds of combustion events influence the SV region, implying different fuels either of natural or of anthropogenic origin .

Soluble potassium is abundant in vegetation and generally considered as a good indicator of biomass burning events. K^+concentration in NH_4^+events at SV show a rather high variability compared to ammonium. NH_4^+/K^+ratios range between 4 and 100 with a mean value close to 20, which is lower than in preindustrial or pollution impacted boreal fires ($NH_4^+/K^+ \sim 40$, Sillanpä et al. 2005, de Angelis 2010, pers.comm.) and significantly higher than in Amazonian fires (Talbot et al., 1988, $NH_4^+/K^+ \sim 3$) (no data is available for African fires). This may point again to different types of combustion events in relation with fuel composition. However, in figure 4.4(b) we present an exception for this. We found one case of a double peak of NH_4^+(the only case found), which retraces a mixed signature: it contains K^+(as $nssK^+$) in its first portion and it is deprived of K^+in its second portion. Its NH_4^+/K^+ratios are, respectively, 8 and 30. It seems unlikely that a single event retraces 2 separate sources simultaneously (all other measured

species remain consistent between the two parts of this peak). It would rather seem that this changing in the NH_4^+/K^+ratio would retrace the evolution of the combustion event, that may involve in its latter phase a different type of vegetation of the same area.

Although most fires contain HCl (black numbers in the ternary plot), only one event (event 9) shows high chloride excess values ($0.86\mu eq.L^{-1}$as a mean). Semi-arid African vegetation fires show high HCl content (Gao et al., 2003) while boreal and amazonian fires contain more Na^+than Cl^-(Sillanpä et al., 2005; Talbot et al., 1988). This indicates that fires from Patagonian vegetation are generally deprived of important HCl content, but no data are available to confirm or reject this hypothesis.

The insoluble content of event 9 has been investigated by SEM (figure 4.5). Clusters of micro- soot, unequivocal tracers of combustion, were identified. This, combined with preliminary analyses of levoglucosan (Cozic 2009, pers.comm.), a marker of cellulose combustion, and the presence of long chain carboxylic acids (C8 to C16) dominated by acids with odd C number (Jacob 2009, pers.comm.) confirms a biomass burning origin for this event. Compared to other samples analysed by SEM (representative of marine, dust, and background levels), event 9 was the most densely populated by insoluble particles. They ranged mostly from 10 to 50 μm. Some of them were rather large and dense (such as ferrite, P13 in figure 4.5), likely remobilized from soil surface by pyroconvection. We also observed diatoms known to remobilise from sedimentary basins, as those designed by S in figure 4.1. This suggests a possible eastern Patagonian origin of event 9. However, even if such event clearly contains a local biomass burning contribution, it can also be influenced by a secondary reservoir of nssSO_4^{2-}as sulphuric acid.

As shown in 4.5, the concentrations of formate ($0.250\ \mu eq.L^{-1}$), acetate ($0.081\mu eq.L^{-1}$), oxalate ($0.720\mu eq.L^{-1}$), NH_4^+($1.119\mu eq.L^{-1}$) and NO_3^-($0.947\mu eq.L^{-1}$) are generally lower than in boreal forest fires recorded in Greenland snow by Savarino and Legrand (1998). Only events 9 and 18, which are more concentrated in ionic species, are close to Greenland values. A few events located in the deeper part of the core, between 61.9 and 63.0 m w.e. (events 27 to 31) and peaks located between 35 and 45 m w.e. (numbers 14 to 22) present a composition different from

the other ones. Is this due to a change in burning practices, to temporal trend in relation with anthropogenic sources, or to very different sources (not combustion related)? We will address this issue below.

4.4.2.4 NH_4^+ major contributions and F^- peaks

NH_4^+ peaks located between 35 and 40 m w.e. (peaks 14 to 17) are associated with unusually high amounts of F^- (0.02 -0.06μeq.L^{-1}) compared to the mean F^- content of all other NH_4^+ peaks ($\sim$0.002μeq.L^{-1}). Moreover, these peaks correspond to the highest relative SO_4^{2-} contributions, exceeding 70% of the $NH_4^+ - NO_3^- - SO_4^{2-}$ triplet in the ternary plot (fig. 4.3). Although also emitted in combustion processes and industrial exhausts, F^- is a good tracer of large volcanic eruptions (de Angelis and Legrand, 1994; Mather et al., 2004b). Most of the sulphate in these events was very likely deposited as H_2SO_4 as demonstrated by fluoride and chloride relocation on sulphate peak borders (figure 4.11). This pattern is very similar to the fingerprint of the tropospheric arrival of major volcanic events in Greenland (de Angelis and Legrand, 1994) or at high altitude sites of the southern tropical belt (de Angelis et al., 2003). The presence of NH_4^+ associated with volcanic SO_4^{2-} can be explained by the partial neutralization of volcanic acidic gases by atmospheric ammonia (Mather et al., 2004b).

We are aware that short individual volcanic events can be missing in the SV record due to wind scouring or even to unfavorable transport conditions (e.g., in spite of the proximity of the Cerro Hudson to the SV, its plume was directed to the south east and did not have an important impact in the SV). However, it seems difficult to entirely miss inputs corresponding to a sustained period of volcanic activity (lasting several months or years). The only period of quasi permanent volcanic activity documented for the last century in subtropical southern America is the one corresponding to the Quizapu volcano (35°S, number 1 in figure **??**), which had an eruptive phase starting in 1907 and ending with a major plinian (VEI=5) eruption in 1932 as described by Maksimov (2008); Hildreth and Drake (1992). Thus, we argue that part of Quizapu′s emissions could have been conserved in SV ice (either with precipitation or as dry

Event number	N	Depth m	Depth m w.e.		NH_4^+ µeq.L^{-1}	NO_3^-	$nssSO_4^{2-}$	Cl_{exc}^-	$nssK^+$	$nssMg^{2+}$	$nssCa^{2+}$	Succ	Ox	H^+	F-	NH_4^+/ NO_3^- µeq.µeq^{-1}	$nssSO_4^-$/ NO_3^-	NH_4^+/ $nssK^+$
1	(15)	0,3	0,1 -0,3		0,97	0,51	1,64	-0,03	0,03	0,01	0,28	0,05	0,02	0,90	0,00	1,90	3,33	28,75
2	(26)	1,4	0,6 -0,8		0,85	0,62	0,68	-0,26	0,15	0,01	0,41	0,04	0,09	-0,25	0,01	1,84	1,29	5,78
3	(1)	5,3	2,4 -2,4		1,33	0,28	1,39	-0,19	0,05	0,31	0,31	0,01	0,14	-0,38	0,01	4,68	4,88	27,47
4	(4)	10,3	5,1 -5,1		0,56	1,02	0,28	-0,15	0,00	-0,03	0,03	0,00	0,01	0,60	0,00	**0,87**	0,36	123,36
5	(2)	12,9	6,6 -6,6		1,00	0,37	1,40	-0,11	0,09	0,40	0,52	0,01	0,11	-0,21	0,02	2,64	3,76	11,00
6	(4)	14,1	7,3 -7,3		0,72	0,89	1,48	0,05	0,02	0,04	0,88	0,01	0,02	0,80	0,01	**0,75**	1,60	34,08
7	(6)	20,1	10,7 -10,8		1,43	0,98	4,65	-0,11	0,05	0,28	2,74	0,03	0,08	1,14	0,01	1,45	4,71	27,51
8	(5)	20,4	10,9 -10,9		2,45	1,68	4,26	-0,05	0,08	0,10	1,53	0,04	0,14	1,91	0,01	1,21	2,44	29,08
9	(8)	22,1	11,9 -12,0		3,99	3,67	5,98	0,48	0,79	0,11	0,75	0,27	0,39	5,15	0,01	**0,96**	1,68	5,05
10	(1)	29,2	16,6 -16,6		1,38	1,67	2,12	0,13	0,04	0,06	0,17	0,02	0,03	2,34	0,01	**0,83**	1,27	31,94
11	(8)	33,0	19,2 -19,3		0,41	0,91	3,14	-0,24	0,03	0,29	3,27	0,02	0,00	-0,18	0,01	**0,49**	2,74	11,79
12a	(3)	33,9	20,0 -20,0		2,24	2,11	6,93	0,14	0,22	-0,03	0,08	0,04	0,08	6,79	0,01	**1,13**	3,33	10,14
12b	(6)	34,0	20,0 -20,1		2,22	2,81	10,18	0,23	0,06	0,01	0,14	0,04	0,05	10,90	0,01	**0,79**	3,62	39,74
13	(3)	46,1	29,1 -29,1		0,94	0,78	3,77	0,07	0,04	0,12	1,00	0,02	0,03	2,56	0,00	1,38	4,94	21,24
14	(10)	54,5	35,9 -36,1		1,23	0,71	4,55	-0,23	0,13	0,02	0,92	0,06	0,03	2,83	**0,03**	1,71	6,36	9,62
15	(2)	56,0	37,2 -37,2		1,85	1,12	4,34	0,16	0,05	0,17	1,35	0,06	0,11	2,36	**0,02**	1,59	3,77	34,63
16	(6)	56,8	37,9 -38,0		0,69	0,47	2,26	-0,04	0,07	0,04	1,77	0,02	0,06	0,20	**0,03**	1,52	5,47	9,31
17	(2)	57,0	38,0 -38,1		1,15	1,76	13,01	-0,50	0,37	0,37	15,47	0,11	0,80	-2,23	**0,05**	0,66	7,18	3,11
18	(4)	58,1	39,0 -39,0	Quizapu?	3,33	1,54	4,17	-1,24	0,40	0,06	0,33	0,14	0,27	0,76	**0,03**	2,28	2,28	8,25
19	(2)	59,1	39,9 -39,9		0,76	1,04	-0,33	-0,42	0,03	0,06	0,44	0,02	0,02	-0,97	0,00	**0,70**	-0,35	27,24
20	(6)	59,3	40,0 -40,1		0,58	0,65	1,20	-0,05	0,04	0,03	0,26	0,02	0,01	0,92	0,00	**0,72**	1,85	13,68
21	(2)	60,7	41,2 -41,3		0,95	0,36	-0,58	-4,07	-0,14	-4,93	1,35	0,02	0,05	-1,94	0,02	3,71	1,19	
22	(4)	61,7	42,1 -42,2		2,50	1,28	8,46	0,02	0,16	0,16	0,45	0,07	0,09	6,65	0,01	1,98	6,86	15,64
23	(8)	70,3	49,5 -49,6		1,86	1,05	2,95	0,00	0,17	0,17	2,33	0,01	0,04	-0,49	0,01	1,87	2,86	10,92
24	(3)	73,6	52,3 -52,4		0,99	0,54	1,25	-0,02	0,06	0,11	3,29		0,13	-2,56	0,00	1,38	2,30	16,90
25	(5)	80,7	58,6 -58,6		1,32	0,70	0,76	0,04	0,09	0,05	0,47		0,10	-0,34	0,00	1,72	1,07	14,87
26	(4)	82,0	59,7 -59,7		0,76	0,71	2,43	-0,05	0,02	0,07	0,23		0,11	2,09	0,01	1,15	4,50	31,11
27	(4)	84,6	61,9 -62,0		1,17	0,51	1,01	0,11	0,23	0,15	0,94		0,35	-0,52	0,00	2,11	2,07	5,14
28	(14)	84,7	62,1 -62,3		3,40	1,55	2,12	-0,08	0,42	0,31	3,19		2,41	-1,34	0,00	1,96	1,31	8,05
30	(6)	85,2	62,5 -62,6		2,08	1,07	1,60	0,15	0,11	0,21	2,33		1,04	-0,87	0,00	1,77	1,52	19,37
31	(2)	85,6	62,8 -62,8		1,16	0,64	1,38	-0,04	0,14	0,06	1,45		0,19	-0,67	0,01	1,78	2,25	8,32
32	(6)	89,8	66,5 -66,6		0,67	0,58	1,01	-0,01	0,14	-0,04	1,87		0,01	-1,08	0,00	1,13	1,75	4,83
33	(2)	91,7	68,1 -68,1		1,15	0,65	0,37	0,19	3,17	-0,24	0,93		0,01	-3,84	0,54	1,70	0,56	0,36
Mean (all peaks)					1,46	1,07	3,03	-0,19	0,22	-0,04	1,56	0,03	0,21	0,94	0,03	1,59	2,87	20,26
Std dev (all peaks)					*0,89*	*0,73*	*3,04*	*0,75*	*0,56*	*0,89*	*2,68*	*0,05*	*0,45*	*2,96*	*0,09*	*0,86*	*1,90*	*21,76*
Summit (L) NO_3^-<1.6 µeq.L^{-1}					2,328	1,182			0,03	0,03	0,17	0,05				1,97		
Summit NO_3^->1.6 µeq.L^{-1}					3,806	2,194			0,01	0,08	0,45	0,22				1,73		
Amazonia mixed layer (T) neq m^{-3}					12	4,4	2,6					1,80					0,22	
Amazonia free troposphere					2,2	0,77	0,33					0,21					0,15	
Boreal fire + pollution (S) µeq.L^{-1}					80,33	40,48	102,3											

Table 4.5: Mean ratios and selected species of major NH_4^+peaks. Concentrations are given μeq.L^{-1}and ratios in eq.eq $^{-1}$. Total mean concentrations (average of all events) and corresponding standard deviation in italics. The number of samples per event are given between parenthesis, in the first column next to the sample number. Some reference values are also presented: glaciochemical measurements in Greenland ice, Summit, for fires having NO_3^-<1.6 and NO_3^->1.6μeq.L^{-1}(L, Savarino and Legrand, 1998); reference values for Amazonian fires are deduced from aerosol measurements and given in neq.m^{-3} (T, Talbot et al., 1988); and values for boreal fires having undergone transport through a urban polluted atmosphere (S, Sillanpä et al., 2005). Blue NH_4^+pics are mixed with important Na^+concentrations. Red pics have high concentrations of oxalate, NH_4^+, nssCa^{2+}. A volcanic contribution is depicted in orange (probably the Quizapu). The dashed lines delimit depths with high and low NH_4^+/NO_3^-ratios.

deposits), as northerly contributions are relatively frequent at this site (2.3% northerly +18.3% NW advections, cf. table 2.8).

4.4.2.5 Deep ice NH_4^+major peaks

Events 27 to 31, located between 61.9 and 62.6 m w.e. (fig. 4.6), are characterized by very high oxalate (2-7μeq.L^{-1}), acetate (0.6μeq.L^{-1}) and formate (1-3.6μeq.L^{-1}) concentrations compared to other events, even the most concentrated in oxalate ($\sim$1μeq.L^{-1}, peaks 17 and 9), acetate (0.1 μeq.L^{-1}), or formate (1.6μeq.L^{-1}peaks 23 and 24) of the upper 52 m w.e. We also observe very high amounts not only of nitrate and nssSO_4^{2-}but also of nss$Mg^{2+}$and nssCa^{2+}. The ice is slightly alkaline.

A rather similar association of unusually high concentrations of NH_4^+, formate, oxalate, nss$Mg^{2+}$and nss$Ca^{2+}$was also found in Greenland basal ice (Tison et al. 1998, de Angelis 2010, pers.comm.) and related to the decomposition of vegetal debris, lichen activity and/or animal excreta deposited on the former bedrock deprived from ice. The origin of these peaks in the SV brittle ice remains to be explained, however biomass burning does not seem to account for the whole set of events.

All the previous observations demonstrate the complexity of SV chemical records. NH_4^+major peaks do not always correspond to combustion events, and it is difficult to infer unambiguous origin only based on their chemical composition. Only events 2, 4 and 33 have a signature rather similar to data commonly published for pure vegetation fires, in particular concerning their sulphate content. Nevertheless, the influence of biomass combustion is clearly identifiable even in sulphur rich events (dicarboxylic acids, nssK^+presence, even if it is low at this site).

The high nssSO_4^{2-}concentrations contributing to significantly enhance the snow acidity remain difficult to explain. In some cases they could be attributed to volcanic activity, but given the association with NO_3^-commonly observed, the possible influence of urban pollution cannot be discarded. We can also evoke particular features of Patagonian vegetation: a tentative explanation involves the rather high sulphur content that may be expected in Patagonian soils due to the

presence of evaporitic layers and the formation and subsequent deposition of secondary gypsum formed by the interaction between Andean volcanic passive degassing or eruptive emissions and mineral particles (de Angelis et al., 2003, see for instance). Biomass fire from vegetation growing on sulfur rich soils should emit larger amount of sulphur species than elsewhere.

Amazonian and also Pampean fires can be transported by the low level jet flowing southwards on the eastern side of the Andes cordillera and reach SV when northerly/ northeasterly flow arrive to the site (see figure 2.1, page 41). Forest fires on the western side of the cordillera could also be fast transported by a smaller jet detected on the western side of the Andes (Garreaud, 2009).

4.4.2.6 Additional information provided by succinate?

It has been demonstrated from aerosol sampling that succinate can be an indicator of fire plumes aging (Pio et al., 2008; Sillanpä et al., 2005, plumes aged of more than 1 day). Most of SV NH_4^+major events show high succinate concentrations, markedly above background level (>0.05 μeq.L^{-1}) and sometimes associated with oxalate, which points to the existence of significant combustion sources for SV. However, as it is the case for MS^-, succinate diffusion in snow may be observed (and diffusion is much more marked for succinate than for MS^-). For instance in events 10, 18 (figure 16, 16-17 m w.e., 38.6-39.5 m w.e.), we observe succinate gaussian-like profiles centered on NH_4^+maxima and likely produced by diffusion. Diffusion processes seem to be restricted by the presence of nssCa^{2+}, like in events 7 and 8 (10.4-11.4 m w.e.). This is in agreement with the findings of Sillanpä et al. (2005) that point to the condensation of dicarboxylic acids (oxalate, malonate, succinate) produced by boreal fires on PM10 dust particles. However, not all major NH_4^+peaks are associated with nssCa^{2+}peaks (events 2, 10, 11, 12,18, 20, 21, 22, 26 are not). Events, having nssCa^{2+}concentrations lower than 0.5μeq.L^{-1}, may correspond to fires that did not lead to significant soil particle mobilization (low intensity) or that have been transported in air masses not significantly impacted by soil dust (free troposphere). As for MS^-, succinate tightening on alkaline aerosol may have artificially enhanced former concentrations.

Although succinate cannot provide absolute information on plume ages, we may suggest that

most of the plumes reaching SV have been transported for at least 1 day. Particularly high succinate content compared to ammonium are observed in a few NH_4^+ major events suggesting farther location of source areas or less direct transport pathways (events 1, 2, 9, 13, 14, 16, 18 and 22). As only N/NW backtrajectories seem to pass over the continent, the most probable source of fires containing high amounts of succinate seem to be located northward of the NPI.

4.4.2.7 Temporal evolution of fire composition and dating constraints

In biomass burning events, the NH_4^+/NO_3^- ratio can be used as a fire type indicator. Indeed, flaming fires are more oxidizing and thus, emit more NO_x than smoldering fires (Lebel et al., 1990; Reid et al., 2004). Although plume aging increases the conversion rate of NO_x and organic nitrogen species to nitrate (Andreae et al., 1988), we argue that low NH_4^+/NO_3^- ratio in NH_4^+ events would indicate flaming conditions.

NH_4^+ to NO_3^- molar ratios in individual NH_4^+ events identified as very likely influenced by combustion point to 2 main kinds of contributions: the group of events located between 11.9 and 29.2 m w.e. shows NH_4^+/NO_3^- ratios lower than 1:1 (0.3 to 0.8) while above (from the surface to 10.9 m w.e.) and below (below 35 m w.e.) NH_4^+/NO_3^- ratios are higher than 1:1 (1.3 to 2.1).

This can be due to a temporal trend of fire practices / conditions in Patagonia and it is consistent with the colonization history of the region: fires located deeper than 35 m w.e. may correspond to smoldering conditions that would have been prevailing in a) the early stage of colonization of Chilean Patagonia, when the forest was still densely populated or b) pre colonization wild fires emissions. Lower NH_4^+/NO_3^- ratios observed between 11.9 and 29.2 m w.e would correspond to more flaming fires.

Some dating constraints can be then proposed. The first hypothesis is that fires recorded between 29.2 and 45 m w.e. having NH_4^+/NO_3^- ratios>1:1 would be tracers of forest clearing in Chilean Patagonia (characterized by smoldering conditions) starting in 1890 and fires in the same depth range having a NH_4^+/NO_3^- ratio close to 1 would be tracers of Argentinian Patagonia clearing (characterized by flaming conditions and starting in 1870).

1937 marks the onset of intensive land clearing for cattle settling in western Patagonia (Gonzales and Veblen, 2007; Rodrigo S. and Orrego S., 2007), which may be reflected by higher NH_4^+/NO_3^- ratios in events located above 30-35 m w.e. More flaming conditions may be expected since the forest, once destructed by fire clearing, is progressively replaced by shrubs (the surrounding region has lost at least 50% of its original vegetation cover).

Another hypothesis is that the onset of Patagonian settlement (either in Chile or in Argentina) cannot be clearly deciphered from natural background, and that the increase of fire frequency at ∼43 m w.e. corresponds to the beginning of intensive destruction of the Chilean forest, i.e. 1937. In this last case the sudden transition between smoldering and flaming conditions at 30-35 m w.e could be explained by the exploitation of open vegetated areas in relation with overgrazing farther North (Villagra et al., 2009).

Above 11.9 m w.e., NH_4^+/NO_3^- ratios become again higher than 1:1. This suggests either the return to smoldering fire conditions in relation with a better fire control by state policy, or a recent change in atmospheric equilibrium, i.e. increase of atmospheric ammonia likely to react with acidic air masses.

In conclusion, we propose that most of NH_4^+ peaks are tracers of fires in SV ice. They can retrace burning conditions (flaming or smoldering), which can be due to a change in land use and/or the influence of different sources, some having a more local character than others. They can be used to identify date periods in the ice core although not absolute dating layers can be defined (see section 4.4.5 for more details on the dating hypothesis proposed).

4.4.3 Minor ammonium contributions: soils and vegetation emissions?

In section 4.4.2, the complex fingerprint of NH_4^+ major peaks was attributed to combustion emissions of biomass possibly combined with fuel burning events, volcanic eruptions or urban-like pollution. Minor NH_4^+ peaks are by far less intricate. In table 4.4**b** we present the correlation matrix for minor NH_4^+ contributions, and it appears that

- NO_3^- and NH_4^+ do not correlate. Conversely, NO_3^- is only associated with nssSO_4^{2-} (r=0.44)

while $NH_4^+$is only slighlty correlated to oxalate (r=0.35)

- Mono and dicarboxilic species weakly correlated among themselves (r>0.2)

As oxalate and $NH_4^+$are both end-products of uric acid decomposition of animal waste, they can be found tightly associated in stoechiometric equilibrium in regions influenced by important animal populations(Legrand et al., 1998). The average $NH_4^+$and oxalate concentrations in NH_4^+minor peaks are 1.12 μeq.$L^{-1}$and 0.07 μeq.L^{-1}, respectively, which does not support the decomposition of animal waste as a significant source of ammonium and implies the existence of another ammonium reservoir, such as soil emissions or litter decomposition.

Another important characteristic of these peaks is that they are more frequent between the surface and 11 m w.e. The increase of NH_4^+minor peak frequency observed in the most recent part of the CL122 core can be partly explained by higher sampling resolution in relation with the strong increase of net accumulation rates suggested for the few last years (cf. chapter 1), but we may also evoke the increase of the use of nitrogenous fertilizers that started few decades ago (Zhang and Zhang, 2007).

The good correlation between $NO_3^-$and nssSO_4^{2-}(r = 0.44) may be due to the mixing of polluted air masses transported through the free troposphere with more local soil emissions uplifted to SV altitude. Local emissions of NH_4^+would preferentially take place at the time of maximum soil activity and litter decomposition (i.e. warm periods) and synoptic conditions favoring the uplift of local air masses above the boundary layer. They should also be accompanied by nitrate emissions, which is not supported by the lack of correlation between these two ions. Moreover the Dirac′s shape of NH_4^+peaks is very specific and remains difficult to explain if we assume that $NH_4^+$is deposited by the same processes as NO_3^-or nssSO_4^{2-}. Thus, Dirac′s shaped peaks could not directly reflect the NH_4^+atmospheric content but tentatively be explained by short episodes of NH_4^+dry deposition or formation at the snow surface.

4.4.4 Background ammonium contributions: the intricate contribution of NO_3^-, SO_4^{2-}, and Cl_{exc}^-

The correlation matrix for background NH_4^+ levels (table 4.4**c**) shows that SO_4^{2-} and NO_3^- arrive mostly as acids (r=0.8 and 0.7 with H^+, respectively) and are also rather well correlated (r=0.53).

An example of NH_4^+, NO_3^-, nssSO_4^{2-} and Cl_{exc}^- background concentration profiles is given in figure 4.7 for the 20-26.5 m w.e. core section. A case where these four species peak together (below the background level) is denoted by 'a' in figure 4.7. A detailed examination of depth profiles corresponding to NH_4^+ background shows that NO_3^- and nssSO_4^{2-} occurrences are closely related, although in varying stochiometric proportions (see 'c' in figure 4.7). It appears that not only NO_3^- and nssSO_4^{2-} covary, but that a close relationship exists also with Cl_{exc}^-. Although not visible in the correlation matrix, this relationship must not be neglected. The presence of HCl may be related to HCl production over the ocean (degassing from marine primary aerosol and oxydation of marine chlorocarbons) or to anthropogenic emissions. The preferential association of Cl_{exc}^- with NO_3^- when the relationship of this last species with nssSO_4^{2-} weakens (see 'b' in figure 4.7), may be related to the decomposition of PAN from polluted air transported long range within the cold southern marine atmosphere. (Note that residual SO_4^{2-} in also included in the figure and its spikes confirm non marine contributions to the background SO_4^{2-}).

Background levels of NH_4^+, NO_3^-, nssSO_4^{2-}, Cl_{exc}^- are presented in figure 4.8 alternatively smoothed using: the running average of 31 points (0.3 m w.e.) in fig. 4.8(a); and the first component of resampled and SSA filtered signals in fig. 4.8(b). The latter was built using a filtering window corresponding to the depth covered by 100 samples. SSA was used as a complement of the running average because it is more appropriate to depict the dominant oscillations of a system.

In fig. 4.8(a) we observe that NO_3^- and nssSO_4^{2-} generally covary, with a few additional nssSO_4^{2-} broad peaks (e.g. 30 m w.e.) possibly due to volcanism. Except a broad relative minimum observed at approximately 76 m w.e. both profiles do not show any specific trend up to ∼52 m w.e. Then, markedly higher levels of both ions are observed from 52 up to ∼27 m

w.e. Lower NO_3^- and $nssSO_4^{2-}$ levels are observed above 27 m w.e. No clear NO_3^- trend is observed until approximately 14 m w.e. (ca. 1965). Upper NO_3^- regularly decreases from 14 m w.e. to the surface, while the decrease of $nssSO_4^{2-}$ seems to start a little bit earlier at approximately 20 m w.e. A similar trend may be observed for Cl_{exc}^-, except a decreasing tendency from 83 up to 63 m w.e. also observed for MS^- and suggesting changes in sea surface conditions at this time. The broad peaks observed along the Cl_{exc}^- profile, although scarcer, are always associated to NO_3^- and $nssSO_4^{2-}$ peaks which is similar to what was observed on detailed profiles.

The main trends of NH_4^+ profile are quite different: below 72 m w.e. NH_4^+ does not show any specific trend, with large variations around 0.07 μeq.L^{-1}. Then it progressively decreases from rather high values centered at 1 μeq.L^{-1} at 68 m w.e. to values close to 0.05 μeq.L^{-1} at 45-48 m w.e. It remains more or less constant around 0.07 μeq.L^{-1} up to 27 m w.e. Upper, a two step increase is observed. The first one is rapid, leading to a rather constant level close to 0.07-0.1 μeq.L^{-1} between 25 and 14 m w.e. followed by a marked increase from 0.07 to 0.14 μeq.L^{-1} close to the surface, where the highest values of the whole profile are observed. Besides these general trends, a rather good agreement between the occurrences of NH_4^+ and NO_3^- and/or $nssSO_4^{2-}$ broad peaks may be observed between ∼27 and 52 m w.e.

Average NH_4^+ and NO_3^- background values are 4 to 10-fold lower at SV than pre industrial northern hemisphere values for biomass burning events obtained in Greenland, while $nssSO_4^{2-}$ is in the same range, pointing again to a specific sulfur fingerprint in Patagonia. For the three species, background average values are lower than in ice cores from the South Tropical belt (de Angelis 2010, pers. comm.). Average values calculated for the 20-26 m w.e. core section considered as representative of more recent background conditions are the same as when calculated over the whole profile down to 73 m w.e.

A recent work of Kellerhals et al. (2010) pointed to NH_4^+ as a tracer of temperature in tropical South America, as soils and vegetation productivity increases with temperature. Although vegetation does not emit ammonia, vegetation productivity and the amount of litter available for decomposition (especially in the Pampa and forests) could be related. Thus it cannot be

discarded that the increase of NH_4^+background concentrations at SV would also be reflecting a regional increase of soils emission. Note that NH_4^+emissions in semi-arid Patagonian soils is favoured by the absence of larger precipitation events (dry years), while ammonia emission by litter decomposition is decreased by drought (Yahdjian and Sala, 2008). NH_4^+increasing trend could be the consequence of one or a a combination of the following factors, i) increasing expanse of arid soils of Patagonia in relation with fire land clearing which became intensive on Chilean territory in 1937 ii) increasing temperature: the steady increase of ∼1.5°C observed for minimum temperature values between 46-53 °S, from Aysen to Punta Arenas, since 1933 (Rosenblüth et al., 1997). If true, the ice horizon corresponding to 1933 would be located at 27 m w.e. or a little bit deeper. Note however that at around 41 °S, a cooling of ∼2.3 °C was observed between 1933 and 1992; iii) change in the pluviometric regime over Patagonia leading to drier soil conditions. This last hypothesis must be better checked.

However, no one of the preceding hypothesis could account for the major NH_4^+increase starting at ∼14 m w.e.). This could be a consequence of fertilizer consumption which markedly increases in subtropical south America since the early 1960′s (Bouwman et al., 1997; Zhang and Zhang, 2007). Nitrogenous fertilizer in southernmost South America are mainly used in Argentina between 30 and 40°S and on the western side of the Andes, south of 35°S (Matthews, 1994). This last hypothesis is quite consistent with the only absolute dating horizon we have hitherto i.e.1965, located at approximately 14 m w.e .

Curiously, while $NO_3^-$and SO_4^{2-}background concentrations registers show and increasing trend in northern hemisphere ice core, in SV ice core, they clearly tend to decrease since a few decades along the SV ice core. Background conditions in the SV ice should correspond to free tropospheric arrival. If true, corresponding profiles should allow to track change of atmospheric background conditions rather than the influence of specific local sources. This hypothesis could compare with data from Arctic ice cores: it has been shown that the anthropogenic increase of $SO_4^{2-}$and $NO_3^-$was not recorded in an ice core recovered at the summit of Mount Logan (5340 m.a.s.l., Alaska) as clearly as in other artic ice-cores recovered at lower altitudes. This was

explained by the high altitude of the drilling site, remaining in the free troposphere even during winter, when pollutants accumulate in the polar vortex, and also by the important wind blowing producing incomplete accumulation (Holdsworth, 1985; Yalcin and Wake, 2001).

If background conditions at SV really reflect the composition of the regional atmosphere rather than local influences, the background increase of both SO_4^{2-} and NO_3^- from 52 to 27 m w.e. could be the consequence of large scale pollution. Similarly, the NH_4^+ background increase observed at 14 m w.e. could be related not only to local practices but also to the global nitrification of the whole South American atmosphere due to the increasing fertilizer consumption since 1961. Among potential regional pollution reservoirs, we can mention oil extraction in Argentinean Patagonia starting in 1908, with a steady increase since then, or population increase in major cities and the onset of intensive industrial activity farther North. Technology improvement of oil extraction beginning after 1958 could have partly contributed to marked decrease of SO_4^{2-} and NO_3^- concentrations above 14 m w.e. Even if the precise reasons of the NO_3^- and SO_4^{2-} decrease in SV ice remains unclear, we may hypothesize that such a decrease would have modified the chemical equilibrium of the atmosphere. NH_3 - NO_x- equilibrium is, for instance, constrained by the pH of the atmosphere. pH change may influence either the oxidation of SO_2 to SO_4^{2-} and NO_x to NO_3^- or the more efficient deposition of SO_4^{2-} and NO_3^- when neutralized with NH_4^+. However coupled chemical reactions constrain these processes so that a straightforward relationship is difficult to determine, and a modeling work would be necessary to better assess this change.

In fig. 4.8(b) we observe essentially the same tendencies described in fig. 4.8 (a). Nevertheless, additional information from the PC1s can be obtained: The variability of the background record at a ∼5-year resolution (according with the dating of 0.19 m w.e. proposed by Vimeux et al., 2008) shows that 19% of the variability of NH_4^+ background levels is explained by the PC1, 10% for NO_3^-, 16% for nssSO_4^{2-}, 25% for Cl_{exc}^- and 9% for MS^-. This indicates that 1) the oceanic component depicted by MS^- is governed by different time scales 2)nssSO_4^{2-} is undoubtedly associated to NO_3^- oscillations, but it is also partly associated with Cl_{exc}^-. The SSA application to

our signal is limited due to the lack of dating horizons. As new constrains will be set, a more in-depth work on background signals treated with SSA can be useful depicting the main climatic modes governing this region, and probably unveiling teleconnections among them.

4.4.5 Proposed dating horizons

Several time markers have been mentioned in this document and may be summarized as follows:

Radioactive stratospheric fallouts from the 1962-1963 major nuclear test period show the highest flux in 1965 in Southern Hemisphere. According to preliminary tritium (Schotterer 2009, pers. comm.) and radionuclides profiles (Magand β and γ decay 2008, pers. comm.), 13.82 m w.e. (25.02 m) corresponds to 1965. This unquestionable dating constraint supports the hypothesis that the marked increase of NH_4^+background starting approximately at 14 m w.e. may be related to increasing nitrogenous fertilizer consumption in South America (mostly subtropical and tropical) starting ca. 1960.

Fire events: fire clearing of the Chilean Patagonia by settlers started in ca. 1890 (smoldering fires), and 1937 marks the onset of a period of intense burning of the more open canopy replacing the dense former forest of Chilean Patagonia (flaming fires). $NH_4^+$to NO_3^-ratios as well as the location of a zone of frequent NH_4^+peaks allow us to propose 45 and 35 m w.e. (65.0 and 53.4 m) as approximate markers of 1890 and 1937, respectively. If correct, this first hypothesis would lead to an averaged net accumulation rate of 0.21 m w.e. for the 1890-1937 time period, which is in the same range as the mean accumulation rate deduced for the 1965-2005 time period from SV2005. This hypothesis leads to significantly higher accumulation rate (0.75 m w.e.) for the 1937-1965 time period.

The second hypothesis, i.e. 1937 at 43 m w.e. (62.7 m) suggested by the increase of NH_4^+major peaks associated to biomass burning events having a high NH_4^+/NO_3^-ratio) would lead to a mean snow accumulation rate of 1.04 m w.e. for the 1937-1965 time period. However, it has to be kept in mind that the zone located between 20 and 26.5 m w.e. (34.0 m and 42.7

m) where concentrations are very low for marine as well as continental markers may correspond to washout conditions associated with anomalously high precipitations.

Volcanic events: the main characteristics of a set of fluoride peaks associated to large amounts of nssSO_4^{2-}suggests that the 39-34.5 m w.e. (58.1-52.8 m) depth interval corresponds to the 1932-1907 Quizapu eruptive phase. If true, this would be in agreement with the first dating approach by fire events and would correspond to a similar mean snow accumulation rate: 0.22 m w.e.

Industry and urban development: The increase in nss$SO_4^{2-}$and NO_3^-background concentrations around 52 m w.e. can correspond to 1908, the beginning of oil extraction and urban growthn in Argentinean Patagonia, located eastern from the SV. In this case, the so-called Quizapu period would only contain the emissions for the last eruptive phase, and the first eruptions would not be present in SV ice.

Nevertheless, according to the backtrajectories study, most of continental airmasses influencing the SV originate farther north (or south), not from the east. Thus, the assumption that the higher nss$SO_4^{2-}$and NO_3^-background concentrations between approximately 52 and 27 m w.e. are due to the long range influence of pollutants from industrial and urban centers in eastern Patagonia is not really supported by the general transport pattern of air masses. In that case, the high nss$SO_4^{2-}$and NO_3^-background levels could be related to mining or Amazonia land clearing further north for rubber exploitation (in the late 1800′s). A southern influence of fuel-like emissions could be related to maritime traffic for whaling during the operation of the Gyrytviken whale processing station (South Georgia island) from 1904 to 1965. Another hypothesis can be the influence related to maritime traffic through Magellanic strait prior the opening of the Panama canal in 1914, however, this seems unlikely as the 1914 horizon would be placed in 26.5 m w.e., above the intense fire period, which seems a more robust hypothesis.

All these dating hypothesis need to be confirmed and are presented in table 4.6 and figure 4.9 can be included in the glaciological model (Vincent et al., 1997) currently used to try to reconstruct ice flow at SV. This is in good agreement with the possible large changes of net snow

accumulation rates related with ice location along the flow line (Ginot 2009, pers. comm.).

Table 4.6: Proposed dating horizons. The year 1965 is located at 13.82 m w.e. (25.02 m) according to radiogenic measurements.

Dating hypothesis	**Absolute horizon proposed**	**Depth in m w.e.**	**Depth in m**	**Net accumulation m w.e. yr^{-1}**	**Period covered**
Smoldering fires in early stage colonization	1937	35	53.4	0.21	1890-1937
	1890	45	65.0	0.75	1937-1965
High fire frequency due to intensive land clearing	1937	43	62.7	1.04	1937-1965
	1890	Not given			
Quizapu eruption	1932	34.5	52.8	0.22	1907-1932
	1907	39	58.1	0.62	1932-1965
Industrialization or whaling onset	ca.1908	52.0	73.2	0.67	1908-1965
	Late 1800′s	52.0	73.2		
Hypothesis traffic prior to Panama canal opening	1914	26.5	42.7	0.33	1914-1965
Strange diluted snow		20.0-26.5	34.0-42.7		

4.4.6 Other continental inputs

We will here deeper investigate the part of the continental input at SV which cannot be related to continental biomass emission or combustion events and involves mineral particles emitted by erodible soils and the volcanic contribution briefly mentioned in section 4.4.2.4. In ice cores studies performed by ionic chromatography, nss$Ca^{2+}$is commonly used as a marker of soil dust. Indeed, calcium is a major component of most of soil particles, and it was demonstrated that its soluble part is higher than 80% in polar ice cores (see for instance de Angelis et al., 1992) and ranges from 50 to 80% in tropical ice cores (Correia and de Angelis 2010, pers. comm.). nssSO_4^{2-}alone or associated with halogens (HCl and HF) was used as a valuable proxy of stratospheric or tropospheric volcanic inputs in polar and tropical ice cores.

4.4.6.1 What can be inferred from nssCa^{2+}?

A detailed comparison of SV2005 and CL122 shows that the broad tendencies and major arrivals initially observed along SV2005 are also found along CL122. A large continental arrival taking place after a major burning event corresponding to the NH_4^+major event number 9 in this study, may be observed around 4.7 m w.e. (9.6 m) along the SV2005 profile. This event is centered at 10.9 m w.e. (20.5 m) in CL122. When looking at nssCa^{2+}peaks of similar width as those taken into account by Vimeux et al. (2008) (i.e. larger than 5 cm, which represents ∼3 samples in this study), we observe along CL122 the same general alternation of marine and continental arrivals as along SV2005. However, nssCa^{2+}concentrations are much noisier along CL122 where many Dirac′s delta shaped peaks may be observed, very similar to NH_4^+minor peaks.

An example of such Dirac′s events is presented in figure 4.10(a) where nssSO_4^{2-}, F^-, NH_4^+, nssCa^{2+}concentrations are shown along with $Na^+$and Cl^-. The sequence was chosen in the upper part of the core, where the high accumulation rate allows more detailed investigation than deeper. nssCa^{2+}events are numbered from 1 to 6. We observe that all of them may be related to nss$SO_4^{2-}$and NH_4^+Dirac′s peaks, although event 6 is slightly deported on the left (right side) of corresponding nssSO_4^{2-}(or NH_4^+) peak which is wider. These 6 events are sometimes clearly associated with F^-(peaks number 1, 2 and 3) and $Na^+$and Cl^-close to stoechiometric equilibrium (peaks number 1, 2, 4, 6). All that suggests the common arrival and deposition pathway (very likely dry) of mixed air masses containing volcanic gases (SO_2, HF) and ash (halite and calcium rich minerals) with soil dust and atmospheric ammonia. The highest nssCa^{2+}concentration is observed in event 1 in the same time as for nssSO_4^{2-}, which supports the hypothesis of acidic attack of mineral dust. Lastly we observe two other nssCa^{2+}peaks not associated with other species, suggesting that the volcanic influence is not continuous at SV and depends on meteorological conditions. The presence of many nssCa^{2+}Dirac-shaped peaks along CL122, not only in the firn section corresponding to 2005-2007 but also in the part of the core overlapping SV2005, is certainly partly due to the very high sampling resolution used here and may also be influenced by small-scale topography effects.

Another example of the intricate nssCa^{2+}signature is given in 4.10(b) where the same ionic profiles as in figure a are shown, except the depth that is 10.0-11.6 m w.e., and corresponds to the wide continental event centered at 10.9 m w.e. mentioned above. This figure clearly shows the simultaneous occurrence of nss$Ca^{2+}$and nssSO_4^{2-}peaks as well as narrow halite peaks (denoted by H). Two NH_4^+peaks are observed fitting the two major nssSO_4^{2-}peaks. Only a very weak fluoride increase is suggested. Once deduced the NH_4^+contribution very likely present as ammonium sulphate from nssSO_4^{2-}, we observed a nss$Ca^{2+}$to nssSO_4^{2-}ratio very close to the stoechiometric equilibrium. This suggests that nss$Ca^{2+}$is present as secondary gypsum (denoted G) formed in acidic plumes and points again to the significant impact of volcanic emission on the composition of continental air masses reaching the SV.

Ca^{2+}mean content of SV ice is 0.23 μeq.L^{-1}, which is rather low compared to other cores. It is two times higher than coastal Antarctic values (Moreno, 2007, 0.10μeq.L^{-1}at Talos Dome). It is in the range of Greenland concentrations (de Angelis et al., 1997, 0.35μeq.L^{-1}), but 6-times lower than tropical Andes Values (Herreros et al., 2009, 1.32μeq.L^{-1}at Coropuna). This is explained by the rather low water soluble fraction of nssCa^{2+}at SV. Indeed the comparison between nssCa^{2+}concentrations obtained by ICPMS (total fraction) and IC (soluble fraction) on targeted samples shows that only a few to 20% of nss$Ca^{2+}$are soluble. Such a low soluble part in soil dust reaching a site located in the vicinity of an important arid zone (cf. figure 4.1) and also impacted by acidic emissions points to a very fast transport of dust particles to the site. Short residence time in the atmosphere would generally prevent any acid attack to significantly solubilize dust particles. However and as shown in Figures b, increasing solubilization rate may be observed in the most acidic plumes along with the formation of secondary gypsum. Further investigations are needed to better understand the contribution of erodible soils at SV and to check the relevance of nssCa^{2+}as a soil dust proxy at this site.

4.4.6.2 The possible volcanic fingerprint

Due to wind scouring, the SV cores cannot offer the detailed records required by the reconstruction of past volcanic activity in this region. However, even if a significant part of individual events may be lost we cannot miss long term events. Beside the rather frequent occurrence of air masses impacted by volcanism (either quiescent regional degassing or long range transport of volcanic plumes from remote eruptions), we have also evidenced a period of sustained volcanic activity located between 39.3 and 34 m w.e. This ice section contains the 5 highest fluoride peaks of the whole profile, and was proposed to correspond to the 1907-1933 Quizapu eruptive phase (section 4.4.2.4).

In figure 4.11, we present the upper part (33.5-35.5 m w.e.) of this section, likely tracking the 1933 plinian eruption. The same ions presented in figure 4.10 are shown. The wide F^-peak may be split in two parts corresponding to different compositions of the plume. The first one (denoted 1) correspond to a first arrival of HF and H_2SO_4 and the subsequent removing of HF (the weaker acid) from a pure H_2SO_4 layer as observed in Greenland or Andean ice cores. The second episode (denoted 2) corresponds to the arrival of acidic gases mixed with volcanic ash as shown by the presence of halite (H) and a huge peak of nss$Ca^{2+}$where large amounts of HF are entrapped. Once again we observed the presence of ammonium as a consequence of the formation of ammonium sulphate in the plume. The common occurrence of nssSO_4^{2-}, F^-, NH_4^+, nss$Ca^{2+}$and NaCl is observed in all events of this ice section. Interestingly minor NO_3^-contribution are also observed, as in plume of Lascar and Villarica volcanoes, Chile (Mather et al., 2004a). This led us to think that a more detailed investigation of NH_4^+major and minor events in relation with the association between nss$Ca^{2+}$and nssSO_4^{2-}should provide further information, not only on combustion processes and soil emission but also on volcanic contribution to SV

4.5 Conclusions

Continental imprints on the CL122 glaciochemical record are complex and retrace multiple sources influence: biomass burning, fuel combustion, a probably volcanic background, and soils aridity.

Contrary to well known marine major proxies (Na^+, MS^-), the choice of adequate and unequivocal proxies to depict continental inputs is by far more complicated given the intricate associations of NH_4^+, NO_3^-, $SO_4^{2-}$and Cl_{exc}^-at this site and the high ubiquitous nssSO_4^{2-}concentrations.

Nevertheless, we were able to detect some biomass burning events (2, 4, 9 for instance) and an increase of NH_4^+major peaks between 35 and 45 m w.e. led us to consider this depth range for the land clearing of Patagonia by settlers (1890, 1937 and onwards). We also have identified some volcanic eruptions (events numbers 14 to 17) characterized by their high fluoride content and we attribute them to the Quizapu eruptive phase . Based on these events, we propose some dating horizons for the ice core.

The background trends of the NH_4^+, NO_3^-, $SO_4^{2-}$and Cl_{exc}^-allows us to identify an interesting and unexpected environmental pattern: contrary to an expected increase in anthropogenic pollutants, we observe an unexplained decrease in $NO_3^-$and $SO_4^{2-}$for the last 50 years and a high contribution between 27 and 52 m w.e. (that seems to start in the late 1800′s). This behavior needs further investigation as atmospheric equilibrium would play a role on it.

Another background trend was observed: the NH_4^+increase starting ca. 1965, which is in agreement with the increase of the use on nitrogenous fertilizers in agricultural soils of South America (not the Patagonian case). This would imply that SV registers contain a regional signature (of sources located more than 1000 km far north).

Finally, based on documented land use practices and volcanic activity we were able to propose some dating horizons, that would account for a net accumulation ranging from 0.2 to 1 m depending on the periods and also on the dates attributed to specific events assumed to correspond to Patagonian settlement and volcanic activity.

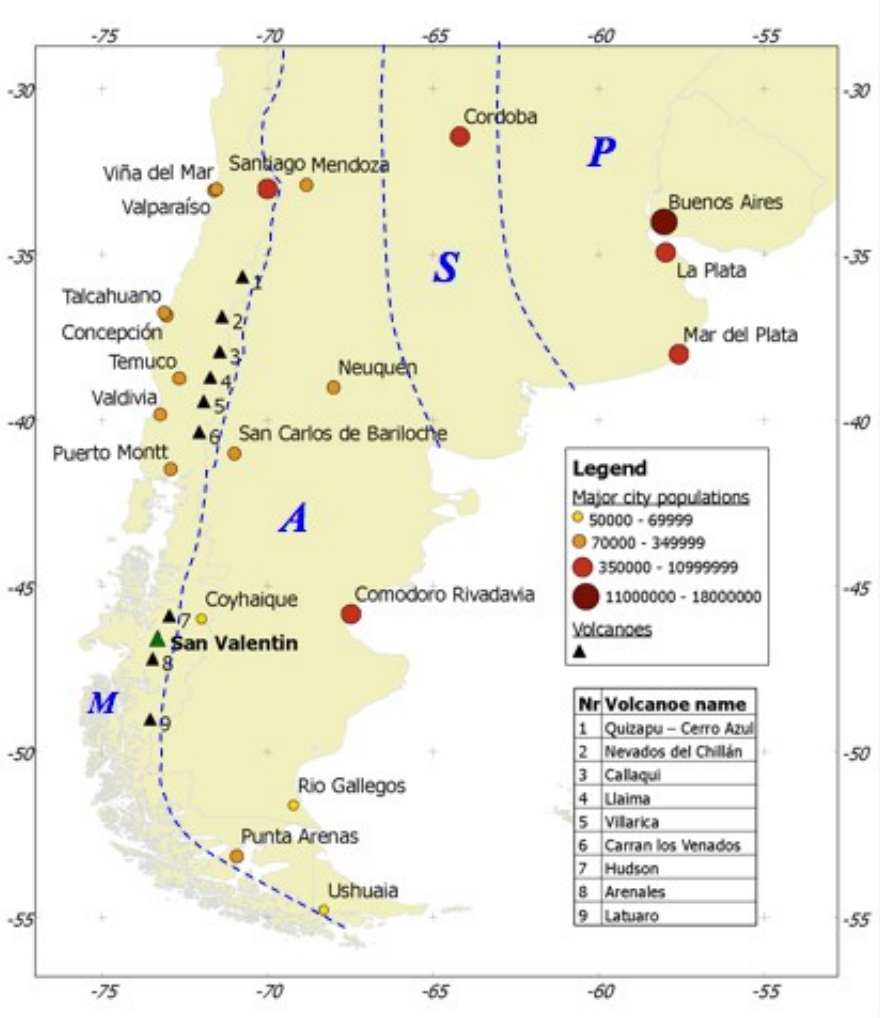

Figure 4.1: Map of southern South America (30-55°S) including the principal cities (circles) and the most active volcanoes (triangles) of the region. The color code of the circles designates the urban population. Soils and vegetation characteristics are defined by P, S, A and M (Buol, 2007; Paruelo et al., 2001). Vegetation maximum activity takes place in October and November in P and A, in October, November and April in S, and in January and February in M.**P** stands for the pampa ecoregion, an area of chemically fertile soil characterized by agricultural production and cattle pastures. **S** corresponds to a mostly aridic region dominated by sediment derived from the Andes. The soil is saline and alkali-affected. Extensive grazing is the primary land use. **A** depicts a broad upland aridic plain crossed by wide valleys. Soils are mineral-rich, contain basalt and volcanic ash. Sand dunes occur in some areas, desert pavement gravels are widespread. Sparse grazing is the primary land use. This zone is referred as Eastern Patagonia in the text. **M** stands for the mountainous Andes, where a rain shadow produces a moist region westwards populated by subantarctic forests and a drier zone located eastwards. The zone located westward the mountain divide is referred as Western Patagonia in the text.

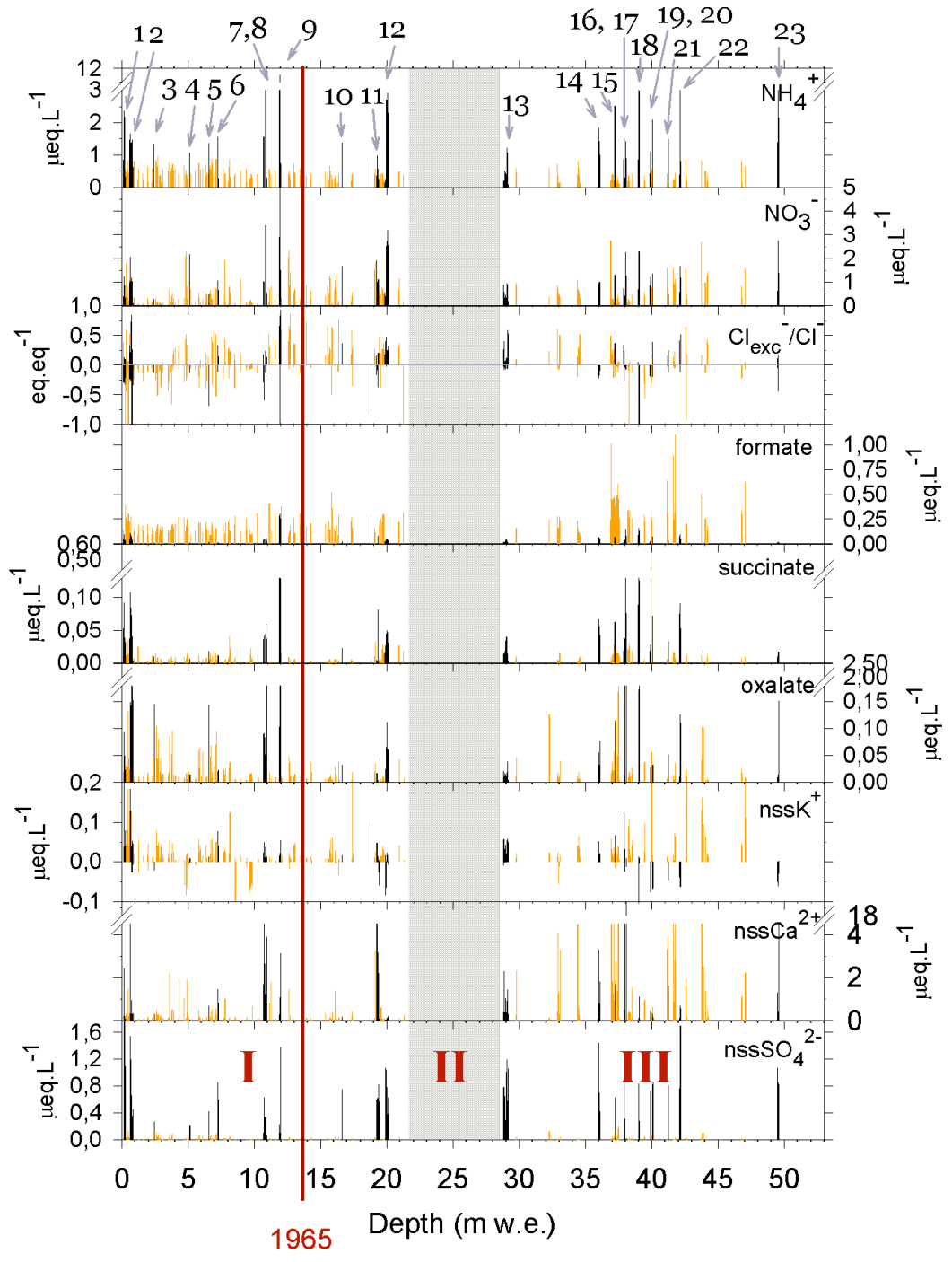

Figure 4.2: Major (black, numbered) and minor (orange) NH_4^+peaks along the first 52 m w.e. of the CL122 core. NO_3^-, the $Cl_{exc}^-$to Cl^-ratio, formate, succinate, oxalate, nssK^+, nss$Ca^{2+}$and nss$SO_4^{2-}$are also presented. Concentrations are given in μeq.L^{-1}, Cl_{exc}^-/Cl^- in eq.eq $^{-1}$. Zones of different characteristics as explained in section **??** are pointed with I, II, III. The red line represents the 1965 level, dated with both ^{3}H (Schotterer 2009, pers. comm.) and β decay counting (Magand 2008, pers. comm.).

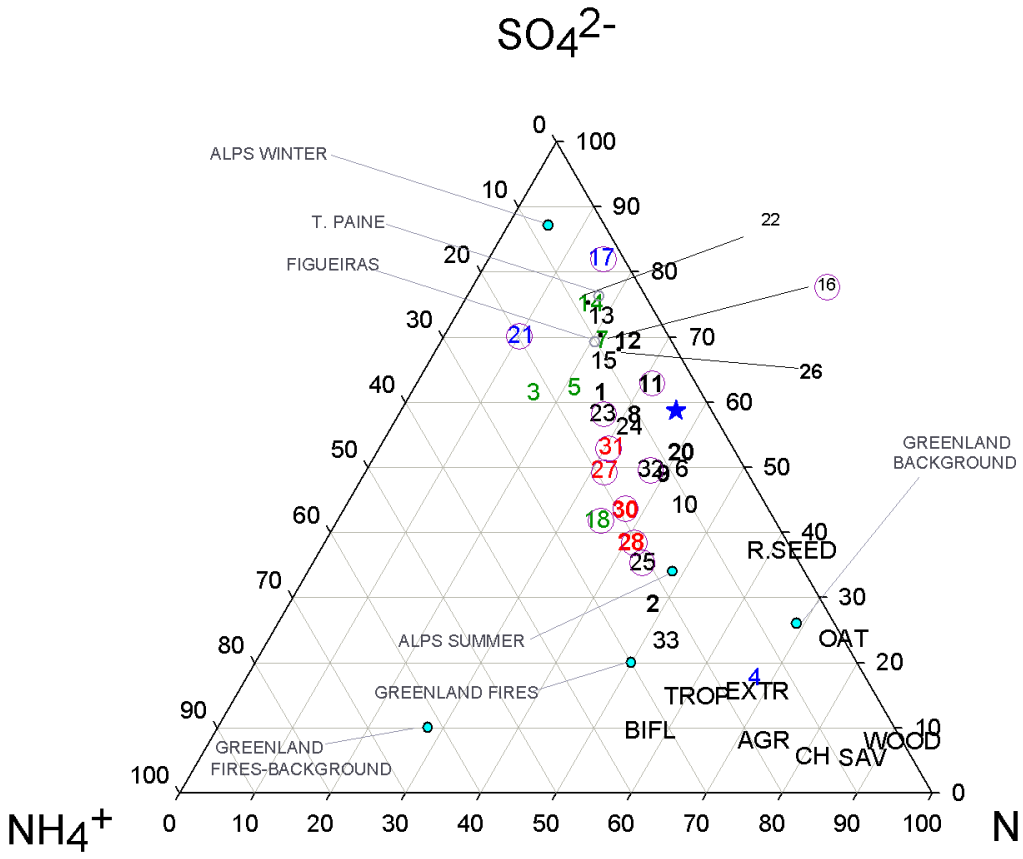

Figure 4.3: Ternary plot of SO_4^{2-}, NO_3^-, $NH_4^+$for major NH_4^+events numbered from 1 to 33 obtained in the complete profile of SV (88 m w.e.) as well as the average values for the 20-26 m w.e. section (blue star) defined as a recent background. Reference values for Alpine Ice (Preunkert et al., 2001, 2003, Col du Dome) and Greenland (GRIP) preindustrial ice (de Angelis 2010, pers. comm.) are also included. Other values corresponding to different combustion processes are: Biofuels, Tropical fires, Extratropical fires, Agricultural waste, Charcoal, Savanna fires (Andreae and Merlet, 2001, compilation from more than 100 publications); Rape Seed, Oat and Wood emissions obtained in a burner (Tissari et al., 2008). Originally reference values were given in SO_2, NO and NH_3 but in this figure they are expressed as if they were SO_4^{2-}, $NO_3^-$and NH_4^+. Finally, rainwater samples (given by the authors in μeq.L^{-1}) from a remote location (Galloway et al., 1996, Torres del Paine) and a site downwind a coal plant (Figueiras, Brazil Flues et al., 2002) are also presented. Event number 19 (39.9 m w.e.) is not included here since nss$SO_4^{2-}$is negative. Green numbers are used for chloride depleted samples (Cl^-_{exc}<0). Red numbers correspond to the events located in the deep core (62 m w.e.) containing high oxalate concentrations. Blue numbers represent major NH_4^+contributions that overlap major Na^+peaks. Circles around fires represent concentrations >0.5μeq.L^{-1}, i.e., for low acidity or alkaline snow. Units: mass percentage.

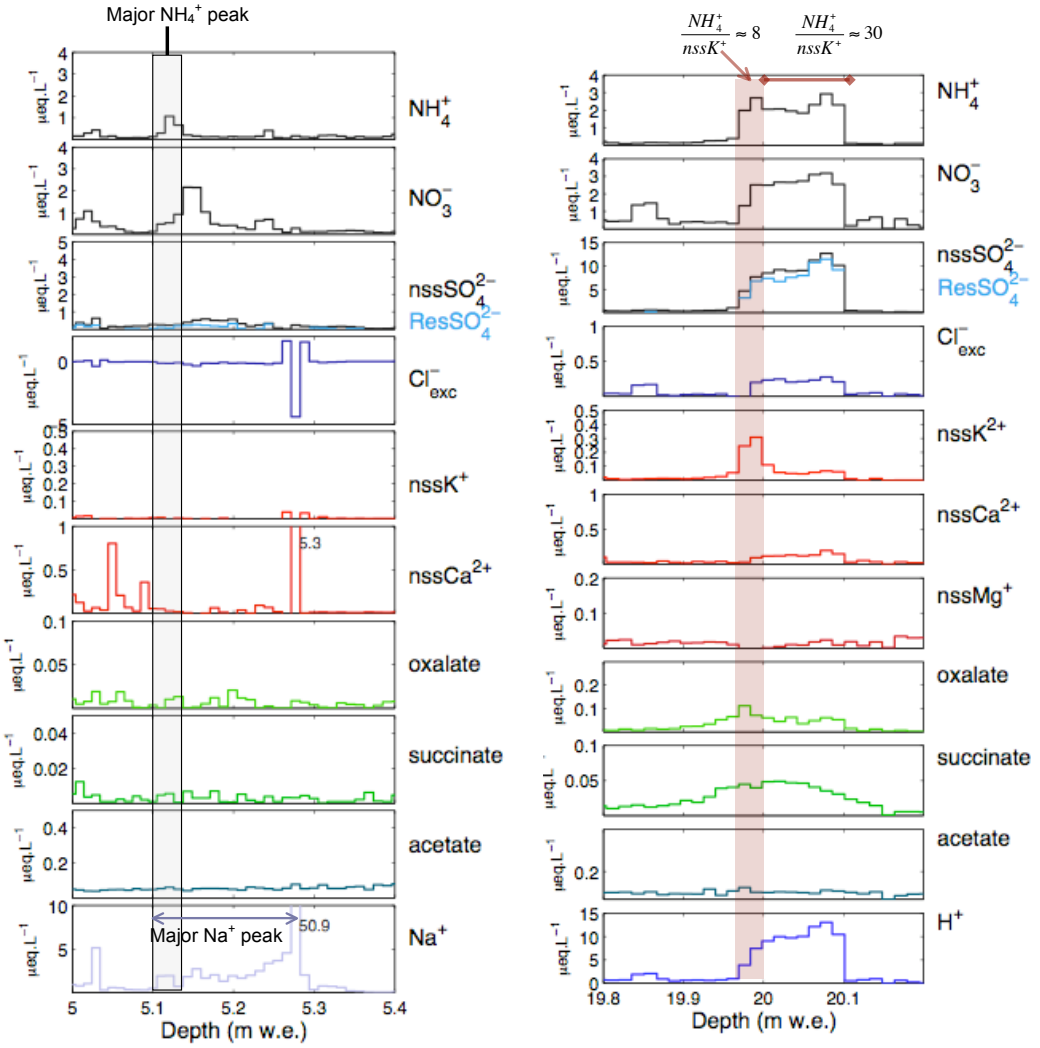

(a) NH_4^+major event number 4

(b) NH_4^+major event number 12

Figure 4.4: (a) Detailed example of a mixed contribution of a NH_4^+major peak (shaded zone) and a Na^+major peak (arrow in the bottom). Note that the NH_4^+major peak chosen (number 4) is one of the few peaks having a biomass-burning like composition, as seen in the ternary plot (fig. 4.3) (b) Detailed example of double peak of NH_4^+that has a zone influenced by nss$K^+$and other lacking nssK^+. The NH_4^+/nssK^+ratio ∼8 for the first zone is twice the value for typical amazonian fires (Talbot et al., 1988), whereas the NH_4^+/nssK^+ratio ∼30 is in the same range of boreal fires (Sillanpä et al. 2005; de Angelis 2010, pers. comm.).

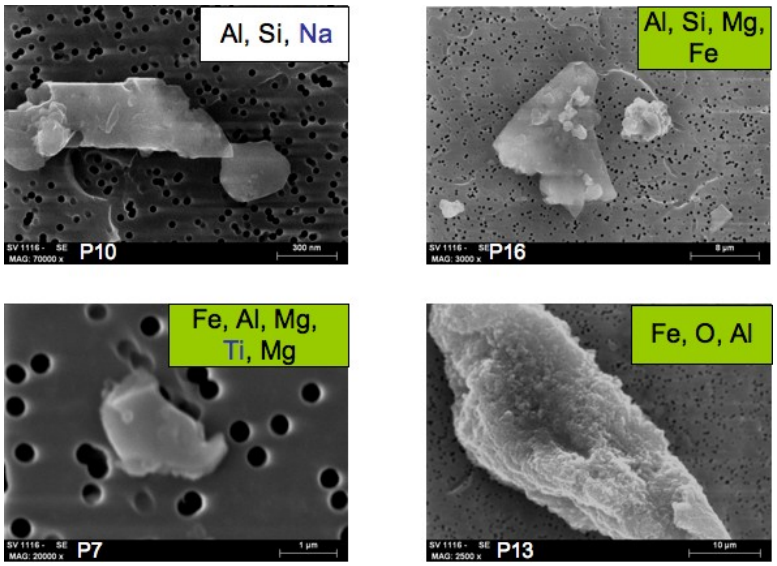

(a) Dust particles

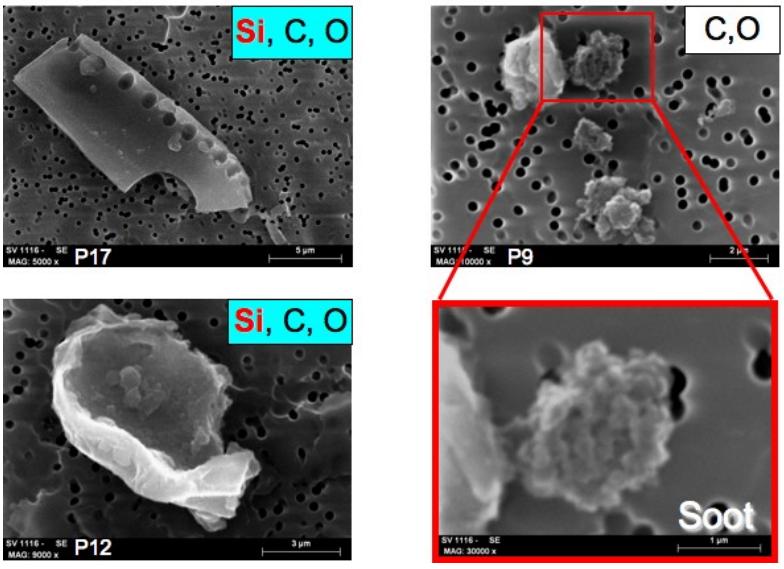

(b) Diatoms and soot

Figure 4.5: Selected images obtained by SEM of insoluble particles found at the NH_4^+peak spanning from 11.9-12.0 m w.e. (samples number 1116 and 1117, 22.2 m) that was also identified in the shallow core 2005. P10, P16, P7 are crustal/dust particles from sizes ranging from 0.3 μm to 10 μm. P13 is the biggest and most dense crustal particle found in this sample (ferrite), having a length of more than 50 μm. P12 and P17 are diatoms. P8 corresponds to soot granular structures.

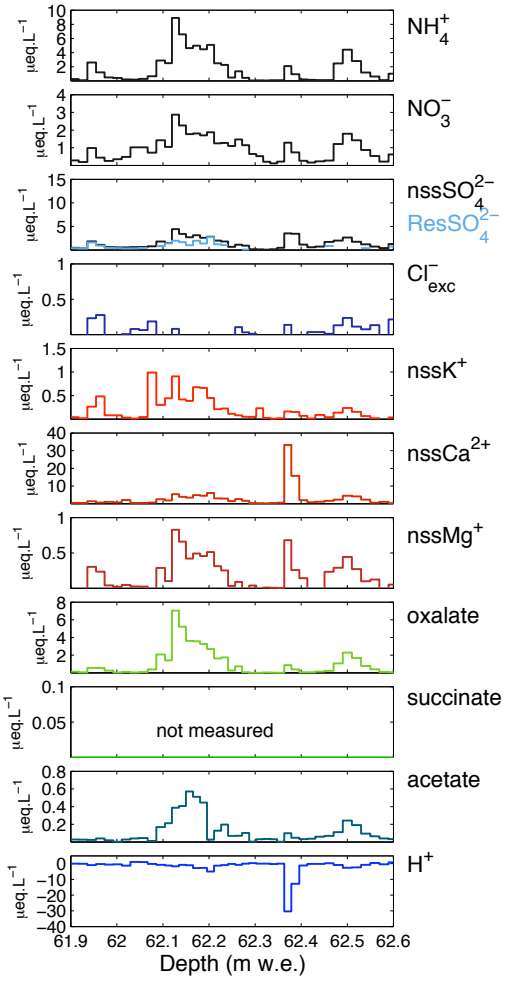

Figure 4.6: Group of peaks presenting very high concentrations of oxalate, $NH_4^+$and $nssCa^{2+}$in the brittle zone. Its origin remains uncertain as the high concentrations of NH_4^+, oxalate and $nssCa^{2+}$do not depict typical biomass burning events, organic matter decomposition of an undetermined origin has been invoked.

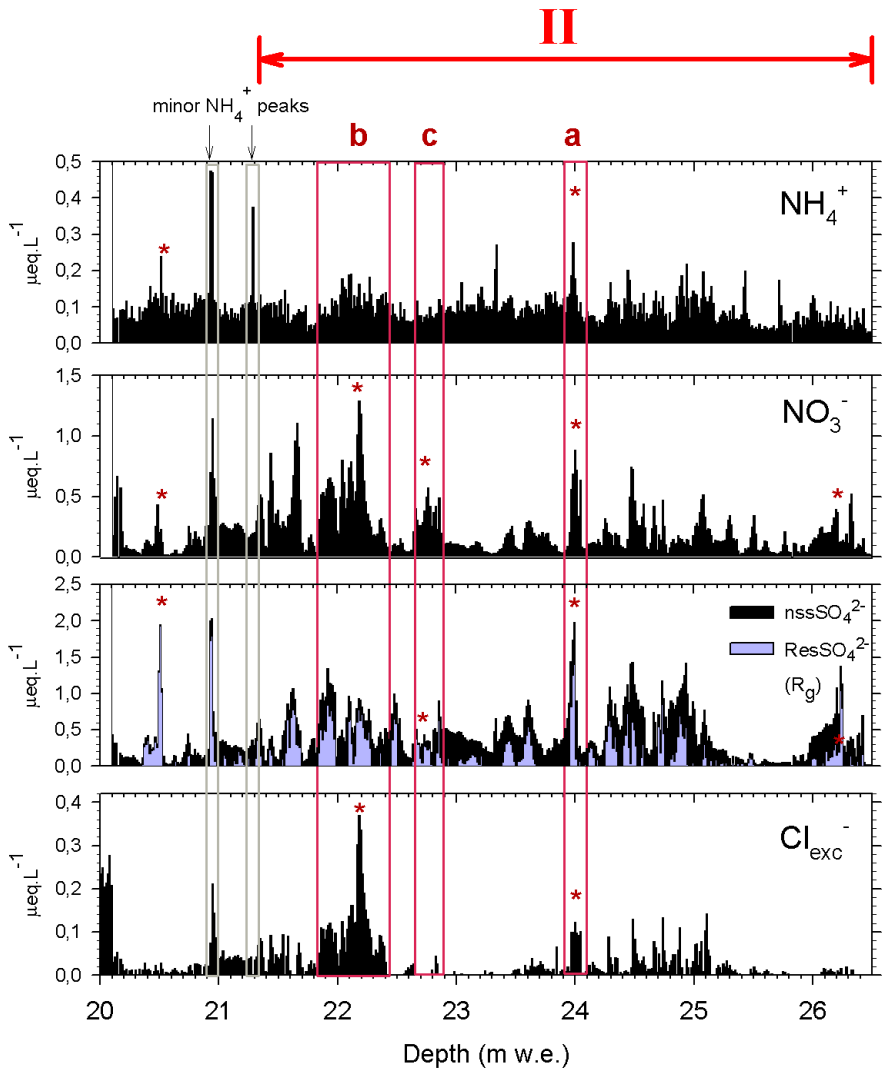

Figure 4.7: Detailed profile between 20 and 20.6 m w.e of NH_4^+, NO_3^-, Cl_{exc}^-, $nssSO_4^{2-}$and residual SO_4^{2-}($ResSO_4^{2-}$calculated with equation 3.13 in blue). The zone labeled II in figure 4.2 is included here. As this zone is deprived of peaks of any specie (including Na^+, not shown) it represents the background composition of recent snow. Focus (asterisks) is made on some examples of synchronous occurrences of these species at the background level: **a.** A case when NH_4^+, NO_3^-, $nssSO_4^{2-}$(and $ResSO_4^{2-}$) and $Cl_{exc}^-$are all correlated. **b.** When the most prominent correlation is between $NO_3^-$and Cl_{exc}^-(although NH_4^+, $nssSO_4^{2-}$and $ResSO_4^{2-}$are present). **c.** $NO_3^-$and $nssSO_4^{2-}$(and $ResSO_4^{2-}$) when $NH_4^+$and $Cl_{exc}^-$are absent.

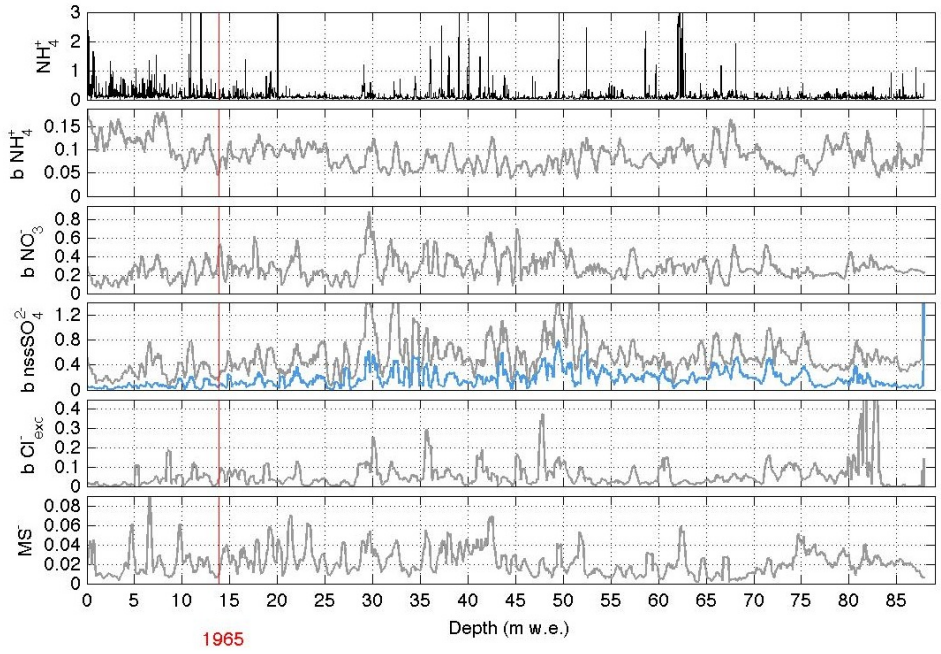

(a) Running average (31 points = ∼0.3 m w.e.)

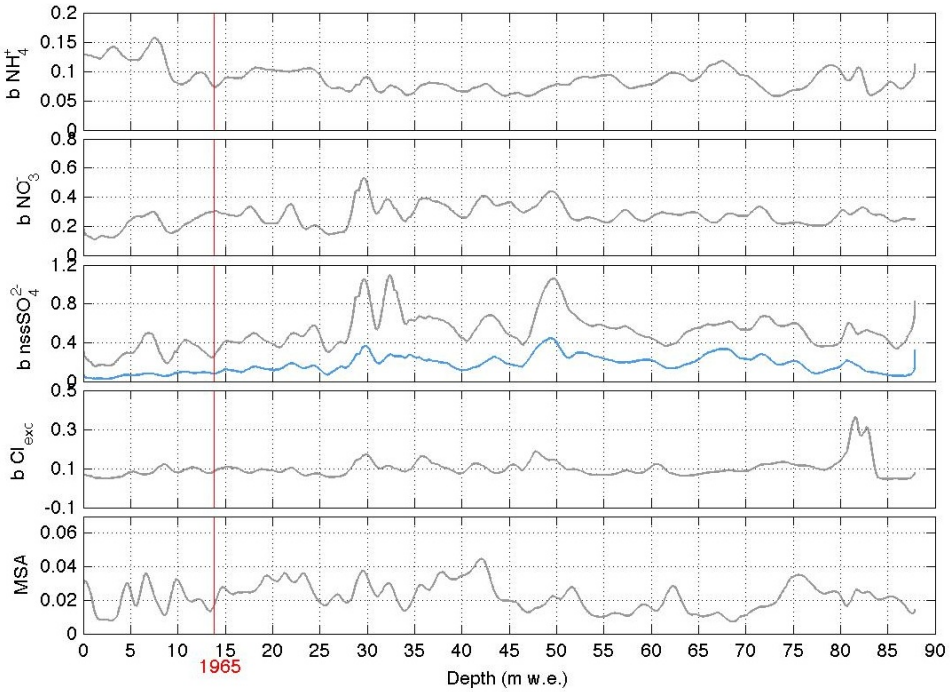

(b) PC1-SSA (Embedding dimension M = 100, ∼1 m w.e.)

Figure 4.8: (a) Complete NH_4^+profile (black), and the 31-point running average of background levels of NH_4^+, NO_3^-, $nssSO_4^{2-}$, $Cl_{exc}^-$and MS^-(gray). $ResSO_4^{2-}$calculated with equation 3.13 is shown in blue. Background levels where obtained removing major and minor NH_4^+peaks presented in figure 4.2 and major MS^-contributions described in section 3.4.2.1. (b) The first principal component (PC1) of background levels of NH_4^+, NO_3^-, $nssSO_4^{2-}$, $Cl_{exc}^-$and MS^-, obtained with Analyseries (Paillard et al., 1996). The PC1 reflects 19%, 10%, 16%, 25% and 9% of the background variability of the aforementioned species.

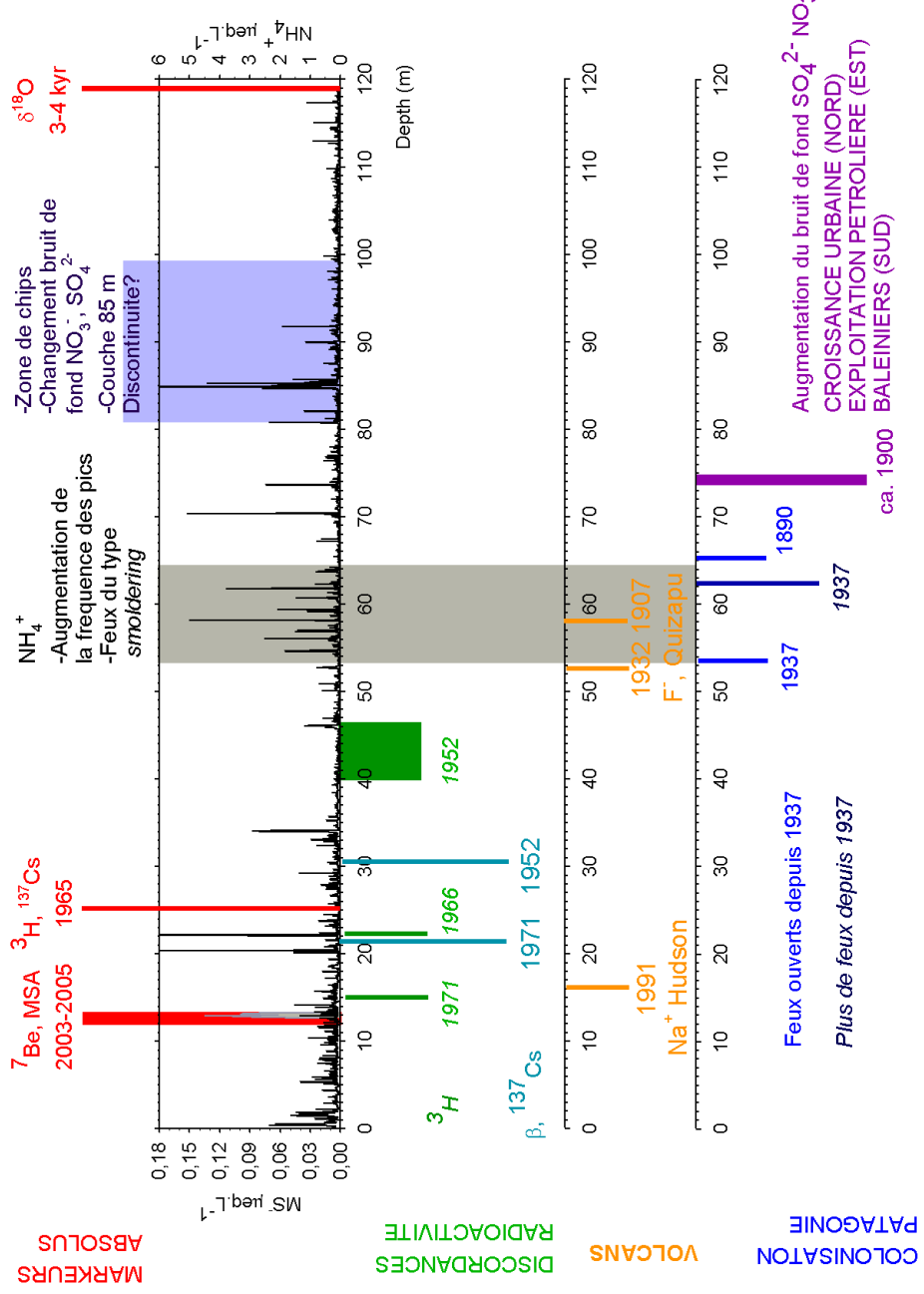

Figure 4.9: Current dating horizons as presented in section 4.4.5. In red, absolute horizons. In green/turquoise: Radioactive data under debate. In orange: volcanic eruptions. In blue: settlers influence in forest fire type/frequency in Patagonia. In violet: industrialization or whaling onset

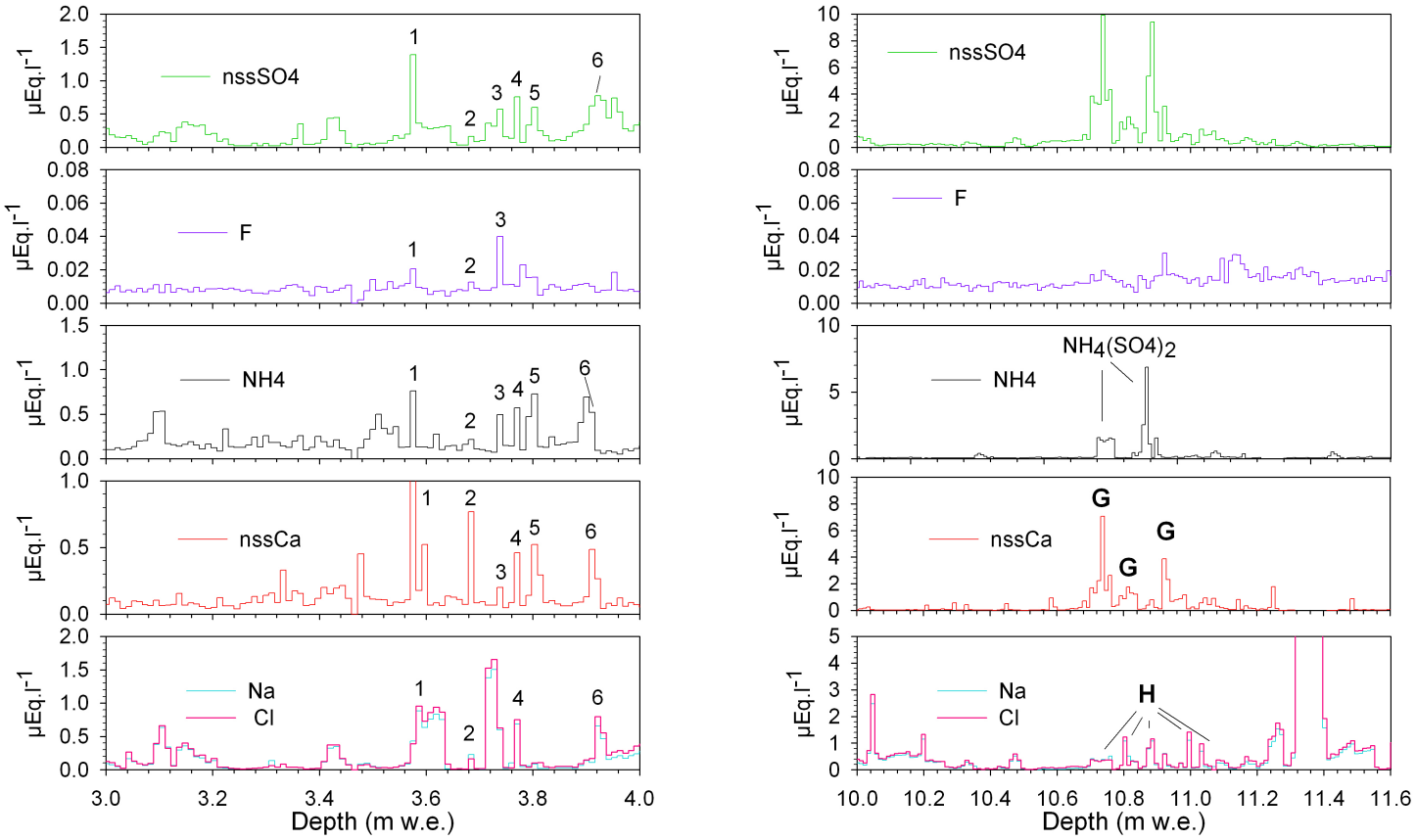

(a) Detailed example of 6 Dirac-shaped nssCa^{2+}contributions

(b) Detailed example of gypsum-like contributions

Figure 4.10: Detailed example of dust contributions of selected sections of the CL122 core. nssSO_4^{2-}, F^-, NH_4^+, nssCa^{2+}, $Na^+$and Cl^-concentrations are given in μeq.L^{-1}. H stands for halite (NaCl) and G for gypsum-like ($CaSO_4$) contributions.

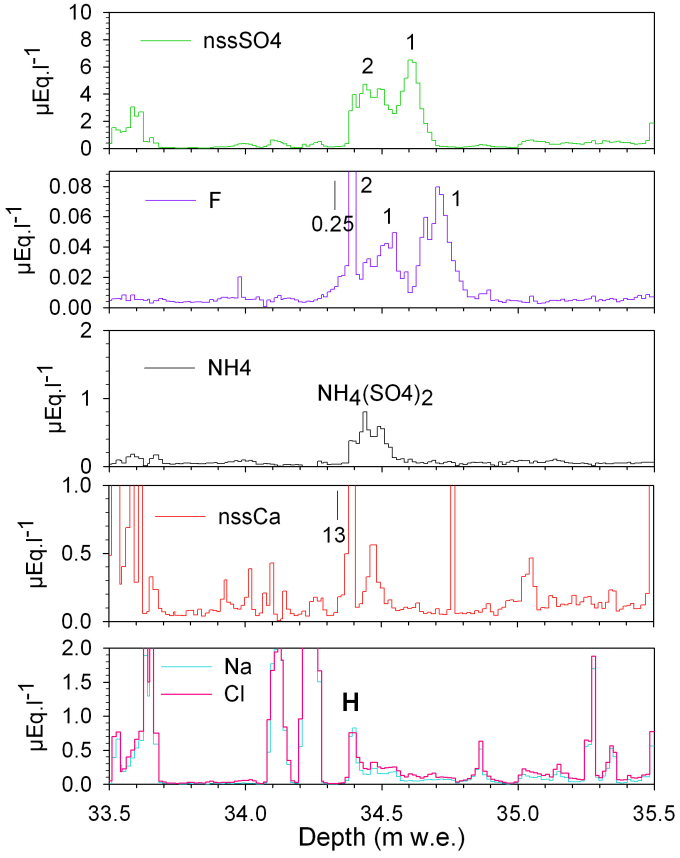

Figure 4.11: Detailed example of two (numbered 1 and 2) possible volcanic contributions to SV ice. nssSO_4^{2-}, F^-, NH_4^+, nssCa^{2+}, $Na^+$and Cl^-concentrations are given in μeq.L^{-1}. H stands for halite (NaCl) contributions.

Conclusions and prespectives

Contribution of this study to the characterization of southern mid-latitudes environment

The first objective of this work was to provide a high resolution data base of major and minor ions along the 122 m long ice core recovered in 2007 at the Monte San Valentin (46°S), in order to help to document past atmospheric variability along the Equator-Pole transect. In consequence, a complete ionic dataset was produced based on the analysis of the the 73 upper meters (52 m w.e.) and the last 14 meters (from 80 to 88 m w.e.) reaching the bedrock.

The first step of my work was devoted to analytical developments including organic trace species. A specific care was paid to contaminations estimate and control. Detailed profiles at ∼2 cm resolution were established for Na^+, K^+, NH_4^+, Ca^{2+}, Mg^{2+}, MS^-, F^-, Br^-, Cl^-, SO_4^{2-}, $NO_3^-$and $NO_2^-$and the following carboxylates: formate, acetate, lactate, pyruvate, propionate, oxalate, succinate and glutarate. The database produced is available under request and it constitutes a contribution to fill the environnmental data gap existing between 35 and 60°S.

Ionic profiles as well as water isotope profiles (the latter obtained and discussed by Herreros, 2010) were compared with preliminary results obtained from a shallow core extracted in 2005 in the same area. This intercomparison presented evidence of a recent increase of the net annual snow accumulation rate, namely from 20 cm w.e. per year for the 1965-2005 time period to more than 3 m w.e. per year for the past 2 years. This was explained by the varying influence of snow blowing along the glacier flow line leading to a progressive increase of the net snow accumulation

rate for the last few years. High annual precipitation rates predicted by the PRECIS and GFS models for the SV summit (8 and 4 m w.e., respectively) are quite consistent with the net accumulation rates observed for the last few years.

This important spatial variability on net accumulation precluded the establishing of an absolute dating of the ice core, as the accumulation processes appeared to be more complex than previously evaluated. It seems that the combination of ice flow and surface exposure to wind blowing affects the net accumulation at the summit plateau of the SV, where the ice cores were retrieved. Thus, **the interpretation of the chemical profiles was made in terms of events′ characterization** and not in a temporal basis.

The second part of this work was devoted to the understanding of the climatic conditions governing the Mount San Valentin site using available reanalysis data (NECP-NCAR, ERA-40 and ERA-Interim), forecast data (GFS model), surrogate climatology (PRECIS) and precipitation and wind observations from neighboring stations (Coyhaique, Balmaceda, San Pedro and Cabo Raper). The chapter including these analyses provided an important basis for the interpretation of the chemical and isotopic signals of the ice cores.

According to GFS precipitation predictions at this site, we would expect to have an ice archive dominated by marine contributions: precipitations originating from the Pacific and Southern Oceans were predicted to occur in 92% of the days, bringing 97% of the annual precipitation. The original source of moisture at this site is the Pacific Ocean, nevertheless, based on $Na^+$and MS^-profiles, proxies of marine primary salt and marine biogenic inputs, respectively, we demonstrated that ice layers corresponding to precipitation containing an important marine imprint account for only ∼45% of the ice archive (∼30% for $Na^+$and ∼15% for MS^-). This confirms that marine proxies are underepresented in the glaciochemical archive of the Monte San Valentin, which increases the relative importance of the continental record.

Concerning westerly transport, major ions inputs, δD , deuterium excess and precipitation predictions indicate that marine biogenic contributions can originate from both the South Eastern Pacific and the Southern Oceans, whereas important inputs of primary marine aerosol are

transported mainly from the South Eastern Pacific Ocean. These contributions are asynchronous and likely underrepresented in winter.

Northern and northeastern sources would influence this site bringing most of the continental markers (∼3 % of the precipitation and also dry deposit). Northwesterly flow (∼20% of the precipitation) can also produce mixing between stratified marine air masses and continental air masses aloft. All this is reflected by the complex continental contributions unveiled at this site composed by biomass burning-like events, volcanic background and a possible influence of anthropogenic pollution more likely transported from the subtropics than of local origin. Conversely, southern flow would be characterized by more pristine and rather scarce precipitation (∼1% of precipitation).

Easterly flow, rather rare and mostly non-precipitating, would be responsible of thin concentrated nssCa^{2+}layers due to dry deposits. This type of deposit is likely to favor chemical interactions near the snow surface and the formation of secondary species involving nssCa^{2+}, $NH_4^+$and SO_4^{2-}.

The high SO_4^{2-}content observed in precipitation of both marine (SO_4^{2-}/Na^+ratio close to 0.25eq.eq $^{-1}$) and continental origins (e.g. SO_4^{2-}content of combustion-like events is always higher than reported values) points to an important atmospheric reservoir of SO_4^{2-}at these latitudes that is only partly explained by the marine biogenic source. We estimate that the non marine SO_4^{2-}accounts for at least 50% of the total SO_4^{2-}.

After having examined the possible link between major NH_4^+events recorded along the core with the documented activity of the Quizapu volcano (1907-1932) and the arrival of settlers to Patagonia (ca.1870-1937), we were able to propose some dating horizons.

The only long term trend attributed to an anthropogenic influence is the increase of NH_4^+background levels after 1965 possibly related to increasing nitrogenous fertilizer consumption in South America since ca.1960.

Finally, and surprisingly, background continental contributions of NO_3^-, $Cl^-$and SO_4^{2-}do not seem to retrace any significant anthropogenic influence over the last decades. This last issue

motivates further environmental research in terms of continental sources and transport in this intriguing region.

Unresolved issues and next steps

- The lack of accurate depth-age scale at this site is the main issue to be resolved. We expected to cover the Holocene with this record, but, as this study suggests, the first 73 m of the core would rather span approximately 120 years, with variable net accumulation rates.

- Once dating is provided, the chemical signal can be interpreted in terms of mesoscale patterns: Northwesterly and Northerly flow (especially in terms of continental markers) would retrace subtropical variations (e.g. PDO, ENSO) whereas westerly (Na^+peaks) and southwesterly flow (likely the periods with diluted snow) would retrace Southern Anular Mode (SAM) fluctuations.

- Our understanding of marine contributions to this site is rather complete, but continental contributions remain to be fully studied. An important proxy still to be better understood is SO_4^{2-}. For this, we propose to use the same methodology as used before by grouping the types of peaks, now with the advantage of having gathered information on other processes (such as events associated with NH_4^+).

- We did not document pre industrial environmental and atmospheric variability during this study. For this, the deepest ice located below the brittle zone offers a unique opportunity to obtain unprecedented information on preindustrial reference levels and possibly part of the natural atmospheric variability in the southern mid-latitudes. The extensive dataset produced has still to be exploited in combination with other proxies such as water stable isotopes.

- The study of an anthropogenic influence in this site is still incomplete. We expect that

the trace element analyses conducted at the LMTG would help to better investigate it, confirming the dating hypothesis proposed here in relation with the colonization of the Patagonian region, volcanic events (Quizapu eruptive phase) and/or longer-range transport of polluted air masses from northern locations. Glacier flow modeling would be then better constrained to allow the continuous dating of the core, at least above the brittle zone.

- Other studies can be proposed to investigate the origin of SO_4^{2-}. As SV snow is characterized by high SO_4^{2-}levels, it provides the opportunity to study the oxidation pathways leading to sulfate formation, and sulfur origin using sulfur and oxygen isotopes of SO_4^{2-}: ^{34}S, ^{37}S, ^{16}O, ^{17}O and ^{18}O.

- In order to complete climatic and chemical studies at SV, a coupled analysis of weather regimes and sulfate outputs of the model MOCAGE covering the 2005-2007 period can be done. As the SV site has conserved a detailed glaciochemical archive of this time period, we would improve our understanding of the puzzling SO_4^{2-}source influencing this site. For this, collaboration is possible with the Centre de Recherches de Climatologie (B. Pohl) and the atmospheric chemistry group of the LGGE (M. Ménégoz).

Appendix

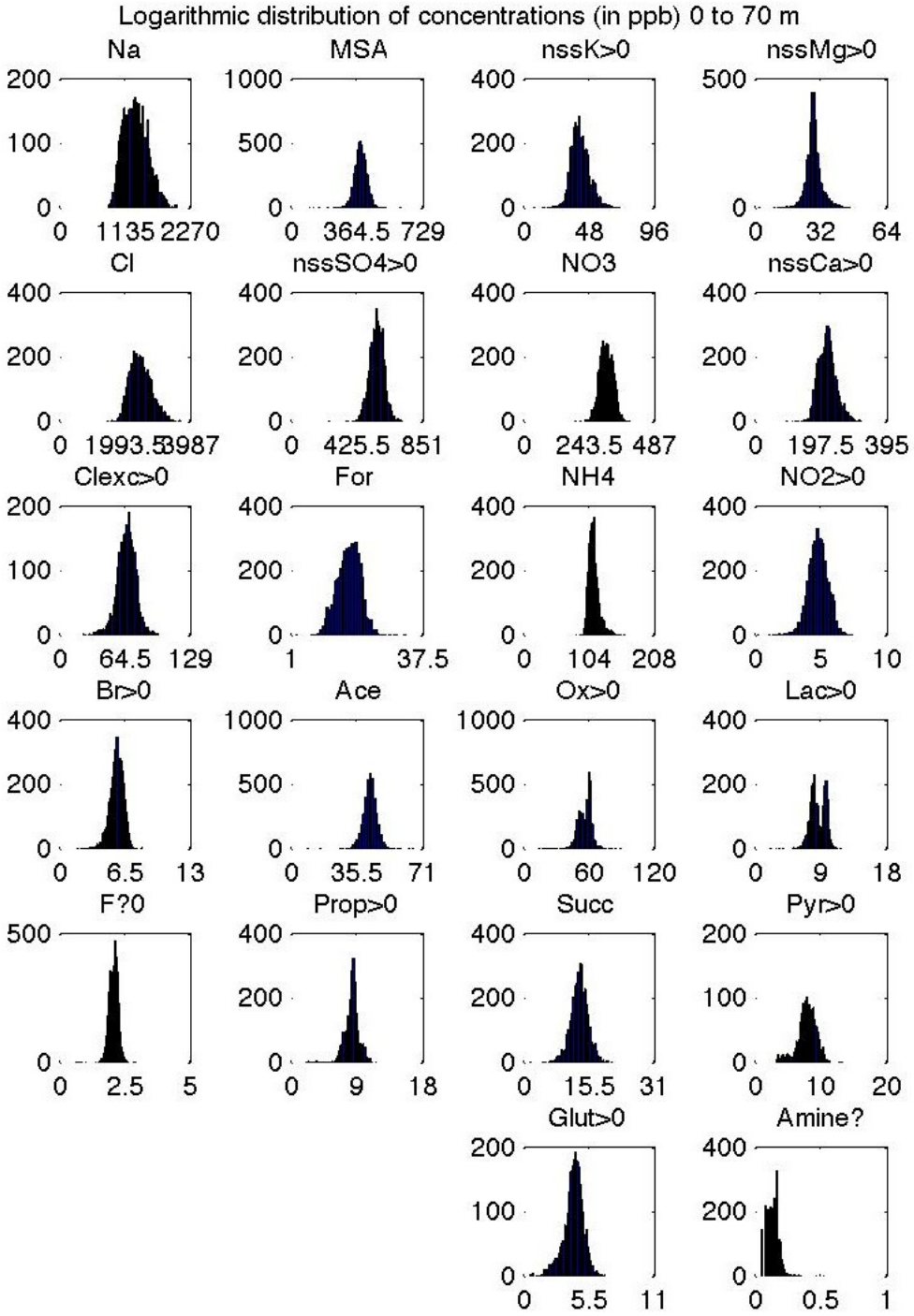
Logarithmic distribution of concentrations (in ppb) 0 to 70 m
Na
MSA
nssK>0
nssMg>0
Cl
nssSO4>0
NO3
nssCa>0
Clexc>0
For
NH4
NO2>0
Br>0
Ace
Ox>0
Lac>0
F?0
Prop>0
Succ
Pyr>0
Glut>0
Amine?

Volcanic activity close to the Northern Patagonian Icefield during the last century

Listed below are the known recent eruptions as reported by the Global Volcanism Program (http://www.volcano.si.edu/). The list is not exhaustive as other volcanoes are identified in the region, although no known recent eruptions have been reported for those. The Chilean Southern Volcanic region (33ºS -46º S) is very active as it is influenced by the Nazca plate subduction. The Austral Volcanic region (47º S -55º S), influenced by the Antarctic plate, shows much less volcanic activity since the plesitocene (Amigo, 2004), Eruptions with a Volcanic Explosivity Index (VEI) higher than 3 are highlighted. Ejected (VEI=3 tephra ejected 3-15 km height; VEI=4, 10-25 km; VEI=5, >25 km)

	Altitude m a.s.l.	Latitude S	Longitude W	Known eruptions
Quizapu – Cerro Azul	3788	35.653	70.761	1967 (august 9) VEI\approx2 1949 (april 15 \pm 5 days) VEI\approx2 1933-1938 (july 25) VEI=2 **1916-1932 (april 21) VEI=5+** **1914 (sep 8) VEI=3** 1913 (jan 15\pm 45 days) VEI\approx2 1912 VEI=2 1907 (jul 28) VEI=2 1906 VEI=2 1903 (jan) VEI\approx2 1846 (nov 26) VEI=2
Nevados del Chillán	3212	36.863	71.377	2003 (Aug 29-Sep29) VEI=1 1973 (July) -1986 1972 1965 1946-1947 VEI\approx2 1945 1935 VEI\approx2
Callaqui	3164	37.92	71.45	1980 (Oct)
Llaima	3125	38.692	71.729	1979 (Oct 15)– 1980 (April 25)
Villarica	2847	39.42	71.93	1980 (June 20)– 1980 (September 24)
Carran los Venados	1141	40.35	72.07	1979 (April 14– may 20)
Arenales	3437	47.20	73.48	1979 (ca. march 8) VEI\approx1 (or Lautaro eruption)
Latuaro	3607	49.02	73.55	1979 (ca. march 8) VEI\approx2 (or Arenales

				eruption) 1978 (June) 1972 1961 (October) VEI=2 1959 (December 28) VEI=2 1945 (January 15 \pm 15 days) VEI=1 1933 (February) VEI\approx2 1879 1878 (January 18) VEI=1 1876 (October) VEI\approx2
Hudson	1905	45.90	72.97	**1991 (August 8, – October 27) VEI=5$^+$** **1971 (August 12 to September 18) VEI=3** 1891 1740\pm 150 years 860AD \pm 100 years 390AD \pm 150 years and other eruptions during the Holocene

Bibliography

Alexander, B., Savarino, J., Kreutz, K. J., and Thiemens, M. H. (2004). Impact of preindustrial biomass-burning emissions on the oxidation pathways of tropospheric sulfur and nitrogen. *J. Geophys. Res.*, 109(D8):D08303.

Amigo, A. (2004). Volcán láscar: Aporte y dispersión de azufre oxidado a la atmósfera regional. Master's thesis, Departamento de Geología, Universidad de Chile.

Andreae, M. O., Browell, E. V., Gregory, G. L.and Harriss, R. C., Hill, G. F., Sachse, G. W., Talbot, R. W., Garstang, M., and Jacob, D. J.and Torres, A. L. (1988). Biomass-burning emissions and associated haze layers over Amazonia. *Journal of Geophysical Research*, 93:1509–1257.

Andreae, M. O. and Merlet, P. (2001). Emission of trace gases and aerosols from biomass burning. *Global Biogeochem. Cycles*, 15(4):955–966.

Aravena, J. C. and Luckman, B. H. (2008). Spatio-temporal rainfall patterns in Southern South America. *International Journal of Climatology*, 9999(9999):n/a (on line version). 10.1002/joc.1761.

Aristarain, A. and Delmas, R. (1993). Firn-cor study from the southern Patagonia ice cap, South America. *Journal of Glaciology*, 39(132):249–254.

Arlander, D. W., Cronn, D. R., Farmer, J. C., Menzia, F. A., and Westberg, H. H. (1990).

Gaseous oxygenated hydrocarbons in the remote marine troposphere. *J. Geophys. Res.*, 95(D10):16391–16403.

Baroni, M. (2006). *Etude des anomalies isotopiques du soufre et de l'oxygene dans le sulfate d'origine volcanique enregistré dans les archives glaciaires.* PhD thesis, Université Joseph Fourier.

Bates, T. S., Calhoun, J. A., and Quinn, P. K. (1992). Variations in the methanesulfonate to sulfate molar ratio in submicrometer marine aerosol particles over the South Pacific Ocean. *Journal of Geophysical Research*, 97(D9):9859–9865.

Berrisford, P., D., D., Fielding, K., Fuentes, M., Kållberg, P., S., K., and Uppala, S. M. (2009). The ERA-Interim archive. Technical report, European Centre for Medium-Range Weather Forecasts.

Bouwman, A. F., Lee, D. S., Asman, W. A. H., Dentener, F. J., Van Der Hoek, K. W., and Olivier, J. G. J. (1997). A global high-resolution emission inventory for ammonia. *Global Biogeochem. Cycles*, 11(4):561–587.

Buol, S. (2007). Soils. In Veblen, T., K.Young, and Orme, A., editors, *The Physical Geography of South America*. Oxford University Press.

Carmona-Moreno, C., Belward, A., Malingreau, J.-P., Hartley, A., Garcia-Alegre, M., Antonovskiy, M., Buchshtaber, V., and Pivovarov, V. (2005). Characterizing interannual variations in global fire calendar using data from Earth observing satellites. *Global Change Biology*, 11(9):1537–1555.

Casassa, G. (2009). Personal communication.

Casassa, G., Rivera, A., Lange, H., and Carvallo, R. (1998). Radar and GPS studies at Horseshoe Valley, Patriot Hills, Antarctica. Technical report, FRISP report.

Centritto, M., Di Bella, C. M., Baraldi, R., Eugenia Beget, M., Kemerer, A., Rapparini, F., Oricchio, P., Rebella, C., and Loreto, F. (2008). Monoterpene emissions from three Nothofagus species in Patagonia, Argentina. *Journal of Plant Interactions*, 3(2):119 – 125.

Chebbi, A. and Carlier, P. (1996). Carboxylic acids in the troposphere, occurrence, sources, and sinks: A review. *Atmospheric Environment*, 30(24):4233–4249.

Cole-Dai, J., Mosley-Thompson, E., Wight, S. P., and Thompson, L. G. (2000). A 4100-year record of explosive volcanism from an East Antarctica ice core. *J. Geophys. Res.*, 105(D19):24431–24441.

Correia, A., Freydier, R., Delmas, R. J., Simões, J. C., Taupin, J.-D., Dupré, B., and Artaxo, P. (2003). Trace elements in South America aerosol during 20th century inferred from a Nevado Illimani ice core, Eastern Bolivian Andes (6350 m asl). *Atmospheric Chemistry and Physics*, 3.

Correia, J. and de Angelis, M. (2010). Personal communication.

Covert, D. S., Kapustin, V. N., Bates, T. S., and Quinn, P. K. (1996). Physical properties of marine boundary layer aerosol particles of the mid-Pacific in relation to sources and meteorological transport. *J. Geophys. Res.*, 101(D3):6919–6930.

Cozic, J. (2009). Personal communication.

Dalia Pereira, K. C., Evangelista, H., Pereira, E. B., Sim oes, J. C., Johnson, E., and Melo, L. R. (2004). Transport of crustal microparticles from Chilean Patagonia to the Antarctic Peninsula by SEM-EDS analysis. *Tellus B*, 56(3):262–275.

Dansgaard, W. (1964). Stable isotopes in precipitation. *Tellus*, 16(4):436–468.

de Angelis, M. (2010). Personal communication.

de Angelis, M., Barkoy, N. I., and Petrov, V. I. (1992). Sources of continental dust over Antarctica during the last glacial cycle. *Journal of Atmospheric Chemistry*, 14(1):233–244.

de Angelis, M. and Legrand, M. (1994). Origins and variations of fluoride in Greenland precipitation. *Journal of Geophysical Research*, 99(D1):1157–1172.

de Angelis, M., Sim oes, J., Bonnaveira, H., Taupin, J.-D., and Delmas, R. (2003). Volcanic eruptions recorded in the Illimani ice core (Bolivia): 1918-1998 and Tambora periods. *Atmospheric Chemistry and Physics*, 3:1725–1741.

de Angelis, M., Steffensen, J. P., Legrand, M., Clausen, H., and Hammer, C. (1997). Primary aerosol (sea salt and soil dust) deposited in Greenland ice during the last climatic cycle: Comparison with east Antarctic records. *Journal of Geophysical Research*, 102(C12):26681–26698.

del Valle, H. F., Elissalde, N. O., Gagliardini, D. A., and Milovich, J. (1998). Status of desertification in the Patagonian region: Assessment and mapping from satellite imagery. *Arid Land Research and Management*, 12(2):95–121.

Delmas, R. J., Kirchner, S., Palais, J. M., and Petit, J.-R. (1992). 1000 years of explosive volcanism recorded at the South Pole. *Tellus, Series B - Chemical and Physical Meteorology*, 44B(4):335–350.

Delmonte, B., Andersson, P., Schöberg, H., Hansson, M., Petit, J., Delmas, R., Gaiero, D., Maggi, V., and Frezzotti, M. (2010). Geographic provenance of aeolian dust in East Antarctica during Pleistocene glaciations: preliminary results from Talos Dome and comparison with East Antarctic and new Andean ice core data. *Quaternary Science Reviews*, 29(1-2):256 – 264.

Denman, K., Brasseur, G., Chidthaisong, A., Ciais, P., Cox, P., Dickinson, R., D. Hauglustaine, C. H., Holland, E., Jacob, D., Lohmann, U., Ramachandran, S., da Silva Dias, P., Wofsy, S., and Zhang, X. (2007). Couplings between changes in the climate system and biogeochemistry. Technical report, Climate Change 2007: The Physical Science Basis. Contribution of Working Group I to the Fourth Assessment Report of the Intergovernmental Panel on Climate Change.

Dentener, F., Kinne, S., Bond, T., Boucher, O., Cofala, J., Generoso, S., Ginoux, P., Gong, S., Hoelzemann, J. J., Ito, A., Marelli, L., Penner, J. E., Putaud, J.-P., Textor, C., Schulz, M., van der Werf, G. R., and Wilson, J. (2006). Emissions of primary aerosol and precursor gases in the years 2000 and 1750 prescribed data-sets for AeroCom. *Atmos. Chem. Phys.*

DGF (2007). Estudio de variabilidad climática en Chile para el siglo XXI - Cambios climáticos regionales para fines del siglo XXI obtenidos mediante el modelo PRECIS. http://www.dgf.uchile.cl/precis/.

Draxler, R. and Rolph, G. (2003). HYSPLIT (HYbrid Single-Particle Lagrangian Integrated Trajectory) Model access via NOAA ARL READY Website (http://www.arl.noaa.gov/ready/hysplit4.html).

Enomoto, H. and Nakajima, C. (1985). Recent climate fluctuations in Patagonia. Technical report, Jap. Soc. Snow and Ice.

EPICA, c. m. (2004). Eight glacial cycles from an antarctic ice core. *Nature*, 429(6992):623–628.

Escobar, F., Fernando, V., and Garin, C. (1992). Water balance in the Patagonia Icefield. Technical report, Jap. Soc. Snow and Ice.

Eyzaguirre, R. (2010). Personal communication.

Falvey, M. (2009a). Personal communication.

Falvey, M. (2009b). Regional simulation with the precis model. In *Climate Change in the Magellan and Antarctic Regions: Evidence and Challenges for the Future*, Punta Arenas, Chile.

Favier, V. (2010). Personal communication.

Favier, V., Falvey, M., Rabatel, A., Praderio, E., and López, D. (2009). Interpreting discrepancies between discharge and precipitation in high-altitude area of chile′s norte chico region (32°s). *Water Resour. Res.*, 45(2):W02424.

Ferrari, C. P., Clotteau, T., Thompson, L. G., Barbante, C., Cozzi, G., Cescon, P., Hong, S., Maurice-Bourgoin, L., Francou, B., and Boutron, C. F. (2001). Heavy metals in ancient tropical ice: initial results. *Atmospheric Environment*, 35(33):5809–5815.

Finlayson-Pitts, B. J. and Pitts, J. N. (2000). *Chemistry of the upper and lower atmosphere.* Academic Press, 1st edition.

Fischer, H., Wagenbach, D., and Kipfstuhl, J. (1998a). Sulfate and nitrate firn concentrations on the greenland ice sheet 1. large-scale geographical deposition changes. *J. Geophys. Res.*, 103(D17):21927–21934.

Fischer, H., Wagenbach, D., and Kipfstuhl, J. (1998b). Sulfate and nitrate firn concentrations on the greenland ice sheet 2. temporal anthropogenic deposition changes. *J. Geophys. Res.*, 103(D17):21935–21942.

Flues, M, Hama, P, Lemes, M. J, L., Dantas, E. S, K., Fornaro, and A (2002). *Evaluation of the rainwater acidity of a rural region due to a coal-fired power plant in Brazil*, volume 36. Elsevier, Kidlington, UK.

Fredier, R. (2009). Personal communication.

Fujiyoshi, Y., Kondo, H., Inoue, J., and Yamada, T. (1987). Characteristics of precipitation and vertical structure of air temperature in the northern patagonia. *Bulletin of Glacier Research*, 4:15–23.

Galloway, J. N., Keene, W. C., and Likens, G. E. (1996). Processes controlling the composition of precipitation at a remote southern hemispheric location: Torres del paine national park, chile. *Journal of Geophysical Research*, 101(D3):6883–6898.

Gao, S., Hegg, D. A., Hobbs, P. V., Kirchstetter, T. W., Magi, B. I., and Sadilek, M. (2003). Water-soluble organic components in aerosols associated with savanna fires in southern africa: Identification, evolution, and distribution. *Journal of Geophysical Research (Atmospheres)*, 108(D13):SAF 27–1.

Garreaud, R. (2007). Precipitation and circulation covariability in the extratropics. *Journal of Climate*, 20(18):4789–4797.

Garreaud, R. and Aceituno, P. (2007). Atmospheric circulation and climatic variability. In Veblen, T., K.Young, and Orme, A., editors, *The Physical Geography of South America*. Oxford University Press.

Garreaud, R. D. (2009). The andes climate and weather. *Adv. Geosci.*, 22:3–11.

Garreaud, R. D., Vuille, M., Compagnucci, R., and Marengo, J. (2007). Present-day south american climate. *Palaeogeography, Palaeoclimatology, Palaeoecology*.

Ginot, P. (2009). Personal communication.

Ginot, P., Casassa, G., Patris, N., Moreno, I., Herreros, J., de Angelis, M., Magand, O., and Vimeux, F. (2009). How representative is a unique deep ice core extracted from high summit glacier: the case of san valentin (chilean patagonia). Poster at MOCA confrence.

Ginot, P., Kull, C., Schwikowski, M., Shotterer, U., and Gäggeler, H. W. (2001). Effects of postdepositional processes on snow composition of a subtropical glacier (cerro tapado, chilean andes). *Journal of Geophysical Research*, 106(D23):32,375–32,386.

Ginot, P., Stampfli, F., Stampfli, D., Schwikoski, M., and Gäggeler, H. (2002). FELICS, a new ice core drilling system for high-altitude glaciers. Technical report, National Institut of Polar Research. Japan.

Gondwe, M., Krol, M., Gieskes, W., Klaassen, W., and de Baar, H. (2003). The contribution of ocean-leaving dms to the global atmospheric burdens of dms, msa, so2, and nss so4 =. *Global Biogeochem. Cycles*, 17(2):1056.

Gonzales, M. E. and Veblen, T. (2007). Incendios en bosques de araucaria araucana y consideraciones ecológicas al madereo de aprovechamiento en áreas recientemente quemadas. *Revista chilena de historia natural*, 80(2):243–253.

Gordon, C., Cooper, C., Senior, C. A., Banks, H., Gregory, J. M., Johns, T. C., Mitchell, J. F. B., and Wood, R. A. (2000). The simulation of sst, sea ice extents and ocean heat transports in a version of the hadley centre coupled model without flux adjustments. *Climate Dynamics*, 16(2):147–168.

Goto-Azuma, K. and Koerner, R. M. (2001). Ice core studies of anthropogenic sulfate and nitrate trends in the arctic. *J. Geophys. Res.*, 106(D5):4959–4969.

Graedel, T. E. and Keene, W. C. (1995). Tropospheric budget of reactive chlorine. *Global Biogeochem. Cycles*, 9(1):47–77.

Guiry, M. and Guiry, G. (2010). AlgaeBase. World-wide electronic publication, National University of Ireland, Galway. accesed on 17 October 2010.

Gutierrez, F., Gioncada, A., González Ferran, O., Lahsen, A., and Mazzuoli, R. (2005). The hudson volcano and surrounding monogenetic centres (chilean patagonia): An example of volcanism associated with ridge-trench collision environment. *Journal of Volcanology and Geothermal Research*, 145(3-4):207–233.

Haberle, S. G. and Lumley, S. H. (1998). Age and origin of tephras recorded in postglacial lake sediments to the west of the southern andes, 44°s to 47°s. *Journal of Volcanology and Geothermal Research*, 84(3-4):239–256.

Hardy, J. T. (1982). The sea surface microlayer: Biology, chemistry and anthropogenic enrichment. *Progress In Oceanography*, 11(4):307–328.

Herreros, J. (2010). *Interpretations sur le dernier siécle du profil isotopique de l'eau dans deux carottes de glace andines (Coropuna, Pérou, 15° S et San Valentin, Chili, 46° S)*. PhD thesis, Université Montpellier II.

Herreros, J., Moreno, I., Taupin, J.-D., Ginot, P., Patris, N., de Angelis, M., Ledru, M. P., Delanchaux, F., and Schotterer, U. (2009). Environmental records from temperate ice on nevado coropuna saddle, southern peru. *Adv. Geosci.*, 22:27–34.

Hildreth, W. and Drake, R. E. (1992). Volcán Quizapu, Chilean Andes. *Bulletin of Volcanology*, 54:93–125.

Hoffmann, G. (2009). Personal communication.

Hoffmann, G., Werner, M., and Heimann, M. (1998). Water isotope module of the echam atmospheric general circulation model: A study on timescales from days to several years. *J. Geophys. Res.*, 103(D14):16871–16896.

Holdsworth, G.; Peake, E. (1985). Acid content of snow from a mid-troposhere sampling site on mount logan, yukon territory, canada. *Annals of Glaciology*, 7:153–160.

Holton, J. R. (2004). *An introduction to dynamical meteorology*, volume 88 of *International Geophysics Series*. Elsevier Academic Press, 4th edition.

Hong, S., Bravante, C., Boutron, C., Gabrielli, P., Gaspari, V., Cescon, P., Thompson, L. G., Ferrari, C., Francou, B., and Maurice-Bourgoin, L. (2003). Atmospheric heavy metals in tropical south america during the past 22 000 year recorded in a high altitude ice core from sajama, bolivia. *JEM*, 6:322–326.

Hong, S., Candelone, J.-P., Patterson, C. C., and Boutron, C. F. (1996). History of ancient copper smelting pollution during roman and medieval times recorded in greenland ice. *Science*, 272(5259):246–249.

IFFN (2000). International forest fire news. Technical report, FAO/ECE/ILO Committee on Forest Technology, Management and Training.

Infobae, p. e. l. (2006). accessed on 30 September 2009.

Iriondo, M. (2000). Patagonian dust in Antarctica. *Quaternary International*, 68-71:83–86.

Jacob, V. (2009). Personal communication.

Jones, R., Noguer, M., D.C., H., Hudson, D., Wilson, S., Jenkins, G., and Mitchell, J. (2004). Generating high resolution climate change scenarios using PRECIS. Exeter, UK.

Jouzel, J., Masson-Delmotte, V., Cattani, O., Dreyfus, G., Falourd, S., Hoffmann, G., Minster, B., Nouet, J., Barnola, J. M., Chappellaz, J., Fischer, H., Gallet, J. C., Johnsen, S., Leuenberger, M., Loulergue, L., Luethi, D., Oerter, H., Parrenin, F., Raisbeck, G., Raynaud, D., Schilt, A., Schwander, J., Selmo, E., Souchez, R., Spahni, R., Stauffer, B., Steffensen, J. P., Stenni, B., Stocker, T. F., Tison, J. L., Werner, M., and Wolff, E. W. (2007). Orbital and millennial antarctic climate variability over the past 800,000 years. *Science*, 317(5839):793–796.

Jouzel, J. and Merlivat, L. (1984). Deuterium and oxygen 18 in precipitation: Modeling of the isotopic effects during snow formation. *J. Geophys. Res.*, 89(D7):11749–11757.

Kaallberg, P., Simmons, A., Uppala, S. M., and Fuentes, M. (2004). The era-40 archive. Technical report, European Centre for Medium-Range Weather Forecasts. available from www.ecmwf.int/publications.

Kalnay, E., Kanamitsu, M., and Baker, W. E. (1990). Global numerical weather prediction at the national meteorological center. *Journal Name: Bulletin of the American Meteorological Society; (USA); Journal Volume: 71*, pages Medium: X; Size: Pages: 1410–1428.

Kalnay, E., Kanamitsu, M., Kistler, R., Collins, W., Deaven, D., Gandin, L., Iredell, M., Saha, S., White, G., Woollen, J., Zhu, Y., Leetmaa, A., Reynolds, R., Chelliah, M., Ebisuzaki, W., Higgins, W., Janowiak, J., Mo, K. C., Ropelewski, C., Wang, J., Jenne, R., and Joseph, D. (1996). The ncep/ncar 40-year reanalysis project. *Bulletin of the American Meteorological Society*, 77(3):437–471.

Kanamitsu, M. (1989). Description of the nmc global data assimilation and forecast system. *Weather and Forecasting*, 4(3):335–342.

Kawamura, K., Seméré, R., Imai, Y., Fujii, Y., and Hayashi, M. (1996). Water soluble dicarboxylic acids and related compounds in antarctic aerosols. *Journal of Geophysical Research*, 101(D13):18,721–18,728.

Keene, W. C., Pszenny, A. A. P., Galloway, J. N., and Hawley, M. E. (1986). Sea-salt corrections and interpretation of constituent ratios in marine precipitation. *Journal of Geophysical Research*, 91:6647–6658.

Kellerhals, T., Brütsch, S., Sigl, M., Knüsel, S., Gäggeler, H. W., and Schwikowski, M. (2010). Ammonium concentration in ice cores: A new proxy for regional temperature reconstruction? *J. Geophys. Res.*, 115(D16):D16123.

Kerminen, V. M., Teinilä, K., and Hillamo, R. (2000). Chemistry of sea-salt particles in the summer antarctic atmosphere. *Atmospheric Environment*, 34:2817–2825.

Kerminen, V.-M., Teinilä, K., Hillamo, R., and Pakkanen, T. (1998). Substitution of chloride in sea-salt particles by inorganic and organic anions. *Journal of Aerosol Science*, 29(8):929–942.

Kitzberger, T. and Veblen, T. T. (1999). Fire-induced changes in northern patagonian landscapes. *Landscape Ecology*, 14(1):1–15.

Kitzberger, T., Veblen, T. T., and Villalba, R. (1997). Climatic influences on fire regimes along a rain forest-to-xeric woodland gradient in northern patagonia, argentina. *Journal of Biogeography*, 24(1):35–47.

Kohshima, S., Takeuchi, N., Uetake, J., Shiraiwa, T., Uemura, R., Yoshida, N., Matoba, S., and Godoi, M. A. (2007). Estimation of net accumulation rate at a patagonian glacier by ice core analyses using snow algae. *Global and Planetary Change*, 59:236–244.

Lamarque, J. F., Bond, T. C., Eyring, V., Granier, C., Heil, A., Klimont, Z., Lee, D., Liousse, C., Mieville, A., Owen, B., Schultz, M. G., Shindell, D., Smith, S. J., Stehfest, E., Van Aardenne, J., Cooper, O. R., Kainuma, M., Mahowald, N., McConnell, J. R., Naik, V., Riahi, K., and van Vuuren, D. P. (2010). Historical (1850-2000) gridded anthropogenic and biomass burning emissions of reactive gases and aerosols: methodology and application. *Atmos. Chem. Phys. Discuss.*, 10(2):4963–5019.

Lara, A., Solari, M., Rutherford, P., Thiers, O., Trecaman, R., Molina, R., Prieto, R., and Montory, C. (1999). Cobertura de la vegetacion original de la ecoregion de los bosques valdivianos en chile hacia 1550. Technical report, WWF/Universidad Austral de Chile.

Lebel, P. J., Vay, A., and Roberts, R. D. (1990). Ammonia and nitric acid emissions from wetlands and boreal forest fires. In Levine, J. S., editor, *Global biomass burning - Atmospheric, climatic, and biospheric implications*, volume 71, pages Medium: X; Size: Pages: 1075–1077. Cambridge, MA, MIT Press.

Leck, C. and Persson, C. (1996). Seasonal and short-term variability in dimethyl sulfide, sulfur dioxide and biogenic sulfur and sea salt aerosol particles in the arctic marine boundary layer during summer and autumn. *Tellus B*, 48:272–299.

Legrand, M. (1997). Ice-core records of atmospheric sulphur. *Philosophical Transactions of the Royal Society B: Biological Sciences*, 352(1350):241–250.

Legrand, M. and de Angelis, M. (1995). Origins and variations of light carboxylic acids in polar precipitation. *Journal of Geophysical Research - Atmospheres*, 100(D1):1445–1462.

Legrand, M. and de Angelis, M. (1996). Light carboxylic acids in greenland ice: A record of past forest fires and vegetation emissions from the boreal zone. *Journal of Geophysical Research*, 101(D2):4129–4146.

Legrand, M., Ducroz, F., Wagenbach, D., Mulvaney, R., and Hall, J. (1998). Ammonium in coastal antarctic aerosol and snow: Role of polar ocean and penguin emissions. *Journal of Geophysical Research*, 103(D9):11,043–11,056.

Legrand, M., Feniet-Saigne, C., Saltzman, E. S., and Germain, C. (1992). Spatial and temporal variations of methanesulfonic acid and non sea salt sulfate in antarctic ice. *Journal of Atmospheric Chemistry*, 14(1):245–260.

Legrand, M. and Mayewski, P. (1997). Glaciochemistry of polar ice cores: a review. *Reviews of geophysics*, 35(3):219–243.

Legrand, M. and Wagenbach, D. (1999). Impact of the cerro hudson and pinatubo volcanic eruptions on the antarctic air and snow chemistry. *Journal of Geophysical Research*, 104(D1).

Legrand, M. R. and Delmas, R. J. (1988). Formation of hcl in the antarctic atmosphere. *Journal of Geophysical Research*, 93:7153–7168.

Li, L. and Pomeroy, J. W. (1997). Estimates of threshold wind speeds for snow transport using meteorological data. *Journal of Applied Meteorology*, 36(3):205–213.

Lopez, P., Chevallier, P., Favier, V., Pouyaud, B., Ordenes, F., and Oerlemans, J. (2010). A regional view of fluctuations in glacier length in southern south america. *Global and Planetary Change*, 71(1-2):85–108.

Lopez, P., Sirguey, P., Arnaud, Y., Pouyaud, B., and Chevallier, P. (2008). Snow cover monitoring in the northern patagonia icefield using modis satellite images (2000-2006). *Global and Planetary Change*, 61(3-4):103–116.

Lopez, P. P. (2007). *Impact de la variabilité climatique sur la cryosphere du Campo de Hielo Norte : apport de la télédectection.* PhD thesis, Univ. Montpellier II.

Magand, O. (2008). Personal communication.

Maksimov, A. (2008). A physicochemical model for deep degassing of water-rich magma. *Journal of Volcanology and Seismology*, 2(5):356–363.

Marshall, G. J. and Harangozo, S. A. (2000). An appraisal of ncep/ncar reanalysis mslp data viability for climate studies in the south pacific. *Geophys. Res. Lett.*, 27(19):3057–3060.

Mather, T. A., Allen, A. G., Davison, B. M., Pyle, D. M., Oppenheimer, C., and McGonigle, A. J. S. (2004a). Nitric acid from volcanoes. *Earth and Planetary Science Letters*, 218(1-2):17–30.

Mather, T. A., Tsanev, V. I., Pyle, D. M., McGonigle, A. J. S., Oppenheimer, C., and Allen, A. G. (2004b). Characterization and evolution of tropospheric plumes from lascar and villarrica volcanoes, chile. *J. Geophys. Res.*, 109(D21):D21303.

Matsuoka, K. and Naruse, R. (1999). Mass balance features derived from a firn core at hielo patagonico norte, south america. *Arctic, Antarctic, and Alpine Research*, 31(4):333–340.

Matthews, E. (1994). Nitrogenous fertilizers: Global distribution of consumption and associated emissions of nitrous oxide and ammonia. *Global Biogeochem. Cycles*, 8(4):411–439.

Ménégoz, M. (2009). *Modélisation globale des interactions atmosphere-aérosols*. PhD thesis, Université de Toulouse.

Ménégoz, M. (2010). Personal communication.

Merlivat, L. and Jouzel, J. (1979). Global climatic interpretation of the deuterium-oxygen 18 relationship for precipitation. *J. Geophys. Res.*, 84(C8):5029–5033.

Meyerson, E. A., Mayewski, P. A., Kreutz, K. J., Meeker, L. D., Whitlow, S. I., and Twickler, M. S. (2002). The polar expression of enso and sea-ice variability as recorded in a south pole ice core. *Annals of Glaciology*, 35:430–436.

Molina, A. (2009). Personal communication.

Molina, M. J. and Molina, L. T. (2004). Megacities and atmospheric pollution - critcal review. *Air & Waste Manage. Assoc.*, 54:644–680.

Moreno, I. (2007). Variabilité régionale de l′environnement Antarctique au cours de l′Holocène : étude par chromatographie ionique de différents indicateurs au site de Talos Dome, comparaison avec les sites centraux du plateau Antarctique. Master's thesis, Laboratoire de Glaciologie et Géophysique de l′Environnement, Université Joseph Fourier, Grenoble.

Moy, C. M., Dunbar, Robert B.and Moreno, P. I., Francois, J.-P., Villa-Martínez, R., Mucciarone, D. M., Guilderson, T. P., and Garreaud, R. D. (2007). Isotopic evidence for hydrologic change related to the westerlies in sw patagonia, chile, during the last millennium. *Quaternary Science Reviews*, 27(13-14):1335–1349.

nez, P. S. (2008). personal communication.

Nichols, C. A. M., Guezennec, J., and Bowman, J. P. (2005). Bacterial exopolysaccharides from extreme marine environments with special consideration of the southern ocean, sea ice, and deep-sea hydrothermal vents: A review. *Marine Biotechnology*, 7(4):253–271.

Olivares, G., Gallardo, L., Langner, J., and Aarhus, B. (2002). Regional dispersion of oxidized sulfur in central chile. *Atmospheric Environment*, 36(23):3819–3828.

Paillard, D., Labeyrie, L., and Yiou, P. (1996). Macintosh program performs time-series analysis eos trans. agu, 77: 379.

Pakkanen, T. A., Kerminen, V.-M., Hillamo, R. E., Màkinen, M., Makela, T., and Virkkula, A. (1996). Distribution of nitrate over sea-salt and soil derived particles - implications from a field study. *Journal of Atmospheric Chemistry*, 24(2):189–205.

Paruelo, J. M., Beltrán, A., Jobbágy, E., Sala, O. E., and Golluscio, R. A. (1998). The climate of patagonia: general patterns and controls on biotic processes. *Ecologia Austral*, 8:85–101.

Paruelo, J. M., Jobbágy, E. G., and Sala, O. E. (2001). Current distribution of ecosystem functional types in temperate south america. *Ecosystems*, 4(7):683–698.

Parungo, F., Ackerman, E., Caldwell, W., and Weickmann, H. K. (1979). Individual particle analysis of antarctic aerosols. *Tellus*, 31.

Pasteur, E. C. and Mulvaney, R. (2000). Migration of methane sulphonate in antarctic firn and ice. *Journal of Geophysical Research*, 105(D9):11,525–11,534.

Patagonia-Argentina (2010). Memorias de un pueblo minero; accessed on 28 september 2009. http://www.patagonia-argentina.com/e/atlantica/sierra/hipasam.php.

Patris, N. (2009). Personal communication.

Peuch, V. (1999). Mocage chimie-transport et bien plus encore. Technical report, Méteo France, Centre National.

Pio, C. A., Legrand, M., Alves, C. A., Oliveira, T., Afonso, J., Caseiro, A., Puxbaum, H., Sanchez-Ochoa, A., and Gelencsér, A. (2008). Chemical composition of atmospheric aerosols during the 2003 summer intense forest fire period. *Atmospheric Environment*, 42(32):7530–7543.

Pomeroy, J. W., Marsh, P., and Gray, D. M. (1997). Application of a distributed blowing snow model to the arctic. *Hydrological Processes*, 11(11):1451–1464.

Prenni, A. J., Demott, P. J., Rogers, D. C., Kreidenweis, S. M., Mcfarquhar, G. M., Zhang, G., and Poellot, M. R. (2009). Ice nuclei characteristics from m-pace and their relation to ice formation in clouds. *Tellus B*, 61(2):436–448.

Preunkert, S., Legrand, M., and Wagenbach, D. (2001). Sulfate trends in a col du dome (french alps) ice core: A record of anthropogenic sulfate levels in the european midtroposphere over the twentieth century. *J. Geophys. Res.*, 106(D23):31991–32004.

Preunkert, S., Wagenbach, D., and Legrand, M. (2003). A seasonally resolved alpine ice core record of nitrate: Comparison with anthropogenic inventories and estimation of preindustrial emissions of no in europe. *J. Geophys. Res.*, 108(D21):4681.

Prospero, J. M., Ginoux, P., Torres, O., Nicholson, S. E., and Gill, T. E. (2002). Environmental characterization of global sources of atmospheric soil dust identified with the nimbus 7 total ozone mapping spectrometer (toms) absorbing aerosol product. *Reviews of geophysics*, 40(1):2.1–2.31.

Ramirez, E., Hoffman, G., Taupin, J. D., Francou, B., Ribstein, P., Caillon, N., Ferron, F., Landais, A., Petit, J., Pouyaud, B., Schotterer, U., Sim oes, J. C., and Stievenard, M. (2003). A new andean deep ice core form nevado illimani (6350 m), bolivia. *Earth and Planetary Science Letters*, 212:337–350.

Rasmussen, L. A., Conway, H., and Raymond, C. F. (2007). Influence of upper air conditions on the patagonia icefields. *Global and Planetary Change*, 59(1-4):203–216.

Reid, J. S., Koppmann, R., Eck, T. F., and Eleuterio, D. P. (2004). A review of biomass burning emissions, part II: Intensive physical properties of biomass burning particles. *Atmos. Chem. Phys. Discuss.*, 4(5).

Renwick, J. A. (1998). ENSO-related variability in the frequency of South Pacific blocking. *Monthly Weather Review*, 126(12):3117–3123.

Renwick, J. A. and Revell, M. J. (1999). Blocking over the South Pacific and Rossby wave propagation. *Monthly Weather Review*, 127(10):2233–2247.

Rignot, E., Rivera, A., and Casassa, G. (2003). Contribution of the patagonia icefields of south america to sea level rise. *Science*, 302(5644):434–437.

Rivera, A., Benham, T., Casassa, G., Bamber, J., and Dowdeswell, J. A. (2007). Ice elevation and areal changes of glaciers from the northern patagonia icefield, chile. *Global and Planetary Change*, 59(1-4):126–137.

Rodrigo S., P. and Orrego S., J. P. (2007). *Patagonia chilena, sin represas.* Ocho libros editores.

Rosenblüth, B., Fuenzalida, H. A., and Aceituno, P. (1997). Recent temperature variations in southern south america. *International Journal of Climatology*, 17(1):67–85.

Salawitch and Ross, J. (2006). *Biogenic bromine*, volume 439. Nature Publishing Group, London, UK.

Santibañez, P., Kohshima, S., Scheihing, R., Jaramillo, J., Shiraiwa, T., Matoba, T., Kanda, D., Labarca, P., and Casasa, G. (2008). Glacier mass balance interpreted from biological analysis of firn cores in the chilean lake district. *Journal of Glaciology*, 54(186).

Savarino, J. and Legrand, M. (1998). High northern latitude forest fires and vegetation emissions over the last millenium inferred from the chemistry of a central greenland ice core. *Journal of Geophysical Research*, 103:8267–8279.

Schläppi, M. et al. (2009). First ice core record from pio xi glacier, southern patagonia ice field 49°s. Poster at EGU AvH4 confrence.

Schlesinger, W. H. (1996). *Biogeochemistry. An analysis of global change.* Academic Press, London, second editon edition.

Schneider, C. and Gies, D. (2004). Effects of el niño-southern oscillation on southernmost south america precipitation at 53°s revealed from ncep-ncar reanalyses and weather station data. *International Journal of Climatology*, 24(9):1057–1076.

Schneider, C., Glaser, M., Kilian, R., Santana, A., Butorovic, N., and Casassa, G. (2003). Weather observations across the southern andes at 53°s. *Physical Geography*, 24(2):97–119.

Schotterer, U. (2009). Personal communication.

Schwikowski, M., Brütsch, S., Casassa, G., and Rivera, A. (2006). A potential high-elevation ice-core site at hielo patagonico sur. *Annals of Glaciology*, 43:8–13.

Seinfeld, J. H. and Pandis, S. (1998). *Atmospheric chemistry and physics : from air pollution to climate change*, volume A Wiley-Interscience Publication. New York, NY: Wiley.

Shiraiwa, T., Kohshima, S., Uemura, R., Yoshida, N., Matoba, S., Uetake, J., and Godoi, M. A. (2002). High net accumulation rates at campo de hielo patagonico sur, south america, revealed by analysis of a 45.97 m long ice core. *Annals of Glaciology*, 35:84–90.

Sillanpä, M., Saarikoski, S., Hillamo, R., Pennanen, A., Makkonen, U., Spolnik, Z., Van Grieken, R., Koskentalo, T., and Salonen, R. O. (2005). Chemical composition, mass size distribution and source analysis of long-range transported wildfire smokes in helsinki. *Science of The Total Environment*, 350(1-3):119–135.

Simões, J. C., Ferron, F. F., Bernardo, R. T., Aristarain, A. J., Stiévenard, M., Pourchet, M., and Delmas, R. J. (2004). Ice core study from the king george island, south shetlands, antarctica. *Pesquisa Antártica Brasileira*, 4:9–23.

Simões, J. C., Taupin, J.-D., Ribstein, P., Petit, J.-R., Angelis, M. d., Ramirez, E., Hoffmann, G., Correia, A. L., Delmas, R. J., Dupré, B., Ginot, P., and Francou, B. (2003). Forty years of environmental record from the nevado illimani ice core, central-eastern andes.

Simkin, T. and Siebert, L. (2002). Smithsonian institution, global volcanism program digital information series, GVP-5; accessed on 11 july 2008.

Simmons, A., Uppala, S. M., Dee, D., and Kobayashi, S. (2006). Era-interim: New ecmwf reanalysis products from 1989 onwards. *ECMWF Newsletter*, 110:25–35.

Sinclair, M. R. (1996). A climatology of anticyclones and blocking for the southern hemisphere. *Monthly Weather Review*, 124(2):245–264.

Smith, R. B. and Evans, J. P. (2007). Orographic precipitation and water vapor fractionation over the southern andes. *Journal of Hydrometeorology*, 8(1):3–19.

Song, C. H. and Carmichael, G. R. (1999). The aging process of naturally emitted aerosol (sea-salt and mineral aerosol) during long range transport. *Atmospheric Environment*, 33(14):2203–2218.

Stichler, W., Schotterer, U., Fröhlich, K., Ginot, P., Kull, C., Gäggeler, H., and Pouyaud, B. (2001). Influence of sublimation on stable isotope records recovered from high-altitude glaciers in the tropical andes. *Journal of Geophysical Research*, 106(D19):22613–22620.

Talbot, R. W., Andreae, M. O., Andreae, T. W., and Harriss, R. C. (1988). Regional aerosol chemistry of the amazon basin during the dry season. *J. Geophys. Res.*, 93.

Tassi, F., Aguilera, F., Vaselli, O., Medina, E., Tedesco, D., Delgado Huertas, A., Poreda, R., and Kojima, S. (2009). The magmatic- and hydrothermal-dominated fumarolic system at the active crater of lascar volcano, northern chile. *Bulletin of Volcanology*, 71(2):171–183.

Thompson, L. G., Davis, M. E., Mosley-Thompson, E., Sowers, T. A., Henderson, K. A., Zagorodnov, V. S., Lin, P. N., Mikalenko, V. N., Campen, R. K., Bolzan, J. F., Cole-Dai,

J., and Francou, B. (1998). A 25,000-year tropical climate history from bolivian ice cores. *Science*, 282:1858–1864.

Thompson, L. G., Mosley-Thompson, E., Davis, M. E., Lin, P. N., Henderson, K. A., Cole-Dai, J., Bolzan, J. F., and Liu, K. b. (1995). Late glacial stage and holocene tropical ice core records from huascarán, peru. *Science*, 269(5220):46–50.

Thompson, L. G., Mosley-Thompson, E., and Henderson, K. A. (2000). Ice-core palaeoclimate records in tropical south america since the last glacial maximum. *Journal of Quaternary Science*, 15(4):377–394. Special Issue: Quaternary Climate Change and South America.

Tison, J.-L., Souchez, R., Wolff, E. W., Moore, J. C., Legrand, M. R., and de Angelis, M. (1998). Is a periglacial biota responsible for enhanced dielectric response in basal ice from the greenland ice core project ice core? *J. Geophys. Res.*, 103(D15):18885–18894.

Tissari, J., Sippula, O., Kouki, J., Vuorio, K., and Jokiniemi, J. (2008). Fine particle and gas emissions from the combustion of agricultural fuels fired in a 20 kw burner. *Energy & Fuels*, 22(3):2033–2042.

Uetake, J., Kohshima, S., Nakazawa, F., Suzuki, K., Kohno, M., Kameda, T., Arkhipov, S., and Fujii, Y. (2006). Biological ice-core analysis of sofiyskiy glacier in the russian altai. *Annals of Glaciology*, 43:70–78.

Uppala, S. M., Kaallberg, P. W., Simmons, A. J., Andrae, U., Bechtold, V., Fiorino, M., Gibson, J. K., Haseler, J., Hernandez, A., Kelly, G. A., Li, X., Onogi, K., Saarinen, S., Sokka, N., Allan, R. P., Andersson, E., Arpe, K., Balmaseda, M. A., Beljaars, A. C. M., Berg, L. V. D., Bidlot, J., Bormann, N., Caires, S., Chevallier, F., Dethof, A., Dragosavac, M., Fisher, M., Fuentes, M., Hagemann, S., Hólm, E., Hoskins, B. J., Isaksen, L., Janssen, P. A. E. M., Jenne, R., McNally, A. P., Mahfouf, J.-F., Morcrette, J.-J., Rayner, N. A., Saunders, R. W., Simon, P., Sterl, A., Trenberth, K. E., Untch, A., Vasiljevic, D., Viterbo, P., and Woollen, J. (2005). The ERA-40 re-analysis. *Quarterly Journal of the Royal Meteorological Society*, 131:2961–3012.

Vautard, R. and Ghil, M. (1989). Singular spectrum analysis in nonlinear dynamics, with applications to paleoclimatic time series. *Physica D: Nonlinear Phenomena*, 35(3):395–424.

Villagra, P. E., Defossé, G. E., del Valle, H. F., Tabeni, S., Rostagno, M., Cesca, E., and Abraham, E. (2009). Land use and disturbance effects on the dynamics of natural ecosystems of the monte desert: Implications for their management. *Journal of Arid Environments*, 73(2):202–211.

Vimeux, F. (2009). Personal communication.

Vimeux, F. (2010). Personal communication.

Vimeux, F., Angelis, M. d., Ginot, P., Magand, O., Casassa, G., Pouyaud, B., Falourd, S., and Johnsen, S. (2008). A promising location in patagonia for paleoclimate and paleoenvironmental reconstructions revealed by a shallow firn core from monte san valentín (northern patagonia icefield, chile). *Journal of Geophysical Research*, 113(D16118).

Vimeux, F., Ginot, P., Schwikowski, M., Vuille, M., Hoffmann, G., Thompson, L. G., and Schotterer, U. (2009). Climate variability during the last 1000 years inferred from andean ice cores: A review of methodology and recent results. *Palaeogeography, Palaeoclimatology, Palaeoecology*, 281(3-4):229–241.

Vimeux, F., Maignan, F., Reutenauer, C., and Pouyaud, B. (2011). Evaluation of cloudiness over Monte San Valentín (Northern Patagonia Icefield) from 2000 to 2008 using MODIS observations. Submitted. *Journal of Glaciology*, 57(202):221–230.

Vimeux, F., Masson, V., Jouzel, J., Stievenard, M., and Petit, J. R. (1999). Glacial-interglacial changes in ocean surface conditions in the southern hemisphere. *Nature*, 398(6726):410–413.

Vincent, C., Vallon, M., Pinglot, J. F., Funk, M., and Reynaud, L. (1997). Snow accumulation and ice flow at Dôme du Goûter (4300 m), Mont Blanc, French Alps. *Journal of Glaciology*, 43:513–521.

Wagenbach, D., Ducroz, F., Mulvaney, R., Keck, L., Minikin, A., Legrand, M., Hall, J. S., and Wolff, E. W. (1998). Sea-salt aerosol in coastal antarctic regions. *J. Geophys. Res.*, 103(D9):10961–10974.

Warren, C. R. and Sugden, D. E. (1993). The patagonian icefields: A glaciological review. *Arctic and Alpine Research (Boulder, Colorado)*, 25:Pages: 316–331.

Weller, R., Traufetter, F., Fischer, H., Oerter, H., Piel, C., and Miller, H. (2004). Postdepositional losses of methane sulfonate, nitrate, and chloride at the european project for ice coring in antarctica deep-drilling site in dronning maud land, antarctica. *J. Geophys. Res.*, 109(D7):D07301.

Wendt, J. (2007). Personal communication.

Whitlow, S., Mayewski, P., Dibb, J., Holdsworth, G., and Twickler, M. (1994). An ice-core-based record of biomass burning in the arctic and subarctic, 1750-1980. *Tellus B*, 46(3):234–242.

Wylie, D. J. and Mora, S. J. d. (1996). Atmospheric dimethylsulfide and sulfur species in aerosol and rainwater at a coastal site in new zealand. *Journal of Geophysical Research*, 101(D15):21,041–21,049.

Yahdjian, L. and Sala, O. E. (2008). Do litter decomposition and nitrogen mineralization show the same trend in the response to dry and wet years in the patagonian steppe? *Journal of Arid Environments*, 72(5):687–695.

Yalcin, K. and Wake, C. P. (2001). Anthropogenic signals recorded in an ice core from eclipse icefield, yukon territory, canada. *Geophysical Research Letters*, 28(23):4487–4490.

Yamada, T. (1987). Glaciological characteristics revealed by 37.6-m deep core drilled at the accumulation area of san rafael glacier, the northern patagonia icefield. *Bulletin of Glacier Research*, 4:59–67.

Yeatman, S. G., Spokes, L. J., and Jickells, T. D. (2001). Comparisons of coarse-mode aerosol nitrate and ammonium at two polluted coastal sites. *Atmospheric Environment*, 35(7):1321–1335.

Zhang, W. and Zhang, X. (2007). A forecast analysis on fertilizers consumption worldwide. *Environmental Monitoring and Assessment*, 133(1):427–434.